Absolute Long-distance measurements with (sub)-micrometer accuracy for formation flight applications

Flatscher, R.; Cabral, A.; Abreu, M.; Verlaan, A.L.; Witte, S.; Ubachs, W.M.G.

2008

document version
Publisher's PDF, also known as Version of record

Final Report

Compilation of updated Technical Notes produced under this contract, including performance models and any produced output files.

	Name	Signature
Prepared by	R. Flatscher (ASG) A. Cabral and M. Abreu (INETI) A.L. Verlaan (TNO) S. Witte W. Ubachs(LCVU)	
Checked by		
Approved by		

DISTRIBUTION LIST

External:		TNO:	
• ESA ESTEC	8x	Archive	1x

DOCUMENT CHANGE RECORD

Issue	Date	Number of pages	Short description	Page
1	See header	See header	New document	All

List of Contents

List of Figures

List of Tables

1 Documents & Abbreviations

1.1 Applicable Documents

	Applicable Documents	Document number	Issue
AD01	SOW in Appendix 1 to AO/1-5070/06/NL/HE	GS 05/B20	1.0
AD02	Absolute long distance measurement with (sub-) micrometer accuracy for formation flight applications (Technical Proposal)	TNO-ALDM-PROP-002	1.0
AD03	TN1 State-of-the-art Technology Review and Preliminary HAALDM Concepts	HAALDM-TN1	1.0
AD04	TN2 Technology Status Review and Refined Femtosecond-based HAALDM Concepts	HAALDM-TN2	2.0
AD05	TN3 Parametric HAALDM System Study	HAALDM-TN3	2.0
AD06	TN4 Femtosecond-based Distance Metrology Systems for XEUS and Darwin	HAALDM-TN4	2.0
AD07	TN6 “Recommended R&D Programme for Spaceborne Femtosecond-based Distance Metrology Systems: (A) General, (B) Darwin, (C) Xeus”	HAALDM-TN6	1.0

1.2 Reference Documents

The reference documents have been moved to Annex 1

1.3 Abbreviations

ADM	Absolute Distance Measurement
ADR	Adiabatic Demagnetisation Refrigerator
ALDM	Absolute Long Distance Metrology
AM	Amplitude Modulated
AOM	Acoustic Optic Modulator
APD	Avalanche Photodiode
ATV	Autonomous Transfer Vehicle to ISS
BBO	Beta-Barium Borate
CCD	Charge Coupled Device
CHAMP	Challenging Mini-satellite Payload
COM	Centre of Mass
CRDF	fsLALDM with a Double Repetition Frequency in Coherent regime
CRFS	fsLALDM with a Repetition Frequency Sweep in Coherent regime
CW	Continuous Wave
DARWIN	The InfraRed Space Interferometer Mission
DORIS	Doppler Orbitography and Radiopositioning Integrated by Satellite
DSC	Detector Spacecraft
DWARF	DarWin AstRonomical Fringe sensor
EADS	European Aeronautic Defence and Space Company
EH	Electrical Heterodyning
EOL	End of Life
ESA	European Space Agency
ESSP	Nasa's Earth Science Pathfinder Program

FEEP	Field Emission Electrical Propulsion
FM	Frequency Modulated
FSI	Frequency Sweeping Interferometry
FsL	Femtosecond Laser
fsLALDM	femtosecond Laser Absolute Long Distance Metrology
GFZ	GeoForschungsZentrum
GNSS	Global Navigation Satellite System
GOCE	Gravity and Steady-State Ocean Circulation Explorer
GPS	Global Positioning System
GRACE	Gravity Recovery and Climate Experiment
HAALDM	High-Accuracy Absolute Long-Distance Measurement
HPOM	High Precision Optical Metrology for SMART-2
ICC	Interferometer Constellation Control
ICR1	fsLALDM with Incoherent and Coherent regimes
ICRN	fsLALDM with Incoherent (n>1) and Coherent regimes
INETI	Instituto Nacional de Engenharia, Tecnologia e Inovação
IRSI	Infrared Space Interferometer
ISim	Astrium's Interferometer Simulation program
ISS	International Space Station
ITT	Invitation to Tender
JPL	Jet Propulsion Laboratory
LCVU	Laser Centre of the Vrije Universiteit
LDI	Laser Doppler Interferometer

LED	Light Emitting Diode
LEO	low earth orbiting
LISA	Laser Interferometer Space Antenna
MSC	Mirror Spacecraft
MSM	Metal-Semiconductor-Metal
MWI	Multiple Wavelength Interferometry
NASA	National Aeronautics and Space Administration
NEP	Noise Equivalent Power
NFI	Narrow Field Imager
OB	Optical Bench
OFS	Optical Frequency Synthesizer
OH2LE	Optical Heterodyning with 2Lasers Intensity Cross Correlation Envelope Detection
OHD	Optical Heterodyning Dispersive time to space conversion
OHOSE	Optical Heterodyning with OPD Scan and Intensity Cross Correlation Envelope Detection
OOK	On-Off Keying
OPD	Optical Path Difference
PIN	Positive - Intrinsic - Negative
PLL	Phase Locked Loop
PM	Proof Mass
QD	Quantum Dot
RF	Radio Frequency
SA	Saturatable Absorber
SAR	Synthetic Aperture Radar
SC	Spacecraft
SHG	Second Harmonic Generator
SNR	Signal to Noise Ratio
SOW	Statement of Work

SSI	Satellite-Satellite Interferometry
SST	Satellite-to-Satellite Tracking
STJ	Super-conducting Tunnel Junctions
TNO	Technisch Natuurwetenschappelijk Onderzoek
TOF	Time-of-flight
TPA	Two-Photon Absorption
TTN	Three Telescope Nuller
USO	Ultra-Stable Oscillator
WFI	Wide Field Imager
XEUS	X-ray Evolving Universe Spectrometer
XMM	X-ray Multi-Mirror

2 Introduction

This document is the final report of the HAALDM project. (Absolute Long Distance Measurement with (sub-) micrometer Accuracy for Formation Flight Applications, ESA Contract number 20183/NL/HE)

The objective of the study is to assess the feasibility of FS-laser-based absolute long distance metrology in space and to explore its range of applications. The work comprises a parametric study for various FS-metrology schemes. These schemes represent a number of missions. Important aspects here are not only the required measurement range resolution, but also the role in the mission scenario and corresponding specifications in terms of spacecraft constellation and distance. To achieve this, the study investigates:

- Limitations of FS-metrology. This can be divided in
- Fundamental limitations
- Technological limitations
- Technical realisation
- Maturity of the involved technology
- Applicability of FS-metrology to different space mission scenarios
- Demands on system level

Where needed (where critical parameters are not documented sufficiently in literature) the study is supported by a limited experiment. In addition to the assessed performance of the FS-metrology schemes, they are compared to potential alternative measurement techniques, like frequency sweeping interferometer or dual wavelength interferometer. For the Darwin and the XEUS missions a HAALDM set-up is designed.

This final report consists of a compilation of updated Technical Notes produced under this contract, giving an overview of the research findings and a description of the derived designs for Darwin and XEUS. It includes performance models and their output. In this document the findings and results are critically reviewed.

3 Review of technology

3.1 Control of the fs-laser parameters

3.1.1 The frequency comb principle

A modelocked laser operates on a large number of longitudinal modes inside a laser cavity, which are all made to lase simultaneously. When all these optical modes are locked in phase, the final output of the laser will be a train of regularly spaced ultrashort optical pulses. Locking the phases of all these modes with respect to each other can be done in several ways, of which Kerr-lens modelocking is by far the most popular technique. To achieve stable modelocking inside a laser cavity, several elements need to be in place:

- A broadband gain medium, allowing the amplification of a large number of modes.
- Optics and a gain medium that can withstand the megawatt peak intensity circulating inside the cavity.
- Dispersion management inside the cavity, to ensure that modes of different frequencies can oscillate simultaneously.
- A method to initialise the modelocking.

The most common type of modelocked oscillator is the Kerr-lens modelocked Ti:Sapphire laser, which typically produces pulses with several nJ energy and a pulse duration in the 10-100 femtosecond range. The repetition rate of these lasers typically is typically in the MHz-GHz range.

The relation between time and frequency domain of such a modelocked laser is shown in Fig. 2.1. In the time domain, the laser output is an infinite train of ultrashort laser pulses, regularly spaced with a time interval T, which is simply the cavity roundtrip time related to the laser repetition rate by $f_{rep} = 1/T$. Since the group velocity and the phase velocity in the laser cavity are usually different, the carrier wave and the pulse envelope propagate at different velocities inside the cavity, which leads to a carrier-envelope phase shift $\Delta\varphi$ between the pulses in the train. In the frequency domain, this pulse train corresponds to a comb of discrete frequency modes, regularly spaced by f_{rep}. The carrier-envelope phase shift leads to a constant frequency shift of all the comb modes by an amount $f_{ceo} = (\Delta\varphi/2\pi)\, f_{rep}$, where f_{ceo} is known as the carrier-envelope offset frequency [RD52; RD73].

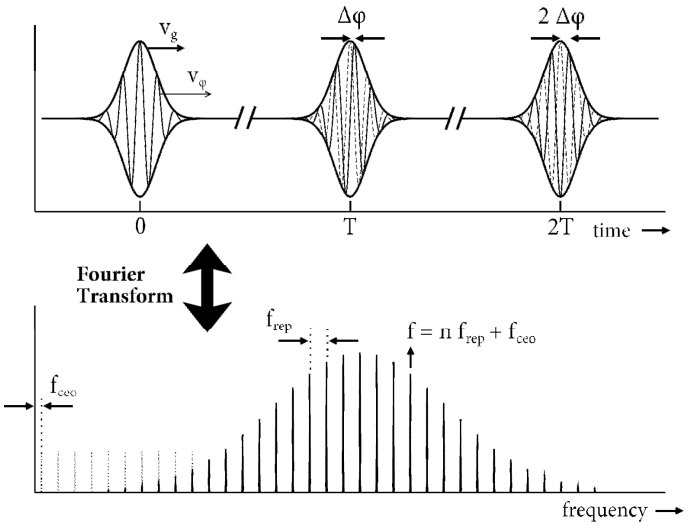

Fig. 2.1 - The relation between time and frequency domain of the output of a modelocked laser

This remarkably simple picture forms the basis of optical frequency measurements using a femtosecond frequency comb. The absolute frequencies of all the modes in the comb are given by $f = n f_{rep} + f_{ceo}$, where n is the mode number. Since both f_{rep} and f_{ceo} are in the RF domain, they can easily be compared to an absolute frequency standard such as a Cs clock. Stabilization of f_{rep} and f_{ceo} to such a frequency standard leads to an array of $\sim 10^6$ optical modes of which the absolute frequencies are all precisely known [RD48; RD52; RD73].

3.1.2 Repetition frequency

Stabilization of the repetition frequency f_{rep} of the frequency comb is conceptually straightforward, and it can be achieved by stabilizing the length of the laser cavity. A measurement of the repetition frequency is typically performed by detecting the modelocked pulse train on a fast photodiode. From this pulse train signal, f_{rep} can be obtained through electronically filtering. This measured f_{rep}-signal is then mixed with the signal from a stable RF frequency generator, which is referenced to the primary frequency standard (e.g. an atomic clock). The mixing product is used as a feedback signal to a PID regulator that controls the cavity length. Typically, this is achieved by mounting one of the cavity mirrors on a piezo-electric transducer and controlling the voltage on this piezo to change the cavity length.

The stability of the frequency comb at the frequency of the optical modes is mostly determined by the stability of f_{rep}. This can easily be seen by writing the frequencies of the respective optical modes as $f = n \times f_{rep} + f_{ceo}$, which highlights the fact that f_{rep} is multiplied by a large integer (typically $n \sim 10^5$), and therefore the stability of f_{rep} is much more critical to the final stability of the optical modes than any uncertainty in f_{ceo}. It should be stressed here that the relative frequency stability of the RF reference source is maintained in the optical domain, and that phase noise on this RF source does not simply accumulate because of upconversion to higher frequencies (a phenomenon known as carrier collapse), since the optical modes of the frequency comb are tightly phase-locked due to the modelocking process of the laser oscillator [RD12].

Although primary RF frequency standards provide excellent stability and accuracy (the stability of a commercial Cs clock reaches $5 \times 10^{-12}\ \tau^{-1/2}$, accuracy $\sim 10^{-14}$), transferring this stability to the frequency comb requires care. Since the feedback loop effectively reacts to phase shifts of the f_{rep}-signal compared to the reference frequency signal, a tighter lock is achieved when a faster oscillation (i.e. a higher frequency) is used in the locking scheme, as a given phase shift then corresponds to a shorter time period Δt. As a result, the relative timing jitter decreases with the locking frequency, and it is beneficial to employ a higher harmonic of f_{rep} in the feedback loop. While the final accuracy of the comb may not improve significantly, it will have a significant effect on the stability, and the required accuracy can be reached on shorter timescales [RD12]. Therefore, an oscillator with f_{rep}=100 MHz should preferably be locked using e.g. its 100^{th} harmonic at 10 GHz. This does require the use of faster electronics, and in practice the maximum locking frequency that can be achieved is limited by the RF generator and the speed of the photodiode that is used to detect the pulse train. This has been explored in detail by Shelton et al., who show that by using higher harmonics of the repetition frequency the residual frequency stability and timing jitter can be reduced [RD68]. They exploited this feature to reduce the timing jitter between two separate femtosecond lasers to less than 5 fs. With an additional coherent cross-correlation technique, they could even reduce the timing jitter to below 1 fs, leading to some degree of phase-coherence between the two independent femtosecond oscillators.

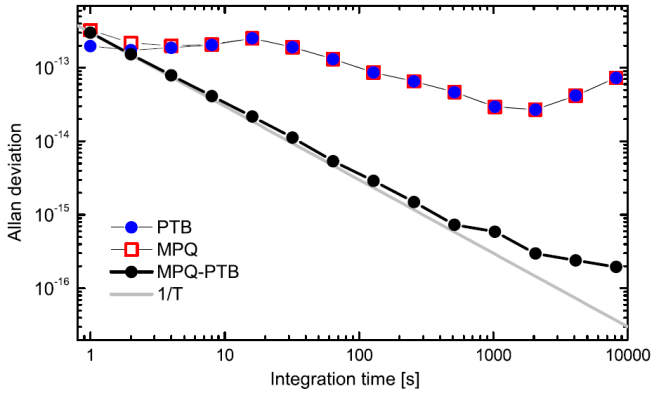

Fig. 2.2 - Measured Allan deviation between two fiber-based frequency comb lasers stabilized to a common hydrogen maser RF reference (Taken from [RD58]).

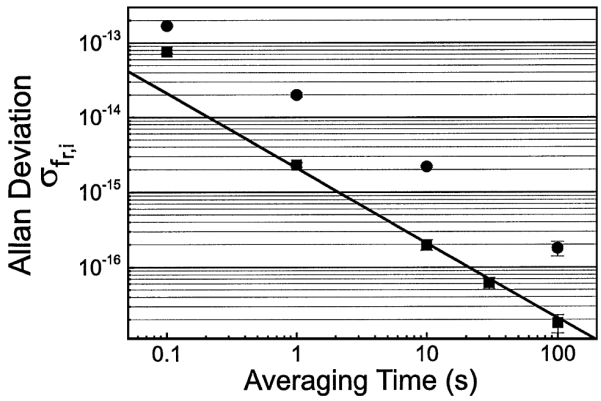

Fig. 2.3 - Measured Allan deviation between two frequency comb lasers stabilized to a common optical reference frequency at 456 THz. The solid line represents the measurement limit (Taken from [RD40], see text for details).

An even higher frequency stability can be achieved when an optical frequency reference is used to stabilize the frequency comb [RD73; RD12]. In principle, this is an extension of the previous discussion on using higher harmonics of f_{rep} to improve the frequency comb stability, by using optical frequencies directly for locking the comb modes. Typical frequency comb oscillators have a rather low cavity finesse, which is limited by the high gain of laser materials employed in such oscillators. By locking the oscillator to an external reference cavity with a much higher finesse, high-frequency noise on the cavity modes can be eliminated more effectively, leading to an improved short-term stability of the frequency comb. A comparison between typical RF and optically stabilized frequency combs is obtained from Fig. 2.2 and Fig. 2.3. The Allan deviation between the optically referenced combs can be more than an order of magnitude better than the RF referenced combs [RD40; RD58]. An even more impressive experiment has been performed by Ma et al. [RD60], who compared four different optically referenced frequency combs and found agreement in measured frequency down to a level of 10^{-19}.

Fig. 2.3 shows the Allan deviation between two frequency comb lasers that have been stabilized to a common optical frequency reference at 456 THz (λ=657 nm) in the form of a laser diode with Hz-level linewidth [RD40]. The squares represent the Allan deviation between the two combs as measured using optical cross-correlation, from which it can be seen that these frequency combs have a relative stability of 2×10^{-15} in 1 s. At 0.1 s the measured stability is already 7.6×10^{-14}, caused by acoustic vibrations in the detection setup. From these Allan deviations, the residual timing jitter between the pulses from these two frequency comb lasers is only 0.45 fs between 1-100 Hz, and 1.5 fs in 1-100 kHz. This should be compared to the stability achieved by Shelton et al. [RD68] who achieve 5 fs jitter between 1-160 Hz using an RF

reference source at the 100th harmonic of the laser frequency, as mentioned above. The circles represent the Allan deviation for an RF frequency signal at 1 GHz that has been electronically synthesized from the respective frequency combs. This RF signal is found to have a stability of 2×10^{-14} in 1 s, which improves to a few parts in 10^{-16} after 100 s averaging time. This shows the superior stability of optically referenced frequency combs compared to RF referenced combs. However, it should be noted that the synthesized RF signals have lost about an order of magnitude in stability compared to the optical signals that they were derived from. The source of this stability degradation is not completely clear at present.

A setup that implements an all-optical frequency comb stabilization technique is shown in Fig. 2.4, where both the average frequency of the comb modes and f_{rep} have been locked to an external reference cavity [RD53]. With this setup, a frequency stability of 5×10^{-13} was achieved in 0.1 seconds. Note that in this particular case, the etalon was free-running: to obtain a true frequency comb, an RF or optical reference frequency source is still required to control the drift of the etalon. An interesting aspect of this particular type of system is that an octave-wide spectrum is not required, as long as the length of the reference cavity is stabilized with respect to e.g. an optical atomic transition.

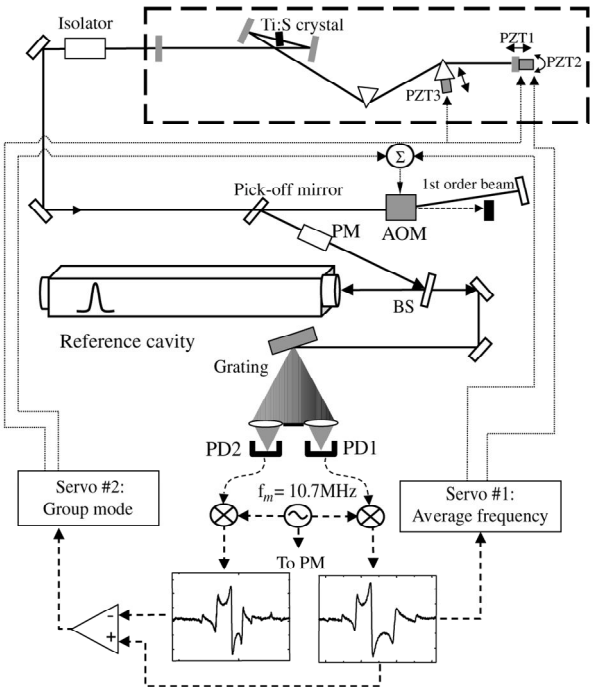

Fig. 2.4 - Stabilization of the average comb mode frequency and frep to a high-finesse reference cavity (Taken from [RD53]).

Furthermore, locking the frequency comb to an optical reference can in the future also improve the overall accuracy, since optical frequency reference sources have been demonstrated to provide higher accuracy than the best RF clocks that are currently available. The stability of optically referenced frequency combs can be further improved by the use of optical reference cavities with a higher finesse and an improved passive stability [RD65; RD59]. By taking advantage of a optical cavities constructed from ultralow expansion (ULE) glass in a stable mounting configuration (see Fig. 2.5), a frequency stability of 1×10^{-15} in 1 s has been demonstrated. The measured fractional frequency stability of two independent cw lasers stabilized to two separate high-finesse cavities is shown in Fig. Fig. 2.5. This graph also shows that especially on short timescales (<1 s), optical referencing provides much better stabilization compared to RF reference sources. Note that in this particular example, 10^{-13} stability is already achieved with only 1 ms averaging time.

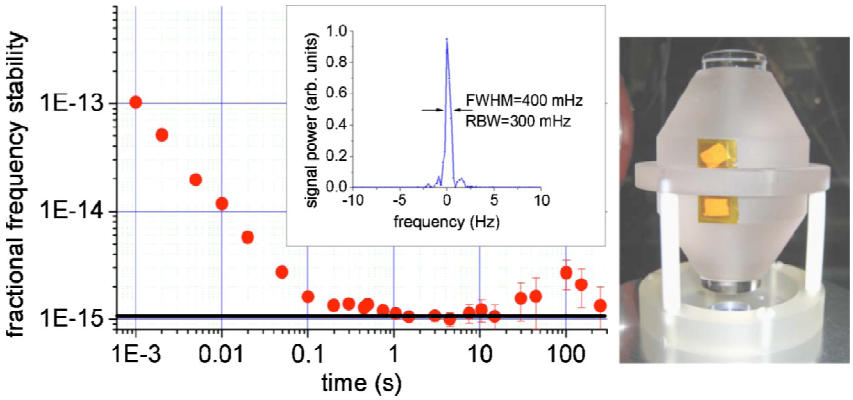

Fig. 2.5 - Left: Relative stability of two independent cw lasers stabilized to separate ultrastable reference cavities. Right: Picture of a vertically mounted ULE reference cavity (Taken from [RD59]).

Available values for the repetition frequency depend mostly on the cavity design and the type of oscillator that is used in the frequency comb laser system. Typical values that are common in the field range between 10 MHz and 1 GHz. As f_{rep} is simply related to the cavity length, a compact, mechanically stable oscillator would automatically imply a higher repetition frequency, typically in the 300 MHz – 1 GHz range. Several oscillator designs and frequency combs have been demonstrated at these high repetition frequencies, optimized for various practical situations such as low power consumption [RD57], and ultrabroadband oscillator spectrum [RD61; RD33].

3.1.3 Tuning the repetition frequency

An issue that may be of importance for distance metrology is the tunability of the repetition frequency of a frequency comb laser system. However, not many experiments using f_{rep}-tunable frequency comb systems have been reported. One notable exception is the development of a fiber laser-based frequency comb with tunable repetition frequency by Washburn et al. [RD35]. They report on a frequency comb laser with a repetition frequency that can be continuously tuned over a range of 800 kHz, from 49.3 to 50.1 MHz (relative scan range of 1.6%). In the optical domain around a wavelength of 1550 nm, this corresponds to a wavelength scan of one comb mode over 25 nm (3 THz). A scanning speed of up to 20 kHz/s has been achieved, while maintaining f_{rep}- and f_{ceo}-stability. This corresponds to a pulse-to-pulse time delay change of about 8 ps/s. To keep f_{ceo} locked during scanning, the pump power has to be adjusted by a few mW. Aside from a few cycle slips, the stabilization of f_{ceo} remained good enough to maintain the frequency comb accuracy at the 10^{-14}-level. The limiting factor on the scanning speed were mechanical vibrations induced by the scanning, which made stabilization of f_{ceo} more difficult.

Although f_{rep}-tunable Ti:Sapphire-based frequency comb have not been actively researched, they should be achievable in the same way as this particular fiber-laser-based example of Washburn et al. [RD35]. Of course, the relative scan range will be higher for a smaller cavity length (i.e. a higher repetition frequency). In practice, the limitations on the scan range are set by the stability range of the laser cavity and by the requirements on the alignment of the cavity. The maximum achievable scan speed will be determined by the robustness of the laser with respect to acoustical and mechanical vibrations induced by the scanning, and by the ability to keep f_{ceo} and f_{rep} stabilized when tuning the cavity length.

3.1.4 Carrier-envelope offset frequency

The basic principle underlying the detection of the carrier-envelope offset frequency f_{ceo} is known as the f-to-2f scheme [RD48; RD52], which is illustrated graphically in Fig. 2.6.

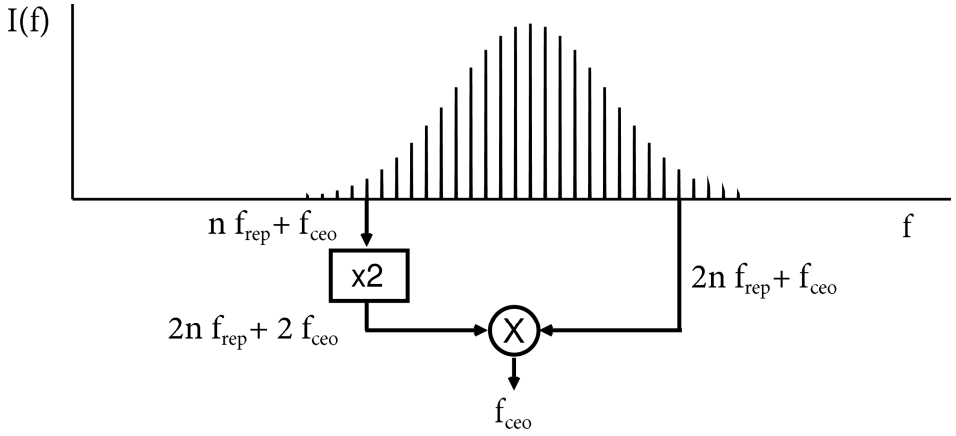

Fig. 2.6 - The f-to-2f measurement principle for carrier-envelope offset frequency detection.

The major requirement for this measurement scheme to work is that the width of the spectrum exceeds one full optical octave, i.e. that there exist frequencies f and 2f with a nonzero intensity. In this case, f_{ceo} can be measured by generating a beat signal between a high-frequency comb 2f mode and the second harmonic of a low-frequency comb mode f. Such optical second harmonic generation can routinely be performed using nonlinear crystals such as BBO (β-$BaBO_2$). The difference frequency between these comb components is then given as:

$$2 \times (n f_{rep} + f_{ceo}) - (m f_{rep} + f_{ceo}) = f_{ceo}$$

when comparing the mode numbers n and m=2n with each other.

3.1.5 Implementation of the f-to-2f scheme

A practical implementation of the f-to-2f scheme is shown in Fig. 2.7, and is based on a Mach-Zehnder interferometer. The output beam from the frequency comb oscillator is sent into a photonic crystal fiber (PCF) for spectral broadening to a full octave (see paragraph 3.1.6). Behind the PCF, the high and low frequency components are split using a dichroic mirror. The low-frequency components are frequency-doubled in a nonlinear crystal, after which the beam is recombined with the high-frequency part using polarizing optics (note that the second harmonic is generated with a 90° rotated polarization). The path lengths should match to overlap the pulses in time, as well as in space. A beat signal between the two interferometer arms is generated on an avalanche photodetector, yielding f_{ceo}. This setup has been constructed and tested at LCVU, and a typical output signal is shown in Fig. 2.8.

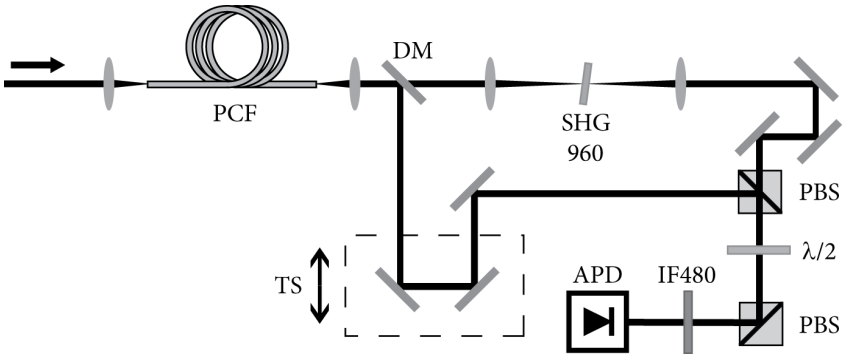

Fig. 2.7 - Implementation of the f-to-2f scheme using a Mach-Zehnder interferometer. DM: Dichroic mirror, SHG 960: BBO crystal for second harmonic generation of 960 nm light, PBS: Polarizing beamsplitter, IF 480: Interference filter for 480 nm light, TS: Translation stage, APD: Avalanche photodetector.

Besides a strong signal corresponding to f_{ceo}, we also detect the laser repetition frequency f_{rep}, as well as higher harmonics of f_{ceo}, and linear combinations of f_{rep} and f_{ceo}. To isolate the f_{ceo}-signal bandpass filters are used, followed by a low-noise electronic amplifier which increases signal strength to facilitate locking to an RF generator. A frequency spectrum of the stabilized f_{ceo}-signal is shown in Fig. 2.8B, demonstrating a 60 dB signal-to-noise ratio in a 1 Hz resolution bandwidth (1 Hz video bandwidth). The 3 dB width of this signal is 1 Hz, limited by the spectrum analyzer resolution. This f_{ceo} stabilization has been maintained for hours, and this can be extended to much longer timescales when external disturbances are properly controlled.

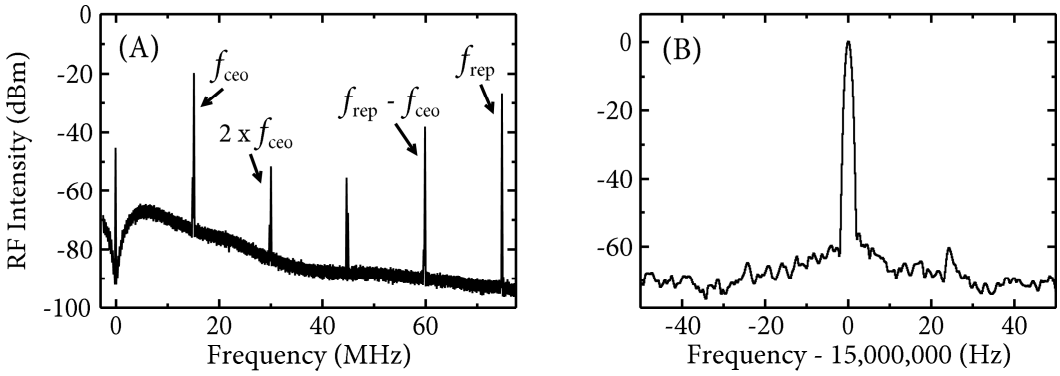

Fig. 2.8 - Measurement of fceo using the Mach-Zehnder interferometer from Fig. 2.7. (A) Besides the f_{ceo}-signal, the laser repetition frequency and several combination peaks are detected. (B) High-resolution scan of the stabilized f_{ceo} peak at 15 MHz.

To minimize the path over which the high- and low-frequency components are separated inside the interferometer, a new implementation of the f-to-2f scheme was constructed at LCVU. This setup is based on a Michelson interferometer, and has been designed to be less sensitive to external perturbations. A schematic of this setup is shown in Fig. 2.9.

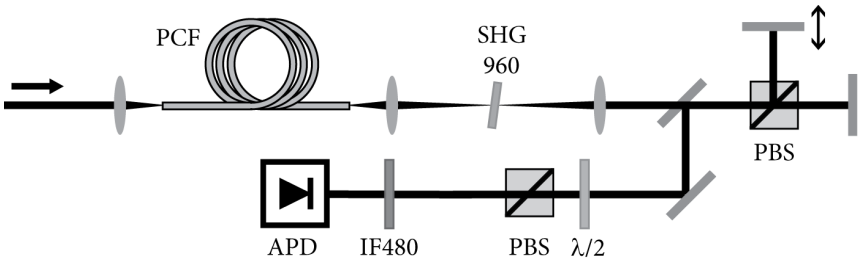

Fig. 2.9 - Implementation of the f-to-2f scheme based on a Michelson interferometer. Abbreviations identical to Fig. 2.7.

This setup uses the fact that the fundamental and second harmonic pulses have orthogonal polarizations, by employing a polarizing beamsplitter in the interferometer. It has the advantage that the various frequency components are only separated inside the Michelson interferometer, which can be kept to a few millimeters of optical pathlength. Such an f-to-2f interferometer is also smaller, and requires less optics than the Mach-Zehnder-based setup.

To electronically stabilize f_{ceo}, the signal first needs to be phase-locked to an RF reference frequency. This reference frequency is provided by a waveform generator locked to the atomic clock that works as the primary RF reference. The output signal from the avalanche photodetector is bandpass-filtered to remove the spurious peaks at f_{rep} and at linear combinations of f_{rep} and f_{ceo} from the signal. After filtering and possibly amplification, this signal is sent into a phase-detector along with the reference signal from the waveform generator. The output from this phase-detector is then used as the input signal for a PID regulator that controls the pump power to the laser oscillator [RD12].

For convenient stabilization of f_{ceo}, the frequency of the detected beat signal should be well-separated from the other frequency components as well as from zero, which is required for accurate phase detection. Typically, f_{ceo} is locked to a subharmonic of f_{rep} (typically $1/4^{th}$ or $1/5^{th}$), so that the reference frequency used for phase-locking can be derived from the same waveform generator that is used to lock f_{rep}. Locking f_{ceo} to zero is therefore not entirely trivial. This can be achieved by placing an AOM in one interferometer arm of the f-to-2f setup, to add a frequency offset to one of the comb components before creating the beatnote on the photodetector. If this frequency offset equals the frequency of the reference source to which the beat signal is phase-locked, then f_{ceo} is effectively set to zero [RD12]. A possible way of implementing such a zero-offset stabilization scheme is shown in Fig. 2.10.

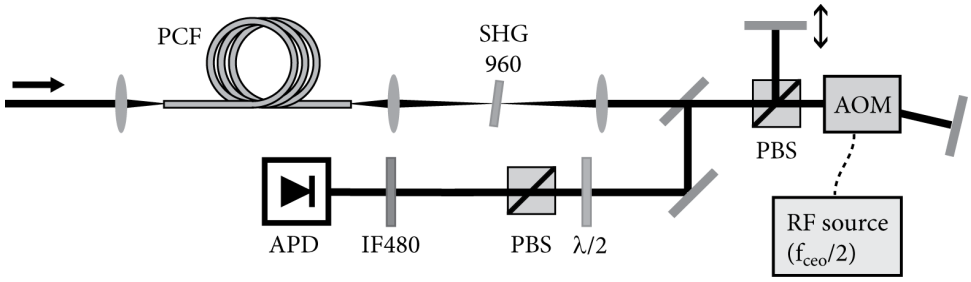

Fig. 2.10 - Implementation of the f-to-2f scheme for locking fceo to zero frequency (Note the RF frequency fceo/2, since the AOM is double-passed).

Another possibility of generating a frequency comb with zero f_{ceo} is through the use of difference frequency generation (DFG) [RD44; RD79]. By taking the comb components at the edges of the spectrum and

combining them inside a nonlinear crystal, a new frequency comb structure is produced at the difference frequency of these comb components. The frequency of these difference-frequency comb lines is then:

$$f_{DFG} = (n \times f_{rep} + f_{ceo}) - (m \times f_{rep} + f_{ceo}) = (n - m) \times f_{rep}$$

From this relation it can be seen that the f_{ceo} has been cancelled out by the DFG process, and an offset-free frequency comb is produced. A typical setup to produce such a comb is shown in Fig. 2.11.

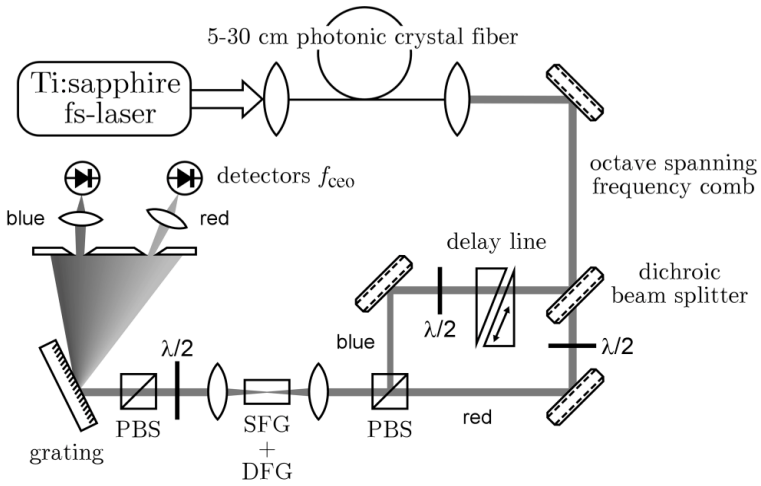

Fig. 2.11 - Setup for generation of an offset-free frequency comb through difference-frequency generation (Taken from [RD79]).

The main drawback of this technique is that it requires an ultrabroadband spectrum to begin with, to ensure that the frequency difference between the outer edges of the spectrum is large enough to generate difference frequency components at optical frequencies [RD44]. As a result, the central frequency of the comb depends on the initial width of the spectrum, and is usually in the mid-IR or at even longer wavelengths. Furthermore, DFG is not a very efficient process, leading to a frequency comb with a very low power per mode. For most practical purposes, additional amplification of the generated spectrum is required, leading to a complex and costly setup.

While locking f_{ceo} to zero provides a train of identical pulses in the time domain, it only adds a constant offset frequency to each comb line in the frequency domain. Therefore, from a frequency metrology point of view, it is not particularly advantageous to lock f_{ceo} to zero, as it only adds to the complexity of the frequency comb setup. Scanning the locked f_{ceo}-frequency can be achieved by sweeping the pump intensity over a certain range. However, this should be performed with caution, since the pump intensity also influences the laser output power and the modelocking stability. Especially for a Kerr-lens modelocked laser, stable modelocking is usually only maintained within a limited pump intensity range. A typical practically achievable scan range for f_{ceo} is on the order of several MHz. Another method of varying f_{ceo} is by changing the amount of dispersive material inside the cavity by inserting e.g. a pair of fused silica wedges. By moving one of the wedges in and out of the beam, f_{ceo} can be varied. This can typically be used for initial tuning of f_{ceo} to a convenient value for stabilization, but a full locking scheme based on e.g. a piezo-mounted wedge is too slow for accurate stabilization.

A practical issue in the stabilization of f_{ceo} is the fact that efficient input coupling of the laser pulses into the small core of the PCF can be problematic, as it is highly alignment sensitive. In most practical situations, the time over which f_{ceo}-stabilization can be maintained is limited by drifts of the optical components that are involved in the fiber coupling. Although the stabilization time can be lengthened considerably by using compact and robust setups, a considerably less alignment-sensitive solution has been demonstrated by Fuji et al. [RD45], and is shown in Fig. 2.12. This setup uses a periodically poled MgO:LN crystal to broaden the

spectrum and generate the difference frequency between low- and high-frequency components simultaneously. The beat signal between the broadened low-frequency components and the generated difference-frequency signal is then detected directly behind the crystal using the light that leaks through a mirror. This is a monolithic f-to-2f scheme that does not involve any fibers, making it much less alignment-sensitive. The only important alignment parameters are the focusing inside the nonlinear crystal, and the chirp of the pulse that determines the overlap between the various spectral components on the detector (to produce the beat signal). This chirp can be controlled using a pair of fused silica wedges and a set of chirped mirrors. Using this monolithic f_{ceo}-stabilization scheme, beat signals with 55 dB signal-to-noise have been demonstrated, and stable phase-locking over several days can routinely be achieved. The setup in Fig. 2.12 has the additional advantages that the full oscillator power is available for the nonlinear interaction, and that most of the phase noise generated in the spectral broadening process can be controlled away be the feedback loop (up to the frequency bandwidth of the feedback electronics). A drawback of this scheme is that the amount of spectral broadening that can be achieved is limited, and therefore the oscillator pulses should already have a bandwidth that is close to an octave (on the order of $\Delta\lambda/\lambda \sim 0.4$).

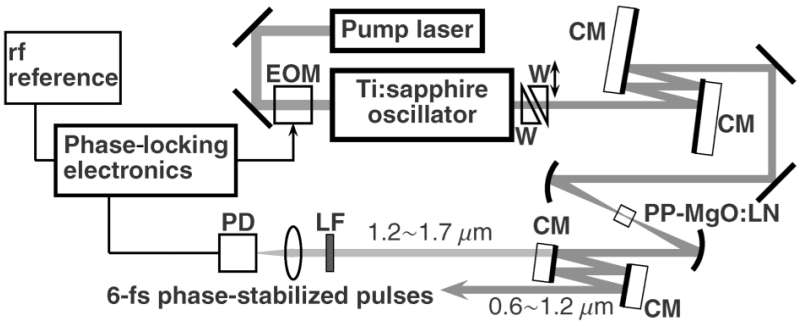

Fig. 2.12 - Setup for monolithic f-to-2f detection (Taken from [RD45]).

For the case of cross-correlation between different pulses from the frequency comb pulse train, it does make a difference whether f_{ceo} is locked to zero, since it influences the position of the cross-correlation fringes underneath the envelope. However, when the number of pulses is already known from e.g. a time-of-flight measurement, then knowledge of the value of f_{ceo} is sufficient to calculate the time delay between the maximum of the envelope and the central peak of the cross-correlation signal. In addition, by locking f_{ceo} to a subharmonic of f_{rep} one can ensure that e.g. every 4^{th} pulse is identical (when locking f_{ceo} to $f_{rep}/4$), thus limiting the number of possible delays between cross-correlation and envelope maxima. In this way, a nonzero f_{ceo} still allows the fringe-resolved analysis of cross-correlation signals for use in length metrology, as shown in Fig. 2.13.

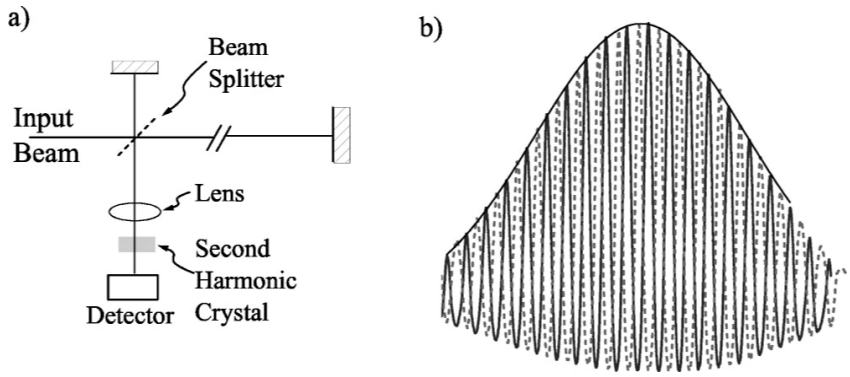

Fig. 2.13 - Time-domain example of cross-correlation. a) Schematic of a cross-correlator. b) Two typical cross-correlation signals, for two cases with a relative phase shift $\Delta\varphi_{ceo} = \pi$ (Taken from [RD12]).

The accuracy with which f_{ceo} can be stabilized is limited by the phase-detection and locking scheme, the bandwidth of the feedback loop, and ultimately by the RF frequency reference standard that is used. For state-of-the-art Ti:Sapphire-based frequency comb systems, the stability of the locked f_{ceo}-signal approaches the stability of the clock to which it is referenced, which for a commercial Cs-clock is as low as $5\times10^{-12}\ \tau^{-1/2}$, with an accuracy approaching 1×10^{-14}. With a 50 kHz bandwidth feedback loop, mHz linewidths can be achieved for f_{ceo}. It should be stressed here that for frequency metrology the stability of f_{ceo} is not the limiting factor, as it enters the equation for the absolute optical frequency only once, while the repetition frequency is multiplied by the mode number n, which is typically on the order of 10^5. Therefore, stabilization of f_{ceo} with a moderate stability of only 10^{-10} in 1 second would already lead to a stability of 10^{-15} in 1 second in the optical domain.

In the time-domain, the carrier-envelope phase stability can be followed directly by monitoring the phase of the RF reference frequency signal and the stabilized f_{ceo}-signal simultaneously, and looking at the phase difference. Such a measurement needs to be performed outside of the feedback loop that is used to stabilize f_{ceo}, so that any noise that is generated inside the feedback loop (e.g. by the electronics or the spectral broadening) can be detected independently. At LCVU we have constructed a second f-to-2f interferometer to carry out these measurements. We track both the reference signal and f_{ceo} by recording the time-domain signals directly with a digital oscilloscope (4 GHz bandwidth) for 4 ms (3×10^5 pulses), and calculate the instantaneous phase differences between them. Typical results are shown in Fig. 2.14, demonstrating a phase stability down to 152 mrad (RMS). Since a delay time of 4 ms corresponds to a distance of 1.2×10^6 metres, these measurements confirm that time-domain cross-correlation can be used to obtain high-contrast fringe-resolved patterns from which the optical path length can be extracted with an accuracy of a fraction of an optical cycle.

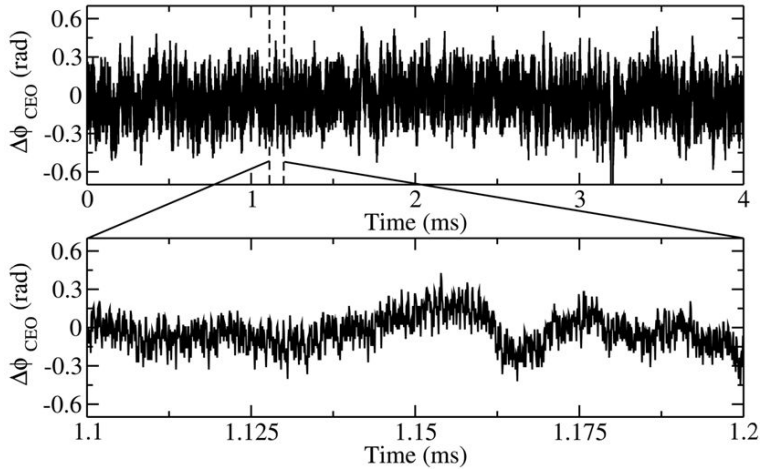

Fig. 2.14 - Instantaneous carrier-envelope phase deviations measured in time. We stabilized f_{ceo} at 11 MHz during these measurements (Taken from [RD13]).

3.1.6 Spectral broadening mechanisms and nonlinear fibers

Since the frequency spectrum emitted by a typical modelocked oscillator does not span the full optical octave required for implementation of the f-to-2f scheme, a method is needed to broaden the spectrum to the desired width. This can be achieved through nonlinear interaction of the intense ultrashort laser pulses (which can reach focused intensities of ~10^{11} W/cm^2) with a solid target. However, in practice it turns out that at these pulse intensities interaction with at least several centimetres of material is needed for sufficient broadening.

This poses a problem, since it is difficult to keep such an ultrashort pulse focused in space, but also in time due to material dispersion. The breakthrough that has enabled supercontinuum generation with modelocked oscillator pulses has been the development of photonic crystal fibers (PCFs), which consist of a small core surrounded by a lattice of airholes. By tuning the size of the core and the structure of the air lattice, the dispersion characteristics can be tuned such that the zero-dispersion-wavelength of these fibers lies at the central wavelength of the input pulse spectrum. As a result, the pulse will remain short over extended interaction lengths, while the small fiber core ensures that the intensity remains high. These PCFs allow the generation of octave-wide supercontinua with nJ energy input pulses, and have enabled the construction of the first self-referenced frequency combs.

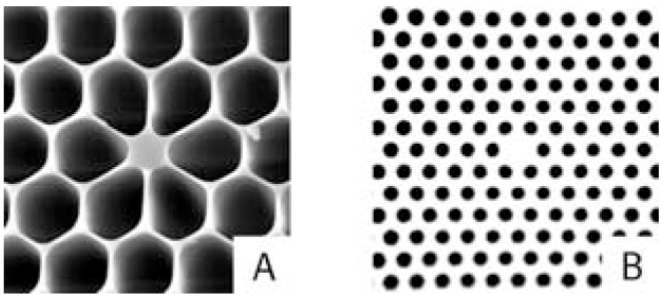

Fig. 2.15 - A) Scanning electron microscope pictures of a photonic crystal fiber for supercontinuum generation with 800 nm input pulses. B) Optical microscope picture of a PCF with zero-dispersion-wavelength in the telecommunications range (Taken from [RD46]).

Although the spectrum that is produced inside a PCF may be wide enough for f-to-2f detection, it is not obvious that the PCF preserves the phase of the input pulses. Since the pulse-to-pulse phase coherence of the modelocked pulse train is an essential ingredient of a frequency comb, this point requires special attention. It has been shown that several different nonlinear processes contribute to the spectral broadening [RD46; RD43], and not all of these broadening mechanisms preserve phase coherence. As a result, only a limited regime of input pulse parameters allows spectral broadening inside PCFs without compromising the frequency comb stability [RD42; RD43]. Which broadening mechanisms occur in a given type of fiber depends for a large part on the dispersion regime that the pulse is in, on the input pulse intensity, and on the input pulse duration. A list of typical nonlinear effects that occur in a PCF is shown in Fig. 2.16.

Table 1. Nonlinear effects involved in supercontinuum generation.

Dispersion	Important nonlinear effects
Normal	•SPM •Raman scattering •Stimulated Raman scattering [54] •Parametric four-wave mixing [54]
Anomalous	All effects seen in the normal regime plus: •Higher order soliton fission into fundamental red-shifted solitons and non-soliton radiation [55,56] •Third order dispersion •Phase matching •Self-frequency shifting by intra-pulse Raman scattering

Fig. 2.16 - List of nonlinear effects involved in supercontinuum generation (Taken from [RD46]).

Table 2. Supercontinua generated at different pumping conditions.

Pumping condition	Resulting supercontinuum
Far below zero-dispersion wavelength in the normal regime	Smooth narrow and stable output, which is insensitive to power fluctuations in the pump. Output is suitable for pulse-compression or applications where the results depends on the Fourier transform of the spectrum like OCT
Close to zero-dispersion wavelength in the normal regime	Medium broad spectrum with peaks forming above the zero-dispersion wavelength. The part of the spectrum above the zero-dispersion wavelength is sensitive to fluctuations in pumping power due to the presence of solitons
Close to zero-dispersion wavelength in the anomalous regime	Very wide output with large amount of features and often a dip at the zero-dispersion wavelength. Spectrum is very sensitive to pumping power fluctuations

Fig. 2.17 - Properties of the supercontinuum generated in a PCF for various dispersion regimes (Taken from [RD46]).

In Fig. 2.17 a list of properties is given for supercontinua produced in a PCF for different dispersion regimes. Depending on the application, this allows selection of the fiber dispersion properties and input pulse parameters to optimize the spectrum of the supercontinuum. It should be noted here, that the spectral broadening in PCFs is not only the result of the enhanced nonlinearity, but that the dispersion characteristics of the fiber are equally important. This can clearly be seen from Fig. 2.18, which shows simulations of spectral broadening in a PCF for different central wavelengths of the input pulse. With a constant input peak power, the spectral shape changes dramatically as the input pulses go from the normal dispersion regime (λ<780 nm) into the anomalous dispersion regime (λ>780 nm).

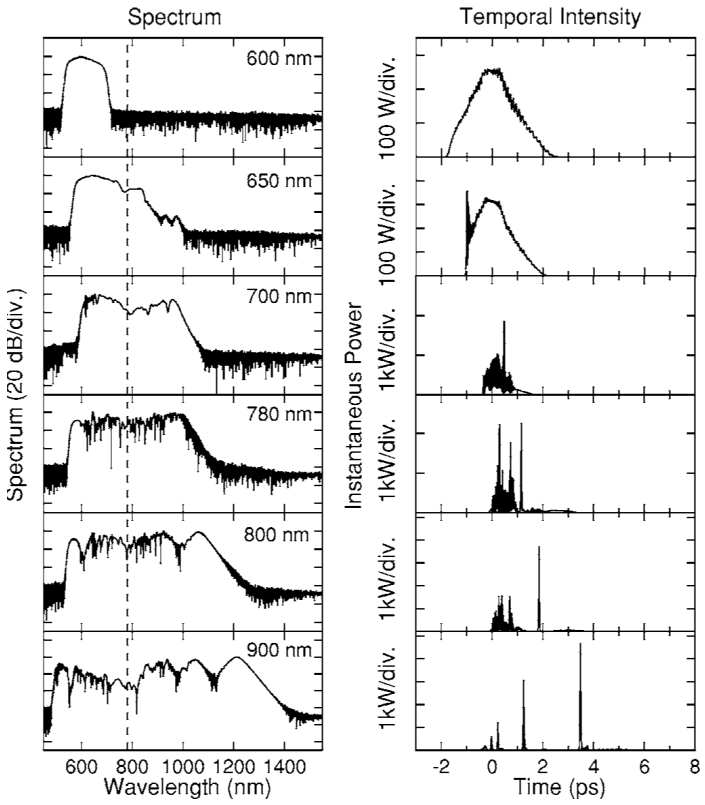

Fig. 2.18 - Spectral and temporal output from a 15 cm long PCF with a zero-dispersion-wavelength of 780 nm (dashed line), for different input wavelengths. The input pulses are 50 fs long and have 10 kW peak power (Taken from [RD43]).

As already noted in Fig. 2.17, the anomalous dispersion regime allows the generation of solitons and the process of soliton fission, as well as phase-matching processes such as modulation instability and dispersive wave generation in the presence of higher-order dispersion. In the normal dispersion regime, self-phase-modulation and stimulated Raman scattering dominate the spectral broadening process for pulses in the femtosecond range, leading to the smooth spectra as shown for the case of 600 nm input wavelength. However, due to the normal dispersion, pulse stretching rapidly leads to a decrease in peak power, which limits the amount of spectral broadening. In the anomalous regime much broader spectra are observed, although the spectral structure becomes increasingly complex, with deep holes especially above the zero-dispersion-wavelength of the PCF.

For frequency metrology applications the coherence of the generated supercontinuum is of major concern. In several cases, research groups working with frequency combs reported a degradation of coherence after spectral broadening in PCFs [RD48; RD41; RD77], although systematic studies into this effect are difficult to perform experimentally [RD41; RD64]. Simulations on the mechanisms of spectral broadening in PCFs have recently shed more light on the issue of coherence degradation [RD42; RD43]. In particular, a clear dependence of the coherence on input pulse duration has been found, as is displayed in Fig. 2.19.

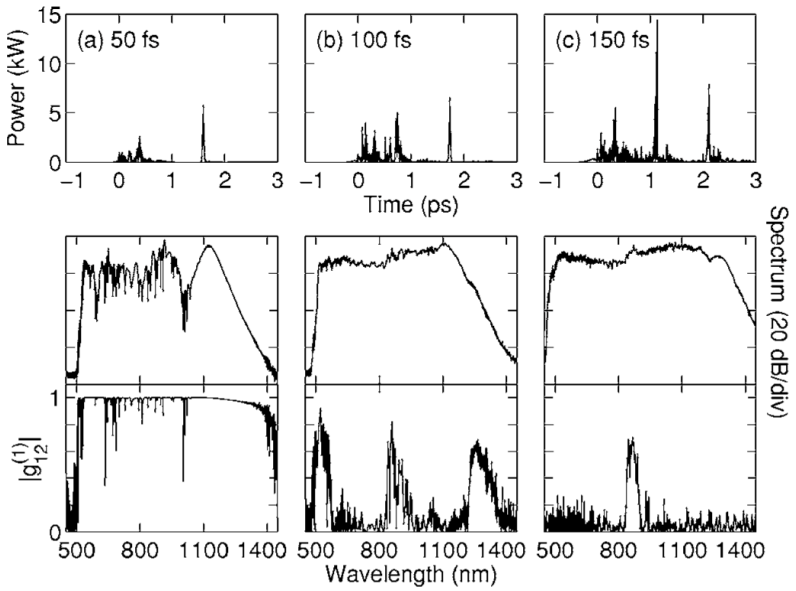

Fig. 2.19 - Spectral and temporal intensity of supercontinua generated in 10 cm of PCF with 50, 100 and 150 fs input pulses. The bottom panels show the first-order coherence |g12| as a function of wavelength. The input peak power is 10 kW in all cases, and the central input wavelength is 835 nm (Taken from [RD43]).

Although the spectral widths are comparable in all three cases, a dramatic degradation in coherence is observed when the pulse duration increases [RD43]. This is largely explained by the fact that the bandwidth of the shortest input pulses is already relatively wide, and initially broadens more rapidly due to the stronger effects of self-phase-modulation and soliton formation for shorter pulses. Therefore, the spectral width of the shorter pulses is already broad early in the fiber, and will overlap with the regions where modulation instability gain is maximal before this modulation instability can cause significant amplification of the incoherent noise background. As a result, the modulation instability will mostly be seeded by coherent spectral parts of the broadened input pulse, thus preserving phase coherence. Instead, with a longer narrow-band input pulse, modulation instability can become the dominant feature associated with spectral broadening in the anomalous dispersion regime, and will lead to the amplification of incoherent shot noise on

the pulse spectrum. This will still result in an ultrabroadband supercontinuum, but seeded by noise and therefore without the coherence properties of the input pulse.

The influence of the interaction length on the coherence can be seen in Fig. 2.20, showing the evolution of both the spectral intensity and the coherence as a function of propagation distance through the PCF (corresponding to the output spectra shown in Fig. 2.19B and C, respectively). From these graphs, one can see that while the initial spectral broadening occurs with preservation of coherence in the case of 100 fs pulses, decoherence rapidly sets in at longer interaction lengths. For the case of 150 fs pulses one can see that initially sidebands are formed around 750 and 950 nm, which are formed from noise photons through modulation instability. These sidebands have no phase coherence with respect to the initial pulse to begin with, which is in contrast with the newly formed frequencies in the 100 fs pulse case that are the result of soliton generation. For both cases, the spectral broadening continues at longer interaction lengths, but the phase coherence progressively decreases.

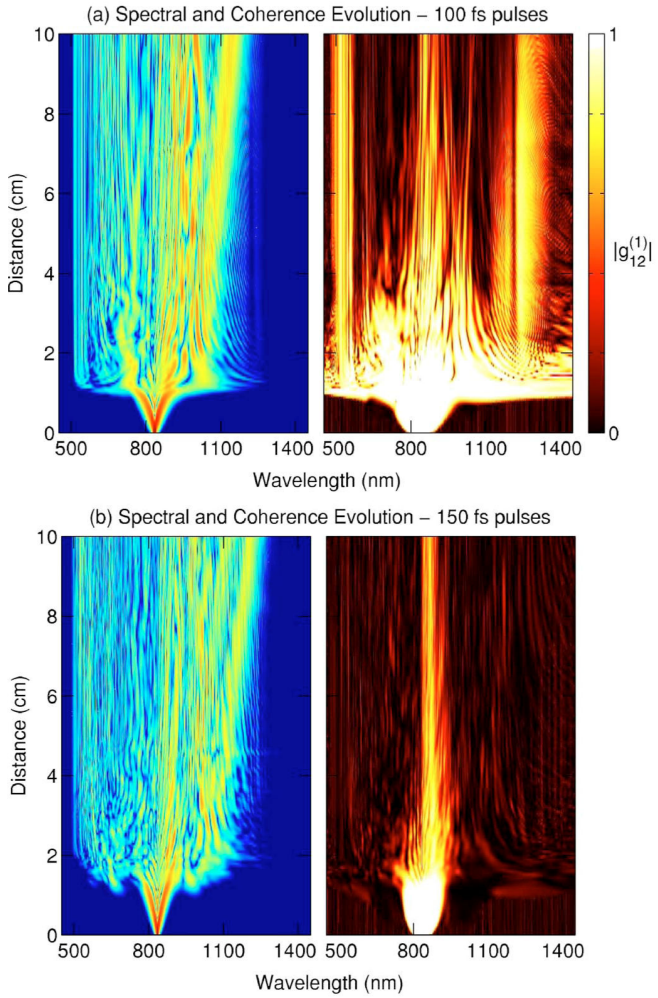

Fig. 2.20 - Evolution of the spectral intensity and degree of coherence for supercontinuum generation with 10 kW pulses at 835 nm of 100 and 150 fs duration (Taken from [RD43]).

To provide more insight in the parameter range for which coherence is preserved during spectral broadening in PCFs, Fig. 2.21 shows the resulting coherence of the generated supercontinuum (averaged over the entire output spectrum) as a function of both input wavelength and pulse duration. From this figure it becomes clear that the use of sub-50 fs pulses is very advantageous when a highly coherent supercontinuum is

required, as is the case for frequency metrology applications. This also explains the necessity of using such ultrashort pulses for the generation of stable frequency combs, as was already noted by the earliest studies on frequency comb technology [RD48; RD52].

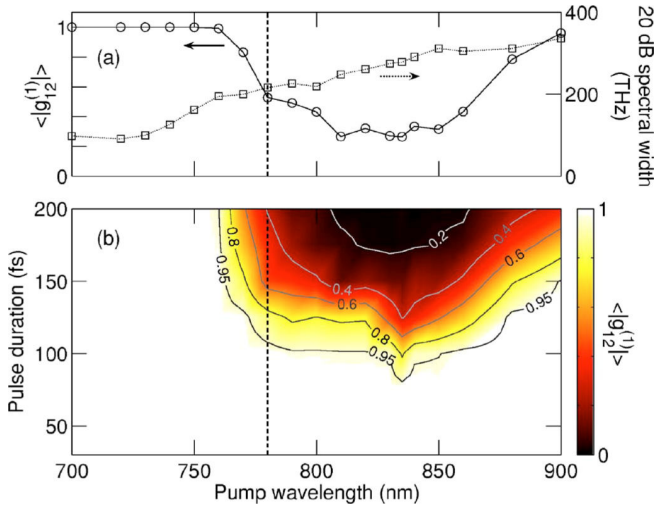

Fig. 2.21 - Dependence of the average coherence on the input wavelength and pulse duration, for a 10 cm long PCF pumped with 4 kW pulses. The top panel shows a cut through the data for the case of a 150 fs input pulse, along with the width of the generated spectrum (Taken from [RD43]).

An interesting aspect of Fig. 2.21 is that the coherence seems to improve again for longer input wavelengths. This is caused by the earlier onset of soliton fission for input pulses so far in the anomalous dispersion regime. The fission products can then effectively seed the modulation instability, resulting in a better coherence of the spectral components generated through modulation instability (see [RD43], and references therein).

To summarize, the use of shorter pulses is highly beneficial to preserve the coherence during spectral broadening in PCFs. While octave-wide spectra can be generated with longer pulses (even up to pico- and nanosecond timescales), these spectra will be incoherent, even in the case of fully coherent input pulses. In addition, the use of shorter fibers is advantageous for coherence preservation. The broadest supercontinua can be generated when the input pulses are far into the anomalous dispersion regime, i.e. the wavelength of the input pulses is significantly longer than the zero-dispersion-wavelength of the PCF. However, pulses in this regime are also the most susceptible to coherence degradation. In practice, this means that a laser system should provide pulses with a duration of ~50 fs or (preferably) shorter to be useful for implementation in a frequency comb system.

3.2 Types of femtosecond lasers for frequency comb applications

An important issue in the generation of ultrashort laser pulses is the relative spectral gain bandwidth of a laser medium, defined as the ratio of the spectral gain bandwidth and the central laser wavelength $\Delta\lambda/\lambda$. To allow the stabilization of f_{ceo} in a frequency comb, an output spectrum with $\Delta\lambda/\lambda > 1$ is required (i.e. an optical octave). As discussed in paragraph 3.1.6, the processes involved in nonlinear spectral broadening can lead to a loss of coherence through various amplitude-to-phase coupling mechanisms and other phase-degrading effects. To minimize the required amount of spectral broadening, it is essential to start out with a laser that already provides output pulses with a high $\Delta\lambda/\lambda$.

Table 2. Spectroscopic and material parameters of broadband transition-metal-doped laser materials. All parameters refer to room temperature. $\Delta\lambda/\lambda_0$: relative emission bandwidth; λ_0 (nm): maximum gain wavelength; $\Delta\lambda$ (nm): gain bandwidth (FWHM); σ_{em} (10^{-20} cm^2): emission cross section at λ_0; τ (µs): upper laser level lifetime; n_2 (10^{-16} cm^2/W): nonlinear refractive index at 1.06 µm, unless specified otherwise; κ (W/(m·K)): thermal conductivity (for colquiriites, the main value corresponds to the c-axis, value in parenthesis to a-axis); dn/dT (10^{-6} K^{-1}): thermo-optic coefficient (for colquiriites, the main value corresponds to the c-axis, value in parenthesis to a-axis)

Material	$\frac{\Delta\lambda}{\lambda_0}$	λ_0	$\Delta\lambda$	Pump source	σ_{em}	τ	n_2	κ	$\frac{dn}{dT}$	Ref.
Ce^{3+}:LiCAF	0.14	290	40	Nd-, Yb-lasers (4ω) Excimer	600	0.03	0.54[a]	5.1 (4.6)	−4.6 (−4.2)	[278, 279, 358, 359]
Ti^{3+}:Al_2O_3	0.3	790	230	Ar^+-laser, Nd-, Yb-lasers (2ω)	39	3.2	3.2	28	12.6	[13, 90]
Cr^{3+}:LiCAF	0.16	780	125	Kr^+-laser, diodes	1.3	170	0.4	5.1 (4.6)	−4.6 (−4.2)	[74, 75, 101, 102, 278]
Cr^{3+}:LiSGaF	0.21	842	180	Kr^+-laser, diodes	3.3	88	1.2	3.6 (3.4)	−1.8 (−2.7)	[101, 103, 112]
Cr^{3+}:LiSAF	0.22	855	190	Kr^+-laser, diodes	4.8	67	0.8	3.3 (3.0)	−4.0 (−2.5)	[101, 102, 112]
Cr^{4+}:Mg_2SiO_4 (Cr:forsterite)	0.2	1250	250	Nd-, Yb-lasers	14.5	2.7	2	5	3.8	[30, 183]
Cr^{4+}:YAG	0.2	1450	300	Nd-, Yb-lasers, diodes	33	4	6.2	10	8.9	[30, 90]
Co^{2+}:MgF_2	0.3	2050	650	Nd-laser (1.3 µm)	0.11	∼ 40	0.8	3.1	1	[90, 267]
Cr^{2+}:ZnS	0.38	2350	890	Tm-lasers, Er-fiber, diodes	140	4.3	90[b]	27	46	[254, 280]
Cr^{2+}:ZnSe	0.37	2450	900	Tm-lasers, Er-fiber, diodes	130	5.5	120[b] 110[c]	18	70	[225, 280, 281]

[a] at 532 nm [b] at 1.3 µm [c] at 1.55 µm

Fig. 2.22 - Overview of parameters for various broadband laser materials suitable for use in frequency comb laser systems (Taken from [RD70]).

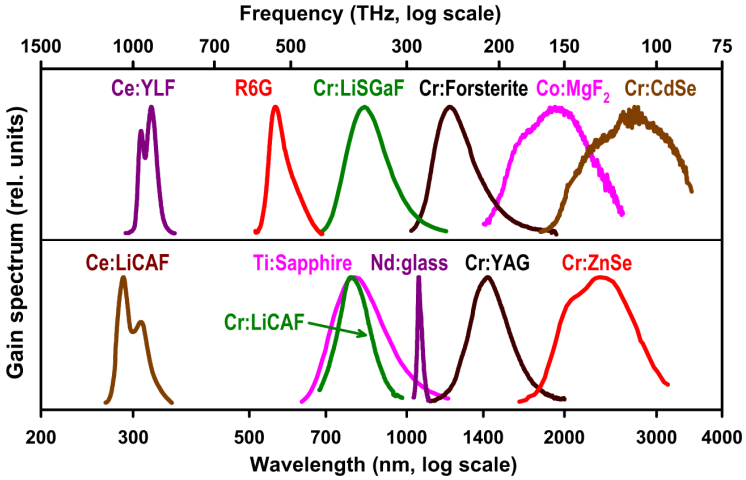

Fig. 2.23 - Spectral gain bandwidth of various broadband laser materials (Taken from [RD70]).

3.2.1 Ti:Sapphire laser

As mentioned above, Ti:Sapphire is by far the most common gain medium used in femtosecond lasers. The main reasons for this are its broad gain bandwidth (690-1100 nm), its high saturation fluence and damage threshold, and its good thermal conductivity. Of all known laser materials, Ti:Sapphire has the widest value of $\Delta\lambda/\lambda$ (~0.3) in the near-infrared and visible spectral range. Since Ti:Sapphire has its strongest absorption band in the range 480-550 nm, it can be efficiently pumped using the second harmonic of well-developed Nd- or Yb-based lasers, which are widely available commercially. The high saturation fluence allows construction of relatively high-energy oscillators, with typical modelocked output powers of up to 1 Watt at 10 Watt pump energy. The large gain bandwidth allows the direct production of two-cycle laser pulses, and due to the short central wavelength this corresponds to a pulse duration of only 5 fs. With a sufficiently high nonlinear interaction inside the laser cavity, substantial spectral broadening in excess of the normal gain bandwidth can be achieved, leading to the production of an optical octave (at -20 dB intensity) directly from the oscillator.

Because of the convenient pump lasers, the high output power and the short pulse durations, Ti:Sapphire lasers have become the standard workhorse of the present-day ultrafast laser physics community. Not surprisingly, the first frequency combs were based on Ti:Sapphire oscillators, and this type of laser is still employed in the vast majority of frequency comb laser systems around the world. As a result, researchers have gained lots of practical experience in the construction, maintenance and (long-term) performance of Ti:Sapphire-based frequency combs. Ti:Sapphire-based frequency combs hold the record for highest demonstrated frequency stability and accuracy. Commercial Ti:Sapphire frequency combs are available (MenloSystems GmbH), although they are still not completely turn-key systems.

An advantage of Ti:Sapphire oscillators is the flexibility in cavity design, resulting in a large range of possible repetition frequencies. Typical Ti:Sapphire lasers operate around 100 MHz, but oscillator designs have been demonstrated with repetition rates between a few MHz and >1 GHz. While the lower repetition frequencies are advantageous for nonlinear optics (spectral broadening, SHG autocorrelation, etc.), the higher repetition frequencies are beneficial for frequency metrology (easier mode identification, more output power per mode, less time-of-flight between subsequent pulses) [RD61; RD33; RD57].

While the Ti:Sapphire laser obviously has proven itself as a reliable and highly accurate frequency comb system, there are several drawbacks that might make it less suitable for space applications:

The threshold for laser operation is rather high. This is a feature that is inherent to any laser medium with such a large bandwidth and short central wavelength. Furthermore, the optimum pump wavelength for Ti:Sapphire lies in the green spectral region. As a result, a high-energy green pump laser is required, which at present rules out the possibility of direct diode laser pumping. Instead, frequency-doubled Nd:YAG, Nd:YVO_4, or possibly an Ytterbium-based solid state laser is required as a pump source. Although these lasers can be diode-pumped, the total electrical-to-optical conversion efficiency for a Ti:Sapphire-based frequency comb is low.

In addition, the alignment sensitivity of a Ti:Sapphire oscillator is a point that requires attention. A strong point of Ti:Sapphire is the high single-pass gain, which allows the pulses to reach their full energy in only a limited number (~10) of roundtrips. However, typical Ti:Sapphire lasers operate on Kerr-lens modelocking, which requires a strongly focused pump beam inside the Ti:Sapphire crystal, as well as a good overlap between this focused pump beam and the cavity mode. This condition may be alleviated somewhat by using an intracavity saturable absorber (such as a SESAM, a Semiconductor Saturable Absorber Mirror) to induce modelocking, but only at the expense of a longer output pulse duration.

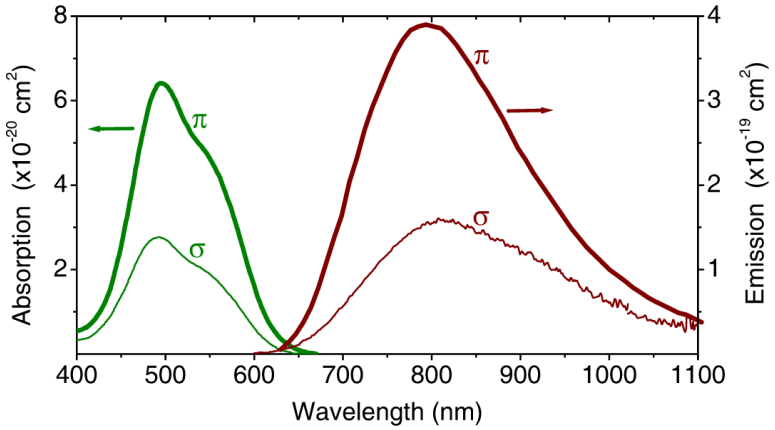

Fig. 2.24 - Absorption and emission cross sections of Ti:Sapphire as a function of wavelength. Note the fivefold vertical scale difference between absorption and emission (taken from [RD70]).

3.2.2 Erbium fiber laser

A type of laser that is rapidly gaining interest in the frequency comb community is the Erbium-doped fiber laser. These lasers operate in the telecommunications wavelength range, at a centre wavelength of 1.55 µm. The major advantage of fiber-based lasers systems is their robustness, since fiber lasers require almost no alignment. Although most fiber laser systems still employ a small free-space path length inside the oscillator to allow starting of the modelocking process, modelocked all-fiber laser systems have already been demonstrated [RD77]. Besides the Ti:Sapphire and Cr:Forsterite lasers, the Erbium-doped fiber laser is the third type of laser oscillator that has been successfully employed as a self-referenced frequency comb system. At present, frequency comb laser systems based on Er-doped fiber lasers are already commercially available from MenloSystems GmbH.

Because Erbium-fiber lasers operate at telecommunications wavelengths, these lasers are very well-suited for implementation of frequency comb technology into optical communications systems. Another advantage of this wavelength range is that high-quality optics, modulators and other components have been developed and are commercially available. Erbium-doped fibers have their absorption band around 980 nm, which allows direct diode-laser pumping. As a result, the electrical-to-optical conversion efficiency of such a fiber laser system can be relatively high.

The pulse energy that can be obtained from a fiber oscillator is usually limited to the sub-nJ range, which is usually not sufficient for spectral broadening to an octave-wide spectrum. However, the use of external Er-doped fiber amplifiers to boost the power has been shown to preserve the phase of the oscillator pulses to a high degree. With such an oscillator-amplifier arrangement, a frequency comb system can be built [RD67; RD77]. Although the peak intensity of the pulses is still rather low after the fiber amplifier, the development of special highly nonlinear fibers (HNLF) has allowed supercontinuum generation with ever lower pulse intensity. These HNLFs are a special type of PCF with an enhanced nonlinearity, caused by doping the fiber with ions that have a higher nonlinear response (bismuth, for example). Fig. 2.25 shows a schematic of an Er-fiber-based frequency comb, which makes use of two external fiber amplifiers in parallel. While one amplifier is used to provide sufficient power for phase and repetition rate stabilization, the second amplifier branch can be used for spectroscopy and metrological applications [RD37; RD51]. However, it should be noted that the f_{ceo} beat signal in a fiber laser-based frequency comb is usually much broader (in the 100 kHz range) than what is observed for Ti:Sapphire-based combs. Although this hardly affects the frequency

stability of the frequency comb, it might have an impact on the short-term pulse-to-pulse phase coherence in the time domain. Several research groups have investigated this issue [RD36; RD25], leading to the development of fiber laser-based frequency combs with f_{ceo}-linewidths at the Hz-level [RD47; RD24].

A major advantage of fiber lasers for the construction of frequency combs is their capability to integrate components into an all-fiber network. By fusion splicing of several different types of fiber, the oscillator, amplifiers, dispersion compensation, and even the PCF for continuum generation can all be connected together, eliminating the need for separate alignment of all these components. The frequency comb system displayed in Fig. 2.25 is a good example of such an integrated fiber-based frequency comb. Especially the alignment of the PCF for spectral broadening is usually very sensitive to perturbations, making this fiber-splicing a strong point of the fiber laser approach to frequency comb construction.

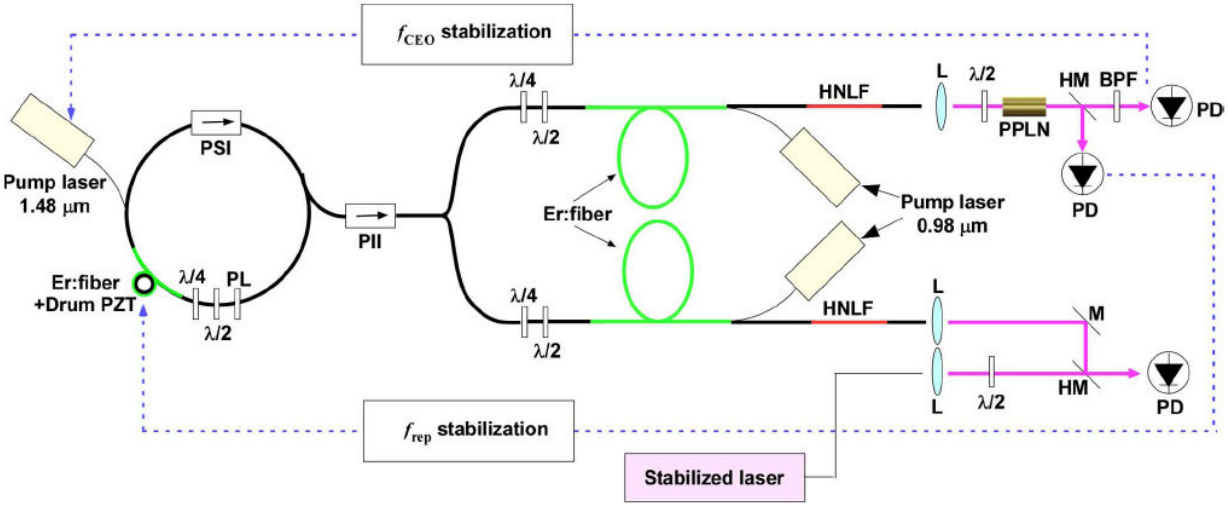

Fig. 2.25 - Example of a frequency comb based on an Erbium-doped fiber oscillator with two parallel fiber amplifiers (Taken from [RD51]).

A possible drawback of fiber lasers for space-based applications is the vulnerability of fibers to the radiation levels in space. Both gamma radiation and high-energy protons that are abundant in space cause degradation to the Erbium-doped fibers in the laser system, which can shorten the lifetime of the laser system considerably. Several studies have been performed on this subject [RD78; RD75], which led to the conclusion that standard erbium-doped silica fibers are susceptible to both gamma radiation and high-energy protons, and lasers based on such fibers can degrade to unacceptable levels within a few years of operation. A solution to this problem may be to include a dopant in the fibers, which may increase the fibers resistance to high radiation levels. This has been demonstrated for several materials, e.g. by doping a Nd:YAG rod with 1% Cr^{3+} ions [RD66]. The Cr-ions reduced the effect of radiation-induced color centering in Nd:YAG, increasing its radiation hardness.

Another issue with fiber oscillators, is that the cavity length is usually longer than what can be achieved using e.g. Ti:Sapphire lasers. This is caused by the required lengths of fiber to achieve sufficient gain, but also for dispersion compensation and modelocking. As a result, the repetition frequency of fiber lasers is usually in the 40-200 MHz range.

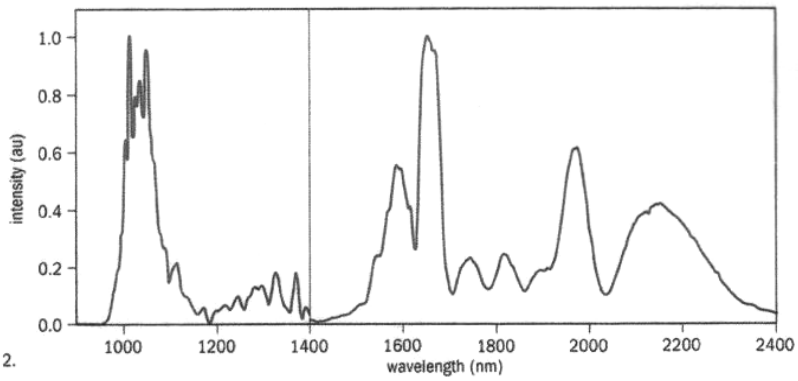

Fig. 2.26 - Output spectrum from a femtosecond fiber laser after broadening in fiber (reproduced from Product guide Toptica).

3.2.3 Cr:LiSAF, Cr:LiCAF and Cr:LiSGaF lasers

An interesting alternative to Ti:Sapphire as a laser gain medium in the near-infrared are Cr^{3+}-doped colquiriite crystals Cr:LiSAF (Cr^{3+}-doped $LiSrAlF_6$), Cr:LiCAF (Cr^{3+}-doped $LiCAlF_6$) and Cr:LiSGaF (Cr^{3+}-doped $LiSrGaF_6$). These crystals have a large $\Delta\lambda/\lambda$ of up to 0.22 (see Fig. 2.22), allowing the generation of few-cycle pulses directly from an oscillator. While colquiriite lasers operate in the same wavelength range as Ti:Sapphire lasers (roughly between 750 and 950 nm), their strongest absorption band lies at much longer wavelengths, between 600 and 700 nm (see Fig. 2.27). This allows direct diode pumping, as diode laser technology is much better developed at these longer wavelengths.

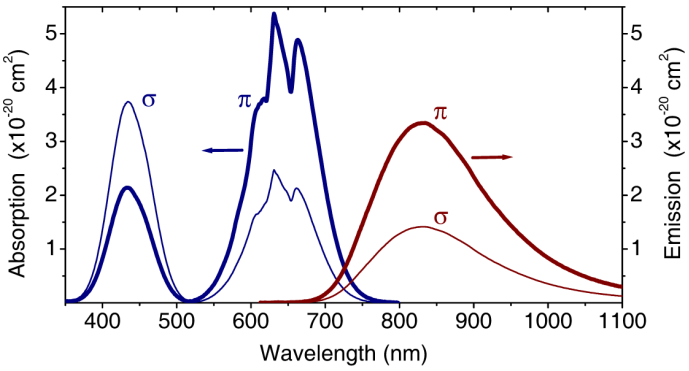

Fig. 2.27 - Absorption and emission spectra of Cr:LiSGaF (taken from [RD70]).

Colquiriite-based lasers are very promising for the development of compact, high-efficiency ultrabroadband laser oscillators, which would be very suitable for frequency comb applications. At present, a directly diode-pumped sub-10 fs Cr:LiSAF laser has already been demonstrated [RD74], as well as a 10 fs Cr:LiCAF laser with ~1% electrical-to-optical conversion efficiency [RD76]. Also, a 150 fs Cr:LiSAF laser has been developed with 5% electrical-to-optical conversion efficiency, with a footprint of 22 x 28 cm [RD50].

Although a fully stabilized frequency comb has never been realized with a colquiriite-based oscillator, the suitability of this type of laser system for frequency comb applications has been confirmed by Holzwarth et al.[RD49], who measured the carrier-envelope offset frequency of a Cr:LiSAF laser using standard f-to-2f interferometry. Figure 3.2-5 displays a measured RF spectrum containing an f_{ceo}-signal with a signal-to-noise

ratio of 40 dB in a 100 kHz bandwidth, which is sufficient for high-fidelity phase locking. The narrow linewidth of f_{ceo} indicates that phase noise generated during spectral broadening is limited.

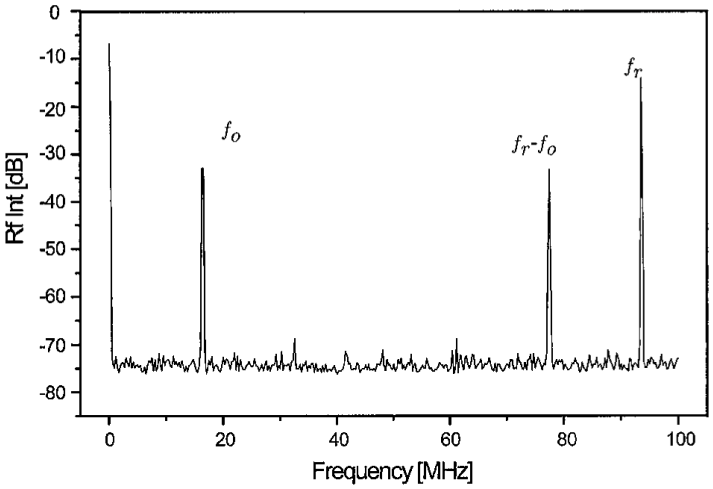

Fig. 2.28 - RF spectrum (100 kHz bandwidth), showing the carrier-envelope offset frequency signal of a Cr:LiSAF laser (Taken from [RD49]).

While Cr^{3+}-doped colquiriite crystals are promising laser materials for use in frequency comb systems, the first fully stabilized frequency comb based on such a material still needs to be constructed. Another drawback of these materials is that due to the relatively short center wavelength, the lasing threshold is relatively high (similar to Ti:Sapphire). In addition, since the oscillator cavity design is very similar to Ti:Sapphire, the same alignment issues need to be overcome. The maximum power that can be obtained from diode-pumped colquiriite lasers is presently limited by the available pump laser diodes, which need to produce sufficient power while maintaining a good beam profile. Note that the pump beam needs to be focused tightly to obtain reliable Kerr-lens modelocking, especially for such high-threshold materials. Therefore, a good pump beam profile is essential for modelocked lasers. Also for colquiriite lasers, a relatively large range of repetition frequencies can be employed, similar to the Ti:Sapphire oscillators (roughly 10 MHz – 1 GHz).

3.2.4 Cr:Forsterite laser

A less-common type of frequency comb laser is the Cr^{4+}-doped Forsterite laser. However, this system has some advantages over e.g. a Ti:Sapphire-based frequency comb. The cavity design of Cr:Forsterite lasers is rather similar to that of Ti:Sapphire, allowing the same range of repetition frequencies to be accessed. An interesting aspect of Cr:Forsterite is its longer absorption and emission wavelengths: it allows for direct diode pumping, and lases in a wavelength range of 1100 to 1400 nm. As a result of these longer wavelengths, the lasing threshold will be somewhat lower than for Ti:Sapphire. Cr:Forsterite oscillators are relatively well studied, and are commercially available: typical specifications are 20-40 fs pulse duration, 2 nJ pulse energy, and repetition rates in the 100-400 MHz range. The most commonly used pump source for these oscillators is an Ytterbium fiber laser, at a wavelength of 1075 nm.

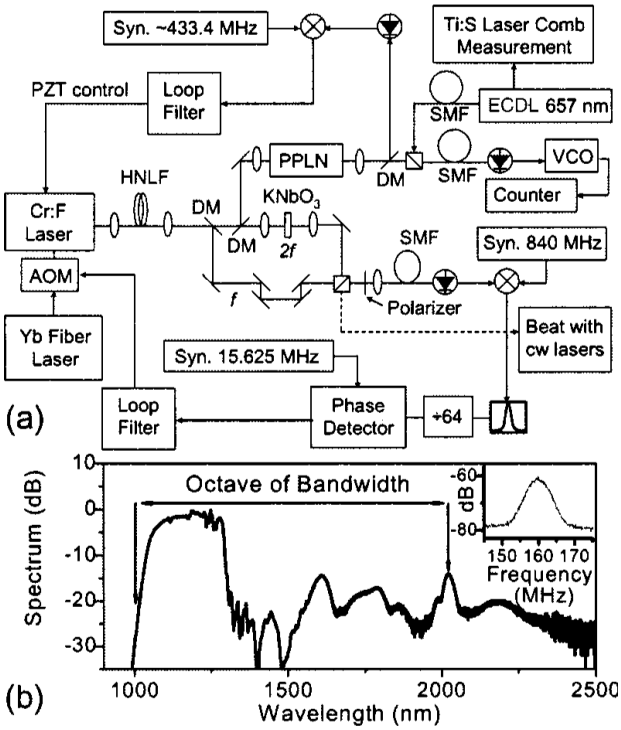

Fig. 2.29 - Schematic of a Cr:Forsterite frequency comb setup (Taken from [RD55]).

Fully stabilized frequency combs based on a Cr:Forsterite laser system have been demonstrated, with high frequency stability and accuracy [RD55]. The accuracy of the Cr:Forsterite frequency comb has been measured by measuring the frequency of an ultrastable diode laser at 657 nm (10 Hz linewidth) with both a Cr:Forsterite frequency comb and a Ti:Sapphire frequency comb simultaneously [RD56]. Both combs are found to agree within an accuracy of 6×10^{-17} in 10 s (measurement limited). A fractional frequency instability (Allan deviation) of $2.9 \times 10^{-13}\ \tau^{-1/2}$ has been found for a Cr:Forsterite comb, and this measurement was limited by the stability of the H-maser that was used as the RF reference source.

It should be noted that the f_{ceo} beat signal that has been reported for the Cr:Forsterite frequency comb is 6.7 MHz wide [RD55], which is exceptionally broad compared to Ti:Sapphire-based frequency combs. Although a high frequency stability can still be obtained, this wide beat signal raises questions about possible sources of phase noise in this frequency comb system. A possible source of such phase noise may be the 2 metres long highly nonlinear fiber (HNLF) that is used to produce an octave-wide bandwidth. Such a long nonlinear interaction length can very well lead to significant phase distortions. As a result of this broad f_{ceo} beat, a sophisticated locking scheme is required, involving multiple highly stable RF synthesizers and a large frequency division step.

3.2.5 Cr:YAG laser

Another laser gain material based on Cr^{4+}-ions which is being developed rapidly is Cr:YAG. Although at present it is a less commonly used material in ultrafast lasers, it has several attractive features that may make it interesting for frequency comb applications [RD69; RD70].

In contrast to Cr^{4+}-doped Forsterite, the Cr:YAG laser operates around a central wavelength of 1.5 µm. As this wavelength is close to the commonly used telecommunications band around 1.55 µm, it can take

advantage of well-developed optics for this wavelength, as well as its compatibility with fiber laser technology and Erbium-doped fiber amplifiers that operate in this wavelength range. Using Cr:YAG, 26 fs pulses (five-optical cycles) have been generated from a self-starting Kerr-lens modelocked oscillator, at an average output power of 250 mW at 100 MHz repetition frequency [RD62]. While this particular oscillator was pumped by an Yb-fiber laser, direct diode-pumping of Cr:YAG is possible as well, and 60 fs pulses at an average power of 15 mW have been produced this way [RD63]. To induce self-starting modelocked operation and to improve modelocking stability, the use of a SESAM is highly benificial, although this leads to somewhat longer pulses at lower power. Using the Yb-fiber-pumped system with a SESAM, 57 fs pulses at 200 mW output power have been obtained [RD62]. Although further development is still needed on this type of laser, the prospects for a compact, low-cost and efficient diode-pumped ultrabroadband laser system based on Cr:YAG seem very good.

A drawback of Cr:YAG is the present state of crystal growing technology for this material. Although YAG has been around as a laser host material for a long time (mostly in Nd:YAG lasers) and can be grown with high quality, pure and reproducible doping of YAG with the Cr^{4+}-ions is still problematic. In addition, a fully stabilized frequency comb system has not yet been demonstrated with a Cr:YAG oscillator. Recent experiments employed a Cr:YAG laser with stabilized repetition frequency for relative frequency metrology on acetylene molecules [RD38]. However, the carrier-envelope offset frequency of a CR:YAG laser has not been detected or stabilized yet.

While Cr:YAG lasers may not be sufficiently developed for implementation in low-maintenance frequency metrology systems, the development of this type of laser towards frequency comb applications seems promising, and should be kept in mind for long-term projects.

3.2.6 Cr:ZnS, Cr:ZnSe, Cr:CdSe lasers

A relatively new class of laser materials that are being developed rapidly are the Cr^{2+}-doped zinc chalcogenides, in particular Cr:ZnSe and Cr:ZnS [RD69; RD70]. Although these relatively new materials have not yet been studied extensively as laser gain media, they are some of the most promising crystals that are around in ultrafast laser physics. Zinc chalcogenides have a good hardness and crystal stability, and have a thermal conductivity comparable to Ti:Sapphire. More importantly though, they have a relative spectral gain bandwidth $\Delta\lambda/\lambda$ of up to 0.38, which is the highest of any known laser medium. This allows the generation of ultrabroadband laser pulses of only a few-cycles in duration directly from the oscillator. Another interesting property of both Cr:ZnSe and Cr:ZnS is that the nonlinear refractive index n_2 is 30-40 times higher than in Ti:Sapphire. This facilitates intracavity spectral broadening through nonlinear interactions, and opens up the possibility of generating octave-wide spectra directly from the laser oscillator.

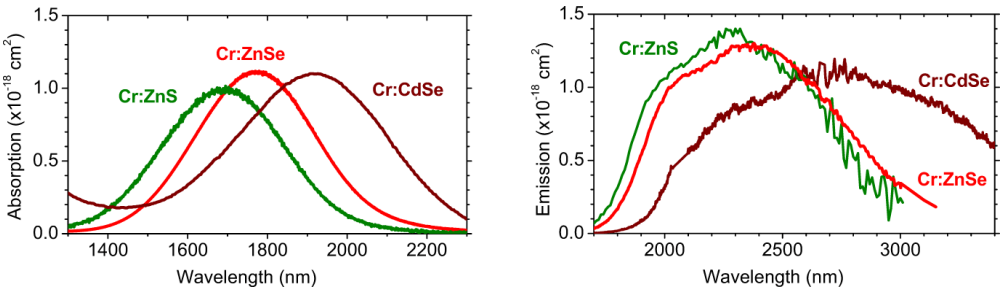

Fig. 2.30 - Absorption and emission cross sections of Cr2+-doped materials (Taken from [RD70]).

As shown in Fig. 2.30, the central operating wavelength of these laser media is in the mid-IR, roughly between 2 and 3 μm. The absorption bands lie between 1.4 and 2 μm, and allow pumping with an Erbium-

doped fiber laser or directly with diode lasers. Therefore, both Cr: ZnSe and Cr:ZnS allow the construction of cost-effective, compact and efficient laser oscillators. Very efficient multi-Watt lasers have been built using Cr:ZnSe, direct diode-pumping has been demonstrated, CW lasers tunable over hundreds of nanometres have been built, and several Watts of modelocked power are feasible with this material.

However, it should be stressed here that the full potential of these materials has not been realized yet. Cr:ZnSe is being researched intensively by various groups, but real few-cycle oscillators have not been demonstrated yet, let alone frequency comb systems. The development of femtosecond optics such as chirped mirrors and high-intensity optical coatings in the mid-IR is not as advanced as it is for the Ti:Sapphire and Erbium-fiber (telecom) wavelength ranges, which at present limits the achievable bandwidth. While Cr:ZnSe can be produced at good optical quality, the growth of Cr:ZnS single crystals is still somewhat problematic. Therefore, although Cr:ZnS has even better properties for intense few-cycle pulse generation, this material should be considered as a more long-term candidate for use in frequency comb laser systems.

3.2.7 Diode lasers

A very compact laser source with high electrical-to-optical conversion efficiency is the diode laser. This type of laser is already very well established in the realm of continuous-wave lasers, but modelocked diode lasers are being developed rapidly as well. While the pulse energy and peak intensity of such laser systems is still very low, diode lasers might be an interesting option for a frequency comb with low power consumption. A picture of a typical state-of-the-art modelocked diode laser is shown in Fig. 2.31. This laser produces 1 ps pulses at 27 GHz repetition frequency, and is integrated on a chip [RD39]. However, due to the high repetition rate and the low average power of only a few mW, the peak power of the output pulses is still very low. Therefore, diode lasers with longer cavities need to be developed to decrease the repetition rate and increase the peak intensity. Also, the pulse duration of these lasers is still too long for phase-coherent continuum generation in PCFs (see section 3.1.6). Therefore, diode-laser-based frequency combs should be considered as a long-term goal, but the possible scale reduction in both size and power consumption offered by the use of diode lasers seems promising.

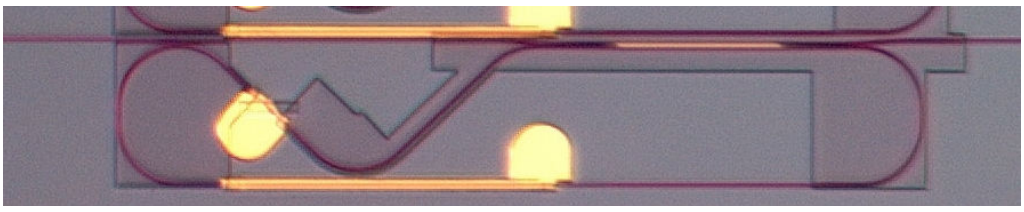

Fig. 2.31 - Photograph of a 27 GHz passively mode-locked bulk InGaAsP ring laser on chip of 1.3 mm by 0.25 mm with active-passive integration. Indicated are the semiconductor optical amplifier (SOA) and the saturable absorber sections (SA), the dark lines are waveguides. The laser produced 1 ps pulses [RD39].

3.3 Practical issues in frequency comb generation

While the first two sections described the principles of frequency comb generation and the practical implementations for stabilization and laser systems, more information is required to allow a realistic assessment of the possibilities for space-based frequency comb applications. In this section, we discuss various properties of frequency comb laser systems, as well as the critical components that are required for frequency comb operation.

As an introduction to this section, we discuss the implementation of a frequency comb laser system that has been constructed at LCVU. This introduction, consisting of paragraphs 3.3.1 and 3.3.2, demonstrates the typical complexity and layout of a typical laboratory-based frequency comb setup which is operated on a daily basis for frequency metrology purposes.

3.3.1 The LCVU frequency comb stabilization scheme

As an example of a practical frequency comb setup, the setup that was developed at LCVU is depicted in Fig. 2.32. In this scheme, an 11 fs, 7 nJ, 75 MHz Ti:Sapphire oscillator has been used as the frequency comb laser. The repetition rate of this laser is measured using a fast photodiode (EOT type ET-4000, 10 GHz speed). The signal from this photodiode is mixed with the output of an highly stable low-noise RF generator (Agilent E8241 PSG-L), which has been phase-locked to a GPS-disciplined Rb atomic clock (Stanford Research Systems PRS-10, 10 second Allan variance $< 1 \times 10^{-11}$). The mixer output is then sent to a PID controller, which provides an appropriate feedback signal to drive both a piezo-transducer glued to one of the cavity mirrors and a baseplate temperature control system to stabilize the cavity length.

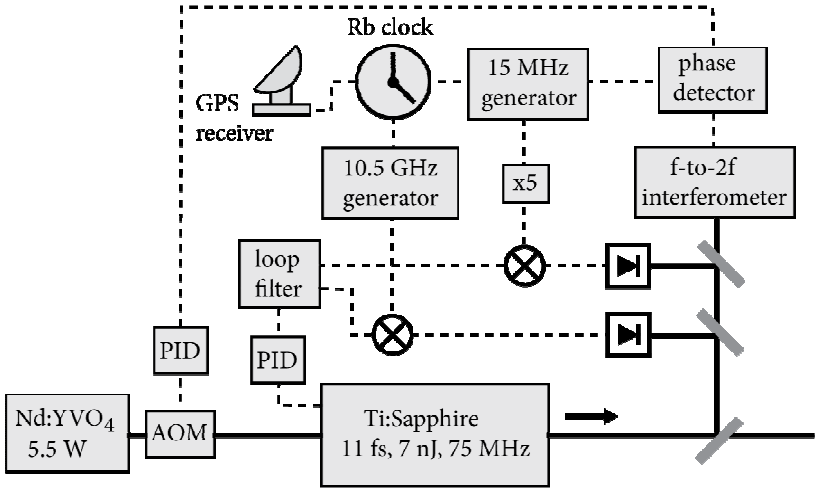

Fig. 2.32 - Schematic layout of the LCVU frequency comb setup.

Stabilization of the carrier-envelope offset frequency requires a more sophisticated approach, as the Ti:Sapphire laser does not emit any output power at the frequency f_{ceo} directly. A way to measure f_{ceo} is by means of an f-to-2f interferometer, as was already explained in paragraph 3.1.4. If the frequency comb is so broad that it spans a full octave, then f_{ceo} can be measured by generating a beat signal between a high-frequency comb mode and the second harmonic of a low-frequency comb mode. Such optical second harmonic generation can routinely be performed using nonlinear crystals such as BBO (β-$BaBO_2$). The difference frequency between these comb components then corresponds to f_{ceo}. The output of the f-to-2f interferometer is then sent to a phase detector, to reference the f_{ceo}-signal to the output of a 15 MHz RF generator which is also stabilized to the Rb clock. The frequency f_{ceo} can be modulated by changing the pump power, since this influences the cavity dispersion through the Kerr effect. Therefore, to lock f_{ceo} we send the output of the phase detector to a PID controller, which controls an AOM in the pump beam that modifies the pump intensity.

3.3.2 Spectral broadening and practical f-to-2f interferometry

A complication of the f-to-2f scheme is that typical modelocked lasers do not emit a spectrum containing a full octave. Therefore, additional spectral broadening of the laser output is required, as discussed in paragraph 3.1.6. Because the spectrum of our 11 fs pulses is already quite broad, only a limited amount of additional spectral broadening is required to reach a full octave. This can readily be achieved using a 6 cm long PCF with a core diameter of 1.7 μm, and a zero-dispersion-wavelength of 770 nm. A typical spectrum of the output of a frequency comb laser before and after broadening in this 6 cm long PCF is shown in Fig. 2.34, and pictures of the typical fiber output are shown in Fig. 2.33.

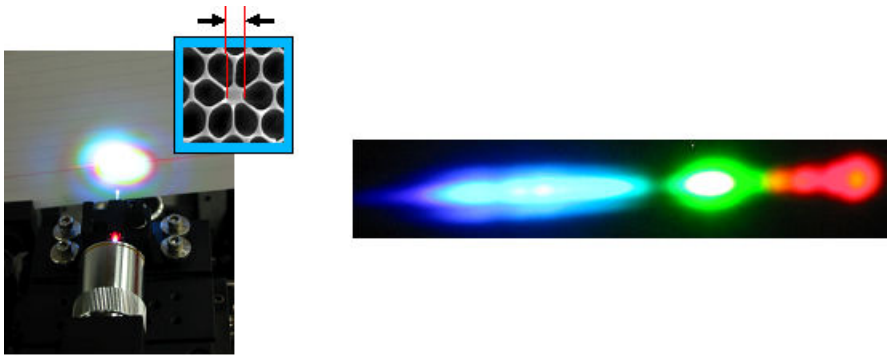

Fig. 2.33 - Pictures of the broadened output spectrum after propagation through 6 cm of PCF. Left: Output of the PCF, and a picture of the PCF structure. Right: The spectrum of the pulse, made visible by dispersing the various wavelength with a grating.

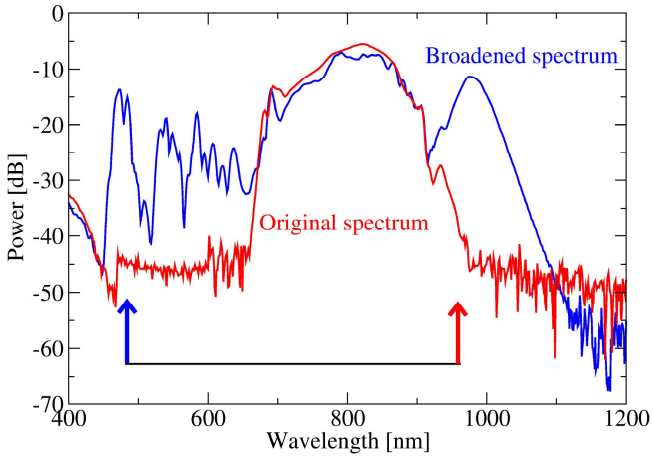

Fig. 2.34 - Broadening of the laser spectrum using a photonic crystal fiber.

It has been shown that the comb structure remains stable during these highly nonlinear spectral broadening processes, and that no significant phase noise is added to $\Delta\varphi$ by the PCF. Therefore, the ultra-broadband output spectrum emitted the PCF can be used to stabilize f_{ceo}, and the modes of this spectrum can be successfully employed for frequency metrology. The f-to-2f interferometer that we use to detect f_{ceo} has already been discussed in detail in section 3.1.5, and is schematically shown in Fig. 2.35. Therefore, we will limit ourselves here to a more practical discussion on the various components that are included in the f-to-2f interferometer.

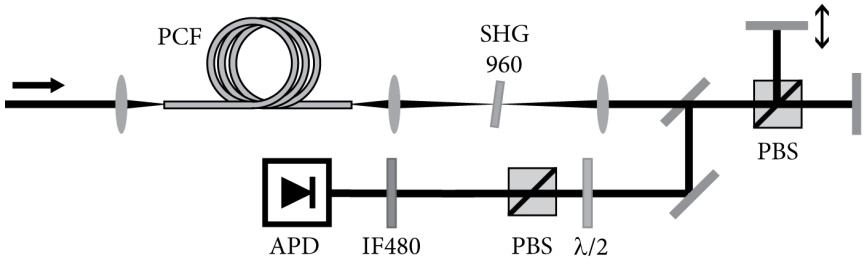

Fig. 2.35 - Implementation of the f-to-2f scheme using a Michelson interferometer, as implemented in the LCVU frequency comb system. DM: Dichroic mirror, SHG 960: BBO crystal for second harmonic generation of 960 nm light, PBS: Polarizing beamsplitter, IF 480: Interference filter for 480 nm light, TS: Translation stage, APD: Avalanche photodetector.

The most critical component in the f-to-2f interferometer is the PCF that is employed for spectral broadening. As the fiber core has a diameter of only 1.7 μm, efficient incoupling into this fiber is extremely sensitive to alignment. The lenses that are schematically drawn in Fig. 2.35 are in fact 25× magnifying microscope objectives, which may be replaced by achromatic doublet lenses. Nevertheless, typical incoupling efficiencies into the PCF do not exceed 20%, and depend critically on beam-pointing stability and robustness of the optical component mounts. Note that the processes that are responsible for spectral broadening in the PCF are highly nonlinear, and therefore the generated output spectrum also depends critically on the alignment stability of the beam that is coupled into the fiber. This alignment sensitivity can be alleviated substantially by using tapered fibers, or by using a PCF that has been spliced between two pieces of normal single-mode fiber. As this single-mode fiber has a larger core (typically 3-4 μm diameter for a wavelength of 800 nm), incoupling into such a fiber is easier and less sensitive to alignment.

After the octave-wide spectrum has been generated in the PCF, the low-frequency part of the spectrum has to be frequency-doubled inside a nonlinear crystal (usually BBO or KTP). This crystal is typically 1 mm long. While a longer crystal would lead to higher conversion efficiency due to the increased interaction length, a shorter crystal is capable of frequency-doubling a wider spectrum, since the phase-mismatch that governs (and eventually limits) the frequency-doubling process is proportional to the interaction length. Therefore, the crystal length is a tradeoff between conversion efficiency and the amount of modes that participate in the doubling process (i.e. the spectral bandwidth).

The detector that is used to produce a beat signal is a low-noise, high-bandwidth (250 Hz - 80 MHz) silicon avalanche photodiode (Analog Modules Inc. 712A-4), with a nominal gain of 77 V/μW and typical noise of

20 fW $Hz^{-1/2}$. Such a high gain, low-noise avalanche photodiode allows the detection of the f_{ceo} beat signal with over 40 dB signal-to-noise ratio (SNR), which is sufficient for reliable phase-locking of the frequency comb for extended periods of time (> hours). In practice, the time that f_{ceo} can remain stabilized depends mostly on environmental changes that affect the laser cavity (e.g. temperature changes and air flow), as well as on alignment drifts of the f-to-2f interferometer. Especially the optics involved in coupling the light into the PCF need to be robust, since these changes in input coupling efficiency can lead to changes in the SNR of the f_{ceo} detection that can cause the lock to fail. With the use of a tapered or a spliced fiber (see above) this input coupling can be made more stable, increasing the locking time considerably. For our particular laser system, the monolithic f-to-2f scheme discussed in section 3.1.5 is not applicable, as our 11 fs laser pulses do not have sufficient spectral bandwidth. However, when e.g. a 7 fs pulse laser is employed, this monolithic scheme is can be much more stable, and would allow phase-locking on longer timescales.

3.3.3 Cavity design and modelocking considerations

The generation of ultrashort laser pulses requires several cavity design considerations beyond the standard stability and finesse analysis that is used for typical cw and Q-switched lasers. The most straightforward of these extra design issues is the requirement that the laser should operate with a broadband spectrum, which means that a large range of wavelengths need to be resonant inside the cavity simultaneously. Therefore, any intracavity dispersion, which is always present due to e.g. the amplifier crystal, dielectric mirror coatings, etc. needs to be compensated already inside the oscillator. This can be achieved by the use of a prism compressor, by using materials with dispersion of opposite sign, or by the use of chirped mirrors. Prism compressors are bulky, alignment sensitive, and only provide proper dispersion compensation up to the second order. Therefore, prisms will not be considered in this study.

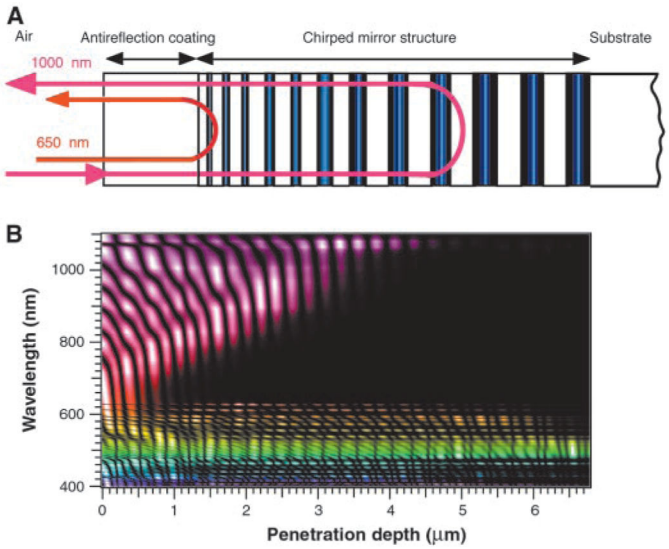

Fig. 2.36 - Top panel: Principle of chirped multilayer mirrors for dispersion control. Bottom panel: Standing-wave patterns in a chirped mirror structure as a function of wavelength (Taken from [RD71]).

Material dispersion is difficult to control. Moreover, especially in the visible and near-infrared wavelength ranges almost all bulk materials exhibit positive dispersion up to the third order. When going to longer wavelengths, however, this is not necessarily true anymore, and materials may be used for dispersion compensation. A more practical example, however, is the use of optical fiber technology. By changing the waveguiding structure of the fiber, the dispersion of the fiber can be tailored. This can be achieved by changing the core radius, or by creating a fiber structure with e.g. a lattice of airholes surrounding the core. Such photonic crystal fibers (PCFs) are being developed ever more precisely, and allow the engineering of the fiber dispersion characteristics (up to higher orders). Although such PCFs are not practical to implement in a laser cavity, they are very suitable for dispersion compensation in fiber lasers. By splicing a piece of PCF to a piece of normal single-mode fiber (doped with the gain medium), a ring cavity with zero net dispersion can be created.

In a standard mirror-based laser cavity, convenient and accurate dispersion compensation can be provided by chirped mirrors. These so-called chirped mirrors are standard optical substrates which are coated with a multilayer structure that effectively provides a different penetration depth for each frequency, thereby causing a phase shift between different frequencies. Fig. 2.36 shows the schematic principle of a chirped multilayer mirror, along with a typical standing-wave pattern that is generated inside the mirror coating by an incident ultrashort pulse. The difference in penetration depth as a function of wavelength in this interference pattern clearly shows the influence on the dispersion for the wavelength range between 600-1100 nm. The methods for designing and production of such chirped mirrors have developed rapidly over the past few

years, and commercial coating manufacturers can provide sets of chirped mirrors that are optimized for broad wavelength ranges (although the Ti:Sapphire and NIR wavelength ranges are better controlled than other spectral regions). The use of chirped mirrors allows the construction of compact cavities with much less alignment sensitivity than prism-compensated lasers, and repetition rates of Ti:Sapphire oscillators can exceed 1 GHz when chirped mirrors are employed. Also, octave-wide spectra directly from a mirror-dispersion-controlled Ti:Sapphire oscillator have been demonstrated [RD61; RD33]. An example of typical dispersion and reflection curves of commercially available chirped mirrors is shown in Fig. 2.37. The dispersion oscillations as a function of wavelength are typical for such chirped mirrors: usually, they are designed in matched pairs of mirrors with opposing dispersion oscillations, so that the total dispersion is well-behaved.

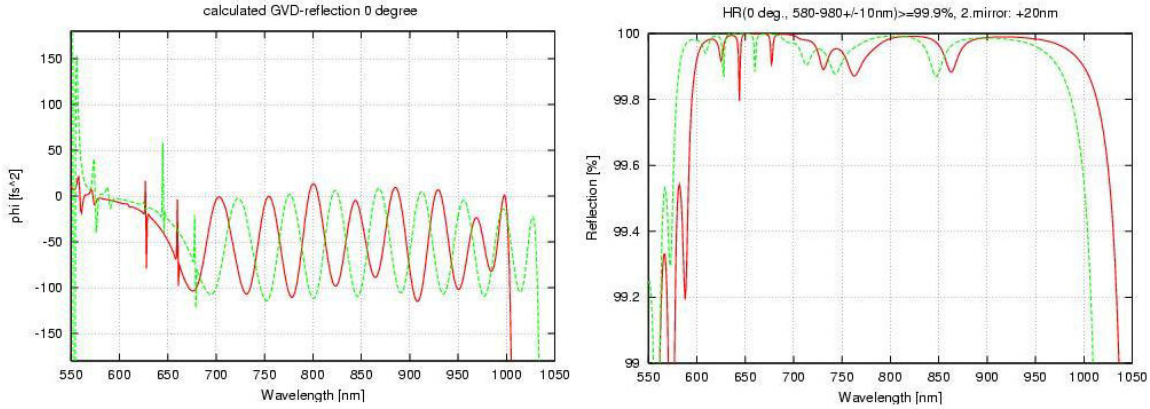

Fig. 2.37 - Dispersion (left graph) and reflection (right graph) curves for a pair of commercially available chirped multilayer mirrors (Layertec GmbH).

Although dispersion compensation inside a laser cavity is of course required for ultrashort pulse generation, this is by itself not sufficient to induce the modelocking process that creates the ultrashort pulse. Active modelocking based on an intracavity modulator (e.g. an AOM) usually only works in a limited wavelength range, and can produce pulses with ~ps duration. To generate the shortest pulses, passive modelocking should be used. The two most popular ways to induce passive modelocking are Kerr-lens modelocking and the use of an intracavity saturable absorber. Kerr-lens modelocking uses the Kerr-effect inside the laser gain crystal, which causes an intense pulse to self-focus inside a material with a nonlinear refractive index n_2. The intense ultrashort pulse would thus follow a different path inside the cavity than a cw beam. By placing an aperture in the right position or simply by tightly focusing the pump beam inside the laser crystal, modelocked operation can be made more favourable than cw operation. Kerr-lens modelocking is the technique that has produced the shortest laser pulses directly from a laser oscillator (down to two optical cycles). However, it requires careful alignment, and depending on the exact laser configuration also an external perturbation is still needed to actually start the modelocking. This might make it somewhat less practical for use in a closed, maintenance-free environment. The other possibility for passive modelocking is the use of an intracavity saturable absorber, in the form of a SESAM (Semiconductor Saturable Absorber Mirror). This SESAM also consists of a multiple nanolayer structure of semiconductor material, which causes relatively high losses at low intensity but bleaches at higher intensity, thereby causing a high-intensity ultrashort pulse to reflect from the mirror with relatively high efficiency while a cw beam experiences a much lower reflectivity. As a result, an ultrashort pulse circulates the cavity more efficiently, leading to modelocked laser operation. Although this method has intrinsically higher losses, it is less alignment sensitive and provides self-starting modelocked operation. Another issue with SESAMs is that the laser typically emits slightly longer pulses, as the spectral bandwidth of the SESAM is usually the limiting factor in this respect. However, with carefully designed SESAM mirrors, sub-6 fs Ti:Sapphire oscillators have been constructed with 300 mW average output power at 100 MHz repetition frequency [RD72]. The shortest pulse

duration that can be achieved with SESAM technology depends on the bandwidth and the response time of the semiconductor saturable absorber, and on the bandwidth of the mirror structure on which the absorber is deposited. Some typical structures of SESAM mirrors are schematically drawn in Fig. 2.38. A good review on the development of SESAMs and the design of these devices for various modes of operation is given by Keller et al. [RD54]. Note that saturable absorbers have also been developed for fiber oscillators, in the form of fiber Bragg gratings.

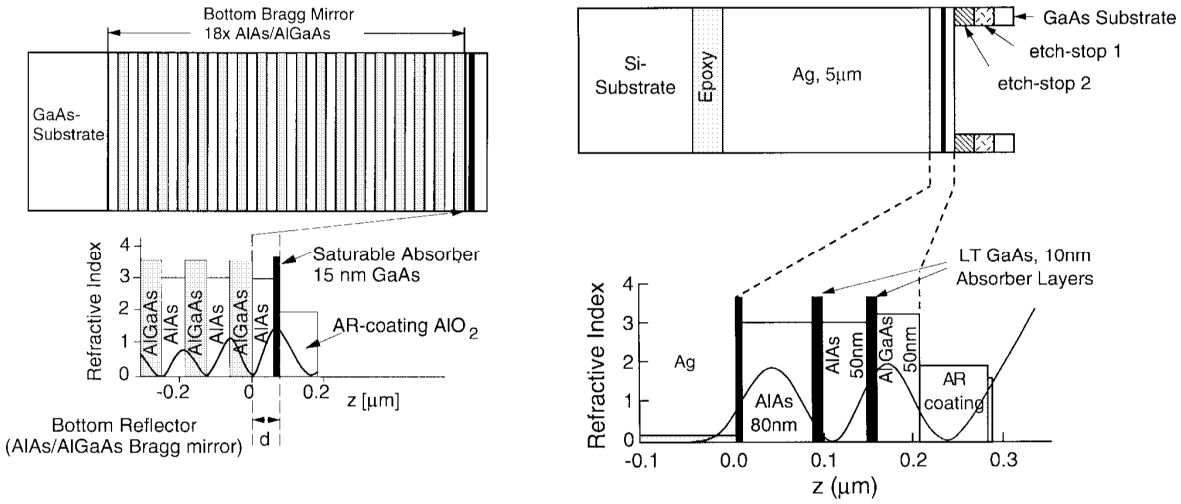

Fig. 2.38 - SESAM devices used for passive modelocking of Ti:Sapphire lasers. Left: SESAM based on a Bragg mirror reflector. Right: SESAM with a silver mirror coating for optimized broadband (sub-10 fs) operation (Taken from [RD54]).

3.3.4 RF frequency references

The stability of a frequency comb system will ultimately be limited by the reference source that is used to lock f_{rep} and f_{ceo}. In section 3.1.2, the advantage of locking to an optical reference instead of an RF source has already been discussed. However, while optical references do increase the stability of the frequency comb, for absolute measurements there should still be a link to an absolute frequency reference such as a cesium clock. In the end, the maximum achievable accuracy on absolute frequency measurements will still be limited by the accuracy and the stability of the RF reference source.

To provide a more quantitative estimate of what is achievable in terms of absolute frequency stability, the projected frequency stability of the space-based cesium fountain clock PHARAO is given in Fig. 2.39. This cesium clock is under development for the ACES project (Atomic Clock Ensemble in Space), and together with a hydrogen maser it will provide a space-based frequency reference at an accuracy and stability at the 10^{-16} level in one day. This ACES clock design represents the current state-of-the-art in RF reference signal generation, when optical reference sources are not taken into consideration (compare e.g. Fig. 2.3). Note that on short timescales, the stability is on the order of 10^{-13} in 1 s. By comparison, the best commercially available primary frequency standard is the Symmetricom 5071A cesium beam clock (formerly sold by HP/Agilent). This clock achieves a frequency accuracy of 2×10^{-13}, and a maximum stability of 10^{-14} after several days (10^{-12} in 1 s). To increase the short-term stability of such a clock, it can be augmented with a commercial hydrogen maser (e.g. Symmetricom MHM2010), which can have stability similar to the red curve in Fig. 2.39.

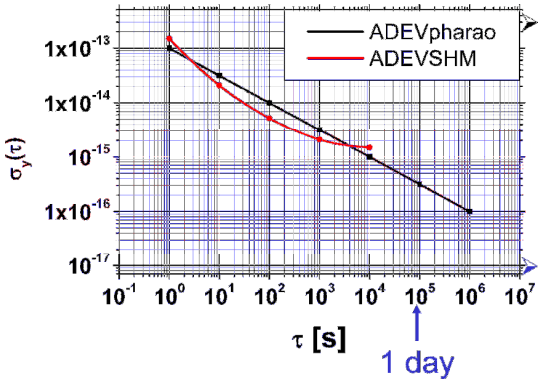

Fig. 2.39 - Projected frequency stability of the ACES cesium fountain clock PHARAO (black trace) and the space-grade hydrogen maser SHM (red trace).

3.3.5 Pump laser considerations

The pump laser source can be a significant issue in the stability of the frequency comb system. This has been demonstrated by Witte et al. for a typical Ti:Sapphire-based frequency comb system [RD13]. In this study, it was found that stabilization of f_{ceo} is facilitated considerably when a single-mode pumplaser is used. In addition, a tighter lock was achieved with the single-mode laser compared to a multi-mode pumplaser. It was found that mode-beating in the multi-mode pump laser induced rapid pulse-to-pulse phase fluctuations in the femtosecond pulse train, leading to a reduction in carrier-envelope offset frequency stability. Fig. 2.40 depicts the measured phase deviations and spectral linewidth of the locked f_{ceo} beat signal of the Ti:Sapphire frequency comb, when pumped by a single-mode Verdi 10 and by a multi-mode Millennia Xs Nd:YVO_4 laser, respectively. These measurements have been performed with a second f-to-2f interferometer outside the f_{ceo} stabilization loop. A striking difference was found between the single-mode and the multi-mode cases: the multi-mode pumplaser is found to induce about a factor of 6 more phase noise on f_{ceo}, depending on the bandwidth of the feedback loop.

These results indicate that care should be taken in the selection of a suitable pumplaser for a frequency comb oscillator, as it can have a significant impact on the stability of the system.

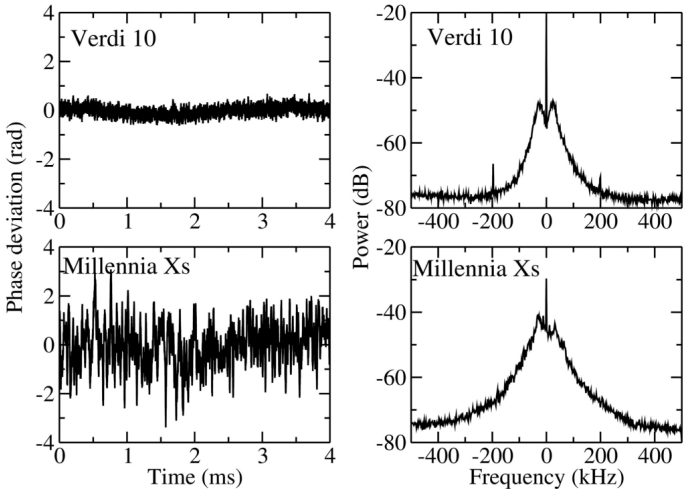

Fig. 2.40 - Measured phase deviations (left panels) and spectrum analyzer traces of the stabilized f_{ceo} beat signal, when using a single-mode Verdi 10 and a multi-mode Millennia Xs Nd:YVO4 laser as a pump source (Taken from [RD13]).

3.3.6 Laser pulse characteristics

The typical output of a femtosecond laser must adhere to several criteria to be useful for long-distance measurement. This paragraph is intended to highlight several characteristics of femtosecond laser pulses that are likely to be of practical importance for length measurement applications.

The first issue is that the diameter of the beam that is coupled out of the oscillator is typically around 2-3 mm. This is not sufficiently large to prevent diffraction effects from becoming noticeable at larger distances. Therefore, beam expanding optics are required to increase the beam diameter. Note that these optics should preferably be reflective instead of transmitting, due to reasons of dispersion.

The second issue is the dispersion of any material that may be in the beam path, such as AOMs or optical components. Especially when material is placed in only one arm of an interferometer, this will cause a difference in pulse duration and chirp between the interferometer arms, leading to a distorted interference pattern. Therefore, dispersion management can become an issue in coherent detection schemes that may be employed for distance measurements. In time-domain cross-correlation, an imbalance in pulse durations between the reference arm and the measurement arm leads to a decrease in fringe visibility and a distorted shape of the interferogram. Furthermore, a difference in material dispersion between reference arm and measurement arm can also lead to a shift of the carrier-envelope phase between pulses, due to the difference between group-velocity and phase-velocity in almost all materials. In spectral interferometry, any imbalance in dispersion between the two measurement arms introduces a wavelength-dependent time delay, which leads to a varying fringe spacing across the pulse spectrum. In this case, only an average value for the time delay can be determined, with an increased measurement uncertainty.

A third issue is the fact that the use of shorter pulses requires the use of broad-bandwidth optics. While shorter pulses may lead to a better measurement resolution, they have a wider spectrum and therefore require the use of high-quality optical coatings to ensure that the entire bandwidth can be used for measurements. Typically, gold- or silver-coated mirrors are used to provide a sufficiently large reflection bandwidth, depending on the exact wavelength range that needs to be covered. Note that while broadband dielectric coatings are also manufactured commercially, care should be taken that the dispersion characteristics of these coatings do not influence the pulse shape significantly.

3.4 Detection of fs-Laser pulses

For the present purpose, specific requirements must be met in order to obtain timing accuracies compatible with ranging resolution on the absolute distance measurement.

The accuracy associated to the absolute distance measurement system depends not only on the capacity to reproduce narrow fs pulses, at a precise repetition frequency, or on a ultra-wide detector bandwidth, but on the complete detection chain, which includes the time discrimination electronics and counters.

In fact, and regarding the jitter associated to pulses, that may show itself in lower or higher extent on the laser source, detector or timing discriminator, add up to a total timing error, referred to the input of timing system, as the square root of the sum of the squares of the contributions of each of the error sources.

The processes involved in the absolute distance measurement, namely time-of-flight measurement and pulse correlation for the final measurement accuracy, have stringent but different requirements.

For time of flight measurement in particular a low jitter/low walk error system is required in order to insure that timing actually reports the true time of arrival of the laser pulse or pulses that travel away to the target/reflector and are bounced back to the detector.

For the non-coherent detection process, the objective is to solve the ambiguity problem of the interferometer. This means that we have to know with accuracy better than $c/(2f_{rep})$ the position of the target. Taking as an example a 200 MHz repetition frequency, this gives a fairly conservative position resolution of 0.75 m, easily obtained with common techniques in ranging systems, either optical or RF.

In order to support the tuning of the interferometer, either by OPD change or f_{rep} tuning, the detection system must be able to discriminate the two pulses and evaluate how close they are from each other and how close they are to start to interfere with each other, thus enabling the trigger of the coherent mode.

In first this case, the detector must be able to detect (expected) weak laser impulses, and reproduce it electrically more or less independently of its shape or amplitude, in order to enable a timing discrimination method with a reduced jitter or walk error. Here, bandwidth and linearity are surpassed by the necessity of having a high signal-to-noise sensing scheme, highly stable detector in order to reduce the sources of jitter and walk error.

Fortunately, and providing that large SNR is available (higher than 10, in order to prevent noise-triggered false alarms) and allowing averaging by measuring in sequence a large number of time intervals between the reference arm pulse and the target pulse, could lead to a reasonable bandwidths of 5-10 GHz (20-10 ps discrimination), attainable with state-of-the-art photosensors and timing discriminators. Fig. 2.41 shows bandwidth requirements facing time discrimination resolution, function of actual SNR and number of pulses averaged.

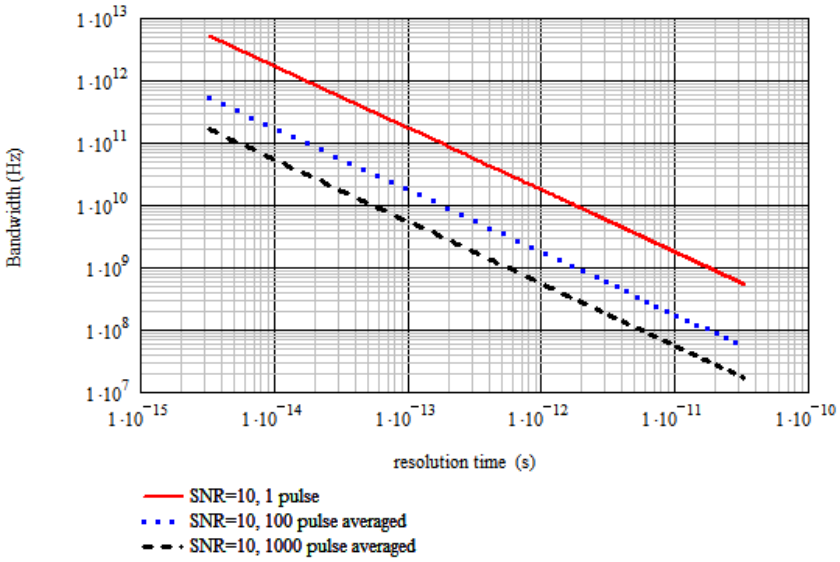

Fig. 2.41 - Bandwidth requirements facing time discrimination resolution, function of actual SNR and number of pulses averaged.

For the coherent detection, related to the pulse correlation process, the detector arrangement must show a highly linear behaviour, with the lowest noise, in order to follow exactly fringe intensity variation during the tuning process.

The detection process during the analysis of the correlation pattern implies that the detection system must be able to discriminate fringe intensity variations while convolving the target pulse over the reference arm pulse, by changing the interferometer arm size with the help of a piezo transducer (although only this option will be referred in the following text, alternatively the correlation pattern can also be obtained by changing the repetition frequency).

The particular architecture of the setup produces singular and very specific requirements from the point of view of the detector system. In fact, the detection system must be able to trigger and measure intensities of pulses that last no more than a couple of hundred fs, showing themselves every few ns (for a repetition frequency in the order of hundreds of MHz), but with intensities only related to the position of the piezo transducer, which can be tuned at frequencies no higher than a few kHz.

The specificity of the problem indicates again that there is no need to have full electrical bandwidth, in order to reproduce linearly the input pulse shape, but that a "slower" detector working as charge integrator or a track-and-hold system could evaluate with enough precision the maximum intensity of each fringe, for each piezo step. Averaging out a set of successive impulses should provide enough measurement precision to correctly identify the fringes of maximum intensity.

To be clear about the specific detection process in the coherent mode, the detector must be capable of sensing fs pulses, which means being able to generate enough photocurrent for such a short pulse and allow the charge to be integrated during several pulses, providing the correct "persistence" for direct viewing or other higher level (slower) processing electronics.

3.4.1 Incoherent fs-pulse detection

As it was mentioned before, the incoherent fs-pulse detection scheme is devoted to remove the ambiguity of the coherent measurement and also to monitor the time lag between the reference pulse and the measurement pulse, during the scanning process.

It is expectable that the metrology chain of the scientific instrument comprises lower accuracy ranging sensors to enable initial beam coupling between spacecrafts (measuring points). Thus, it might not be necessary to use the incoherent detection part to remove the ambiguity. Nevertheless, the incoherent mode is vital to determine how close is the tuning/scanning process to enter in the coherent scheme, which happens when the two pulses are close enough to start to interfere coherently.

In this sense, specific attention is given to new ultra-fast semiconductor arrangements, working as direct detectors (in opposition to any coherent scheme), available today or in the next few years and presenting bandwidths in excess of 5 GHz.

It must be noted that the suitability of these detectors to the realization of the proposed detection arrangement, depend not only on their efficiency, the inherent radiometric balance and on the power/noise budget, but on the complete detection chain, including the detector, amplification stage, time pick-off circuitry and digitizers, that contribute to the overall system performance.

Following are some of the relevant technologies in ultra-fast photodetection.

A metal-semiconductor-metal (MSM) photodetector consists of interwoven metal fingers on a semiconductor, and it detects photons by collecting electric signals generated by photo-excited electrons and holes in the semiconductor which drift under the electrical field applied between the fingers [RD94].

The capacitance of a MSM photodetector with equal finger spacing and width is only one quarter that of a PIN diode having same photosensitive area. Hence, despite the 50% lower efficiency due to blocking of the incoming light with its metal fingers, the MSM detector combined with an integrating receiver would be expected to double the responsivity-bandwidth product which could be obtained using a PIN diode.

Although the MSM technology is one of the candidates for a pure TOF architecture, as these detectors bandwidth is as close to the requirements as the current technology permits (Fig. 2.43), one must remember that the implementation of this solution is always limited by the subsequent complexity and bandwidth of the processing electronics associated to the timing functions.

Rise time	BW	Material	Obs
0.87 ps	510 GHz	GaAs	Low temperature-growing
1.5 ps	300 GHz	GaAs	Semi-insulating substrate
3.7 ps	110 GHz	Si	Crystalline
3.2 ps	140 GHz	Si	*Silicium* on insulator

Fig. 2.42 - Typical characteristics of MSM photodetectors.

We must add also that ultrahigh-bandwidth is presently only available in experimental devices and not exactly as an off-the-shelf product, although this technology shows itself very promising in the close future. Manufacturers like Hamamatsu present some more conservative products, with bandwidths of tens of GHz, already proven in the high demanding market of optical telecommunications [RD95].

Taking into account the specific function associated to the incoherent detection regime, the same requirements can be obtained with "slower" detectors, supported by the relative lower accuracy requirements, supported by the process of averaging, can provide enough precision during the interferometer scanning process.

The table on Fig. 2.43 presents briefly some few other detector types and technologies, whose specifications allow their use in the present application, taking into consideration these latter arguments.

Manufacturer	Model	Type	Material	Bandwidth [GHz]	Wavelength [nm]	Tr [ps]	Tf [ps]
Alphalas	UPD	PIN	GaAs	>10	320-900	<30	
Ultra fast Sensors	HSP50	APD	Si	100	320-900	10	10
ThorLabs	FGA04	PIN	InGaAs	2	800-1800	100	100
Menlosystem	APD310	APD	InGaAs	1	850-1650		
Menlosystem	FPD310	PIN	InGaAs	1.8	850-1650	500	
GigaComm	GGD-OS-A01	PIN	GaAs	5	850		

Fig. 2.43 - Characteristics of non-MSM photodetectors.

3.4.2 Coherent fs-pulse cross-correlation detection

The incoherent regime provides initial, but unambiguous, information about the unknown length in terms of a proper integer multiple of the pulse period, and relies on the time-delay measurement done with a fast photodetector that has the capability to detect pulse separations in the order of few picoseconds. The coherent regime, affords enhanced resolution and accuracy, and relies on the detection of the exact overlap of the two pulses determined with the analysis of the fringes detected with an optical cross correlator. A cross correlator is based on the interferometric autocorrelator commonly used to measure ultrashort pulses,

with the modification that one arm of the interferometer is longer than the other by a multiple of the cavity round-trip time.

At present, only few practical designs for second-order autocorrelators/crosscorrelators are currently used. The most favorable approach for the concepts presented in this work is presented in Fig. 2.44. The setup is based on a Michelson interferometer with a 50/50 beam-splitter and two corner cubes, used to avoid coupling back to the laser source. The corner cube on the reference arm moves back and forth on a piezo translation stage to give access to the cross correlation signal. The fully collinear beams will interfere all along their paths (within the coherence length). The second-order process needed requires a reasonable peak power, and the use of a short focal length lens is advisable. Considering that pulses in the order of tens of fs are being measured, to avoid any pulse broadening before and inside the correlator, a pellicle beam splitter and a thin lens have to be selected.

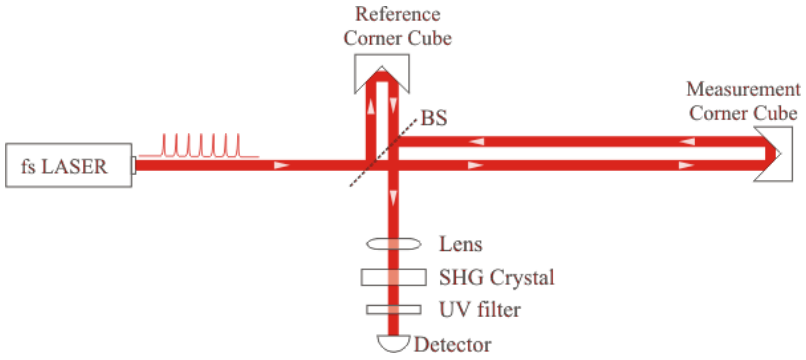

Fig. 2.44 – Schematic of a cross-correlator.

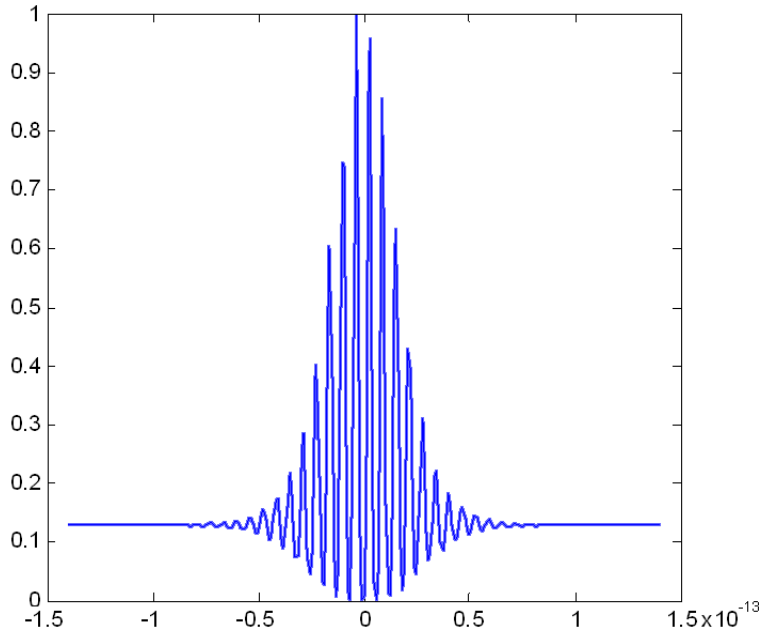

Fig. 2.45 – Typical cross correlation pattern as seen after the SHG (horizontal axis represents time delay between pulses).

Fig. 2.45 represents a typical cross correlation pattern as seen after the SHG (detector signal proportional to I^4). This signal represents, for two pulses with different overlaps, the output of the detector. The horizontal

axis represents time delay between pulses. In practice, each point of this pattern corresponds to a specific OPD (piezo position on the reference arm), or repetition frequency, and will require an integration of several pulses.

To give an order of magnitude of the required variation in the mentioned parameters, consider the following empirical examples:

- For a laser with a repetition frequency of 200 MHz and a pulse width of 100 fs, the ambiguity range is approximately 1.5 m and the number of (ambiguity) periods is around 133. Consider an absolute distance of 100 m.
- To obtain the complete cross correlation pattern using a piezo scan in the reference arm of the interferometer (OPD change), the travel range would have to be at least 15 µm (dependent only on the pulse width).
- To obtain the complete cross correlation pattern changing the repetition frequency, the change would have to be at least 30 Hz (dependent on the pulse width, repetition frequency and measured distance). To achieve the 30 Hz variation, one must change the cavity length by approximately 0.1 µm.

Depending on the particular values of the pulse width, repetition frequency and measured distance, the change in the repetition frequency might not be reasonable enough to enable a correct scan of the cross correlation pattern. Fig. 2.46 shows the required cavity change to obtain the complete fringe pattern for several pulse repetition frequencies as a function of measured distance considering a pulse width of 100 fs.

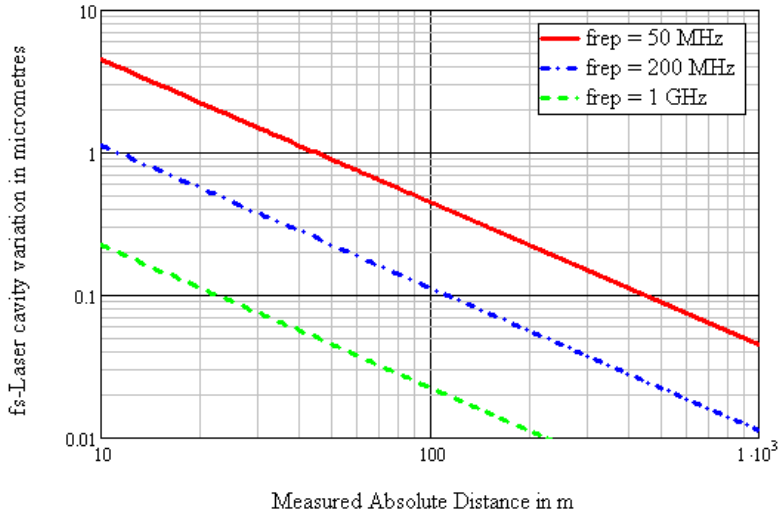

Fig. 2.46 - Required cavity change to obtain the complete fringe pattern for several pulse repetition frequencies as a function of measured distance considering a pulse width of 100 fs.

The relative position of the pulses changes faster for a cavity change (f_{rep} change) than with the OPD change. This will define the strategy for the measurement procedure. Although this issue will be developed in the next stage of the study, Fig. 2.47 presents the possible strategies to reach the final measurement with the desired accuracy (a combination of both might also be considered).

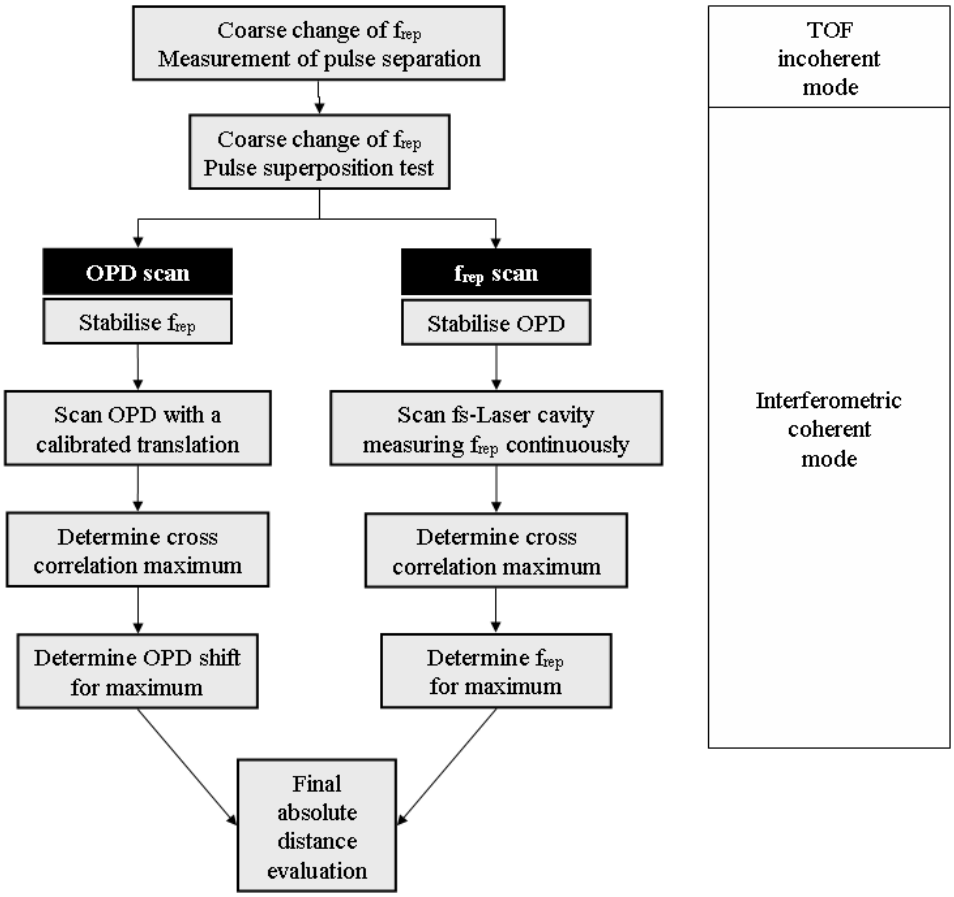

Fig. 2.47 - Possible procedure to obtain the distance measurement from the incoherent and coherent modes of operation.

In order to measure pulse characteristics and detect the peak of the waveforms, intensity autocorrelation using second harmonic generation (SHG) is the most commonly used technique, which gives information on the pulse shape directly. However, the intensity requirement for SHG is high, and group-velocity mismatch can distort the pulses in phase-matched SHG crystals. Phase matching requirements also limit their application due to stringent angle orientation requirements, dependant upon the working wavelength. Since the SHG response is normally of low efficiency, additional care must be taken for the detection of the outcoming pulses, both with filtering and complex avalanche or photomultiplier arrangements.

Two-photon absorption (TPA) in semiconductors is an attractive alternative to second-harmonic generation (SHG) for autocorrelation, because of lower cost and increased sensitivity. TPA can be implemented specific photodiodes or light-emitting diodes (LEDs) for autocorrelation measurement of picosecond and femtosecond laser pulses [RD87; RD91; RD92; RD93].

The laser pulse autocorrelator based on TPA, using large bandgap semiconductor photodetectors, avoids the problems encountered with the autocorrelator based on SHG, and several semiconductors have been found to be able to detect and measure pulses of ultrashort duration.

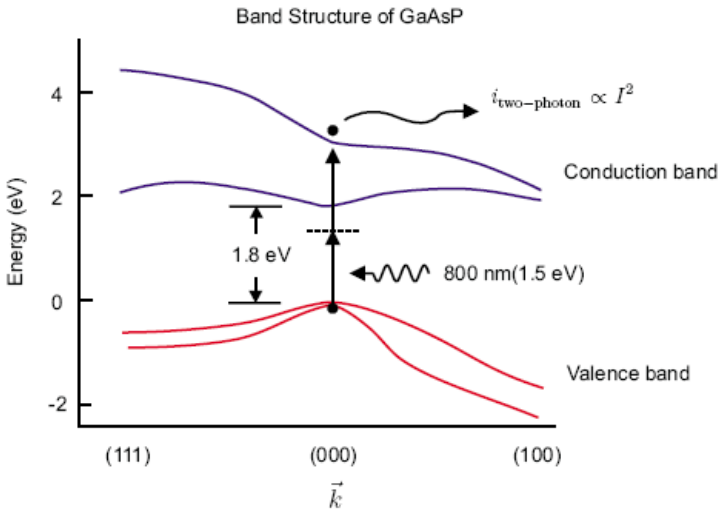

Fig. 2.48 - Two-photon induced photocurrent in semiconductor

For example, an AsGaP photodiode will give excellent results for wavelengths above 600nm, while a standard silicon photodiode will do the same for the near infrared (> 1.2 μm). As it was mentioned before, one can instead use an inexpensive LED whose band gap is adequate, but in this case one has then to worry about the extremely small size of the emitting zone, which is used here as a photodetector.

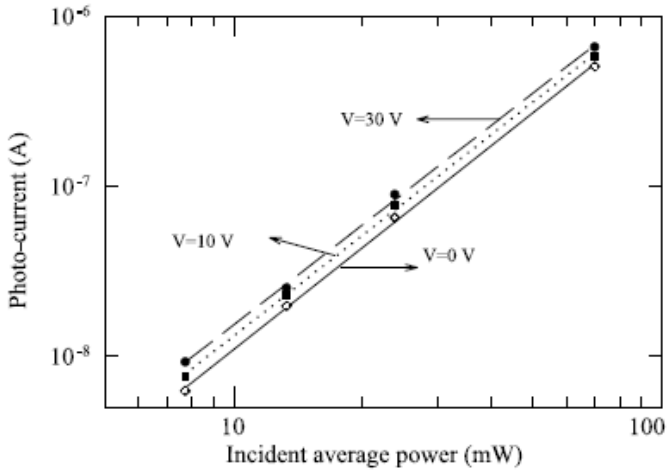

Fig. 2.49 - Two-photon induced response of AlGaAs based LED with respect to incident average power of 200 fs laser for different bias voltages, showing the typical quadratic response of the photocurrent wrt incident average power [RD92]

In order to avoid the difficulties arising from phase-matched nonlinear interactions in both SHG and TPA semiconductors, some recent work relates the use of a metal-semiconductor junction (MS), used to the detection of the short impulses instead of a photodetector [RD32].

Another possible solution for the correlation fringe detection is to use a low-spec streak camera, or a “streak-like device”, working in synchroscan mode, whose sweeping frequency is locked to the piezo scanning waveform.

In this mode, as the sweeping action is in phase with the interferometer reference arm size variation, the correlation figure will be recorded directly and successively on the phosphor or CCD connected to the streak tube. This will allow a very accurate representation of the correlation fringes, obtained with very loose bandwidth constraints.

Fringe contrast could be easily augmented simply by decreasing the sweeping frequency, which is, decreasing the frequency of the signal commanding the piezo, allowing more time to integrate photo-electrons on the streak anode.

Giving an exact correlation between the position of the fringes and the piezo driving stage, the peak of the correlation fringes could be easily found, off-line and without time constraints.

3.5 HAALDM concepts in literature and context

There are several techniques to measure an absolute distance but only a few can achieve high accuracy for long distances. The techniques can be split into tree different categories: Triangulation, Time-of-Flight and Interferometry (Fig. 2.50).

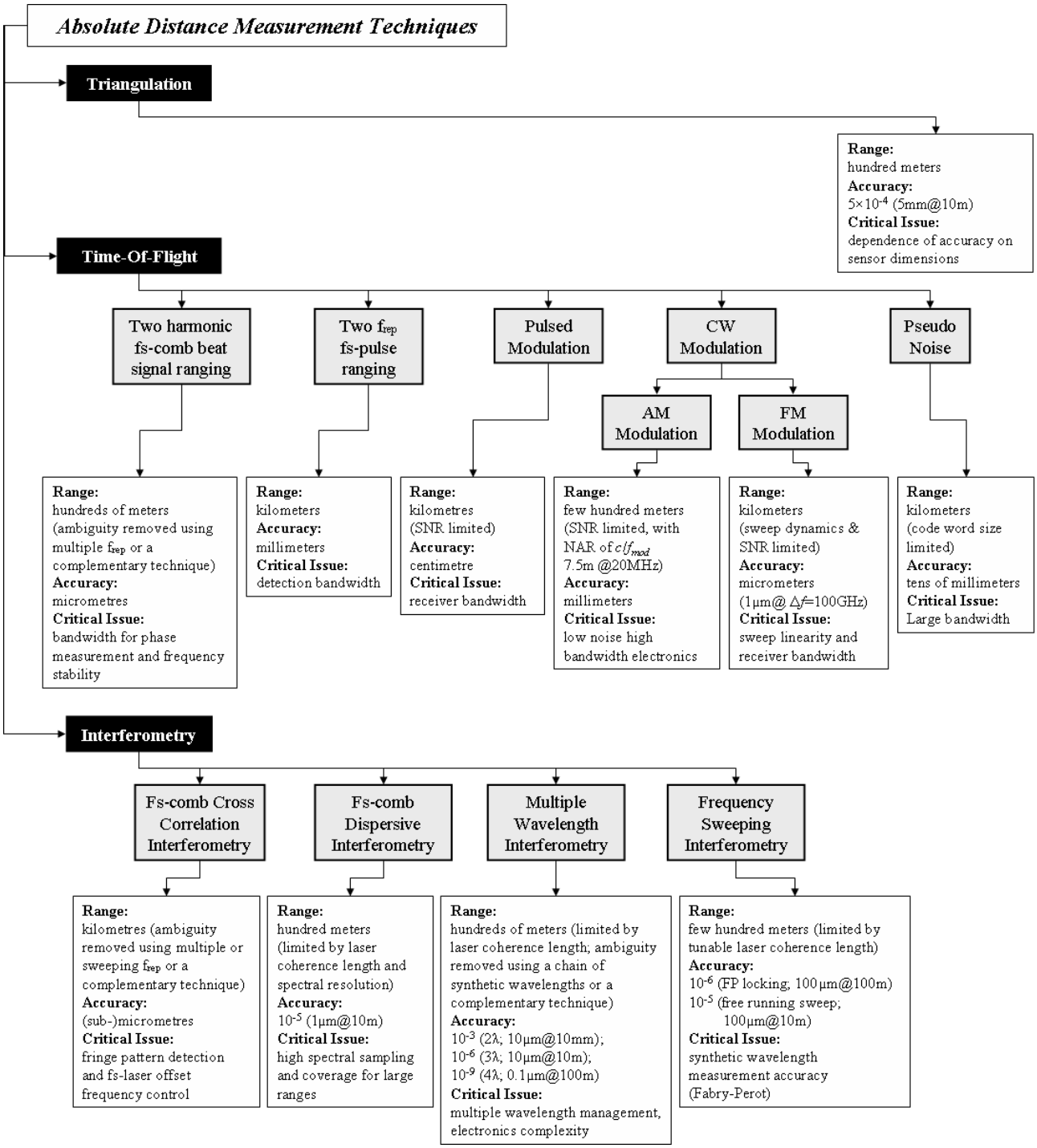

Fig. 2.50 - Graph tree with ADM techniques and corresponding characteristics.

Triangulation can measure distances up to hundred metres but the accuracy at large distances cannot go bellow the millimetre range [RD21].

The TOF method is conceptually the easiest way to make an absolute long distance measurement. To achieve high accuracy at large ranges, different schemes where developed using different types of modulation, corresponding to different levels of complexity [RD21; RD88; RD89].

Optical interferometry uses the phenomenon of interference between light waves to make extremely accurate measurements. It is thus an excellent way to achieve high accuracy at a (sub)micrometer level. Measurements are made without ambiguity, by using either one or several synthetic wavelengths resulting from the beating of two or more wavelengths or from a frequency sweep.

Recent advances in the technology of fs lasers, that emit a constant train of broadband but temporally very short optical pulses, enabled the improvement of some techniques and the development of new ones, based both in TOF and interferometry.

The graph tree on Fig. 2.50 presents the main techniques for ALDM, considering a space application and ranges compatible with the target missions for this (> 10m). The main characteristics of each technique are presented. Several techniques exist that are variations of the indicated techniques but the performances are normally equivalent. Fig. 2.51 shows the location of each technique in an accuracy versus maximum range graph. Clearly some of the techniques cannot be self-sufficient due to the lower accuracy or the short maximum range. Nevertheless, some techniques combined together can overcome the initial constrains and result in an appropriate method. An initial view indicates that TOF techniques are suitable for long range but have poor accuracy, while interferometry techniques can achieve high accuracy but are limited in range (normally due to the inherent ambiguity).

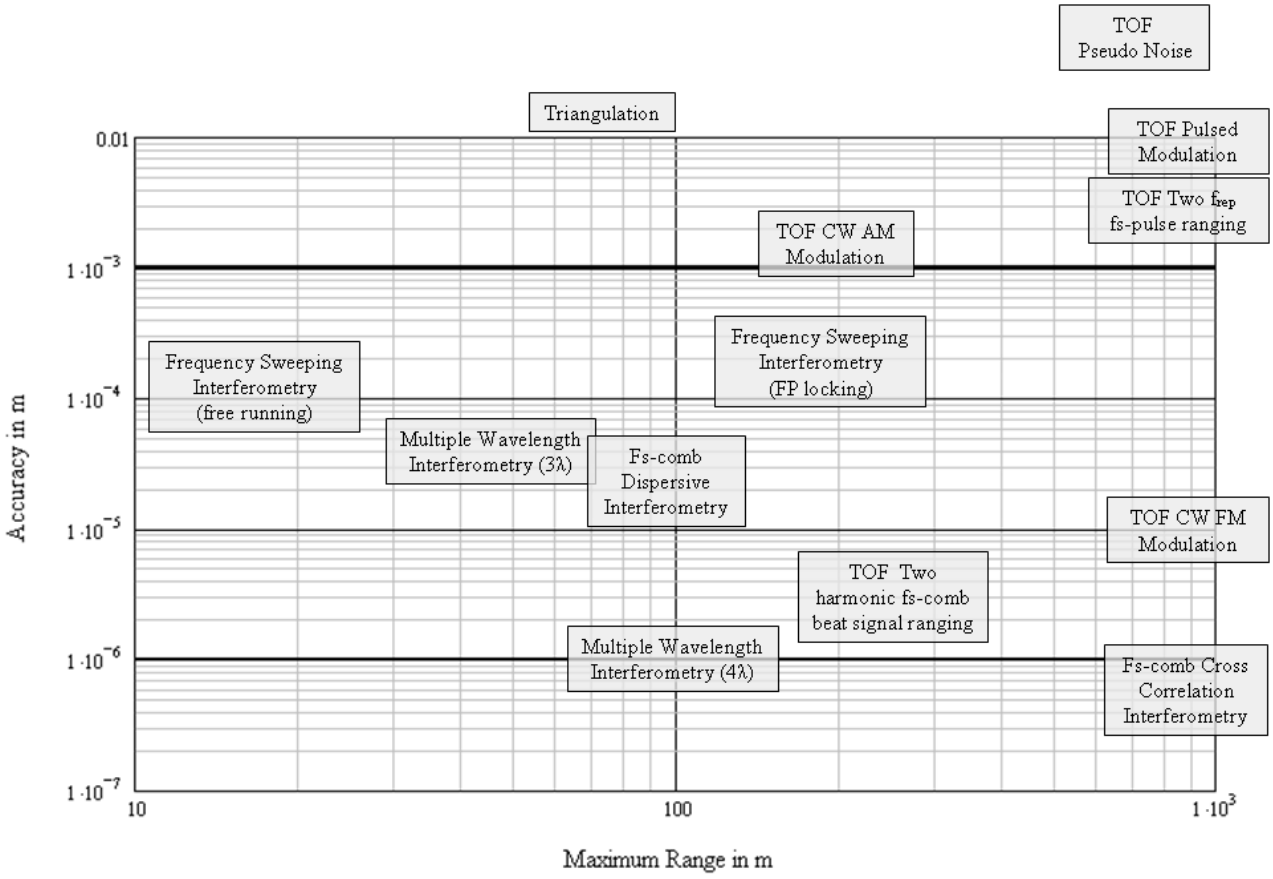

Fig. 2.51 - Accuracy versus maximum range for ADM techniques.

Possible candidates for high accuracy ALDM are all techniques that can achieve, at least, micrometre level accuracy (or tens of) and that can make measurements, at least, at several tens of metres even if there is ambiguity in the measurement. In fact, excluding TOF CW FM Modulation, all techniques capable of high accuracy absolute long distance (HAALD) have an inherent ambiguity that is resolved by a variation of a parameter or using a complementary technique.

TOF CW FM Modulation can, theoretically, measure without ambiguity distances of kilometres with accuracies at the micrometre level [RD88; RD90]. It is typically limited by the coherence length of the laser source and by the phase noise occurring during the modulation at high frequencies. In practice, the requirements on the frequency sweep dynamics and linearity, on the receiver bandwidth and on the SNR make the HAALDM requirements highly complex to achieve [RD21; RD88; RD90].

The TOF CW FM Modulation method (also referenced as FMCW) projects an optical signal whose frequency varies with time as shown in Fig. 2.52. The periodic and linear frequency chirp may practically be performed by applying a saw-tooth bias current to the modulator section of a wavelength tunable laser diode. The reflected signal has the same frequency profile shifted by the propagation time as shown by the dotted lines in Fig. 2.52. The emitted and reflected signals are mixed in a square law detector diode whose main ac output is at the frequency difference f_{if} of the two optical signals. The detector output is fed into an amplifier-limiter so that unintentional amplitude modulation is suppressed. Finally, the intermediate frequency f_{if} is measured with a frequency counter and has a direct relationship with the distance travelled by the light pulse [RD21].

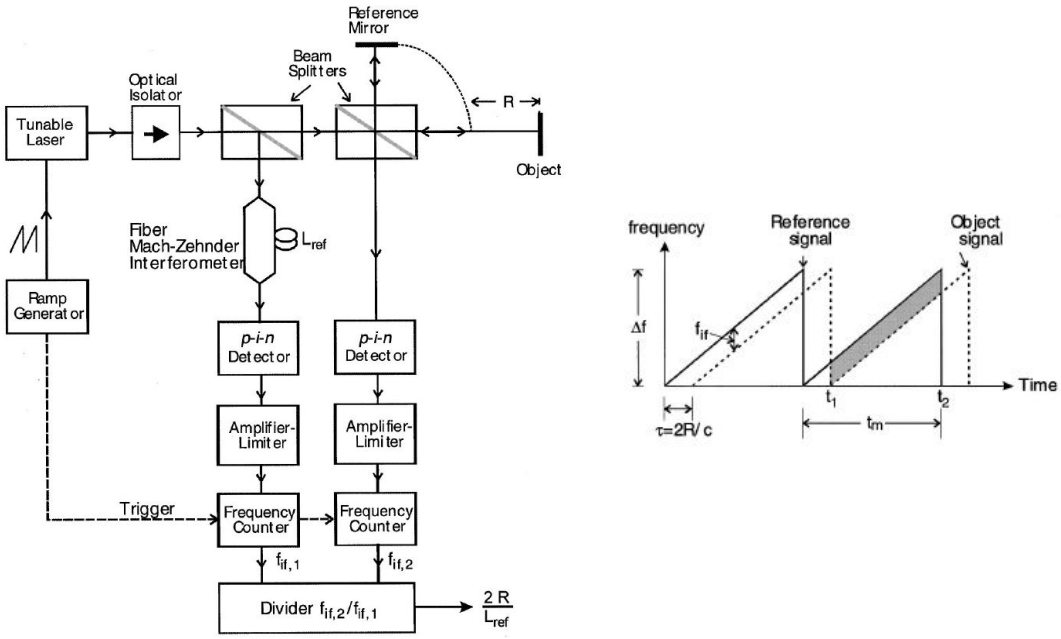

Fig. 2.52 - Setup to implement TOF CW FM Modulation. Taken from [RD21].

Another possibility with TOF is the Two harmonic fs-comb beat signal ranging (Minoshima & Matsumoto approach [RD10; RD11; RD16; RD17], Fig. 2.53). This technique is based on the use of the phase measurement of the inter-mode beats between pairs in the broad and stable optical frequency modes of a optical frequency comb. In this case, for a range up to kilometres, the accuracy can achieve the tens of micrometre level with acceptable complexity (already proved experimentally for 240 m [RD11]).

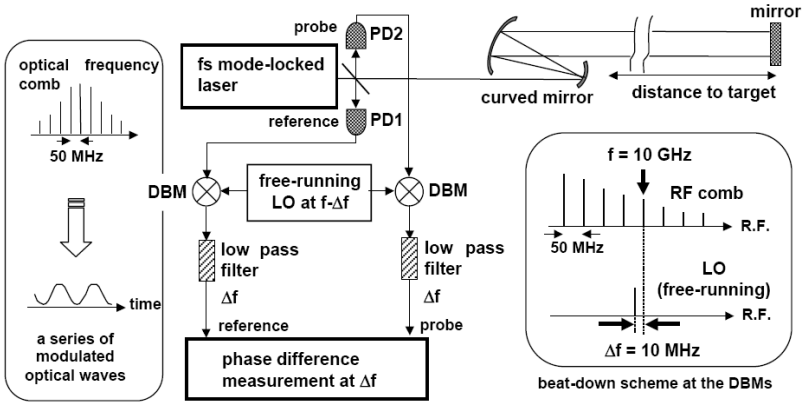

Fig. 2.53 - Setup of the Minoshima & Matsumoto approach implementation. Taken from [RD16].

Interferometry based techniques are inherently high accuracy methods for moderate ranges, limited by the coherence length of the source. Absolute interferometric distance metrology can be implemented by Multiple Wavelength Interferometry (MWI) or by Frequency Sweeping Interferometry (FSI). A synthetic wavelength is generated in both cases, much longer than the optical carrier wavelength; this synthetic wavelength increases with decreasing wavelength difference (in MWI) or sweep range (in FSI). Final resolution depends on phase measurements at the synthetic wavelength.

In MWI, each synthetic wavelength (one or several) is generated using two different and very accurately known optical wavelengths [RD80; RD81], Fig. 2.54. By selecting a small synthetic wavelength it is possible to achieve high resolution (at the micrometer level or even smaller). However the intrinsic ambiguity of the measurement limits the measurement range. As resolution increases, the NAR decreases, and large range absolute measurements are possible only if either MWI with a chain of synthetic wavelengths are used (ensuring that, as the value of the synthetic wavelength decreases, the accuracy associated with each synthetic wavelength is lower than the NAR of the next one), or independent measurements provide a priori range information (for example with TOF). For large ranges, MWI can become indeed a very complex solution.

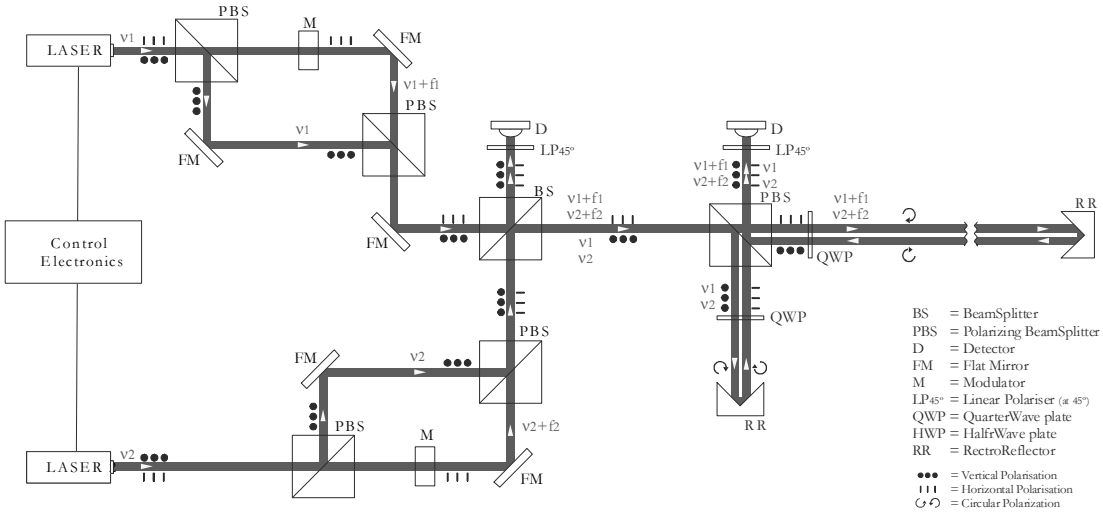

Fig. 2.54 - MWI in super heterodyne mode (one synthetic wavelength). In the main interferometer, beams have different polarizations and frequencies.

The generation of the synthetic wavelength in FSI is based on frequency sweeping the laser source within a given sweep range [RD82; RD83; RD84], Fig. 2.55. As frequency sweeps, detection electronics counts synthetic wavelength maxima (temporal "synthetic fringes") without ambiguity, thus making it particularly interesting for large measurement ranges. Its sensitivity to variations of distance (drift) during the sweep limits the maximum resolution to a few micrometers (although drift can be nulled using an independent metrological system to sense and compensate optical path variations during the sweep). In contrast to MWI, FSI does not requires two independent stabilized and well known laser sources and relies only on a tunable laser and a frequency sweep range measurement subsystem (normally based on a Fabry-Pérot interferometer).

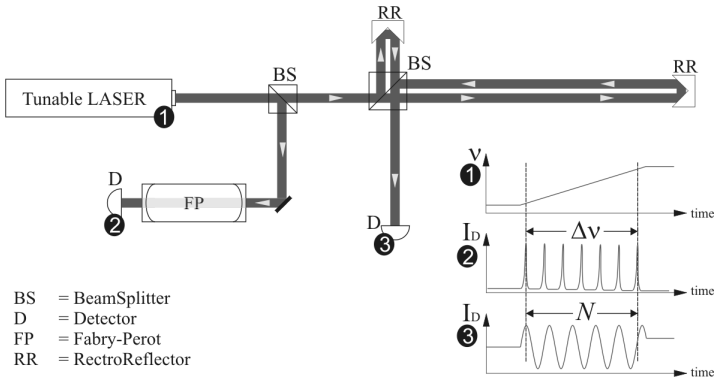

Fig. 2.55 - FSI setup. While the laser sweeps the frequency, the interferometer detector acquires the fringes and a Fabry-Pérot interferometer measures the sweep range by counting the resonances of the cavity.

Other methods to measure absolute distance exist that are, in various ways, based on MWI and FSI (resolutions and ranges are somehow comparable).

A possible solution to achieve high accuracy for large ranges without increasing too much the complexity is to use a DWI (Double Wavelength Interferometry – single synthetic wavelength) sensor with small synthetic wavelength and a FSI based sensor to resolve the NAR. With this combination, accuracies at the micrometre level could be achieved for a range of a few hundred metres.

Recent tunable laser sources for MWI based on a frequency comb generated by a mode-locked fibre laser offer an unprecedent large choice of synthetic wavelengths. Although the complexity associated with the implementation is considerable (the control and management of several synthetic wavelength is far from being a simple issue), the resulting uncertainties are reported to be close to 10^{-7}, enabling nanometre accuracies for large ranges due to the multiple frequency generation [RD85; RD86].

Another possible use of fs-combs for ADM is dispersive interferometry. This technique is normally used for small ranges (< 1m). A work on Fs-Comb Dispersive Interferometry (Seung-Woo Kim approach [RD09; RD14; RD15], Fig. 2.56) demonstrated high accuracy (tenths of micrometers) for an absolute distance of several millimetres. In this technique, the ambiguity is removed using TOF CW AM Modulation. Theoretically, the range can be extended to a few hundred metres. In practice, the requirements on the high spectral sampling and coverage, to cope with the large distance, highly limits the use of the method to long distances.

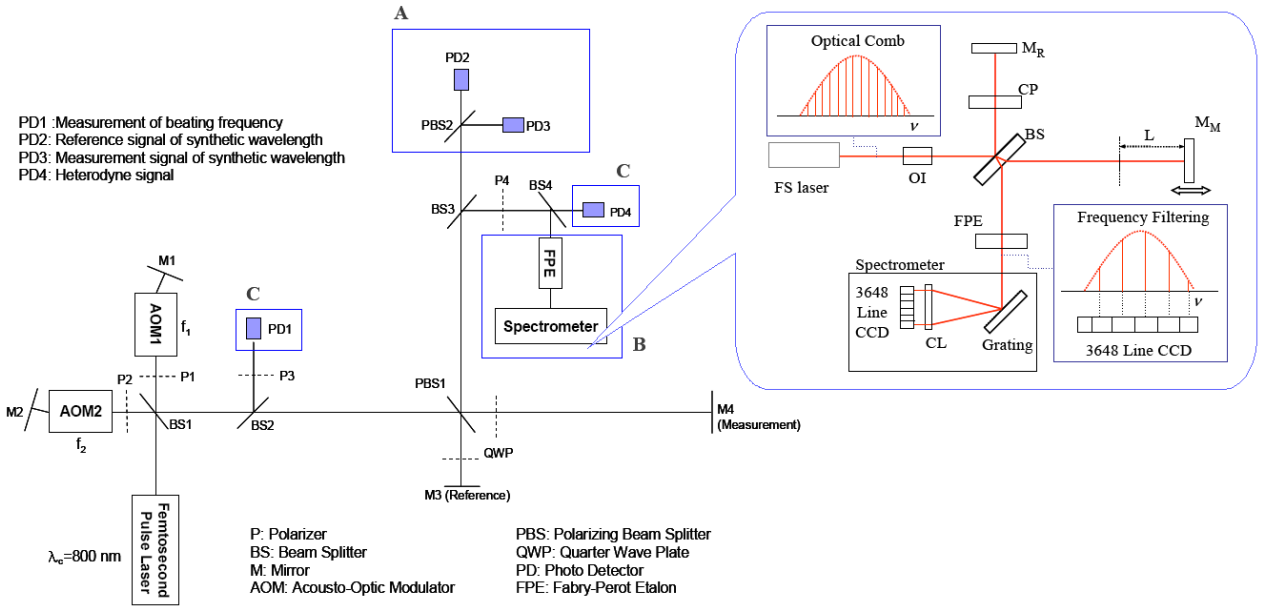

Fig. 2.56 - Setup of the Seung-Woo Kim approach implementation. Taken from [RD09; RD14].

A different approach is the fs-Comb Cross Correlation Interferometry that uses the cross correlation pattern to determine very accurately the absolute distance (Jun Ye approach in coherent mode [RD08], Fig. 2.57). In this case, the maxima of cross correlation tell us that we know that the optical path difference (OPD) is a multiple of the distance between consecutive pulses, with accuracy at the optical wavelength level. The inherent ambiguity can be removed using Two f_{rep} fs-pulse ranging (Jun Ye approach in incoherent mode), by analysing the time interval between a reference and a measurement pulse, retrieving non-ambiguous value of range with low accuracy. It thus seems theoretically possible to achieve kilometres with micrometer (or even sub-micrometer) accuracy, nevertheless considerable requirements on the fs-comb stability have to be complied.

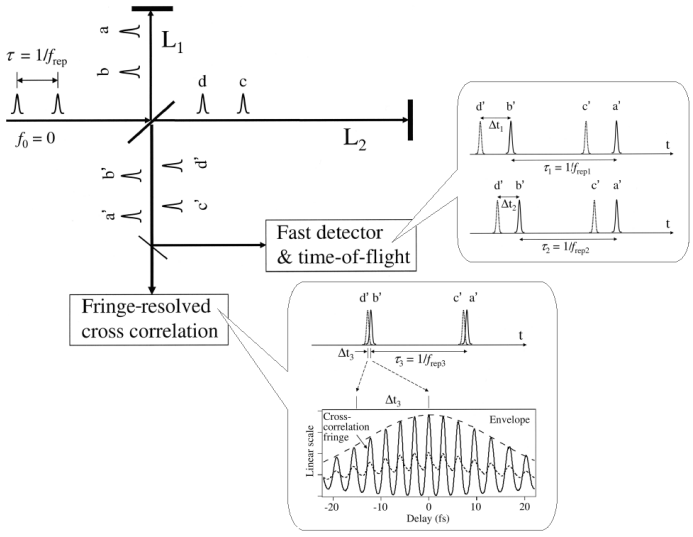

Fig. 2.57 - Setup of the Jun Ye approach implementation. Taken from [RD08].

4 Femto-Second Laser based Concepts

The absolute distance metrology techniques based on fs-Lasers are basically indirect measurements of the time-of-flight or time-delay of fs-Laser pulses. Techniques are based on the measurement of the carrier phase variation or in the determination of an overlapping condition between a reference and a measurement pulse train. The first can be described as an Electrical Heterodyning (EH) method and the second as an Optical Heterodyning (OH) method.

Measuring the carrier phase variation or the overlapping condition parameters will give an accurate but ambiguous measurement of the distance. The absolute distance calculation will only be complete when the integer number of the pulse period is known.

To resolve the number of pulses N in a measurement there are two possibilities: the optical absolute distance sensor based on fs-Lasers must be self-standing, or the metrology system of the instrument, during the high accuracy absolute distance measurement phase, has already information enough to determine N. Several options where already described in the previous Technical Note [AD 4].

The studied concepts were named accordingly to the measurement techniques. Electrical Heterodyning is basically characterised by the carrier phase difference measurement method (between reference and measurement pulse trains). For Optical Heterodyning, considering the option on the measurement approach, on the pulse overlapping procedure and on the detection scheme, several different concepts can be envisaged. In Fact, for optical heterodyning, almost all the combinations of overlapping procedure and detection scheme can generate a concept.

4.1 EH - Electric Heterodyning

Electrical Heterodyning is a technique based on the measurement of the carrier phase variation. This measurement gives an accurate but ambiguous measurement of the distance. The ambiguity is removed with the information obtained with coarse absolute sensors already activated in the metrology chain.

This method is basically characterised by the carrier phase difference measurement method (between reference and measurement pulse trains). The most accurate implementation of EH was done by Minoshima & Matsumoto [RD10; RD11; RD16; RD17], using a two harmonic fs-comb beat signal ranging approach (Figure 4-1). This technique is based on the use of phase measurement of inter-mode beats between pairs in the broad and stable optical frequency modes of an optical frequency comb.

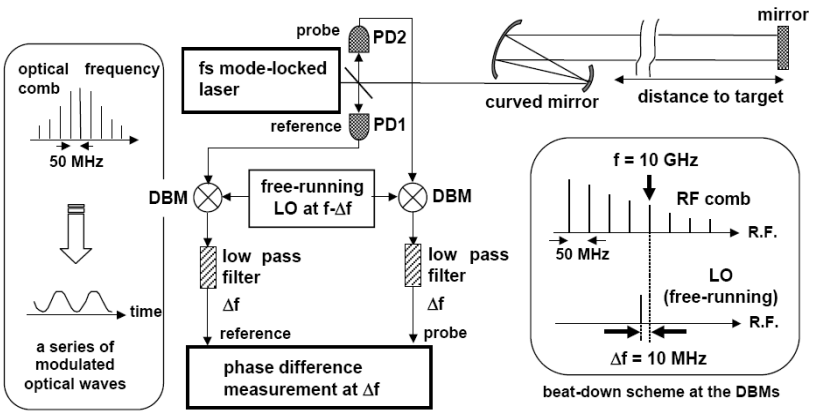

Figure 4-1 - Setup of the Minoshima & Matsumoto approach implementation. Taken from [RD16].

This setup was tested in a 240 m chamber, achieving an accuracy at the micrometre level. The limit on the accuracy results from non-linear residuals with a standard deviation of 1.9 µm, corresponding to a phase accuracy of 0.045º (0.8 mrad) [RD16].

The accuracy of this concept is essentially dominated by the accuracy of the phase measurement. The uncertainty in the f_{rep} measurement is only relevant for distances above the km range.

If the accuracy of the phase measurement, mainly limited by the digital resolution of the phase meter (0.1º for [RD16]), is reduced by a certain factor, or the (10 GHz) frequency is increased, the uncertainties in the distance measurement will decrease accordingly. Considering the current values and the state-of-the-art electronics, although it might be possible, that decrease in accuracy will not be considerable. A possible improvement should also not be done at the cost of a reduction in the measurement frequency. In fact, as it is mentioned in [RD16], each data point was obtained after averaging over 10 s and, to achieve a 10 Hz measurement frequency, a reduction in the accuracy by a factor of 10 might be required $\left(\sqrt{10s/0.1s}\right)$.

4.2 OHFSE - Optical Heterodyning with Frep Scan and Intensity Cross Correlation Envelope Detection

All OH based concepts are based on the determination of an overlapping condition between a reference and a measurement pulse train created in a Michelson interferometer. As the value of the fs-Laser pulse train repetition frequency, f_{rep}, is determined by the dimensions of the laser cavity, a change in the cavity will produce a change in the value of f_{rep}. By changing the cavity it is possible to select/detect the particular value of f_{rep} that, for the particular absolute distance, overlaps the reference and measurement pulse trains of the Michelson interferometer. As different f_{rep} values correspond to different cavity lengths, the required cavity change is a function of both the absolute distance and the selected fs-Laser f_{rep} (Figure 4-2).

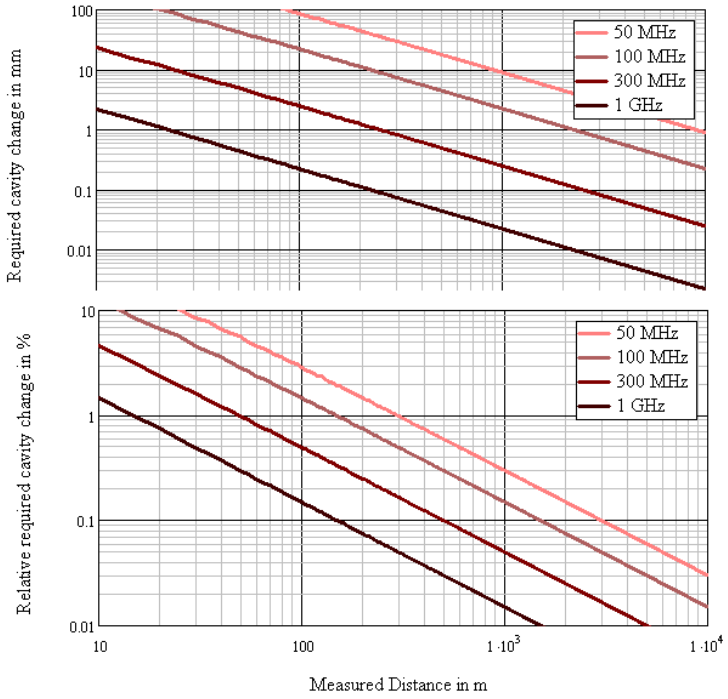

Figure 4-2 – Required fs-Laser cavity change to enable pulse overlapping as a function of the measured distance for different values of frep.

As it is shown on Figure 4-2, the larger the distance and f_{rep} value the smaller is the required cavity change. Considering that the most critical issue of this pulse overlapping procedure is the need to maintain the fs-Laser cavity correctly aligned during the cavity scan, the smaller the required cavity change the less complex is the implementation; this fact puts a constrain in the minimum measurable distance. To achieve small distances, a larger f_{rep} should be selected.

This concept is based on the determination of the maximum of the Intensity Cross-Correlation envelope. Figure 4-3 shows a simulation of the intensity Cross Correlation pattern generated by a mathematical model considering the influence of the different parameters stability level.

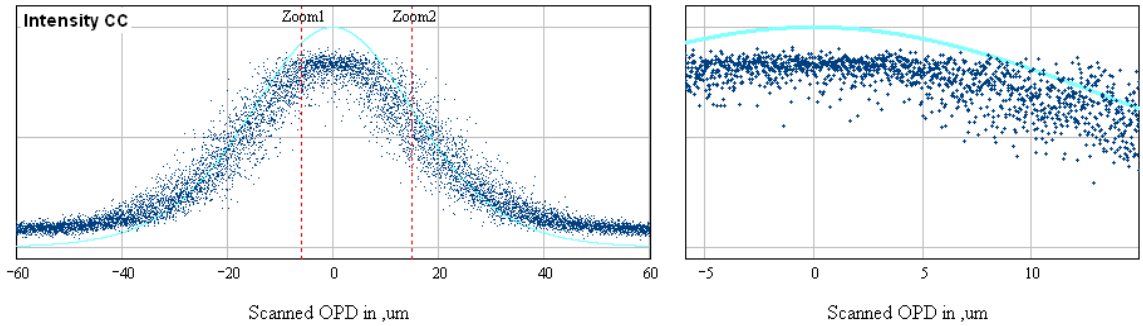

Figure 4-3 – Intensity Cross Correlation patterns for ΔL = 1000 m, frep stabilized to 3x10-12@ms, 2% of multiplicative and additive noise (frep = 100 MHz, pulse width 80 fs).

The range and accuracies obtained are highly dependent on, respectively, f_{rep} value and pulse width. Two different sets of fs-Comb parameters where selected to characterize the concepts, the first corresponding to a Erbium-doped fiber frequency comb with f_{rep} = 100 MHz and pulse width of 80 fs, and the second to a Ti:Sapphire frequency comb with f_{rep} = 300 MHz and pulse width of 25 fs.

The analyses showed that it is possible to achieve sub-micrometre accuracy down to 0.3 µm with an Erbium-doped fiber frequency comb, and down to 80 nm with a Ti:Sapphire frequency comb. The difference is due to the smaller pulse width of the Ti:Sapphire frequency combs, nevertheless, with smaller pulses they become more sensitive to the f_{rep} stability level, requiring for the same distance a higher level of stabilisation. Erbium-doped fibre frequency comb will therefore be able to have a larger measurement range (up to several hundred km).

The different f_{rep} values do not influence the accuracy of the measurement but they are a limiting factor for the minimum measurable distance (100 MHz repetition frequency limits the range down to 100 m, where 300 MHz limits down to 30 m).

4.3 OH2LE - Optical Heterodyning with 2 fs-Laser Phase Tuning and Intensity Cross Correlation Envelope Detection

As an alternative to overlapping the pulses from a reference and a detection arm by scanning the f_{rep}, a scheme can be implemented that overlaps the pulses from the detection arm with pulses from a second fs-laser with its f_{rep} locked to the same reference oscillator. By phase-shifting the electronic signal from the reference oscillator to the f_{rep} stabilization loop of the second laser, the pulses from this laser can be delayed in time with respect to the fs-laser that is used for the length measurement. In this way, the pulses from these two separate lasers can be overlapped in time without the need for moving parts. A phase-shifter at the fundamental f_{rep}-frequency with a tuning range of 2π suffices to tune the delay over the full pulse-to-pulse

time delay T = $1/f_{rep}$. With this technique it should be possible to measure intensity cross-correlations between the pulses from the two separate lasers.

In terms of performance, the difference between OH2LE and the previous concept FSE, is due to the fact that there is an additional timing jitter (the instability of the phase between the two laser pulses) and that we need to measure the phase difference of the two laser pulses with a particular accuracy level.

The uncertainty in the phase measurement completely dominates the concept accuracy, limiting its performances at the micrometer level (considering the same stability of the EH concept). In terms of performance, this concept is similar to the EH concept, being limited in range in the same way as the FSE concept but only for the maximum distance.

4.4 OHOSE - Optical Heterodyning with OPD Scan and Intensity Cross Correlation Envelope Detection

By changing the length of the reference arm, it is possible to change the interferometer OPD in order to make it equal to an integer number of pulse periods (times the speed of light), thus enabling the overlapping of the reference and measurement pulses. The absolute distance is determined knowing how much the length of the reference arm changed from the reference position and the integer number of pulse periods.

This procedure is the less complex to implement as it does not have any influence in the fs-Laser operation. However, to allow a complete scan between consecutive pulse periods, the required scan range, although constant for different measured distances, becomes extremely large for small values of f_{rep}. Although the alignment of this "delay line" in the reference arm is not a critical issue, the fact that the scan must be know with an accuracy bellow the required absolute distance measurement accuracy limits the maximum OPD scan range to a few hundred millimetres. As a consequence, the level of tuning can only be effective (scan from two consecutive pulse overlaps) for f_{rep} values at the GHz level.

To characterize this concept, a Diode laser frequency comb with f_{rep} of 30 GHz and pulse width of 1 ps was considered. The resulting accuracy is at the micrometer level, and the measurement range, depending on the f_{rep} stabilization, can go up to several tens of km (there is no minimum range limit).

4.5 OHFSF - Optical Heterodyning with Frep Scan and Interferometric Cross Correlation Fringe Detection

This concept is based on the determination of the maximum of the Intensity Cross-Correlation envelope a subsequent accuracy improvement by analysing the interferometric fringe pattern (the fringe phase do not necessarily correspond to the envelope maximum, nevertheless this phase can easily be determined). Figure 4-4 shows a simulation of the interferometric Cross Correlation pattern generated by a mathematical model considering the influence of the stability issues of different parameters involved in the distance measurement.

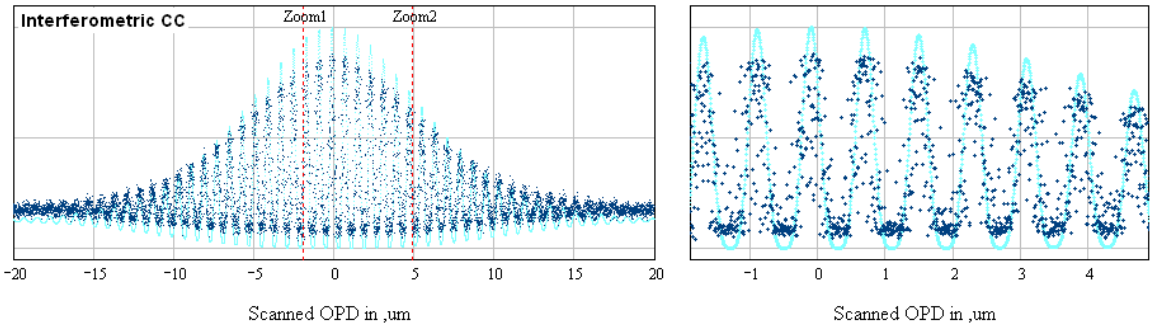

Figure 4-4 – Interferometric Cross Correlation patterns for ΔL = 30 m, f_{rep} stabilized to $3x10^{-12}$@ms, pulse to pulse phase slippage stability $\delta\Phi_{ceo}$ = 150 mrad, 2% of multiplicative and additive noise (f_{rep} = 300 MHz, λ = 800 nm, pulse width 25 fs).

In order to have a smaller pulse width and a maximum level of pulse to pulse phase slippage stabilization, a Ti:Sapphire frequency comb is a preferable choice for this concept, and was thus selected to characterize it. Due to the sensitivity of the fringe pattern to the f_{rep} stability, a higher stabilization (compared with other concepts) is required.

This concept is the most accurate one. Accuracies can even be of only a few nanometres, but at the cost a high stability reference.

4.6 OHFSSSF - Optical Heterodyning with Frep Scan and Interferometric Cross Correlation Single Shot Fringe Detection

In order to reduce the sensitivity of the fringe pattern to the f_{rep} stability, this concept makes use of a single shot detection. In the previous FSF concept, while a delay line scans the OPD a detector acquires a CC pattern showing all the typical effects of timing jitters. In this concept, as the delay line scans the OPD, a single shot detection system detects a clear cross correlation fringe pattern (with the detail defined by the number of CCD pixels) for a particular position of the delay line. That position is affected by the timing jitter, being this the main contribution to the concept uncertainty. The minimum achievable uncertainty of 20 nm, determined by the detail of the CC pattern, is higher than the FSF concept but the measurement range was extended.

4.7 OHD - Optical Heterodyning with Dispersive Time to Space Conversion

The key of this concept is to first convert incoming ultrafast time-domain optical signals into spatial optical signals. The time-to-space conversion technique employs a femtosecond pulse imaging technique that uses time cross correlation between a transform limited reference pulse and the measurement signal pulse. This time cross correlation can be performed with nonlinear three-wave mixing either in the spectral domain or directly in the time domain [RD101].

The time domain approach, also called Transverse Time Delay (TTD) is capable of performing single-shot autocorrelation measurements over a wide range of laser-pulse widths from femtoseconds to picoseconds.

In general terms, this technique allows measurement ranges in the order of tens of picoseconds with resolutions of 20 fs or less (few micrometers in OPL).

4.8 Power Consumption for the Different Detection Methods

The issue of power consumption and laser power requirements, regarding its use in the different concepts illustrated in this document, can be dealt with a bottom-up approach, starting from the minimum power requirements at detector level.

In the Optical heterodyning case, although different methods of detection in the cross-correlator can be considered, like SHG and TPA, different detector materials and structures, literature shows that a common measure of the capability of producing a cross correlator pattern is termed as sensitivity, as presented in previous chapters. Although current and conventional methods point out to a 1 mW^2 sensitivity or higher, recent results obtained using devices with internal gain mechanisms show that is possible to obtain cross-correlation in the 2nd order detectors with values reaching the range of 10^{-4} to 10^{-7} mW^2.

In this bottom up approach, we shall consider a conservative sensitivity value of 1 mW^2 , covering the possibility of using a high-end detector, with sufficient SNR to be able to post-process data, and considering also an expectable coupling loss to the detector surface.

Going up in the metrology sensor chain, a specific loss factor must be considered in the physical implementation of the cross-correlator – interferometer, as well as an external loss factor associated to the telescope coupling efficiencies, retroreflectors and propagation.

Although these loss factors can be engineered to reach minimum levels, by optimizing optical structures, coatings, etc, an overall loss of 6 dB shall be considered. This will mean that only 25% of the raw laser energy will in fact reach the detector.

The Table 4-1 shows the minimum power requirements for the different laser sources, taking into account a 1 mW^2 sensitivity requirement and typical frequency/pulse widths configurations for each laser, according the what was already presented in TN2 [AD 4].

This table also includes the typical Wall Plug Efficiency (WPE) values for each laser source.

Table 4-1 Laser power requirements for 1 mW^2 sensitivity

Laser	$P_{average}$	P_{peak}	$P_{average}$ required after 6dB loss	WPE	Laser Power consumption
Ti:Saph	1.6 µW	0.6 W	6.4 µW	1%	640 µW
Er:doped	2.0 µW	0.5 W	8.0 µW	10%	80 µW
Yb:doped	2.2 µW	0.45 W	8.8 µW	15%	58.6 µW
Diode laser	140 µW	7 mW	560 µW	40%	1.4 mW

In spite of using commonly accepted values in terms of WPE, one must consider that these values correspond to typical equipment configurations and typical power levels in normal operation. This means that this efficiency factor is not exactly scalable, and that this value cannot be used for any laser power level setting, within the equipment dynamic range. In other words, we cannot infer directly that a 50 mW Ti:Saph will consume 5W of electrical power whilst the same laser, working at 0.5 mW average power, will need only 50 mW out of the plug! There are a set of ancillary equipment supporting the laser (cooler, pump laser, electronics, …) that will have a constant power consumption much higher than this. So the values showed in

the previous table as power requirements after considering WPE are only indicative and the real power requirements must be analyzed case by case. In any case, this table indicates that fibre lasers can be the most economic laser sources, when comparing with the other two solutions.

In the Electrical Heterodyning concept scheme, this bottom up approach shall consider different aspects. The concept considered here is the one form Minoshima § Matsumoto, illustrated already in TN2 [AD 4].

In this case, the minimum sensitivity factor is associated to the vector or phase meter, considered as a minimum signal amplitude level to reach the required accuracy. This signal level is function laser source levels, and the loss factors related to propagation, coupling optics, optical/electrical efficiency and finally, losses associated to the different electrical processing stages along the signal network.

It should be noted that, in opposition to the OH schemes, the Electrical Heterodyning processing is basically an all-electrical processing scheme after the optical pickup in the arms of the interferometer. This means that a wider range of amplification schemes can be arranged in order to reduce the minimum power requirements.

At the level of optical detection, linear detectors are used, in opposition to the ones using second order effects – as in TPA – and can be associated to low noise amplifiers with moderate gains (up to 15 dB per stage at these kind of frequencies).

The base sensitivities for this concept are, as mentioned before, the limits of operation of the phase meter. High accuracy systems can resolve 0.1º (or lower) in phase differences by sample averaging, but require significant level of input signal. Typical values of 100mV are the minimum requirements for a standard equipment in high accuracy phase metering, as the HP8508.

Going back in the processing chain, according to Figure 4-1, and analyzing only the network corresponding to the measurement arm of the interferometer, we have different loss sources, as a coupling filter, which have typical values of insertion loss of 1 dB. The DBM, Double Balance Mixer, typically shows higher losses, in the order of 8 dB.

The detector itself, plus its corresponding amplifying chain, and considering a Optical – Electrical conversion factor of 50 (over a 50 Ohm impedance), may reach a positive gain of 30 dBs (in terms of mA in, mV out).

Finally, and considering the same optical configuration, a 6 dB loss is associated to the coupling efficiency at the level of the optics in the telescope, retroreflector and propagation. This will give a net gain of :

$$G = -1\ dB_{filter} - 8\ dB_{DBM} + 30\ dB_{detector} - 6dB_{optical} = +15dB_{net\ gain}$$

Considering a detector responsivity of 1 A/W, this will imply that to obtain a 100 mV signal level at the phase meter we will need 3 mW laser power.

Given a 1% WPE efficiency for the Ti:Saph, we will need at have a 300 mW power consumption. Although the same discussion on the “real” WPE applies here also, this value shows that EH is considerable less efficient than the OH techniques.

The last detection scheme to be considered is the Dispersive time to space concept, already described in TN2 [AD 4]. Figure 4-5 show the typical operating power requirements are a few decades above the other concepts, driving the power levels to the hundred of mW range. This is due to the fact that this scheme uses a parallel processing scheme, this dividing the optical input over a large time window / large number of detectors in the CCD.

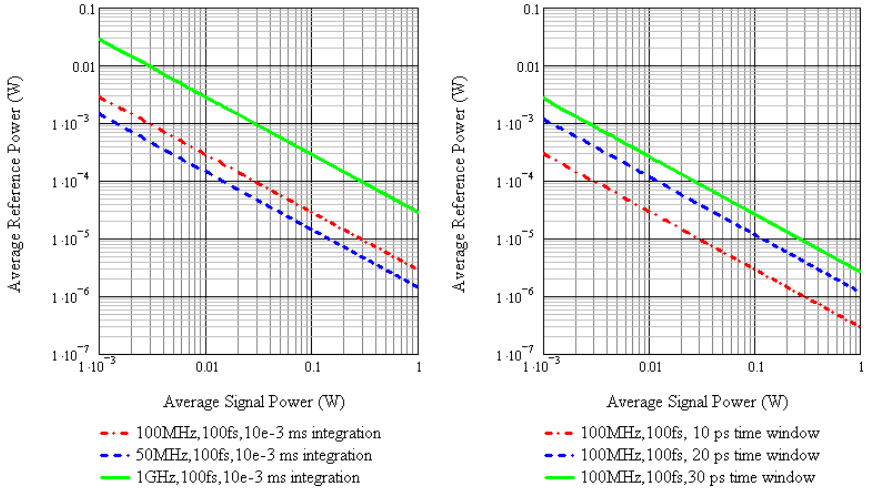

Figure 4-5 - Minimum power requirements for a T2S dispersive implementation, as function of f_{rep} (left), and as a function of the maximum time window, both considering 1 microsecond integration over a 1024 element sensor array.

4.9 Common Issues

The mathematical models used to determine the different concept performances took already in consideration a large number of parameters, leading to a realistic analysis.

There are, however, other factors not considered in the simulations that can influence the sensor performances and thus must be taken into account in the sensor development. The main relevant issues are the laser coherence length, the effect of unbalanced beams in the interferometer, material dispersion, spectral filtering of the measurement beam, and satellite drift.

4.9.1 fs-Combs and Coherence Length

The coherence length of the laser is an important issue when a concept is based in the phenomena of interference. While in a cw laser it is very simple to determine the coherence length, basically of the order of the inverse width of the laser linewidth, in a fs-Comb the issue is not so straightforward.

A fs mode-locked laser, emits a periodic train of ultrashort pulses, all of them related to a single pulse circulating in the laser cavity, and there is a strong phase relation between subsequent pulses, and even between pulses with a large temporal distance. The shape of the coherence function quickly decays on the time scale of a pulse duration, but then it returns at time values corresponding to integer multiples of the pulse spacing, describing the possibility of interference by superposition of such pulses. In a way, we have very long-term coherence, but can only observe it for time delays which allow the overlap of pulses. The Fourier spectrum of such a pulse train is not continuous, but rather has the shape of a frequency comb, and the real coherence time (describing the long-term phase relationship between distant pulses) is of the order of the inverse width, not of the envelope of the Fourier spectrum, but of the single peaks of the frequency comb – and these can be very narrow indeed. The real linewidth is determined by several number of parameters, including the f_{rep} and f_{ceo} noise/stability.

As a practical rule of thumb, people usually measure linewidths on the order of 1 MHz for the comb lines of a Ti:Sapphire laser when only a commercial Cs clock is used for stabilization; this value already imply a

coherence length of several hundred meters. These linewidths can be improved, even to sub-Hz level [RD133], by adding higher short-term stability, for example, by locking to an optical high-finesse cavity or a stabilized cw laser. It is thus possible to say that coherence length will not be a critical issue is measurements are to be made up to a few kilometres.

For distances larger than a few kilometres, special care must be taken in the selection of the fs-laser and of the level of stabilisation of the different parameters that fully characterise the comb. In this case, it will be necessary to determine the temporal coherence of the particular train of ultrashort pulses for the particular fs-laser system [RD28; RD147; RD148].

4.9.2 Unbalanced beams

In the simulations presented in this work, the intensity ratio between the measurement and reference pulses was always considered to be 1. However, a smaller ratio will reduce the fringe visibility in interferometric cross correlation detection and might influence the accuracy of the data processing algorithm. Nevertheless, as is can be seen in Figure 4-6, even with a 0.5 ratio the envelope maximum and the fringes can still be clearly determined. The model was used to test this effect and, with ratio down to 0.5, showed that the level of performances was maintained.

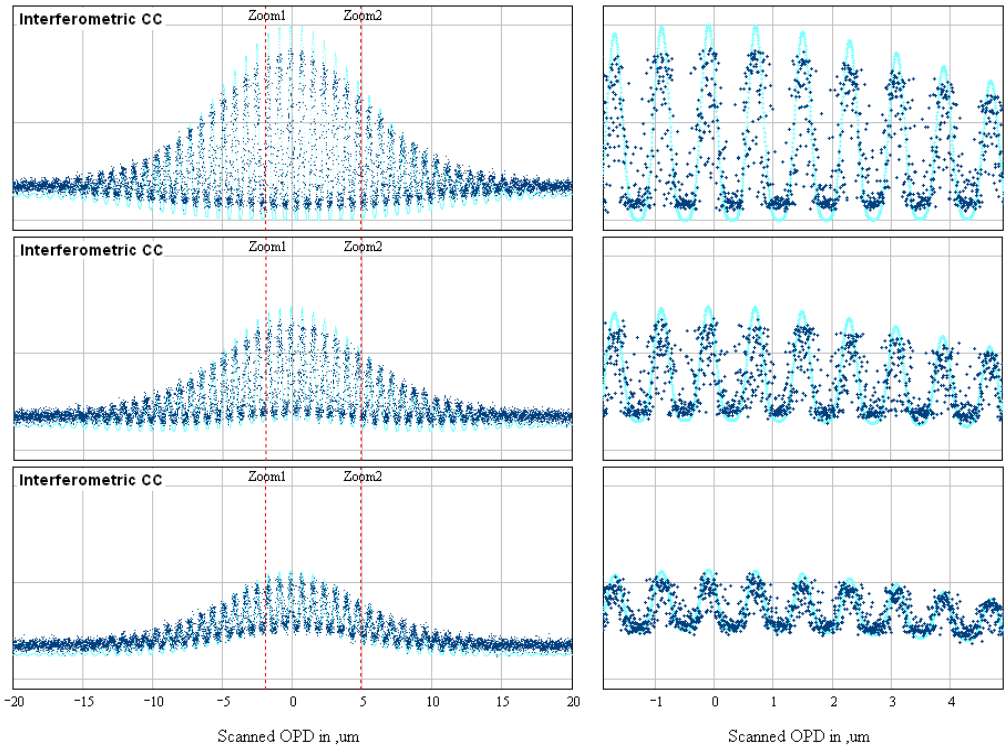

Figure 4-6 - Interferometric Cross Correlation patterns for ΔL = 30 m, f_{rep} stabilized to ACES, pulse to pulse phase slippage stability $\delta\Phi_{ceo}$ = 150 mrad, 2% of multiplicative and additive noise with a measurement to reference pulse intensity ratio of 1 (top) 0.75 (middle) and 0.5 (bottom) (f_{rep} = 300 MHz, λ = 800 nm, pulse width 25 fs).

4.9.3 Material Dispersion

Dispersion on an optical material affects both the shape and the phase of the pulse electrical field. The zero-order term, the phase velocity of light, only adds a general constant phase, i.e., a shift in the carrier-envelope phase. The first-order dispersion (the inverse of the group velocity of the light pulse) does not influence the pulse shape, but leads to a delay in the pulse arrival time at a certain given location. The second-order term is the group velocity dispersion (GVD), which is also known as the linear chirp, leads to a broadening of the pulse in time. The third-order term, also called quadratic chirp, does not simply broaden the pulse in time but leads to a reshaping of the pulse form.

Second and third-order dispersion can affect the cross correlation pattern in two different ways, depending on the location of the dispersive material:

1. If the dispersion occurs before the interferometer beam splitter, then we will have a balanced situation where the correlation between two equal pulses will always lead to a symmetrical pattern (independently of the pulse shape or phase). Nevertheless, the total amount of material equally crossed by the reference and measurement pulses can be of the order of several tens of millimetres.
2. If the dispersion occurs only in the measurement arm, although it seems unlikely to have extremely unbalanced arms, the resulting main question is to know in what extent the small amount of difference between pulses will change the cross correlation pattern and how this change will affect the measurement.

Both conditions were simulated [AD 4] leading to the following conclusions.

In the case of equally affected pulses, the maximum of the intensity cross correlation pattern or the maximum of the envelope of the interferometric cross correlation pattern will never change its position. The only effect of dispersion in an intensity cross correlation will be a symmetrical broadening of the pattern, even in the case of a asymmetric pulse shape (caused by a third order effect). Note that the broadening of the pulse will decrease the accuracy but, at the same time, show less sensitivity to some noise sources as f_{rep} and f_{ceo} instabilities. For the case of interferometric cross correlation detection, as long as the envelope provides an accuracy of at least $\pm\lambda/2$ (to enable the high accuracy detection within the fringes) the performance will not be affected.

In the case of unequally dispersed pulses, for the second order effects, the conclusions are basically the same as the one taken previously for equally dispersed pulses. The only effect is the broadening of the correlation pattern without any influence in the performance of the sensor. The third order effects, as they introduce a shift in the position of the maximum of the correlation envelope, can jeopardize the performances if they are not taken into account in the measurement calculation. Although it is necessary to have a considerable amount of dispersive material (in order to notice the effect in the performances, it was necessary to consider 10 mm of fused silica) special care must be taken with this quadratic chirp in extreme conditions, and unequally dispersion can and should be avoided/controlled.

4.9.4 Spectral Filtering

Another non-ideal situation can be caused by the fact that the telescopes can be smaller than the diffraction spot size. This means that, during the round trip of the measurement pulse train, the fs-laser radiation will suffer a spectral filtering. In this case, if a portion of the red side of the spectrum is lost, it is equivalent to take a longer pulse in the measurement arm, while keeping the phase zero, considering that if spectral components are cut away, then we are effectively increasing the Fourier-limited pulse duration: a broad spectrum is needed to get a short pulse. The consequence is, again, a broadening of the correlation pattern, leading to the same previous conclusions.

4.9.5 Satellite Drift

When a concept is based in an OPD scanning in the reference arm, generating the cross correlation pattern, it is not realistic to assume, at least in space environment, that the distance under measurement is constant during that time frame. Thus, in a situation where the sensor needs some time to perform the measurement, it is important to assess whether the movement during that period of time (normally designated by drift) can be neglected or must be taken into account. The effect of drift in an intensity and interferometric cross correlation pattern results in a shift in the centre of the envelope and an envelope shrinkage/growth effect (depending on drift signal).

To determine if drift can be neglected, three parameters must be taken into account: the drift speed, the measurement duration and the required measurement accuracy. As an example, consider a drift of 1 µm/s and a measurement duration of 0,1 s. In this case, the maximum error introduced by the drift would be 100 nm, which could be neglected if the required accuracy was in the micrometre level. If this effect could not be neglected, more than one option exists to overcome this issue [AD 4]. A possible approach would be to do two consecutive measurements with different OPD scan characteristics. Considering that the drift speed is the same for the two measurements, using a triangular shape for the OPD variation in the reference arm corresponds to a change in the sign of the OPD variation velocity from scan to scan. In this case, any two consecutive pairs of measurements would be affected by the same amount of drift error but with opposite signs. Simple mathematics would immediately give the correct distance and would also be possible to also determine accurately the value of the drift speed.

4.9.6 Pulse Overlapping Procedure

Optical Heterodyning techniques require pulses to overlap or, at least, to be partially overlapped (considering the possible large range of separation). The maximum separation between reference and measurement pulses is a function of the f_{rep}, and equals the non-ambiguity range. The overlapping procedures will take its time and will have implications on the sensor response time when, and only when, the distance to be measured changes significantly (more than the detected cross correlation pattern scan).

It is not possible to do an estimate of the time required to achieve overlapping without specifying the selected concept and the selected concept parameterisation. This duration will clearly depend on the selected procedure and also on the availability of additional information.

As, an example, the coarse knowledge of the absolute distance (for example, from the RF metrology) can be used to help the pulse overlapping procedure by closing down the required ("blind") scanning range. Consider a fs-Laser with f_{rep} = 300 MHz to measure an absolute distance of exactly 100 m. As the pulse period is 0.999308 m, an initial measurement of the distance with an uncertainty of 10 mm indicates that the absolute distance of 100 m (OPD of 200 m) corresponds to 200 complete pulse periods plus an additional fraction of a period. If the technique requires the pulses to overlap by, for example, a change in the f_{rep} value, knowing that the absolute distance is within 100 ± 0.01 m tell us that overlapping is achieved when f_{rep} is within 299.792 ± 0.030 MHz. Thus, to overlap the pulses, it is only required to scan f_{rep} of 0.06 MHz instead of 1.5 MHz (scan for a complete period), reducing both the complexity and increasing the speed of the overlapping process.

In terms of overlapping procedure:

- in f_{rep} scan with f_{rep} = 300 MHz to measure an absolute distance of 100 m, in the worst case, it is required to scan f_{rep} of 1.5 MHz to achieve overlapping, corresponding to a cavity change of 1.2 mm; in

- in OPD scan with f_{rep} = 30 GHz, the ambiguity, or equivalently the required path change to achieve overlapping, is 11 mm.

Thus, the time required to achieve overlapping is dependent on how fast we can scan over the above mentioned (as an example) ranges, i.e., on the speed of the piezo translation table. It seems thus achievable to have sub-second durations.

4.10 Concepts Best Performances

Two basic techniques where studied, Electrical Heterodyning, based on the measurement of the carrier phase variation, and Optical Heterodyning based in the determination of an overlapping condition between a reference and a measurement pulse train. For Optical Heterodyning, several overlapping procedures and detection scheme were identified, and almost all the possible combinations generated a concept.

From a technological point of view, the development of robust, compact and reliable fs-lasers for use in space-based applications is feasible. Also the additional technological challenges of stabilizing f_{rep} and even f_{ceo} in such a laser system seem achievable.

The performance of the different concepts showed a capability to achieve sub-micrometer accuracy for ranges up to several kilometres (Figure 4-7). Different levels of accuracy and measurement ranges will require different level of stability and different types of detection schemes. On the whole, there is a gamut of options that allow a sensor tunability in terms of technological complexity versus requirements.

If, for the one hand, Interferometric Cross Correlation Fringe Detection (OHFSF and OHFSSSF) is the key to create a high accuracy sensor, down to the nanometre level, on the other hand, its sensitivity to timing jitter reduces the measurement ranges to a few kilometres and puts stringent requirements on the frequency stabilisation technology.

Intensity Cross Correlation Envelope Detection can also achieve sub-micrometre (hundreds of nanometre) accuracy (OHFSE). Being less sensitive to timing jitters, it can have a larger measurement range, up to several tens of kilometres, and is less demanding in terms of stability requirements.

If requirements are not better than the micrometer level, other options are available (EH, OH2LE, OHOSE and OHD) with different implementations and different specific characteristics (bandwidth, power requirements, complexity, etc.).

Figure 4-7 illustrates the large variety of possibilities of using fs-laser based concepts in absolute distance metrology.

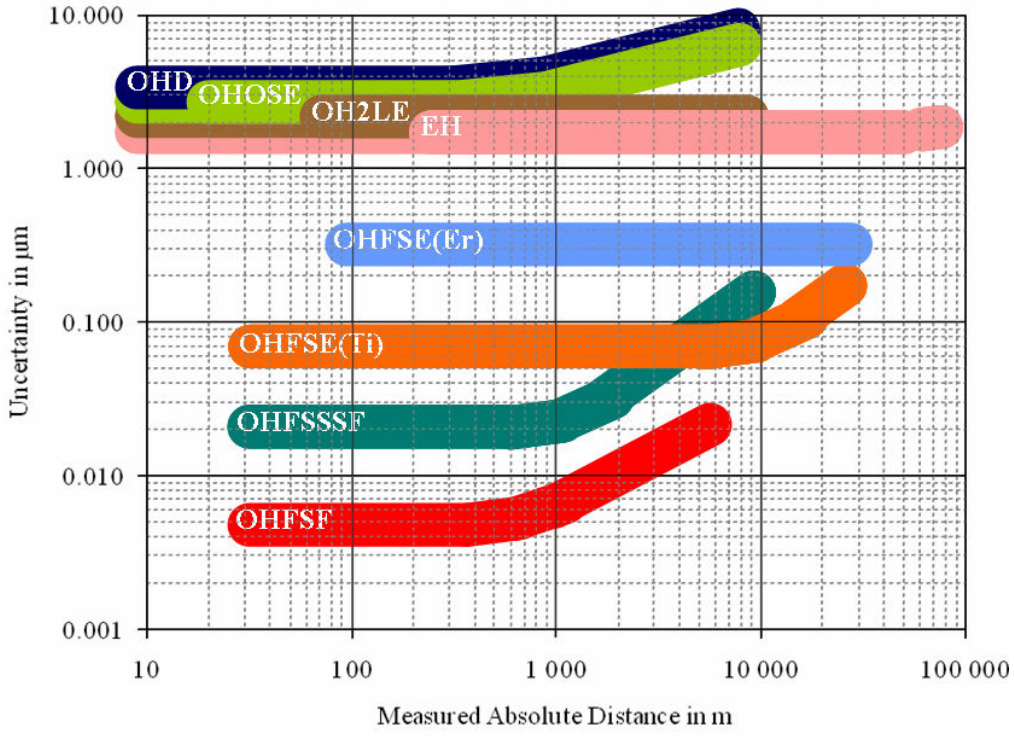

Figure 4-7 – Best performances for fs-Laser based absolute distance metrology concepts.

4.11 Concepts Applied to Absolute Difference and Relative Measurements

Although the objective of this study was the use of fs-Laser based sensors to measure long absolute distances, the use of the previous concepts to perform absolute difference or relative measurements should not be disregarded.

If the goal of the absolute metrology is to enable the co-phasing between telescopes in Free Flyers (FF), which collected light will be recombined in a central hub, then, in order to reduce the OPD between telescopes, we must measure the difference between the distances $\overline{FF1-HUB}$ and $\overline{FF2-HUB}$ (Figure 4-8) and reduce it as much as possible. If the co-phasing is the only objective of the metrology, then it is not necessary to perform the two large distance measurements between FF and hub, and an Absolute Difference measurement configuration where the interferometer arms are defined by the FF (bottom of Figure 4-8). Instead of a reference arm, we have two arms and the absolute measurement will directly give the $OPD = \overline{FF1-FF2}$, with the advantage of reducing the number of sensors to half.

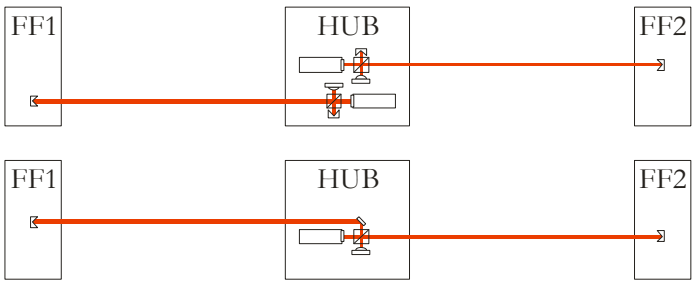

Figure 4-8 – Absolute distance configuration (top) and Absolute difference configuration (bottom).

In terms of concepts, the major difference is that, instead of a measurement using different pulses, we will use exactly the same pulse, i.e., in the case of Optical Heterodyning, from the analysis of a cross correlation pattern we move to an analysis of an auto correlation pattern. Thus, all the issues related with instabilities associated with the correlation between different pulses are gone. The distance between the FF and HUB will only be relevant for the definition of the beam launching optics.

In terms of performances, the concepts would be able do even better than what is presented in Figure 4-7 for the lower ranges, using less complex frequency references, thus becoming less complex. The fact that the overlapping would be much easier to achieve also contributes to the reduction of sensor complexity.

Another possibility is to use the interferometric cross correlation concepts (OHFSF and OHFSSSF) as relative metrology sensors. In this case, the sensor, in an absolute difference configuration, would be locked to a fringe in the cross-correlation pattern (Figure 4-4), enabling a relative accuracy equal or better than the one for the absolute measurement, i.e., at least, at the nanometre level. This type of implementation would have similar performances compared to typical relative metrologies built around cw lasers but, the same sensor, would provide both relative and absolute difference measurements without requiring any hardware change.

5 Missions and requirements

5.1 Changing missions and requirements

At the start of this project (2006) four missions were identified as potential candidates for the use of FS-based metrology for formation flying. These missions were Darwin, XEUS, LISA and the LDI mission for the determination of the Earth's gravity. During the first to phases of the projects it became clear that the LISA requirements were too challenging to meet with the current state of the fs-technology. For the LDI mission the requirements could roughly be met using a high end fs-metrology system. As a consequence however the complexity of such a system would be greater that that of the proposed heterodyne interferometer. Therefore the application of fs-metrology to the LDI mission seemed illogical. The best fitting candidate missions remained Darwin and XEUS. For these two missions a relatively simple fs-based distance measurement system could be designed, which would be very competitive to the proposed DWI or FSI systems.

For WP4000 of this project the XEUS mission has been selected by ESA for studying a detailed fs-based distance metrology system. The metrology system tailored to the XEUS application can be used as well for Darwin with minor modifications. The reason for ranking XEUS at the first place is that this mission has been selected for the Cosmic Vision programme but Darwin not or at least not for the first slot of the programme.

In the meantime the XEUS mission has been replaced by the IXO (International X-ray Observatory) mission and that has been formally announced by NASA, ESA, and JAXA mid of this year (2008). IXO shall be a joint cooperation of NASA, ESA, and JAXA.

Apparently, the IXO mission lost the formation flying part and the free flying mirror spacecraft as well as the in formation flying detector spacecraft are combined now to one single spacecraft. The focal length of the X-ray telescope is further shortened to around 15-20 m (50 m at the very beginning and 35 m during our investigation of the fs-based metrology system).

The detector part of the instrument is deployed via multiple extendable masts that have been developed for the Shuttle SRTM radar mission. SRTM used one extendable mast of 60 m length. The same technology is planned to be used for Nustar needing one extendable mast of 10 m length.

Taking 4 masts instead of 1 increases the stiffness of the construction carrying the detector part. The mast can be covered with a light tight curtain. Any laser ranging technology can be used now without disturbance to the X-ray detection path. Lateral displacement can be detected by a simple camera system like a modified star tracker and some LED targets.

The architecture of the IXO instrument is based of a spacecraft bus carrying the solar panels. The mirror part is rigidly mounted on a stiff cone. The length of this cone is adapted to the fairing of the launcher, an Atlas V 551 rocket. The focal plane is deployed at the other side of the spacecraft bus and the mast length is between 7 and 10 m.

The required metrology to track and stabilise the focal length of the telescope is drastically reduced now and the requirements are very relaxed.

The second application of laser metrology could be the alignment of petals or individual mirror shells within the entire mirror. All mirror concepts and two of them are currently under discussion assume that no alignment of the petals is required. The alignment of the shells will be done already on ground and no realignment is planned in orbit. So, also this measurement is not required anymore.

As the LISA mission cannot be covered by HAALDM and the requirements on an LDI mission are difficult to achieve with HAALDM the remaining application is Darwin. Darwin will be a formation flying instrument with variable distance between the telescope spacecraft and no further reduction of complexity is

possible from the formation flying point of view and the required related metrology. Also for Darwin several possibilities of metrology equipment exist but one instrument performing lateral, tilt, and longitudinal measurements could reduce the complexity of auxiliary equipment.

Darwin relies on a powerful fringe detector during operation and this fringe sensor is capable to measure the distances between the satellites with high precision. During the first setup and deployment of the telescope array respectively during resizing the array or reacquisition of a target considerable time is needed using the standard fringe tracker. A powerful laser metrology instrument assisting during the employment phases could drastically reduce the setup times.

5.2 Darwin Mission for Detecting Earth-like Life

5.2.1 Background of Mission

The European DARWIN mission wants to detect and analyze terrestrial exoplanets orbiting Sun-like stars. Nulling interferometry allows for visual detection and interferometric imaging of such planets. Stringent requirements are imposed onto the instrument because the capability to separate both signals must be excellent due to the close proximity of star and planet. Darwin's operating band is in the mid-infrared and even here the contrast ratio of star and planet is huge. The bandwidth of the instrument ranges from 6.5 µm to 20 µm as absorption lines of the main biomarkers shall be identified at 7-8 µm (methane), 9.6 µm (ozone), 15 µm and 18 µm (carbon dioxide), and 6-8 respectively 17-20 µm (water). A nulling interferometer provides both high on-axis light suppression and high angular resolution. The tremendous requirements given by the Darwin mission call for advanced observation techniques like a rotating telescope array supported by phase chopping and a sophisticated instrument design together with the development of novel subsystems and optical components with so far unrivalled quality.

To achieve deep nulling of the star signal the individual interferometer arms have to be equalised with respect to intensity, phase, and state of polarisation. Modal wavefront filtering of the output signals with single-mode fibres is required for removing the wavefront errors of the affordable and feasible high-quality optics.

5.2.2 Status of Darwin Study

EADS Astrium GmbH is currently performing one of the two awarded Darwin System Assessment Studies. The Astrium team passed successfully both initial tasks, phase 1 and phase 2, and is currently executing phase 3 administrated as a rider to the study and dealing with the consolidation of the baselined concept. The agreed Darwin architecture proposed by Astrium consists of a planar X-array with two different baselines (ratio typically 1:3) and a central hub collecting the light from the four telescopes. The architecture agreed with ESA is shown in Figure 5-1 and an artist's impression is given in Figure 5-2. Phase chopping is proposed to perfectly remove any exo-zodiacal background radiation. Rotating the entire array allows to reconstruct the planet's position with the aid of correlation methods.

A planar configuration consisting of 4 telescopes offers several advantages as compared to a planar respectively a non-planar (Emma) TTN architecture. The most important are summarised as

- best modulation efficiency (100% instead of 93.3%)
- best beam recombination efficiency (100% instead of 75%)
- collecting area increased by a factor of 4/3
- rejection of hardly feasible broadband achromatic phase shifters for nulling and internal modulation (critical devices can be replaced by periscopes made of mirrors)
- high redundancy as degenerated X-array can continue science operation if one CS fails

Figure 5-1: Architecture of X-array and related perfectly symmetric beam routing scheme as proposed by Astrium.

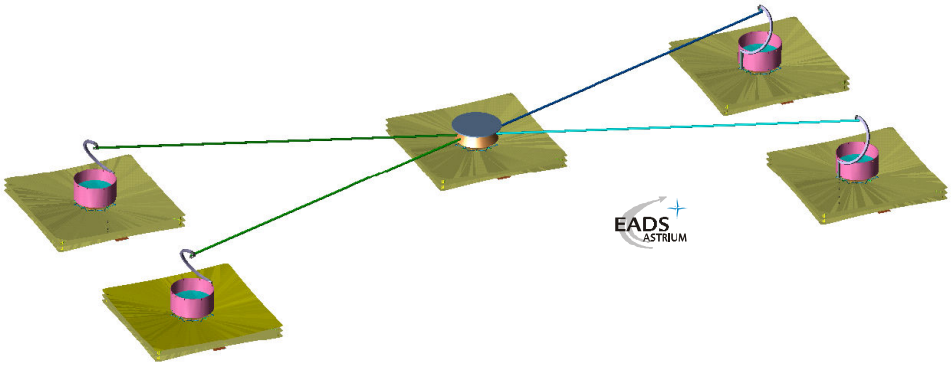

Figure 5-2: Artist's impression of Astrium's X-array equipped with deployable secondary mirrors to fit one Ariane-5 launcher.

A typical modulation efficiency map and correlation map for a single planet scenario orbiting a star at 100 mas distance is shown in Figure 5-3. It should be emphasised here that Astrium's agreed architecture is different to the initial ESA requirement AD3, defining the number of spacecraft to a maximum of three collector spacecraft there. This Three-Telescope-Nuller (TTN) has been later extended by ESA to a non-planar concept (Emma). During the study we got clear indications from our powerful performance simulation tool ISim that a planar 4-telescope architecture performs best. Employing deployable secondary mirrors on the collector spacecraft still allows to fit the entire spacecraft stack (4 CS + 1 BCS) into a single Ariane-5 launcher.

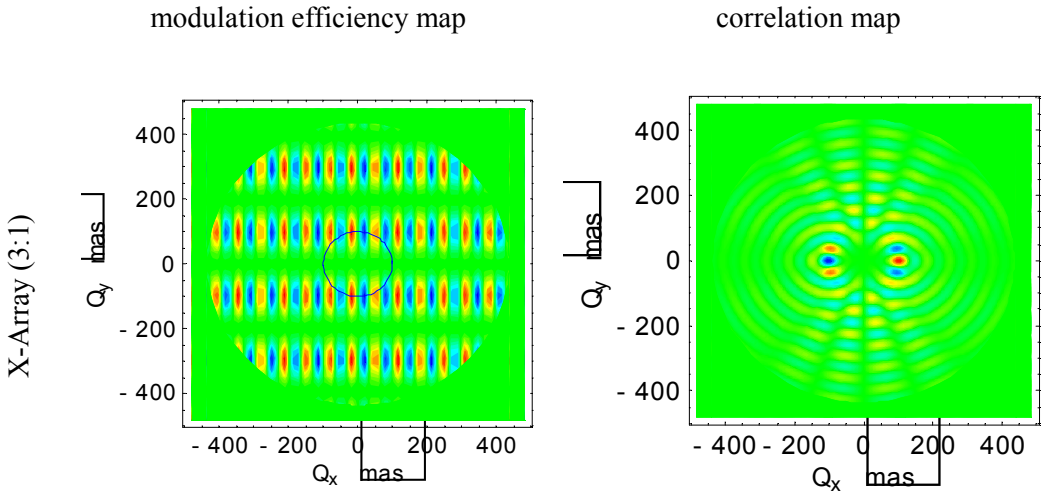

Figure 5-3: Darwin detector signal over planet location after applying phase chopping to subtract exo-zodiacal star dust signal (left). By rotating the entire array and applying correlation methods any target scenery can be reconstructed as shown on the right. The assumed planet is located on the dark circle at the utmost right position. Intensive red indicates a strong positive signal, blue is a strong signal with negative sign. The baseline of the array was optimised to respond best on the assumed location of a single planet at a distance of 100 mas from the star. The planet's position can be reconstructed in a clear non-ambiguous way.

5.2.3 Darwin's Metrology Systems

All arms of the Darwin interferometer must be maintained at the same optical length ranging from the target itself up to the final and critical beam combiner superposing all arms. The total optical path is composed of external optical delay and internal optical delay. Laser metrology can supervise internal optical path delays (OPD) only. Deep nulling occurs only if the sum of external and internal OPD in each interferometer arm is identical and stable to a fraction of the sensing wavelength. This is ensured by a fringe tracker acquiring first the central fringe and tracking it in spite of the moving and rotating telescope array. The required minimal path differences are established and maintained via delay lines. The task to control the external OPD cannot be taken over by laser metrology as the optical path starts at the target star and ends at the last nulling beam combiner.

Internal laser metrology on the other hand maintains a constant distance between the several collector spacecraft and the beam combiner spacecraft. The spatial resolution of Darwin is directly coupled to the separation of the collector spacecraft and the wavelength of course. Internal laser metrology can measure on-axis providing the highest accuracy or laterally shifted decoupling metrology and science path at all. During normal operation, being in measurement mode, the fringe tracker will control all delay lines and metrology is not mandatory. If it is still implemented it would disburden somewhat the control loop of the delay lines.

The real advantage of internal laser metrology is identified in the reduction of the acquisition time of the array. Initial formation deploying, but also regular recalibrations, changing the baseline, jumping to another target star, or changing from detection mode to spectroscopy mode, will need a reorientation of the array being closed by placing all spacecraft in a plane and establishing equal OPD in each interferometer arm. The acquisition time strongly depends on the help of laser metrology.

The architecture of Darwin's metrology systems is shown in Figure 5-4. It is implemented on the cold side of the optical bench of the beam combiner spacecraft. The metrology is split into coarse and fine as well as lateral and longitudinal metrology systems.

The baseline approach is that all spacecraft are brought together via radio frequency metrology to around 10 mm relative distance difference (see AD3, Req. No. 2220) at 1 Hz repetition rate. The remaining budget could be reduced by the fringe tracker alone but is a lengthy procedure as the OPD information of all interferometer arms must be extracted from one fringe sensor. Taking one delay line as reference, three other delay lines must be independently controlled by the fringe tracker and have to be scanned until the strongest central fringe indicates zero OPD. The metrology concept presently available reduces first the OPD drift using the fine longitudinal, lateral and pointing metrology and switches then to the absolute metrology to compute the position of the zero OPD with a given accuracy. In a next and final step the uncertainty range around the zero OPD position is scanned at a speed compatible with the fringe tracker until the central fringe is found and locked at.

Delay lines located on the beam combiner spacecraft are used in open loop to scan the OPD over a maximum stroke of 20 mm, twice the initial error of the RF metrology system. A scan time of not more than 400 seconds (AD3, Req. No. 1310) is needed before fringes are first detected and the fringe tracker takes over and stabilises the OPD by closing the control loop. The delay lines are moved at a rate of 50 µm/s yielding a resolution of 5 µm or half of the observed wavelength at a sample rate of 10 Hz. However, integrating fringe sensors like DWARF must be operated at a lower scan speed. The full width of the fringe packet ΔOPD (coherence length) is related to the bandwidth of the fringe tracker $\Delta\lambda$ and the fringe tracker wavelength λ by $\Delta OPD=2\lambda^2/\Delta\lambda$. An absolute laser metrology resolution higher than the coherence length of the fringe tracker will not provide additional information.

Reducing the uncertainty range of the RF metrology will linearly reduce the fringe acquisition time as the required stroke of the delay line decreases linearly as well. Nevertheless, precise longitudinal metrology does not allow to find faster zero OPD if the instrument is pointing in the wrong direction. Coarse pointing is established by using star sensors with limited angular resolution (1 arcsec). The precise alignment to the target star is performed with the aid of a fine pointing sensor based on a camera with long focal length and is finally confirmed by the fringe tracker. Realignments are required in regular periods and the time required for that can be reduced by precise metrology.

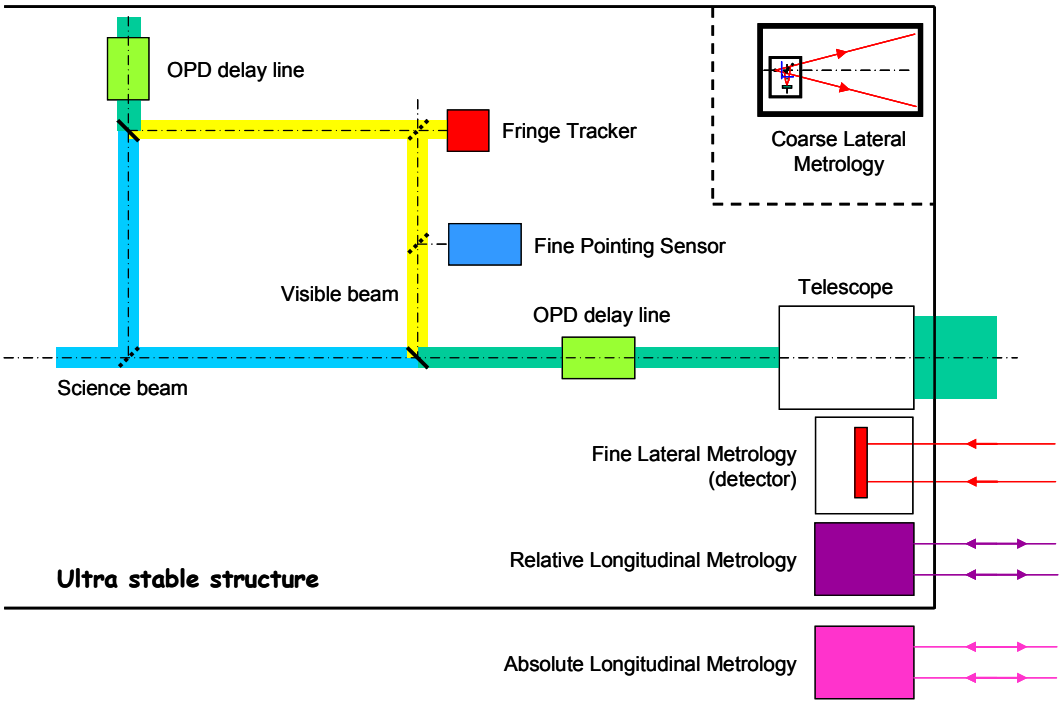

Figure 5-4: Implementation of the metrology systems on the cold side of the optical bench of Darwin's beam combiner spacecraft. Longitudinal and lateral displacements are measured by different coarse and fine metrology sensors.

5.2.4 Laser Metrology Requirements

According to AD4 the distance between two spacecraft is monitored to an accuracy of 32 µm at 10 Hz rate. Here, a white spectral density of the measurement system is assumed with S=10 µm/√Hz. Integrating S between 0 and 10 Hz yields the above rms value. The past IRSI study (done by Alcatel) and the latest information from the HPOM study assumed an accuracy of 70 µm for the absolute longitudinal metrology system to acquire the central fringe within 400 seconds. This absolute longitudinal distance metrology was identified to be necessary to ease and in particular to speed up the fringe acquisition time assuming a "slow" fringe sensor. In the meantime more aggressive fringe acquisition schemes have been studied during the Darwin System Assessment Study (Phase 2 finished and Phase 3 ongoing) and have been considered as feasible confirmed by formation control simulations. Astrium SAS developed a control simulation package (Interferometer Constellation Control, ICC) that is able to assess all impacts of sensor performance and sensor noise on the formation.

In the meantime the outcome of two parallel Darwin System Studies is available. One study has been led by Astrium preferring a 4-telescope in-plane architecture, the second one by Alcatel focussing on a non-planar arrangement. In both studies the requirements on the absolute metrology have been relaxed by assuming a more aggressive fringe acquisition strategy. This implies the use of faster delay lines, e.g. taking magnetic bearings instead of taking the classic voice coil approach, and a faster fringe sensor unit. Astrium proved this new strategy by its ICC (Interferometer Constellation Control) simulation software and considers the approach as feasible together with the more stringent requirements on delay line and fringe sensor. The requirements on the absolute metrology are relaxed to the order of 1 mm allowing the use of conservative techniques for the range measurement like time-of-flight methods.

However, having a sensor providing better information on absolute metrology would always reduce the total acquisition time as it disburdens the fringe sensor. The number of required re-acquisitions during nominal mission operation is still unknown but is assumed to be not very frequently. Currently, the acquisition time of 400 seconds is not seen as a critical parameter and even longer acquisition times are discussed.

The absolute distance between the spacecraft ranges from 15 m up to several hundred metres. The lower end of the scale is defined by the collision risk. The upper end is determined by the planet/star difference and target distance on one hand but also by the processing strategy. A typical and practical range is 200 to 300 m.

In science mode the requirements on the GNC system are summarised in Table 5-1. From these top-level requirements on GNC, the allocations for the different control loops have been derived and are given in Table 5-2. The specifications on the various sensors and subsystems (see Table 5-3) have been elaborated from the top-level requirements.

	Values	Comment
OPD	1 nm rms	Not fully compliant with MRB but preliminary analyses has shown that that performance was compatible with the required nulling depth (control error PSD shape).
Tip/tilt (200mm beam)	70 mas rms	Tip/tilt correspond to BCS-CS relative pointing
Lateral beam displacement (200 mm beam)	3.5 mm rms	

Table 5-1: GNC requirements for DARWIN's science mode.

	Allocation	Origin/comment
Lateral position	0.3 mm rms	ODL stroke (2mm allocation for dynamic control)
Longitudinal position	0.3 mm rms	ODL stroke (2mm allocation for dynamic control)
BCS absolute attitude	1” rms	Lateral beam displacement (462 m ISD). Can be relaxed to 2” for a 230m ISD.
BCS-CS beam relative pointing	1” rms	Lateral beam displacement (462m ISD). Can be relaxed to 1.6” for a 230m ISD.(mirror stroke then becomes the driver).
CS absolute attitude pointing (Z axis)	1” rms	Design goal, No strict constraint on that axis, as no optic amplification factor apply.
OPD control	1 nm rms	
Tip/tilt control	70 mas rms	

Table 5-2: GNC performance allocation to control functions for DARWIN's science mode.

Sensor Actuator	Requirement	Value	Comment
Star-tracker	Readout frequency	1 Hz	
	Bias and mounting error(1)	< 0.5" (3σ)	For transverse axes.
	Noise	< 1" (rms)	For transverse axes.
RF longitudinal measurement	Readout frequency	1 Hz	||x||
	Range for Fine Control	0 -500 m / 5° half cone	
	Bias(1)	< 1 mm (3σ)	Accuracy (noise + biais + all effect) < 1cm (99.9%)
	Noise	< 3 mm (rms)	
RF lateral measurement	Readout frequency	1 Hz	(Y,Z) or (θ,φ)
	Range for Fine Control	0 -500 m / 5° half cone	
	Bias and mounting error(1)	< 0.2° (3σ) half cone	Accuracy (noise + biais + all effect) < 0.4° (99.9%)
	Noise	< 0.07° (rms) half cone	
Coarse Lateral Metrology	Readout frequency	1 Hz	(θ,φ)
	Range	1° half cone, 0-500 m	Margin with respect to RF accuracy
	Noise	< 1" rms	~2.5 mm @ 500 m
	Bias and mounting error(1)	< 0.5" (3σ)	
Fine Longitudinal metrology	Readout frequency	1 Hz	Δx
	Range	0-500 m, ±1 cm lateral	
	Noise	10 µm (rms)	
	Bias and mounting error(1)	< 0.5" (3σ)	
Fine Lateral metrology	Readout frequency	1 Hz	(Y,Z)
	Range	0-500 m, ±1 cm lateral	
	Noise	10 µm (rms)	
	Bias and mounting error(1)	< 1 µrad (3σ)	2.5 mm lateral offset @ 250 m
Fine Pointing Metrology	Readout frequency	10Hz	Relative beam pointing
	Range	300" half cone on 200mm beam	To cover initial bias and mounting errors
	Noise	< 160 mas (rms) on 200 mm beam	Equivalent to 50 mas/√Hz @ 10Hz
	Bias and mounting error(1)	70 mas (3σ) on 200 mm beam	
Fringe Tracker (3)	Readout frequency	50 Hz	OPD
	Range (coherence length)	4 µm	In acquisition, locking, and fine control
	Maximum OPD drift	8.5 µm/s	
	Noise	0.5 nm rms	Intermediate star case (m_v=9)
	Bias	-	Not observable at GNC level

Sensor Actuator	Requirement	Value	Comment
Optical Delay Lines	Command rate	50 Hz	
	Range	±1 cm	For fringe acquisition
	Stability	0.7 nm rms	Around the ODL zero position.
	Response time – Position control	< 20 ms	Staircase profile for fringe acquisition with 100ms step
	Quantification – Position control	~10 nm	Not critical only used for fringe acquisition
	Response time – Velocity control	< 2 ms	For tracking mode (compatibility with control rate)
	Quantification – Position control	1 nm/s	

Sensor Actuator	Requirement	Value	Comment
Tip/tilt mirrors	Command rate	10 Hz	
	Range	±30”	
	Stability	<25 mas rms	
	Response time	< 100 ms	
	Quantification	100 mas	
FEEPs	Command rate	1 Hz	
	Range	0 – 3 mN(3)	Max thrust defined by manoeuvres capability
	Noise	< 2 μN/√Hz	Per axes, including thrust amplitude and thrust direction stability.
	Quantification	1 μN	
	Minimum thrust	1 μN	
	Response time	100 ms	

(1) All biases and mounting errors are to be understood “after calibration and commissioning phase”. The metrology sensor is able to measure in a wide FOV but the error on the desired longitudinal distance value becomes unacceptable high if the specified bias and mounting tolerances are exceeded.
(2) Fringe Tracker is driving the system so these are not recommendations, but hypotheses on which the design is made.
(3) Initial requirement on thrust defined by the durations of the manoeuvres was 14mN. This value is not compatible with the required noise level. A linear scaling of LISA's 150μN-0.1μN/√Hz FEEPs gives a maximum thrust around 3mN. Analyses of Darwin's science performance finally showed that a thrust around 1mN is sufficient.

Table 5-3: Specification on DARWIN's GNC equipment and sensors for the science mode.

5.2.5 Space Environment

Launcher, orbit and hard radiation

Darwin will be brought to the L2 orbit with the aid of a single Ariane 5 rocket and must survive those launch vibrations. The L2 orbit is a stable orbit 1,500,000 kilometres apart from Earth in anti-Sun direction. That Lagrange point is characterised by the fact that the gravitational forces of Sun and Earth are cancelling there and the satellite will orbit around the Sun synchronously to Earth. Hence, the hard radiation environment is similar to an orbit around Earth and 10 krad total dose of ionising radiation may be expected for a nominal

mission lifetime of 5 years. Extended mission operation is specified for a period of twice the nominal duration (see AD3, Req. No. 60).

Temperature

All mid-infrared optics including shields and benches must be operated at 40 K (AD3, Req. No. 3010) to avoid masking of the scientific light by own stray light. Hence, any laser metrology attached to the cold part of the spacecraft must be cooled as well. Measurement devices on the service module could be operated around room temperature (290±20 K from AD3, Req. No. 260).

Service module and optical bench are not only thermally separated but also mechanically decoupled to avoid the transfer of noise from the proportional thrusters (Field Emission Electrical Propulsion FEEP) to the bench. The joints of service module and bench are not stiff enough to transfer the metrology information with reasonable precision. The metrology system must be cryogenically cooled therefore.

Stray light

EADS Astrium details now the Darwin instrument agreed to be a planar architecture. All metrology beams will travel in the plane where the compressed beams from the collector spacecraft are sent towards the beam combiner spacecraft. Any metrology light will deteriorate the fringe tracker operating in the near infrared or the science detection system working in the mid infrared. Optical filters on one side and off-axis metrology paths and baffling can reduce stray light problems. Gating of the fringe tracking and/or science detectors and blanking the detectors during the short metrology measurement time is another way out.

Light used for the fringe tracker and the science light must be spectrally well separated as otherwise the fringe tracker will follow the photo centre of the combined light emitted by the star and the planet and the instrument would be slightly mispointed.

5.3 XEUS Mission for Mapping X-ray Sources

5.3.1 Instrument Description

The X-ray mission XEUS (X-ray Evolving Universe Spectroscopy) is one of the potential future missions in the framework of Cosmic Vision as successor for the highly successful X-ray mission XMM-Newton. XMM used Wolter telescopes with a diameter of 70 cm and a focal length of 7.5 m. XEUS increases the telescope diameter to 4.3 m fitting yet in an Ariane-5 fairing. Preliminary studies have investigated several approaches with focal lengths in the order of 35 up to 50 m. One aspect was kept always constant: a focal length of several tens of metres - with currently 35 m it is too large for a conventional telescope structure. Therefore the XEUS mission will consist of two parts, the Detector Spacecraft DSC and the Mirror Spacecraft MSC flying in formation, this time on a halo orbit around L2. In earlier times also an Earth orbit has been investigated utilising the ISS for the final assembly of the mirror spacecraft. The MSC is free drifting while pointing to the sources of interest. The DSC as the smaller spacecraft will be the active partner and has to maintain its position behind the MSC over the entire mission phase.

As the size and configuration of XEUS will finally depend on the international cooperation - which is not yet fixed - ESA decided to go this time with a purely European solution. This is a fixed optical bench system as large as the Ariane 5 fairing allows. The baseline mission could be accomplished by an instrument complement comprising a Wide Field Imager Narrow Field Imager. Presently two different Narrow Field Instrument designs are available:

- NFI1 is based on a focal plane of super conducting tunnel junctions (STJ), operated at a temperature of <300 mK via a 3He Sorption Cooler (or as an alternative an Adiabatic Demagnetisation Refrigerator (ADR) if temperatures below 250 mK are required)
- NFI2 is based on a focal plane array of micro-calorimeters, operated at about 50 mK via an ADR

In consideration of the expected launcher performance and of the resource demands of both Detector Spacecraft and Mirror Spacecraft, it has been assumed to limit the model payload to the Wide Field Camera

and a single Narrow Field Imager. Both detecting instruments shall be installed on the DSC, and the illumination of the individual focal plane will be enabled by a shift of position - both along the optical axis and on the perpendicular plane - performed by the DSC. Given the early definition stage of the mission, it is not possible to make a definitive choice on the actual NFI design and therefore both designs will be analysed in the context of the XEUS payload accommodation study.

5.3.2 Key Requirements

The yet preliminary requirements taken from the Scientific Requirements of XEUS, issue 2.2, 01, July 2005, Mission Requirement Document, issue 1, 30 Sept. 2005, and the XEUS Payload Definition Document as reference document for the recently released XEUS Telescope Accommodation Study refer to the Formation Flying aspects, in particular to their metrology and are listed below:

- Halo orbit around L2 (eclipse free); direct injection with Ariane 5 or Delta IV Heavy
- Reference scenario: Ariane 5 bringing 6.6 tons to L2 (MSC + DSC)
- Total cruise duration 3-5 months
- Formation flight at ≈ 35 m distance
- Pointing error
  - MSC absolute measurement accuracy <1 arcsecond
  - DSC absolute pointing error <1 arcminute for line of sight
- Field of View
  - 7 x 7 arcminutes for WFI (but detector is oversized)
  - 0.75 x 0.75 arcminutes for both NFI options

5.3.3 Metrology Requirements

According to RD4 (October 2004) RF metrology will bring the DSC to ±12 cm lateral and ± 5 mm longitudinal to the focus of the MSC. Longitudinal metrology maintains the DSC in the focus of the MSC to 0.75 mm. Lateral metrology (cameras) positions the focus to 0.33 mm on a 5 mm detector. Pitch and yaw are measured to ±10 arcsec allowing attitude control with ±1 arcmin accuracy.

Taking RD5 (September 2005) the focal point of the X-ray mirrors mounted on the MSC must be aligned in orbit to an accuracy of ±0.5 mm in all three dimensions. It is not yet defined how the alignment of the numerous petals is performed. Active systems on the MSC based on local laser metrology are the current baseline but the quality of the image of a reference object on the DSC could be used as well for the alignment process.

The DSC must keep its position within ±3 mm (2-σ value) in longitudinal direction and ±1 mm (2-σ value) in lateral direction.

One idea followed in the last time is to use only one metrology system located on the DSC performing both, the petal alignment first and keeping the DSC position second during the formation flight.

The difference between the inertial attitudes of DSC and MSC shall be controlled to less than 1 arcsec.

Recently, the ITT "XEUS Telescope Accommodation Study" has been released (May 2006). This latest and actual document defines XEUS as two separate spacecrafts flying in formation and having a focal length of 35 m obtained without the use of a large deploy-able bench or a telescope tube system. The detector envelopes and focal depth imply that the focal point must be located within about 1 mm, in all 3 dimensions, of the focal reference point. A combination of RF and laser metrology is assumed to provide the distance information. The laser metrology must perform much better than this accuracy.

Figure 5-5 shows the principle of the XEUS telescope with the mirror spacecraft on the left side and the detector on the right side. Both units are free flying as the focal length is too long for a closed classic telescope structure.

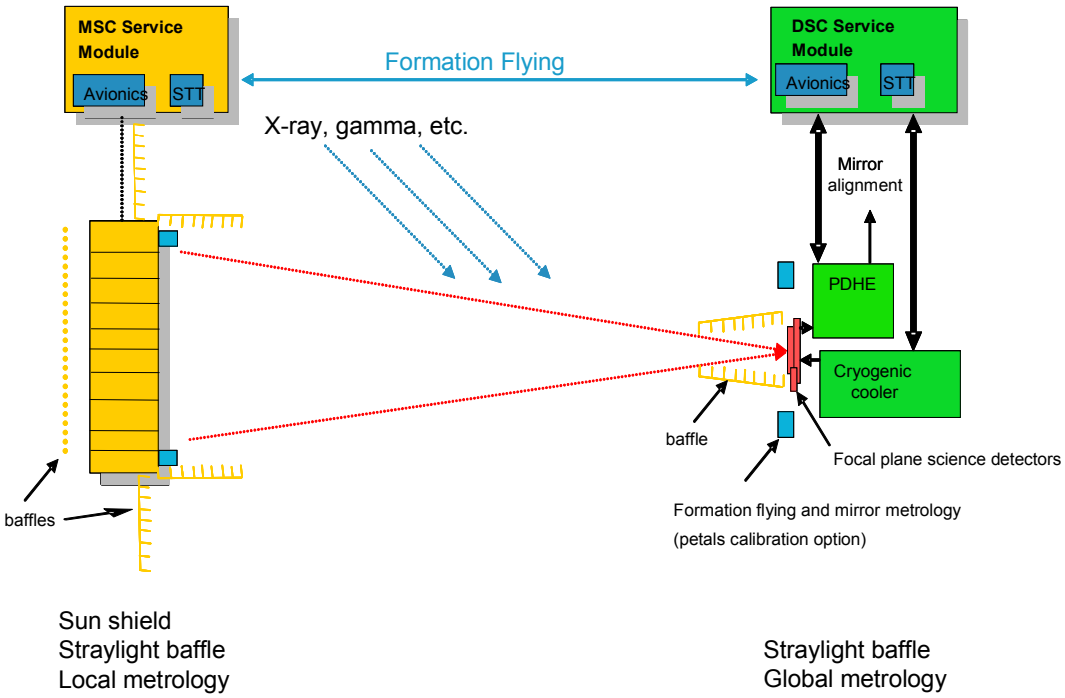

Figure 5-5: Principle function of the "open" XEUS telescope: MSC components are shown in the left and DSC components on the right.

5.3.4 XEUS Metrology approach

In an early state XEUS was equipped with gratings and two options have been considered: Placing the grating at the mirror spacecraft (10 m option) or mounting it in front of the detector spacecraft (50 m option). The 50 m was the focal length assumed in that early state and in the meantime changed to 35 m. The metrology for the gratings had very high requirements for both options ranging from 50 µm lateral up to 60x289 µm lateral for the 50 m configuration. It should be noted here that the grating option has been rejected in the meantime due to the stringent requirements and only the wide-field imager and one narrow-field instrument are left. The metrology requirements are relaxed therefore.

Characteristic in the proposed metrology approach is that the lateral displacements and angular orientation of the DSC with respect to the MSC are determined by multilateration. From three points on the DSC distances are measures to four positions on the corners of the MSC. In Figure 5-6 the simplified version called trilateration is shown. By measurement of the three distances L1, L2 and L3, also the lateral displacement can be determined.

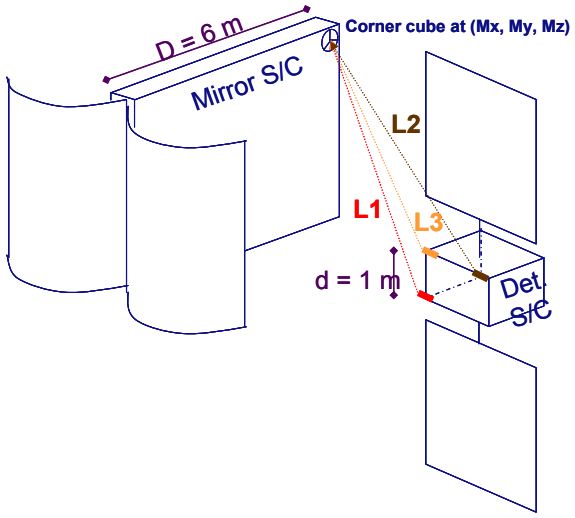

Figure 5-6: Sketch showing the triangulation principle applied to the XEUS configuration

The MSC corner position coordinates $M_{x,y,z}$ with respect to the DSC are given by equations 1 to 3.

$$M_x = \frac{L_1^2 - L_2^2 + d^2}{2d} \qquad \text{Equation 1}$$

$$M_x = \frac{L_1^2 - L_3^2 + d^2}{2d} \qquad \text{Equation 2}$$

$$M_z = \sqrt{L_1^2 - \left(\frac{L_1^2 - L_2^2 + d^2}{2d}\right)^2 - \left(\frac{L_1^2 - L_3^2 + d^2}{2d}\right)^2} \qquad \text{Equation 3}$$

What is clear directly from the sketch of the configuration is that the inaccuracy of the z-coordinate (ISD) is roughly equal to the measurement accuracy it self. In order to asses the lateral accuracies the derivatives of equations 1 and 2 have to be regarded. The error δM_x is then found to be:

$$\delta M_x = \sqrt{\left(\frac{L_1}{d}\right)^2 \delta L_1^2 - \left(\frac{L_2}{d}\right)^2 \delta L_2^2 - \left(1/2 - \frac{L_1^2 - L_2^2}{2d^2}\right)^2 \delta d^2} \qquad \text{Equation 4}$$

As one can see now the errors in the distance measurements L1 and L2 are multiplied by L/d. Taking a spacecraft separation of 35m and 1 m baselength this factor is about 35. In other words the required accuracy of the length measurement is about 35 times higher than the required lateral resolution. The sensitivity to the error of the baselength shows 2 contributions, a first of simply δd/2 and a second part proportional to $\frac{L_1^2 - L_2^2}{2d^2}$. This latter term can vary between zero (when L_1=L_2) and L_1/d +1/2 when L_2=L_1+d. In other words the determination of the baselength is also important for the measurement of the lateral positions, but mainly when the angles are large. (large x/L values).

The comparison between the fs-metrology system capability and the XEUS metrology requirements is an important part of the study. At first glance the fs-laser technology could be an overkill concerning the range precision required for XEUS and considering the complexity of such a system. Nevertheless the fs-laser metrology technology should be considered as one candidate for the XEUS metrology system. XEUS needs information on absolute distance and lateral displacement of the two spacecraft and a fs-laser based system could deliver both information with a single sensor but at possibly reduced sensor size.

5.3.5 Space Environment

Launcher, orbit and hard radiation

XEUS will be launched by a single Ariane 5 or Delta IV Heavy rocket and will travel to the second Lagrange point L2. It has to withstand the related launch vibrations. According to RD4 the nominal mission of the mirror spacecraft MSC is 15 years with an extended option up to 20 years. The DSC requires a lifetime of 5 years with an extended lifetime of additional 2 years. Concerning radiation requirements, a 10% margin on the nominal life-time will be added (extended lifetime no margin). It is planned to replace the DSC at its EOL or if more sophisticated detector systems become available. As all metrology components are located on the DSC the hard radiation environment is similar to Darwin and amounts to 10 krad total dose.

Temperature

The metrology systems can be placed on the warm service module of the DSC as the range accuracy is not that high.

5.4 LISA Mission for Detecting Gravitational Waves

Ground-based interferometers can observe the bursts of gravitational radiation emitted by galactic binaries during the final stages of coalescence when the frequencies are high (≈ kHz) and both the amplitudes and frequencies increase quickly with time. Low frequencies (< mHz) can only be observed in space due to the absence of seismic interference. The LISA mission comprises three identical spacecraft located 5 million km apart forming an equilateral triangle (see Figure 5-7). It resembles a giant Michelson interferometer, with a third arm added to give independent and also redundant information on the two gravitational wave polarisations. The interferometer arm length determines the frequency range in which LISA can make observations. The particular heliocentric orbits for the three spacecraft were chosen such that the triangular formation is maintained throughout the year with the triangle appearing to rotate about the centre of the formation once per year.

5.4.1 Measurement Concept

LISA implements an antenna for low-frequency gravitational waves in the frequency range between 0.03 mHz and 1 Hz.

The laser light going out from the centre spacecraft to the other corners is used to phase-lock the light of the laser onboard of the distant spacecraft. This "regenerated" light is emitted back to the centre spacecraft where it is superposed with the on-board laser light serving as local oscillator in a heterodyne detection scheme (optical transponder). This gives information on the length of one arm modulo the laser frequency. The second arm is treated the same way, giving information on the length of the other arm modulo the same laser frequency. The difference between these two signals will thus allow the detection of any differences between the two arm lengths (i.e. the gravitational wave signal). The sum will give information on laser frequency

fluctuations.

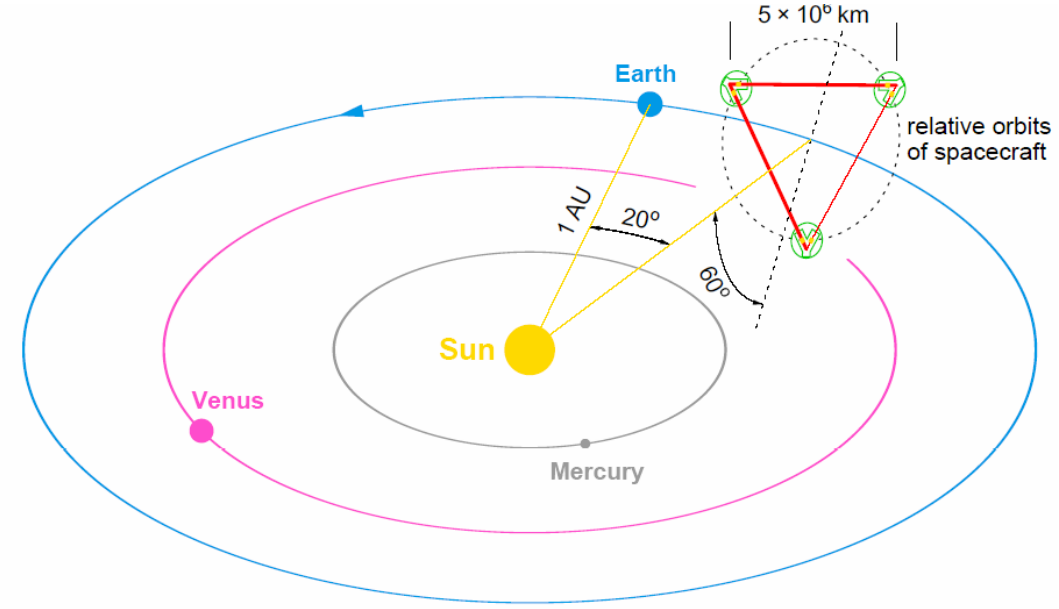

Figure 5-7: LISA constellation flying three widely separated spacecraft in the Earth orbit but lagged by 20 degree.

At the heart of each assembly is a vacuum enclosure containing a free-flying polished platinum-gold cube (proof mass) serving as optical reference ("mirror") for the light beams. The distance fluctuations caused by passing gravitational waves are measured to sub-Angstrom precision. The spacecraft shield the proof masses from adverse effects like solar radiation pressure. The spacecraft must be centred on their respective proof masses by a "drag-free" control system, consisting of inertial sensors and a system of electrical thrusters. Capacitive sensing in three dimensions is used to measure the displacements of the proof masses relative to the spacecraft.

LISA orbits the Sun in the course of one year and the observed gravitational waves are Doppler-shifted by the orbital motion. This allows the direction of the source to be determined.

A passing gravitational wave causes a temporal change of the observable distance between two masses. For a distance of $5 \cdot 10^6$ km a one way measurement accuracy of 12 pm/√Hz at a frequency of 3 mHz is compatible with the scientific measurement requirements.

5.4.2 Key Requirements

The relevant requirements are taken from the LISA Science Requirements Document (version 3) and the LISA Mission Requirements Document and are

- Useful mission duration (at 70% reliability EOL) is 5 years nominal and 8.5 years extended mission, with an additional transfer time of maximum 1.5 years
- Availability >90%
- Latency < 1 week
- Capability to determine the polarisation of a gravitational wave
- Configuration as rotating equilateral triangle 60° rotated with respect to the ecliptic on the earth orbit, a baseline of 5 million km side length, formation 20° behind the Earth
- Simultaneous und continuous availability of all 3 links

5.4.3 Laser Metrology Requirements

The relative and absolute ranging requirements are listed below

- Arm length (= metrology distance) is 5 million kilometres
- Measurement band between 0.03 mHz and 1 Hz
- Allowed single link metrology error for the detection of relative arm length changes is 12 pm/√Hz with a $1/f^2$ roll-off below 2.8 mHz
- Absolute arm length knowledge better than 30 m
- Maximum relative velocity between spacecraft is 15 m/s
- Overall pointing jitter of transmitted beam less than 8 nrad/√Hz
- Required accuracy for pointing acquisition is 1 nrad/√Hz

The critical constraint is the wide separation of the spacecraft and cannot be bridged by a mono-static laser radar of reasonable optical power, even if a cooperative target is implemented. Mono-static radar in this context means that transmitter and receiver are located at the same spacecraft. LISA uses instead a two-fold bi-static approach to overcome the constraints dictated by the range equation. Each spacecraft owns two cw laser sources (1 W optical power from 40 cm telescopes) emitting light at frequencies shifted by 80 MHz to each other. The outgoing light is phase locked to the frequency shifted incoming light by a PLL. One can say that the weak modulated signal received from the counterpart is regenerated and sent back via the second laser.

The knowledge of the absolute position of the counter spacecraft is required to remove the noise produced by the laser source itself. This is done by correlation of the delayed signature with the transmitted noise signature of a laser source. The absolute distance is not important but the relative position of the signature. LISA measures the absolute distance by modulating a pseudo-random sequence on the science signal. A similar sequence as used in the GPS system is proposed, e.g. a 1023 “chip” long code, being transmitted with a frequency of 1.023 MHz. If the codes were actually random, 21023 possibilities would exist. Of these many codes only few are suitable for the auto correlation or cross correlation which is necessary for the measurement of the signal propagation time. The 37 suitable codes are referred to as GOLD-codes (names after a mathematician). For these GOLD-codes the correlation among each other is particularly weak, making an unequivocal identification possible.

The outgoing laser serves in addition as a local oscillator for a heterodyne receiver reducing strongly all 1/f- and dc-drift problems associated with any homodyne receiver. The 80 MHz frequency offset has been chosen such that the expected Doppler shift of maximum 14.1 MHz for a Nd:YAG laser source can be comfortably handled.

The relative spacecraft distance on each side of the triangle is measured by phase comparison of the different heterodyne signals. The enormous phase accuracy required puts stringent requirements on all microwave oscillators (USO ultra stable oscillators) and laser oscillators. One master laser locked to an ultra-stable external cavity serves as reference laser for all spacecraft. The heterodyned signals are directly A/D-converted and all PLL and filtering tasks are performed by digital signal processing. Even the jitter in the sample-and-hold circuitry of the A/D-converter is deteriorating and the sampling frequency is additionally A/D-converted by the same converter for calibration purposes.

Summarising we can say that any external measuring system would have demanding requirements on precision and needs to be part of the entire processing loop for calibrating off all deteriorating effects.

The current baseline of LISA's optical metrology architecture is shown in Figure 5-8. It is based on highly sophisticated heterodyne laser interferometry for the proof mass to proof mass metrology link in three main steps: proof mass PM to optical bench (OB) laser interferometry, which serves also as error signal for the

drag-free attitude control system, optical bench to optical bench metrology (5 million km) and again optical bench to proof mass metrology.

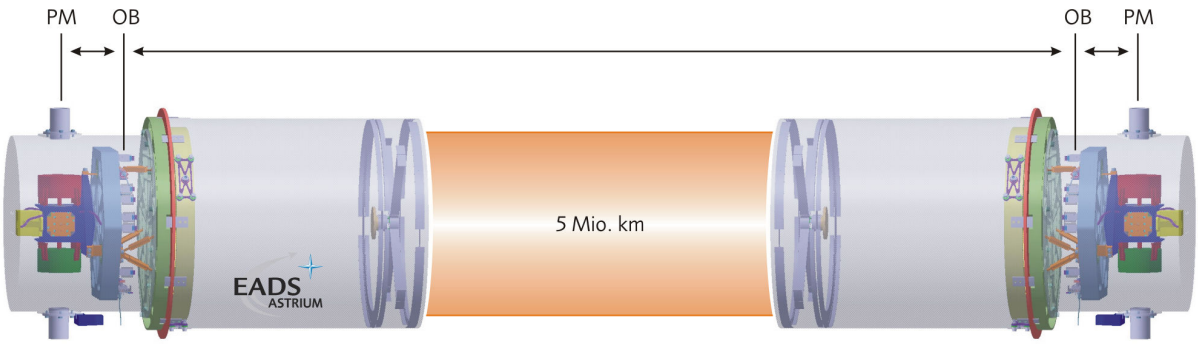

Figure 5-8: Optical metrology architecture baseline for LISA. The distance between the proof-masses (PM) must be determined at pm-level over the huge distance of 5 million km.

5.4.4 Implementation of fs-Laser Based Metrology

The fs-metrology system technology will be assessed in the study with respect to the LISA requirements. LISA requires mainly highly accurate relative distance variation information. Hence, the fs-laser technology is not the favourite candidate for the main science metrology. Nevertheless, a certain relevance to the determination of the absolute distance between the spacecrafts is given. Currently, a metrology concept based on phase comparison of pn-sequences is foreseen. It comes for free as the science signal can be loaded by this information and roughly 30 m accuracy is already sufficient.

Fs-based metrology is much more precise in terms of accuracy but cannot be implemented as a mono-static system. The main challenge is the enormous distance to be bridged by the laser metrology system and mono-static metrology systems are ruled out from the beginning.

5.4.5 Space Environment

Launcher, orbit and hard radiation

The three identical LISA spacecraft will be launched in a composite stack by a single Delta II rocket as produced by the Boeing Corporation into a parking orbit. After several revolutions around Earth, the final launcher burn will manoeuvre the launch stack into an escape orbit. The composite spacecraft are individually released then from the launcher. From the parking orbit, the three spacecraft will be transferred to their final L2 orbits within 14 months from launcher separation, maximising the final injected mass into the target orbits.

Contrary to RD4 the nominal mission duration is 5 years with 3 years extension. The data has been taken from the LISA Mission Formulation Study Astrium is performing since 2004.

The hard radiation environment is similar to Darwin and amounts to roughly 10 krad total dose.

Temperature

All metrology components performing absolute metrology can be located on the warm service module and will not suffer under the stringent temperature requirements of the optical bench where the proof mass is mounted in the order of 1 µK/√Hz.

5.5 Gravimetry Missions

5.5.1 Gravimetry-Mission Classes and Current Missions

In general two principal gradiometer mission classes can be distinguished: the gradiometer mission with a gradiometer instrument on board one SC and the Satellite-to-Satellite Tracking mission forming a giant gradiometer by at least two single SC. Both classes are dedicated to measure the gravity gradient tensor of Earth.

5.5.2 Gradiometer Mission

The prominent representative of this mission class is the currently developed GOCE mission to be launched in 2008. The motivation for this mission is the insufficient knowledge of the Earth's gravity field, which is presently a weak link in the realisation of a globally integrated geodetic/geodynamic observing system. Such a system is needed to derive a comprehensive physical model of the planet Earth. It relies on the combination of three essential components namely:

- geometry and surface deformation
- the Earth's rotation and associated centre of mass variations
- the Earth's gravity field

While substantial progress has been made in determining the first two components (thanks to the use of space methods such as GPS, DORIS, astronomical baseline interferometry, laser ranging, interferometric SAR and satellite altimetry) this is not true for the third component, the Earth's gravity field. Only if all three components are determined independently and have attained the same level of accuracy and spatial/temporal resolution their combination will allow improvements in the monitoring and modelling of a variety of geodynamic, ice and ocean processes as well as their interactions. GOCE will complete this observing system. The GOCE derived gravity field (and the associated geoid) would be a dominant reference for the next decades in geophysical research.

Hence a gradiometer mission is considered as a prime candidate for any future Solid Earth mission, because it basically allows measuring the higher harmonics of the Earth's gravity field with very high precision.

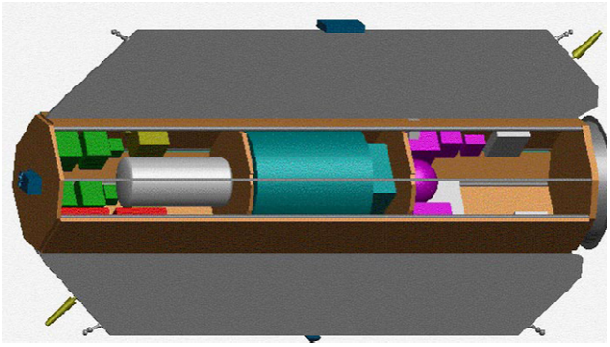

Figure 5-9: GOCE satellite based on a single gradiometer. The streamlined shape of the satellite reduces the atmospheric drag.

A gradiometer mission should be able to measure all nine tensor components by employing a suitable gradiometer supported by a GNSS receiver to allow for high precision orbit determination, while the attitude is derived from star trackers. Taking into account the current development of the GOCE mission, a follow-on Solid Earth mission should offer a significant step beyond the GOCE performance, which has to be realised by the following potential operational and technological improvements:

- Fly at lower altitude than GOCE, i.e. < 250 km

- Gain temporal resolution, i.e. possibly looking for more than one spacecraft
- Solve the related propulsion capacity for a reasonable mission life time
- Improve the measurement accuracy of the accelerometers
- Refine the common mode rejection of the gradiometer
- Optimise the drag free control system
- Investigate the impact of micro vibrations caused by mechanical and thermal variations of the entire satellite

A future Solid Earth mission has to offer measurement accuracies, which are one to two magnitudes better than GOCE will provide meaning that we are looking for performance figures in the range of 1 down to 0.1 mE/√Hz. The gravity gradient (acceleration per metre) is commonly expressed in Eötvös Units where 1 E = 10^{-9} s^{-2}.

5.5.3 Satellite-to-Satellite Mission

Satellite-to-Satellite tracking (SST) missions for Earth gravity field measurement purposes have been studied by ESA since the early eighties. The direct SST metrology principle is shown in Figure 5-10. However, in the late nineties ESA has decided to implement the first Earth gravity field mission based on a gradiometer instrument, a single satellite mission called GOCE. The first pure SST was implemented by NASA in cooperation with JPL and the GeoForschungsZentrum (GFZ) by the GRACE (Gravity Recovery and Climate Experiment) mission. GRACE is an element of NASA's Earth System Science Pathfinder Program (ESSP), intended to address unique, specific, highly focused scientific issues and provide measurements required to support Earth science research.

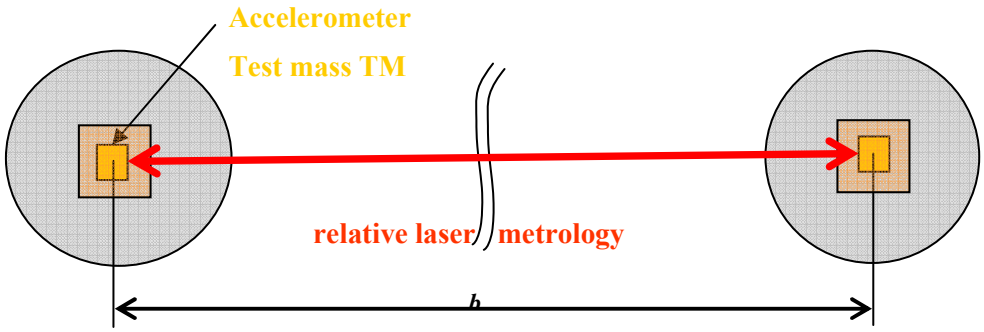

Figure 5-10: Satellite-to-Satellite tracking metrology between two test masses.

The twin GRACE satellites, separated by about 200 km, were successfully launched begin of 2002, with the purpose of collecting data leading to dramatic improvements in the estimates of the long-term mean and temporal variability of the Earth gravity field. GRACE will be able to map the Earth's gravity fields by making accurate measurements of the distance between the two satellites, using GPS data and the RF inter-satellite range-change data. The characteristic orbit is almost polar and near circular starting with an initial altitude between 485 and 500 km. The anticipated lifetime for scientific operation is 5 years. The initial altitude was chosen

- in order to guarantee a multi-year mission duration even under severe solar activity conditions and
- to get a good compromise between gravity field solutions, which desire an even lower altitude, and atmospheric / ionospheric applications, which in contrast would benefit from an higher altitude.

For a number of applications in oceanography, hydrology, glaciology and the solid Earth sciences, the mapping of the static and time varying global gravity field will provide a critical observational and constraint data set. To extend the currently 5 years mission timeline of the GRACE mission, one could imagine to fly a next generation twin satellite mission with further improved range-rate measurements based on an optical interferometry link. Such a mission is considered as a prime candidate for a future Solid Earth mission.

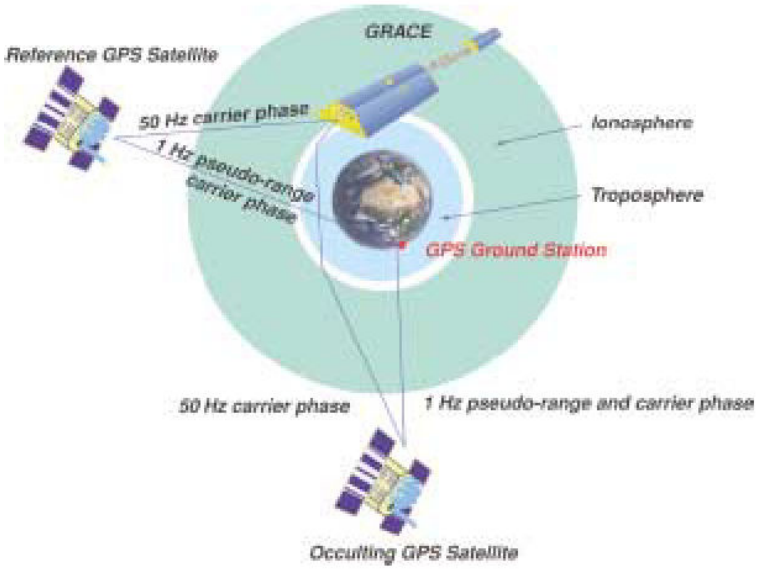

Figure 5-11: GRACE metrology measurement principle based on GPS ranging.

5.5.4 Laser Doppler Interferometry for Earth Gravity Metrology

Satellite-Satellite Interferometry (SSI) or Laser Doppler Interferometry (LDI) defines the Earth gravity field measurement technique based on the tracking of the distance variation between a satellite pair in LEO moving at the same orbital path by means of a laser metrology system.

The variation of the inter-satellite distance is a measure of the gravitational accelerations acting on the satellites and in a next step of the geo-potential. The technique is similar to that adopted on the GRACE mission using Low-Low Satellite-Satellite Tracking. LDI uses a laser interferometer rather than a radio-frequency ranging system for significant in-crease of the precision in the retrieval of the gravity field. The distance measurement is corrected by the measurement of the non-gravitational accelerations acting on the satellites. The objective of the LDI mission is to monitor modifications of the Earth's gravity field up to harmonic degree 180-240 over long periods of time of at least 5 to 10 years. In fact the typical GOCE resolution in the geo-potential variation shall be determined over a time period typical of the CHAMP and GRACE missions.

CHAMP (Challenging Minisatellite Payload for Geophysical Research and Application), a single satellite, used GPS and a laser retro-reflector for precise orbit determination. The GPS method is known as High-Low Satellite to Satellite Tracking. CHAMP was launched in 2000. Its mission duration is nominal 5 years but 8 years are expected. The gravity field can be determined up to harmonics of degree 120 with reduced accuracy for coefficients of degree >70.

GRACE (Gravity Recovery and Climate Experiment) uses already two satellites flying the same orbit but separated by 220 km. The inter-satellite distance is determined by micro-wave metrology working at a precision of 1 µm/second. GRACE was launched in 2002 and shall be in orbit for 5 years. The gravity field determined by GRACE will have a higher accuracy and is predicted up to a degree of 150.

GOCE (Gravity Field and Steady-State Ocean Circulation Explorer) aims at more precise gravity field models than CHAMP and GRACE but uses again a single satellite only. It carries a gradiometer (6

accelerometers), laser retro-reflector, and GPS receiver. GOCE will fly at a mean orbit height of 250 km and will provide higher degrees of the gravity field. In contrast to that CHAMP started at 460 km orbit height and GRACE at 500 km. GOCE will suffer under atmospheric drag due to its low orbit height and is equipped with ion thrusters to correct for that. The ion thrusters with their high electrical power consumption force a Sun-synchronous orbit. Hence, GOCE is limited to daytime measurements contrary to CHAMP and GRACE. The mission duration is 20 months nominal and 30 months extended. GOCE shall determine the static gravity field up to degree 250, possibly 300.

5.5.5 Distance Metrology Requirements

The relative and absolute ranging requirements for a typical LDI mission are taken from the mission parameters section of RD6 and are summarised below

- Orbit height of SSI mission is 325 km
- Inter-satellite distance is 10 km
- Measurement band between 0.1 mHz and 1 Hz
- Measurement error of relative range measurement is 5 nm/√Hz

for frequencies higher than 0.01 Hz

The upper limit of the measurement error of the spectral density of the relative inter-satellite distance over the full measurement bandwidth is shown in Figure 5-12 (taken from RD6).

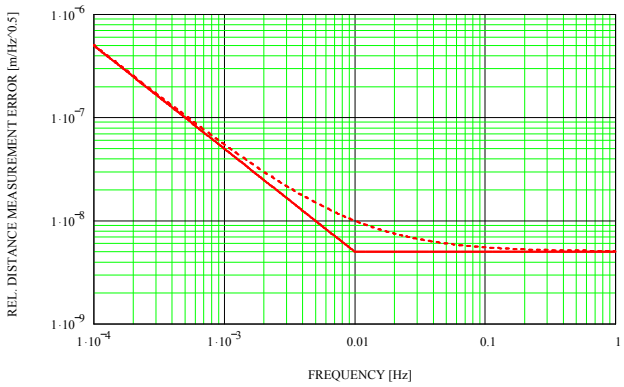

Figure 5-12: Spectral density of maximum relative inter-satellite distance measurement error allowed in the SSI mission.

Figure 5-13 shows a sketch of a SST gradiometer mission based on relative laser interferometry.

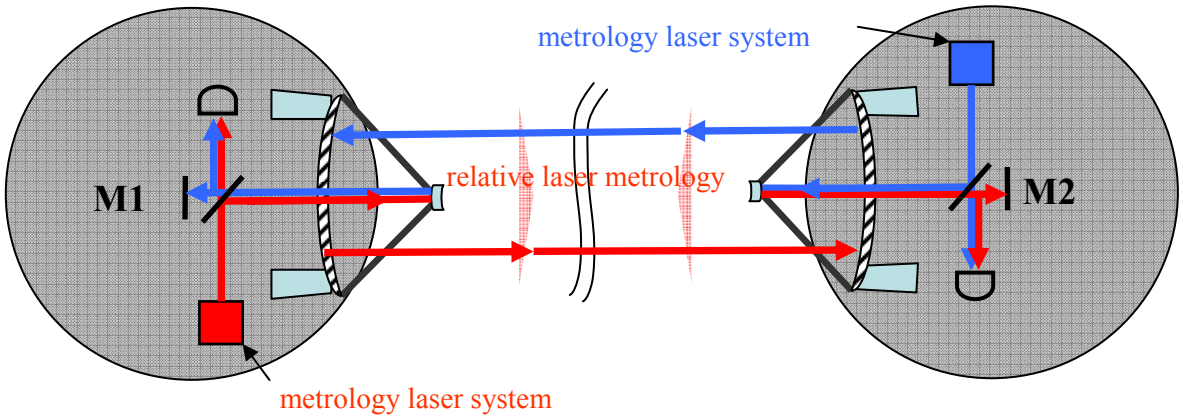

Figure 5-13: Satellite-to-satellite tracking concept base on relative laser interferometry.

Important for the metrology system is the required relative knowledge of the baseline between two spacecraft. The absolute distance knowledge is much more relaxed (≈50 m) and can easily be delivered by the GPS system. The knowledge of the baseline orientation is of main interest for measuring the gravity tensor and separating the gradient of a single direction. The information on the baseline orientation is required on sub-µrad level and is the main challenge for the metrology system applied. To solve this problem highly sophisticated post processing is required fitting a gravity model to the measured data and repeat that procedure iteratively until the optimum guess is found.

At first glance, fs-laser based metrology is not the favoured candidate for an LDI system measuring the gradient of gravity.

5.6 PROBA-3

PROBA-3 is a technology mission demonstrating like PRISMA for the first time formation flying. PROBA-3 is scaled down to fit a reduced cost frame but is representative enough to demonstrate a reasonable formation flying in performance and orbit duration.

PROBA-3 carries a science payload and a demonstration package verifying the formation flying. An additional payload of opportunity can be flown on request.

The science payload is a coronagraph observing the Sun at 530 to 640 nm. The demonstration package consists of a main spacecraft carrying the detector and following the second spacecraft carrying the obscuring shield alone. The mission is quite interesting as the Belgian and the Swedish space agencies will fully finance the two spacecraft.

The main coronagraph function needs metrology sensors as part of the demonstration package. First, a longitudinal metrology system is required to maintain the distance of the occulter. Different variants as required as well in LISA, LDI, XEUS, and Darwin are in discussion. Currently, a sensor similar to the two-wavelengths interferometer as implemented in HPOM is a hot candidate.

The current baseline is to implement a coarse lateral sensor and an absolute longitudinal sensor. Both are mandatory for the coronagraph mission. The lateral sensor is thought to be a kind of star sensor whereas the longitudinal displacement is possibly solved by radio frequency based metrology supported by GPS which is possible in the special Earth orbit of PROBA-3 or LDI but not in L2 orbits as planned for Darwin and XEUS nor for LISA either.

5.6.1 Key Requirements

The relevant requirements are taken from the running PROBA-3 study, Preliminary Concept Review, and can be summarised as

- Highly elliptical orbit around Earth with altitude between 800 km and 160,000 km, 3 days orbit duration, 32 degree inclination, only the perigee time is used for formation flying, mission duration is 2 years nominal
- Perigee passage: safe configuration, LEO type of FF-demonstration, duration 1 hour
- Apogee passage: coronagraph, FF manoeuvre demonstration, duration 60 hours
- Manoeuvre from/to perigee formation: 2 times 5.5 hours
- Separation of main spacecraft to occulting spacecraft typ. 150 m
- Lateral accuracy of better than ±3 mm
- Longitudinal position error of ±100 mm at 150 m inter spacecraft separation
- Individual spacecraft pointing accuracy typ. 4 arcsec
- Wavelength forbidden for metrology: 530- 640 nm
- Diameter of occultation disk: 1.5 m

The add-on sensor shall be representative for the demonstration of future science free-flyer missions and shall support the Darwin or at least the XEUS class of instruments and missions.

The forbidden wavelength range is used by the detector of the coronagraph and shall not be disturbed by metrology signals.

5.6.2 Metrology Requirements for Representativity to Other Science Missions

- Attitude control << 10 arcsec done by AOCS system
- Fine pointing sensor <1 arcsec
  Usually a large aperture star tracker is implemented. The resolution scales with the diameter of the aperture.
- Fine lateral metrology is tied to spacecraft attitude
  Hence, a stand-alone demonstration is not reasonable.
- Fine relative laser metrology in the nm-regime is possible as a stand-alone sensor
  Darwin, LISA, and LDI need this type of sensor. Thruster noise, vibrations by reaction wheels, and orbit micro-vibrations deteriorate the metrology measurement and thrusters are prohibited during the measurement, e.g. for LDI. The required long-term accuracy implies demanding frequency stabilisation of the laser.

5.6.3 Coarse Lateral Sensor

The coarse lateral sensor is based on a light source and a star tracker like telescope. The final implementation is still under discussion and the following variants are possible

- distribution on individual spacecraft
- retro-reflector or divergent light source on other spacecraft
- detector on coronagraph or occulter

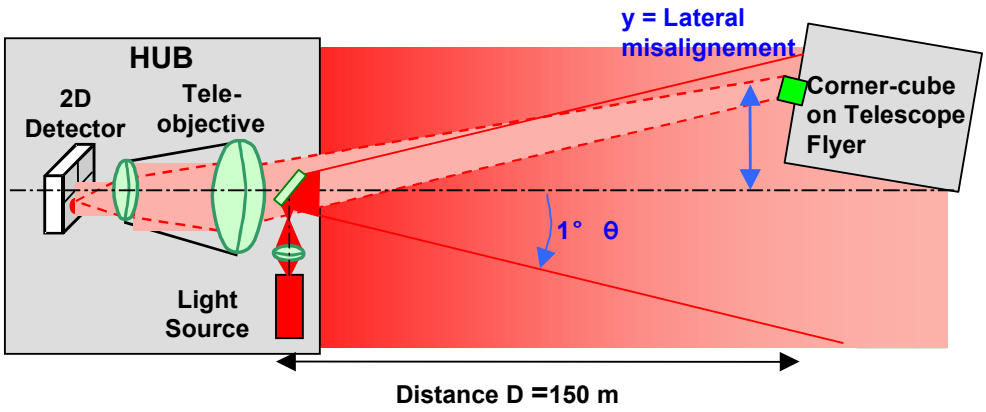

Figure 5-14: Principle of coarse lateral sensor based on light source and star tracker.

The lateral accuracy dy depends on tilt and displacement and is given by

$$dy = D\, d\theta + \theta\, dD$$

Assuming a separation of 150 m and 1 arcsec pointing accuracy yields 1 mm lateral accuracy as well as taking a FOV of 1 degree and 50 mm longitudinal accuracy.

Putting a 10 mW light source on the opposite spacecraft gives a better photon efficiency but also the retro-reflector solution together with a star tracker camera gives much more photons than provided by real stars. Hence, a star tracker like solution will work well on both options.

5.6.4 Absolute Longitudinal Metrology Sensor

The coronagraph of Proba-3 does not need high absolute longitudinal range information. Hence, this measurement is based on rf-metrology. An add-on sensor shall be implemented serving as a fallback solution for the rf-metrology and to demonstrate a representative sensor for future science free-flyer missions like Darwin or at least XEUS.

A scanning frequency interferometer and a dual wavelength interferometer have been studied, breadboarded, and tested within Astrium's HPOM study comprising also lateral and tilt sensors.

ESA currently prefers for the add-on sensor sensor of PROBA-3 the dual wavelength interferometer (DWI). The time-of-flight sensor as proposed by Astrium and developed by Astrium for the ATV fits nicely the coronagraph application of Proba-3 but is not representative enough for future formation flying missions. The advantage of the TOF device is its availability, its maturity, and the high Technology Readiness Level of TRL-8 and with January of next year TRL-9 then.

The DWI is made of two identical non-polarising and superimposed interferometer, one operating at wavelength λ_1 and the second operating at wavelength λ_2. In one interferometer, one beam will be used on the measurement arm between the two satellites and the second beam is used on the reference arm inside the emitting satellite. Both beams are frequency shifted to perform heterodyne detection for utmost sensitivity. The frequency shifting is different for the two superimposed interferometer so they can be distinguished at the receiver. In the final design the AOMs are operated around 80 MHz with frequency shifting of 1 MHz and 3 MHz for the two interferometers to generate the two different heterodyne frequencies.

The first laser operates at 1064 nm and is stabilised to an iodine cell. The second laser operates at 3 GHz offset and is locked to the first laser by a PLL.

The synthetic wavelength depends on the frequency offset alone and is independent on the absolute laser stability. The final phase difference measured is given by

$$\varphi_1 - \varphi_2 = 2\pi \frac{2D}{\Lambda} \quad with \quad \frac{1}{\Lambda} = \frac{1}{\lambda_1} - \frac{1}{\lambda_2}$$

The frequency shifting scheme is given in Figure 5-15 and the interferometer head is sketched in Figure 5-16. Two laser interferometers are superimposed in actual operation because of the dual wavelength measurement. The internal arm (reference) is shown in yellow whereas the external arm (measurement) is sketched in purple. On the external arm a delay line and a beam expander have been added to allow for OPD control and long distance propagation. The reference detector receives the reference beam for each arm and the measurement detector receives the measurement beam. The signals from these detectors are then mixed and the phase difference is evaluated for distance variations.

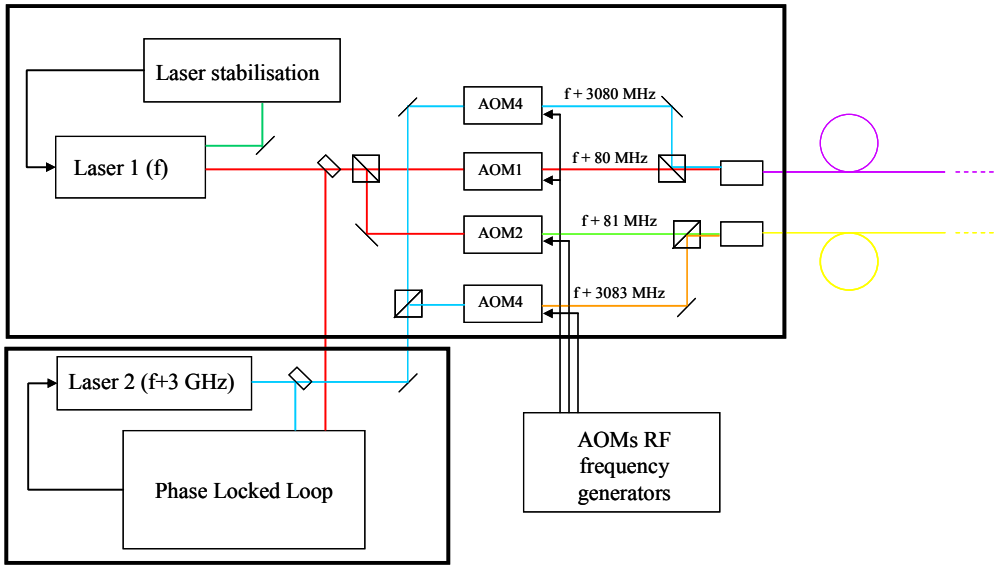

Figure 5-15: Frequency shifting of dual wavelength heterodyne interferometer realised for HPOM and recently proposed as baseline for PROBA-3 demonstration package.

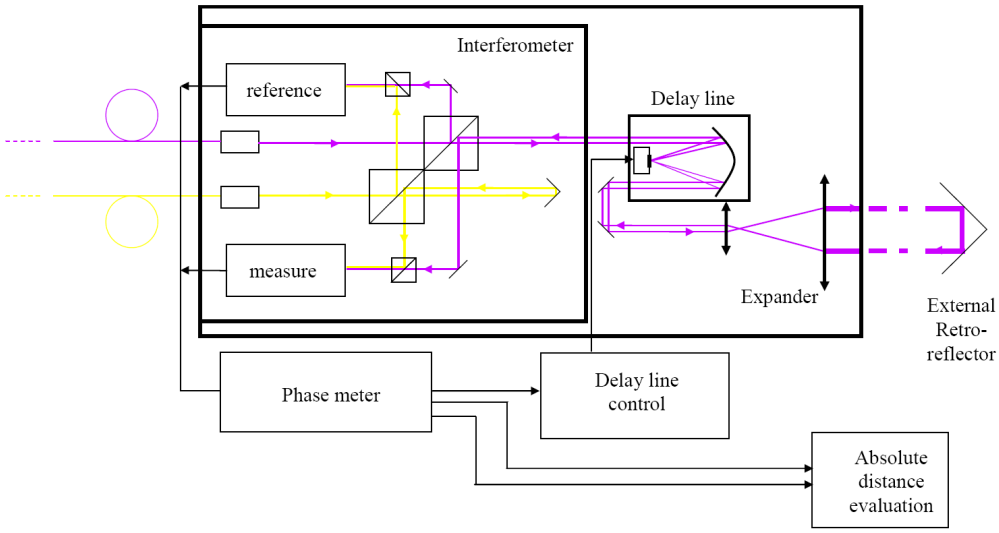

Figure 5-16: Interferometer head of dual wavelength heterodyne interferometer realised for HPOM and recently proposed as baseline for PROBA-3 demonstration package. The yellow interferometer measures the reference arm, whereas the magenta interferometer represents the measurement path. Only one interferometer is shown for clarity.

5.6.5 Recommended Sensor Requirements

The following requirements have been elaborated in the first phase of the PROBA-3 study. An acquisition phase is followed by the coronagraph phase where precise formation flying needs to be established.

Acquisition phase of formation

- Range accuracy: 1 cm
- Line of sight accuracy: 1 degree

Coronagraph phase

- Absolute lateral accuracy: 1 mm
- Absolute longitudinal accuracy: 10 mm

Future FF missions to be eventually demonstrated

- Absolute position metrology: 32 µm (not achieved on PROBA-3)
- Change in absolute position: 10 nm (not possible on PROBA-3)

5.6.6 Preliminary Baseline for Metrology Sensor

The conclusion of the Preliminary Concept Review of the PROBA-3 study was to baseline the EADS Soderne Coarse Lateral Sensor. Until more detailed data is available, a scaling of the EADS Soderne Hydra star tracker has to be used. The specifications of the Hydra star tracker are

- 1 optical head: Mass 0.8 kg, dimensions of 115 mm x 115 mm x 135 mm
- 1 baffle (40°): Mass 0.2 kg, length of 90 mm x 130 mm diameter
- 1 electronic unit: Mass 1.2 kg, dimensions of 140 mm x 140 mm x 70 mm
- typical power consumption for 1 electronic unit and 3 optical heads is 12 W

The required performance improvement by a factor of 2 is proposed by increasing the aperture diameter linearly by a factor 2, and therefore mass of optical head and baffle by a factor of 4. The estimate for the Coarse Lateral Sensor of Proba-3 is based on several minor modifications of Hydra and is given by

- 1 optical head with mass of 3 kg
- 1 baffle with mass of 0.8 kg
- 1 electronic unit with mass of 1.5 kg
- typical power consumption of 12 W

One longitudinal metrology sensor is required for the coronagraph function. Astrium can offer a pulsed laser radar system similar to the sensor as recently built for ATV/HTV. This system is based on a pulsed diode laser and implements the classic time-of-flight technique.

ESA tends to implement a metrology system more adequate to future missions like LISA or LDI. Hence, a dual wavelength interferometer similar to one component of HPOM is under discussion. Currently, this type of sensor is being realised in the course of LISA's LTP (technology package) activity. The LTP electronic equipment dominates in terms of mass, volume, and power demand. This suggests and recommends a dedicated development program for miniaturization especially of these critical electronic components, beyond the intended opto-mechanical development activities.

The system level allocations for a longitudinal metrology sensor on Proba-3 are 15 kg and 16 W. This clearly collides with the interface budget estimate derived from the current LTP development allocations which is 33 kg for mass and 120 W for power consumption.

5.7 Other formation flying missions

Besides the four missions mentioned in the statement of work and the technology demonstrator mission PROBA-3, a number of other European missions is identified that plan to use formation flying. Below an overview (made by ASD-Aerospace) of missions is given.

Mission	No. S/Cs Orbit	Nominal Range (Baseline)	Relative Position Accuracy		Relative attitude accuracy	ISL	Metrology Chain
			Lateral (X,Y)	Longitudinal (Z)			
DARWIN	4; L2	10-1300m	15µm	0.9mm	0.1''	Mbps	RF(coarse/fine) Optical
PROBA-3	2; HEO (72 h)	25m-250m	1mm	100 µm	?	Kbps	RF(coarse/fine) Optical
ASPICS	2; HEO (72 h)	100m-150m	±2.5 mm	±250mm	±40''	?kbps	RF(coarse/fine) Optical
XEUS	2; L2	0.5m-3m lateral; 35m longitudinal	0.15mm	0.1mm	-	kpbs	RF(coarse/fine) Optical
Simbol-X	2; HEO (4 days)	20m (100m)	5mm	30mm	-	kbps	RF(coarse/fine) Optical
MAX	2; HEO or L2	80m-90m	1mm	10mm	-	kpbs	RF(coarse/fine) Optical
GRL	2; L2	500 m	8cm	1m	-	kpbs	RF(coarse/fine) Optical(coarse)
ROMULUS	4; LEO	18m-21m-30m	?	?	?	?	R-GNSS ? RF link ? Optical ?
PEGASE	3; L2	50m-500m	mm	mm	0.1''	?	RF(coarse/fine) Optical

Table 5-4 Overview of European missions that use formation Flying

As can be observed from Table 5-4 the other missions have requirements that are covered when the selected mission scenarios are foreseen with FSL-based alternatives. The operating ranges in the missions varies from 18m for Romulus to 500m for Pegase.

The required accuracies in the table seem to be very low for optical instruments. (Infrared interferometry) The most strict longitudinal accuracy requirement is given for the Pegase mission and is in the order of mm. For Romulus no accuracy values are given. Since the mission objective is to perform aperture syntheses in the visual, accuracies comparable to those in the Darwin mission should be expected.

In the end one finds that most formation flying missions in the near future can be served well with FSL-systems that meet XEUS or Darwin like requirements. Although the XEUS mission is the least demanding mission, its metrology can serve most other formation flying missions and thereby makes it a very interesting case.

In the overview the Swedish PRISMA (Prototype Research Instruments and Space Mission technology Advancement) technology demonstrator is missing. This mission objectives are the demonstration of formation flying, autonomous docking and testing of a wide range of distance and formation sensors and as

well propulsion techniques. Due to the large range of distances and configurations over which the formation flying will be performed, this would be a very nice mission to test the full range of the FSL-systems capabilities.

6 HAALDM Concept trade off

6.1 Darwin trade-off

For the Darwin mission a complex metrology system is anticipated. This system comprises a Dual Wavelength Interferometer (DWI) to determine the absolute optical path length and the use of a single heterodyne interferometer to control the Optical Path Difference (OPD) to the nanometre level. In order to meet the accuracy the primary laser will be locked to an Iodine absorption cell.

Table 6-1 Darwin mission trade-off

System property		***Requirement***	***FSL-system***	***DWI with heterodyne interferometer***
Technical	Range	15-500m	15-1000m	15-500m
	Accuracy / Resolution	10µm rms (abs. dist.) 0.5nm rms (rel.)	3 µm (15 m - 100 m) 3 to 12 µm (100 m to 1 km) - (abs. dist.) nm or sub-nm (relative in difference config.)	10µm rms (abs. dist.) 0.5nm rms (rel.)
	Bandwidth	1-10Hz	10Hz	10Hz
	Satellite motion	2mm/s for abs Few µm/s for rel.	Can cope with drift using a compensation technique	10mm/s (by 10kHz sampling))
	Variation of configuration	ISD 15-500m	15-1000m	15-500m
	Absolute vs. relative	Abs. required Rel. Optional	Abs. yes Rel. yes in diff. config.	Abs. yes Rel. yes
Mass, Volume, Power	Mass	20kg	<10kg	20kg estimate
	Volume	400 X 200X 100mm		
	Power	27Watt	<14W	27Watt estimate
Extra measurements / redundancy	Extra measurements / redundancy		Larger range, higher abs. dist.	2 Relative IFM's

Technical risk	Differences in behavior			
	Sensitivity to perturbations			
	Critical items		Dispersion compensation, a-chromatic design	Wavelength stabilization, IFM synchronization, fiber noise
	Required developments		Laser source	Design electronics

As is clear from Table 6-1, the proposed metrology consisting of DWI and heterodyne IFM meets all requirements. One should not forget however that this metrology has been demonstrated only on a breadboard (HPOM) and on short distances (few m). Additional experiments on longer distances, the design of a FM or EQM and the testing of this design still need to be performed. It is assumed that the mass and power budgets can be met, by analogy to other systems. Therefore the table gives a bit an optimistic view on the proposed metrology. The differences between FSL-systems and the proposed metrology in terms of TRL are not that large. An exception here is the light source. ND-YAG lasers are well developed and being optimised and tested for LISA, whereas FS-lasers have not yet been designed for space-flight operation.

In addition to the mentioned requirements in the Darwin mission documents RD2 and RD3 also the proposed design changes should be regarded. Where previously the relative accuracy of 1nm was required, here it is only optional. As explained in chapter 3 the fringe tracker will deliver the high accuracy data and the proposed relative interferometry only disburdens this fringe tracker a bit. An increase in the knowledge of the absolute distance can be appreciated, since it reduces the blind scanning time.

Technical performance

In terms of technical performance at least four of the FSL-concepts should be regarded, see **Error! Reference source not found.**. Here we should distinguish between systems that replace only the DWI and systems that replace the DWI as well as the relative interferometer. Taking into account the changing mission requirement we propose a high repetition rate diode laser (27GHz) with intensity cross correlation based on an OPD scan in the reference arm. The repetition frequency will be locked to a simple commercial clock (10^{-10} accuracy). As a result we offer a relatively simple system that replaces the DWI, but not the heterodyne interferometer.

The absolute distance measurement is performed more accurately than required (down to a few micrometers), giving some reduction of the required blind scanning time of the delay line. In addition the range over which the FSL-metrology can be operated is larger. Although there's no fundamental limit to the operating range, the frep stabilisation and the power budget will impose constraints at the large distances. (distances over about 1000m)

Satellite motion is dealt with in a different way. The proposed FSL-system will use a compensating technique to find the pulse overlap and then close loop control to maintain the overlap. Due to the high repetition rates of the laser, the first step is the most complicated. The DWI-system provides instantaneous absolute distance information, but needs sufficient sampling to guarantee the required accuracy (and

instantaneous sampling of both interferometers) Therefore this imposes a constraint on the minimum sampling rate.

Mass, volume and power

In terms of mass, volume and power the most FSL-concepts are very comparable to the baseline metrology since the required hardware is very comparable. The DWI uses four AOM's, whereas the frequency combs based systems often use high frequency phase meters. The concept we propose has the lowest complexity and number of components. As a result the mass volume and power consumption will be somewhat lower than that of the proposed DWI and heterodyne interferometer combination.

The mass of the system is mainly determined by the number of components in the optical system and the required system stability. In comparison to the proposed metrology system a large reduction of components is achieved. This is mainly due to the omission of the optical frequency stabilisation. On the other hand we introduce a delay line as an extra part in the system. Altogether the volume and mass will be reduced to less than half of that of the DWI system.

The power consumption is in general dominated by the lasers and electronics devices that are operated at high frequencies. Here the laser conversion efficiency shows significant differences for different types of lasers, but that does not affect the overall power to much. The main advantage of the proposed FSL-metrology is that it uses low frequency electronics with the exception of the clock, the first stage of the detection and the laser it self. On the other hand we introduce a delay line, where no moving parts were present in the previous design. Altogether we estimate as a safe starting point that the energy consumption will be reduced to about half of the DWI metrology.

Extra measurements and redundancy

In terms of extra measurements and redundancy the proposed FSL-concepts is configured to replace the DWI but with an increased accuracy. As a result the blind scanning range of the delay line is reduced. On the other hand we removed the nm-accurate heterodyne interferometer, which will increases the constraints on the fringe-tracker somewhat.

Technical risk

In terms of technical risk more uncertainties are found when choosing the FSL-system. The technology readiness level is not so much different for the DWI and the FSL-systems. Both systems have not yet been flown in any mission. It has to be said that the DWI-optics have been tested in vacuum, which is not the case for the FSL-metrology. In order to perform a decent risk analysis the design concept should be known. Within this project the design activities are performed in the next phase. At this stage the design is known only to the type of component level. For the actual design a simple basic design is assumed. This implies that the actual technical risk will be lower for an optimised design, since there the main sensitivities should be minimised by the design.

System design

- A low dispersion interferometer with a delay line in the reference arm needs to be designed. As has been identified in TN2 [AD 4], the stability properties of this requirement are not yet well known. However no major difficulties are expected here since the system aims at µm-level accuracy and not at the nm-level. Some special care is required for the delay line, since it should be simple, fast and low dispersion.

- The pulse correlation technique needs to be selected as well. Here an important property is that it should give directional information. In addition it would advantageous if the pulse correlator gives instantaneous feedback and can be operated at low frequencies. This will help to reduce the power consumption.
- In the DWI experiments it was identified that the synchronization of the interferometers and the stability of the polarization were critical. A small advantage for the FSL-metrology is that these specific problems will not occur.

Mission related

- Since OPD scanning is used to find and maintain the fringe overlap, the OPD noise is required to be smaller than a small part of the pulse length. Otherwise the overlap could be lost and a new scan should be started. This is very similar to the heterodyning alternative and therefore it imposes no additional risk. Since we use intensity correlation and not fringe position determination the requirement here is relieved by about one order of magnitude.

Optical bandwidth related performance

- Broadband splitters, mirrors, lenses and coatings required instead of narrow band. In general optimization of components over a large bandwidth will be more difficult that over a smaller waveband. This will somewhat reduce the system transmission and increase the polarization leakage, but this does not directly endanger the functionality. In the design this performance should be anticipated.
- Negative dispersion mirrors or dispersion compensation is new in space
- Small laser line width is required for large ISD values. Here a single mode Nd-YAG in a DWI will have a much longer coherence length. However an external cavity laser diode, which is used in an FSI-system will have a smaller coherence length. Altogether one needs to pick the FSL-source carefully. The coherence length should not only be sufficiently large at the start of the mission but also after years of operation.
- For large distance variations a large variation of the FSL-repetition frequency is required. For values larger than a few percent special care is required to maintain the cavity alignment.

Material and component degradation:

- Spectral changes by radiation aging of glass. This effect is no importance to small bandwidth systems. For an FSL-system however the increased absorption in the blue changes the pulse width and shape and that could be interpreted as length changes. In the simulations this effect should be anticipated.
- Fast electronics failure. High speed electronics have a larger risk of failure than low speed electronics due to the smaller lines used in the electronics. Therefore we minimized the use of very fast electronics by choosing detection schemes that work at a lower frequency.
- Diode laser aging.
- Crystal aging. Due to the Kerr lens Mode Locking the peak powers in the crystal are substantially higher than the peak powers in other lasers. Therefore this effect imposes an additional lifetime risk for FSL-systems.

System alignment

- Fiber coupling stability. PCF's have a very small core diameter, even smaller than for a single mode fiber. Therefore the alignment should be preserved somewhat more stable than for a single mode fiber.
- Beam alignment on the detector with respect to the reference beam. Changes in pointing should not be interpreted as signal. If fiber coupling is used here that reduces the system efficiency.
- Reference arm properties are measured as well. This effect is common to any other interferometer and therefore is not more critical here.

External referencing

- The need for external referencing is very similar in the various measurement systems. When for a cw-laser the accuracy divided by the working range is larger than the frequency stability of the emitted light, external referencing is required. Typical numbers could be 10^{-9}. An FS-laser with a tuneable cavity always needs a reference because a signal is required. For very low end applications this could be a clock, whereas for high end applications a more advanced clock can be used. Although primary RF frequency standards provide excellent stability and accuracy (the stability of a commercial Cs clock reaches 5×10^{-12} $\tau^{-1/2}$, accuracy $\sim10^{-14}$), transferring this stability to the frequency comb requires care. Since the feedback loop effectively reacts to phase shifts of the f_{rep}-signal compared to the reference frequency signal, a tighter lock is achieved when a faster oscillation (i.e. a higher frequency) is used in the locking scheme, as a given phase shift then corresponds to a shorter time period Δt.

6.2 XEUS trade-off

In the XEUS mission scenario a distance metrology comprising a laser ranger and a DWI is anticipated. The laser ranger is required to bring the spacecraft safely within the operating range of the DWI. The DWI in its turn is used to align the mirror element and to control the formation. Since the lateral measurements are determined by multilateration multiple DWI's are required. In total a number of three or four DWI-systems is foreseen.

Table 6-2 XEUS-mission trade-off

System property		***Requirement***	***FSL-system***	***DWI with laser ranger***
Technical	Range	35 or 50m ±12cm 35-120m	50.1m ±10cm Larger range optional	0-500m ±5cm DWI@30GHz 10-300m Laser ranger
	Accuracy / Resolution	<1mm ranger ±330µm/50 formation ±50µm/50 petal alignment	±3µm or ±0.3µm to release base length knowledge The metrology will measure both length, lateral and angular parameters	0.25mm ±3µm (not tested) ±0.3µm Open issue
	Bandwidth	1-10Hz	10Hz	>1MHz DWI >Hz Laser Ranger
	Satellite motion	20mm/s during formation Few µm/s during science operation	Can cope with drift using a compensation technique	Ranger: up to large velocity DWI ~10mm/s
	Variation of configuration	±12cm longitudinal <50cm lateral	Not with base system Large range allowed for extended system	Configuration knowledge required to identify the synthetic wave number
	Absolute vs. relative	Abs. required Rel. Optional	Absolute distance measurement	Absolute distance measurement, within a synthetic wave
Mass, Volume, Power	Mass	3.6kg ranger 22.3kg DWI	<20kg (Replace DWI and Laser Ranger) <15kg (Replace Only DWI)	3.6kg ranger 22.3kg DWI

	Volume			
	Power	5W ranger 50W DWI	<50W (Replace DWI and Laser Ranger) <45W (Replace Only DWI)	5W ranger estimate 50W DWI estimate
Extra measurements / redundancy	Extra measurements / redundancy		FLS can be designed to replace laser ranger as well	RF-metrology, laser ranger and DWI show overlapping ranges
Technical risk	Differences in behavior			
	Sensitivity to perturbations			Uncertainty in DWI spacing (base length knowledge)
	Critical items		Dispersion free design Radiation hardness	DWI synthetic wave too short
	Required developments		Space qualified Er-comb laser	DWI accuracy FM

As is clear from Table 6-2, the proposed metrology consisting of DWI and laser ranger meets all requirements. One should not forget however that this metrology has been demonstrated only on a breadboard (HPOM) and on short distances (few m). Additional experiments on longer distances, the design of a FM or EQM and the testing of this design still need to be performed. It is assumed that the mass and power budgets can be met, by analogy to other systems. Therefore the table gives a bit an optimistic view on the proposed metrology system. The actual differences between FSL-systems and the proposed metrology in terms of TRL are not that large.

Here it should be noted that the requirements can also be met using more simple or direct measurements. The baseline system uses triangulation to determine lateral position and tilt. For these measurements some alternatives are available. (Assuming a sufficient stiffness of the MSC)

- Tilt measurement of the MSC can also be performed using an autocollimator and a mirror on the MSC.
- Position measurement of the MSC can also be performed using a collimated beam and position sensor on the DSC and a retro reflector on the MSC.
- Lateral Position measurements can also be performed using accurate (arcsec-level) angle measurements.
- MSC or Petal tilt measurement can be determined very accurately using relative distance measurement (interferometry)
- For the mirror alignment the most direct result would be found by using the X-ray image for analysis. (A wavefront sensor would even be better)

Technical performance

In terms of technical performance several of the more complex FSL-concepts should be regarded. Here we should distinguish between systems that replaces only the DWI and systems that replace the DWI as well as the laser ranger. Taking into account only the replacement of the DWI we propose a Er-doped fiber comb with intensity cross correlation based on an f_{rep} scan. The repetition frequency will be compared to a simple commercial clock (10^{-10} accuracy). As a result we offer a relatively simple system that replaces the DWI, but not the laser ranger. In order to replace also the laser ranger the scan range of the repetition frequency will have to be enlarged substantially. This could complicate the cavity design a bit, but certainly is feasible.

The absolute distance measurement is performed more accurately than required (down to a few tenths of a micrometers), reducing the requirement of the knowledge of the absolute distance between the different measurement heads. (from 1μm to 80μm)

Satellite motion is dealt with in a different way. The proposed FSL-system will use a compensating technique to find the pulse overlap and then close loop control to maintain the overlap. Due to the high repetition rates of the laser, the first step is the most complicated. The DWI-system provides instantaneous absolute distance information, but needs sufficient sampling to guarantee the required accuracy. (As well as the instantaneous sampling of both interferometers) Therefore this imposes a constraint on the minimum sampling rate and the interferometer synchronisation.

Mass, volume and power

In terms of mass, volume and power the most FSL-concepts are very comparable to the baseline metrology since the required hardware is very comparable. The DWI uses four AOM's, whereas the frequency combs based systems often use high frequency phase meters. The FSL-concept we propose has the lowest complexity and number of components. As a result the mass volume and power consumption will be somewhat lower than that of the proposed DWI and laser ranger combination.

The mass of the system is mainly determined by the number of components in the optical system and the required system stability. In comparison to the proposed metrology system a large reduction of components is achieved. This is mainly due to the omission of the optical frequency stabilisation. Up to what extend the optical reference is required is not discussed in the reference documents. Due to the smaller distances for XEUS than those for Darwin, the need for frequency stabilisation is relieved by about one order of magnitude. (Just for the DWI to work, there is no direct requirement to have the stabilisation at all.)

When replacing only the DWI, the power consumption will be very similar than for the DWI. The proposed Er-fiber comb has an efficiency, roughly comparable to the Nd-YAG lasers. However only one laser will be used instead of the two needed for the DWI. The AOM's will be replaced by the high frequency comparison and control. Therefore the overall gain in power consumption is estimated be limited.

Extra measurements and redundancy

In terms of extra measurements and redundancy FSL-concepts can be easily configured to replace both the laser ranger and the DWI. As an alternative to reducing the power consumption the FSL-laser could be planned in a larger number, reducing risk, but at a same level of power consumption.

Technical risk

In terms of technical risk more uncertainties are found when choosing the FSL-system. The technology readiness level is not so much different, with the exception of the laser systems. In order to perform a decent risk analysis the design concept should be known. Within this project the design activities are performed in the next phase. At this stage the design is known only to the type of component level. For the actual design a

simple basic design is assumed. This implies that the actual technical risk will be lower for an optimised design, since there the main sensitivities should be minimised by the design.

System design

For the DWI it is assumed that the design can be scaled to ten times higher synthetic wave frequency at no technical cost. Increasing the synthetic wave frequency implies that the phase measurement/interpolation will be performed at 10 times higher frequencies with the same accuracy. Although it seems feasible using modern electronics, far this has not been proven yet in a DWI design. As a result of the shorter synthetic wave the DWI will also require a mechanism to asses the total number of waves. Where before the number was always fixed, now some variation will occur.

The FSL system needs to be detailed some more to predict the ultimate performance. At this stage the pulse overlap detection scheme design is critical for the performance. Special attention is required here.

Mission related

- When the frequency scanning is used to find the fringe overlap, the OPD noise is required to be smaller than a small part of a pulselength. Otherwise the overlap could be lost. This type of risk is very similar to the heterodyning alternative and therefore it imposes no additional risk. (The sensitivity is lower than for a heterodyning interferometer.)

Optical bandwidth related performance

- Broadband splitters, mirrors, lenses and coatings required instead of narrow band. In general optimization of components over a large bandwidth will be more difficult that over a smaller waveband. This will somewhat reduce the system transmission and increase the polarization leakage, but this does not directly endanger the functionality. In the design this performance should be anticipated.
- Negative dispersion mirrors or dispersion compensation are new in space
- Small laser line width is required for large ISD values. Here a single mode Nd-YAG in a DWI will have a much longer coherence length. However an external cavity laser diode, which is used in an FSI-system will have a smaller coherence length. For the proposed FSL-scheme, the coherence length is not so much an issue since we plan to use intensity correlation rather than fringe correlation. Only for the accuracies really smaller the wavelength of the light coherent measurement and reference beam are required.
- For large distance variations a large variation of the FSL-repetition frequency is required. For values larger than a few percent special care is required to maintain the cavity alignment. For the proposed $1.5^{0}/_{00}$ no specific attention is needed.

Material and component degradation:

- Fiber transmission. Special care is required to prevent the fibers from aging due to the cosmic radiation.
- Spectral changes by radiation aging of glass. This effect is no importance to small bandwidth systems. For an FSL-system however the increased absorption in the blue changes the pulse width and shape and that could be interpreted as length changes. In the simulations this effect should be anticipated.

- Fast electronics failure. High speed electronics have a larger risk of failure than low speed electronics due to the smaller lines used in the electronics. Therefore one should try to minimize the use of very fast electronics by choosing detection schemes that work at a lower frequency.

System alignment

- Fiber coupling stability. PCF's have a very small core diameter, even smaller than for a single mode fiber. Therefore the alignment should be preserved somewhat more stable than for a single mode fiber.
- Beam alignment on the detector with respect to the reference beam. Changes in pointing should not be interpreted as signal. If fiber coupling is used here that reduces the system efficiency. Since we plan to measure in the micrometer range rather than the nm range, no extreme difficulties are expected here.
- Reference arm properties are measured as well. This effect is common to any other interferometer and therefore is not more critical here.

External referencing

- The anticipated external reference is a commercial type electrical clock, which will deliver sufficient frequency stability at a low cost of volume and power consumption.

7 XEUS metrology concept

7.1 XEUS Mission for Mapping X-ray Sources

The X-ray mission XEUS (X-ray Evolving Universe Spectroscopy) is one of the potential future missions in the framework of Cosmic Vision as successor for the highly successful X-ray mission XMM-Newton. XMM used Wolter telescopes with a diameter of 70 cm and a focal length of 7.5 m. XEUS increases the telescope diameter to 4.3 m fitting yet in an Ariane-5 fairing. Preliminary studies have investigated several approaches with focal lengths in the order of 35 up to 50 m. One aspect was kept always constant: a focal length of several tens of metres - with currently 35 m it is too large for a conventional telescope structure. Therefore the XEUS mission will consist of two parts, the Detector Spacecraft DSC and the Mirror Spacecraft MSC flying in formation, this time on a halo orbit around L2. The MSC is free drifting while pointing to the sources of interest. The DSC as the smaller spacecraft will be the active partner and has to maintain its position behind the MSC over the entire mission phase.

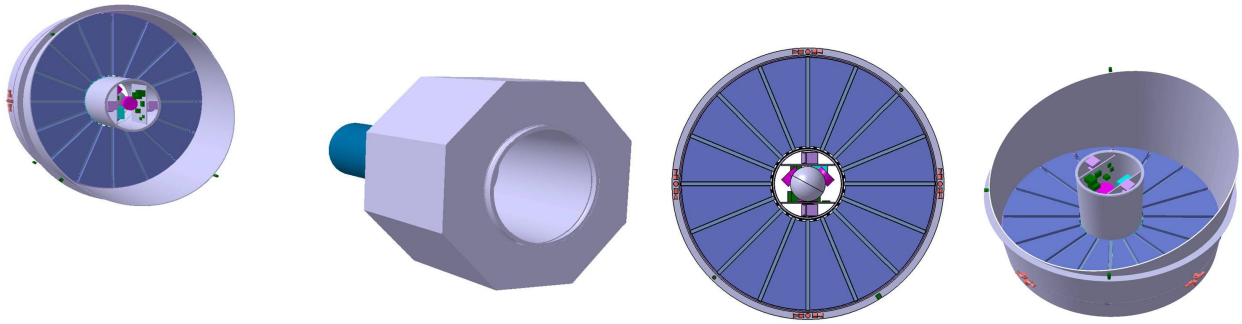

Figure 7-1 Sketches of XEUS spacecrafts Mirror SpaceCraft (MSC) and Detector SpaceCraft (DSC) in the 2006 design with 35m focal length and 5m^2 mirror area (source www.esa.int)

7.1.1 Key Requirements

The yet preliminary requirements taken from the Scientific Requirements of XEUS, issue 2.2, 01, July 2005, Mission Requirement Document, issue 1, 30 Sept. 2005, and the XEUS Payload Definition Document as reference document for the recently released XEUS Telescope Accommodation Study refer to the Formation Flying aspects, in particular to their metrology and are listed below:

- Halo orbit around L2 (eclipse free); direct injection with Ariane 5 or Delta IV Heavy
- Reference scenario: Ariane 5 bringing 6.6 tons to L2 (MSC + DSC)
- Total cruise duration 3-5 months
- Formation flight at ≈ 35 m distance
- Pointing error
  - MSC absolute measurement accuracy <1 arcsecond
  - DSC absolute pointing error <1 arcminute for line of sight
- Field of View
  - 7 x 7 arcminutes for WFI (but detector is oversized)
  - 0.75 x 0.75 arcminutes for both NFI options

7.1.2 Metrology Requirements

According to RD04 (October 2004) RF metrology will bring the DSC to ±12 cm lateral and ± 5 mm longitudinal to the focus of the MSC. Longitudinal metrology maintains the DSC in the focus of the MSC to 0.75 mm. Lateral metrology (cameras) positions the focus to 0.33 mm on a 5 mm detector. Pitch and yaw are measured to ±10 arcsec allowing attitude control with ±1 arcmin accuracy.

Taking RD05 (September 2005) the focal point of the X-ray mirrors mounted on the MSC must be aligned in orbit to an accuracy of ±0.5 mm in all three dimensions. It is not yet defined how the alignment of the numerous petals is performed. Active systems on the MSC based on local laser metrology are the current baseline but the quality of the image of a reference object on the DSC could be used as well for the alignment process.

The DSC must keep its position within ±3 mm (2-σ value) in longitudinal direction and ±1 mm (2-σ value) in lateral direction.

One idea followed in the last time is to use only one metrology system located on the DSC performing both, the petal alignment first and keeping the DSC position second during the formation flight.

The difference between the inertial attitudes of DSC and MSC shall be controlled to less than 1 arcsec.

Recently, the ITT "XEUS Telescope Accommodation Study" has been released (May 2006). This latest and actual document defines XEUS as two separate spacecrafts flying in formation and having a focal length of 35 m obtained without the use of a large deployable bench or a telescope tube system. The detector envelopes and focal depth imply that the focal point must be located within about 1 mm, in all 3 dimensions, of the focal reference point. A combination of RF and laser metrology is assumed to provide the distance information. The laser metrology must perform much better than this accuracy.

In order to establish the baseline for the design of the HAALDM-scheme and consequently the basis for the numerical simulations, based on the information presented in the mission documentation (RD04, RD05 and RD150) and on the ongoing activities and discussions, the following premises where settled:

- XEUS metrology should target to measure all 6 degrees of freedom of DSC relative to MSC (see Figure 7-2),
- The nominal distance is set to 35m but sensor concept/performances should be compatible with any nominal distance within the range 10 to 100m,
- Distance range is set to 35 m with an controlled variation of 1m in all 3 axis, needed e.g. for detector system selection and controlled (de)focusing,
- Most active components (and complexity) to be on the DSC,
- The DSC will be a square with 2 m side and the MSC will be round with 4.3 m diameter.

Table 7-1 presents the numerical values of the relevant parameters for the metrology definition.

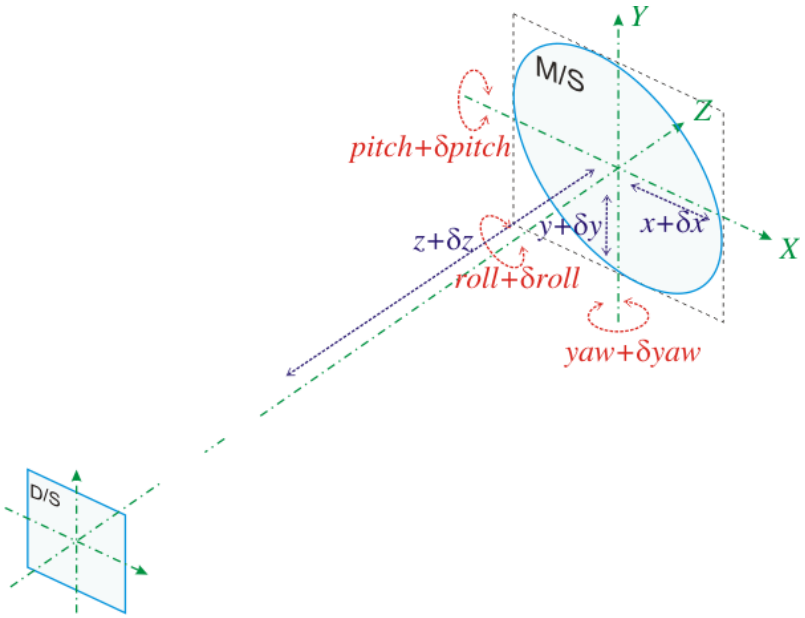

Figure 7-2: XEUS MSC position relatively to the DSC and corresponding degrees of freedom.

Table 7-1 XEUS technical requirements relevant for the metrology system

Parameter (Figure 7-2)	Value and Range	Uncertainty (2σ)
z (ISD)	35 m ± 1 m	300 µm
x & y	0 m ± 1 m	170 µm
pitch & yaw	0 degrees	10 arcsec
roll	0 degrees	TBD (>>10 arcsec)
Required bandwidth	At Hz level	

7.1.3 XEUS Metrology approach

This mission has the least strict requirements of the formation flying missions. Here the motion that the measurement system has to be able to keep up with probably is determined by the slew maneuvers of the configuration. During the measurements the configuration is kept steady and due to the location in L2 the expected perturbation level is very low. However during change of target the constellation rotates the Mirror Space Craft and the Detector Space Craft has to maintain configuration by adjusting its position and orientation. The solution, proposed in the CDF study [RD 4] is to use a trilateration (or multilateration) scheme to obtain both the lateral displacements and angular orientation of the DSC with respect to the MSC from an absolute distance metrology. This scheme would reduce the number of different sensors and the complexity associated with the determination of the position of the Mirror Spacecraft. In trilateration, from three points (or more) on the DSC distances are measured to three (or more) positions on the corners of the MSC. Nevertheless, the requirements on the absolute distance metrology increase considerably to achieve the needed angular accuracy.

Simplified alternative

As an alternative to the triangulation using at least six distance measurement, also a combination of measurements of angles and distances is possible. This approach to a much simplified distance measurement system but in addition also angle need to be determined. Any combination of angles and distances can be used as long as the number of independent measurements is at least six. The most logical approach for the

design of this alternative is too measure three distances and three directions. Practically one needs only one measurement head in the DSC and three retro reflectors on the MSC. This approach is schematically depicted in Figure 7-3.

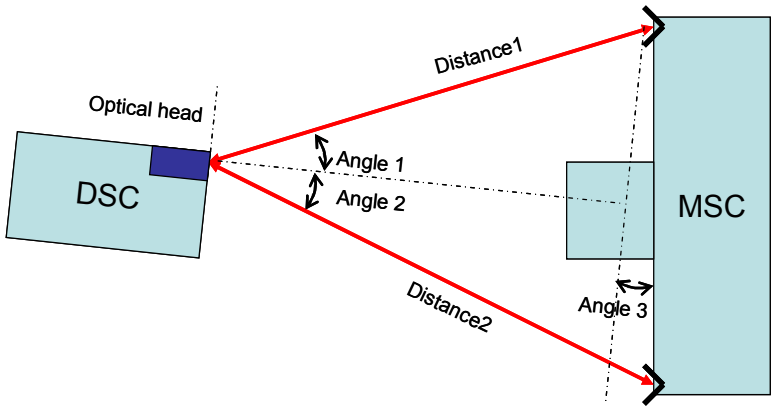

Figure 7-3 Schematic drawing of triangulation using a combination of angular and distance measurements

Basically the distance measurements yield the orientation and position of the MSC with respect to the optical head, whereas the used pointing angles will yield the orientation of the DSC and again the ISD. The required accuracies for the distance measurement in this set-up are identical to the system were only distances were measured.

The required accuracies of the pointing angle measurement need to be approximately 10arcseconds. (Requirement on DSC pitch, yaw and roll) This means that the steering mirrors then need to be equipped with a calibrated sensor for the tilt measurement. However this requirement is only a rough guess. In the real mission the requirement probably is not this strict, since the DSC-orientation has a limited effect on the science performance.

7.2 XEUS Metrology by Trilateration

The trilateration approach followed in this study was to perform four measurements from points located in the DCS (squarely spaced by 2 m) to four retro-reflectors located in the MSC (placed in the outer limit), as sketched in Figure 7-4. It has to be noted that the separation between the optical heads of 2 m is arbitrarily chosen, but has some impact on the system performance. The overall accuracy for lateral displacements roughly depends linearly on the separation d. An increase of the base length can also be used to relax other requirements, such as the laser pulse length or shape, or system stability.

Different measurement schemes can be envisaged, depending on the number of sensors and scanning strategies. Depending on required attitude knowledge update rate and on the sensor bandwidth, it might be possible to use a single sensor to perform the four measurements from a DSC point using a scanning mechanics to scan the four retro-reflectors in the MSC. This issue will be detailed later in this document.

Although measurements from three points to three retro-reflectors were enough, a four-to-four configuration was selected as it introduces redundancy, increases accuracy and makes the system performances symmetric (in relation to the center of the MSC). Since the requirements also have to be met using three optical heads, the calculations are based on three optical heads only. The baseline configuration thus uses only three optical heads and under normal conditions the fourth optical head will be used to increase accuracies and as an integrity check.

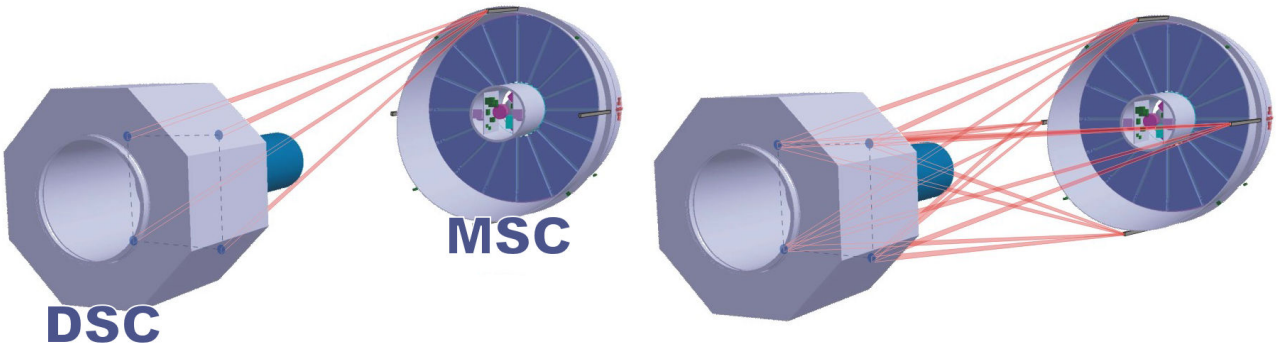

Figure 7-4: XEUS Metrology by trilateration. Single point measurement (left) and overall measurement beams (right) – Although 4 optical heads are shown, the baseline configuration considers only 3.

Considering the coordinate system and the parameters shown in Figure 7-5, the measured distances for a single point *M* are:

$$L_1 = \sqrt{(M_x - d)^2 + (M_y + d)^2 + (M_z)^2}$$ Equation 5

$$L_2 = \sqrt{(M_x - d)^2 + (M_y - d)^2 + (M_z)^2}$$ Equation 6

$$L_3 = \sqrt{(M_x + d)^2 + (M_y - d)^2 + (M_z)^2}$$ Equation 7

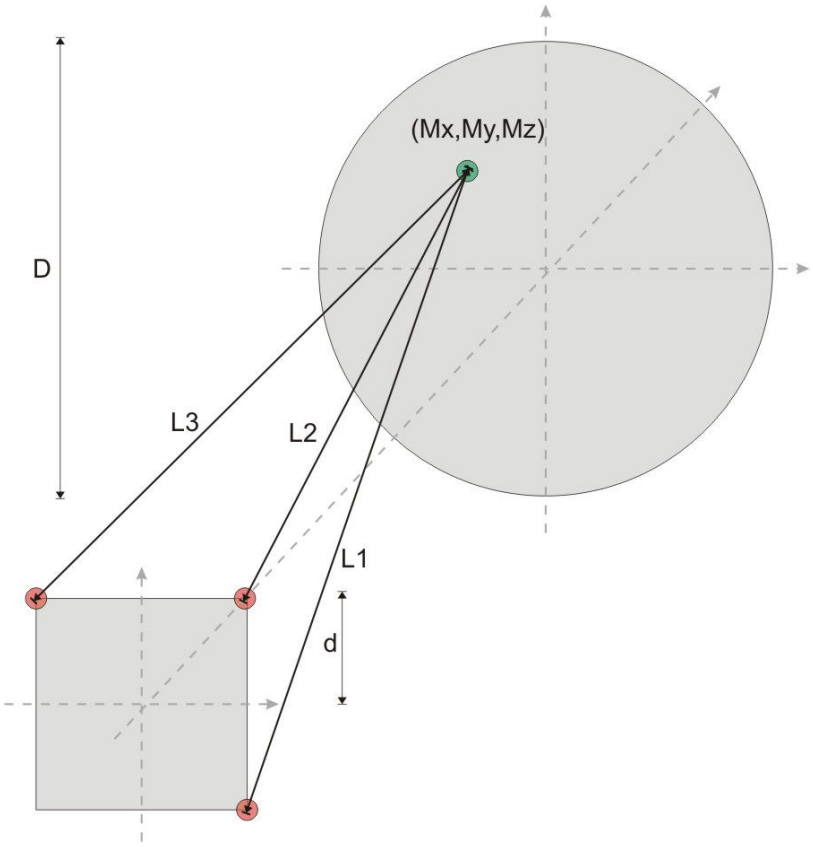

Figure 7-5: Trilateration coordinate system and relevant parameters.

From Equations 1 to 3 we can obtain the coordinates of any point *M* in the MSC from:

$$M_x = \frac{L_3^{\,2} - L_2^{\,2}}{4d}$$ Equation 8

$$M_y = \frac{L_1^{\,2} - L_2^{\,2}}{4d}$$ Equation 9

$$M_z = \sqrt{(L_1)^2 - \left(\frac{L_3^{\,2} - L_2^{\,2}}{4d} - d\right)^2 - \left(\frac{L_1^{\,2} - L_2^{\,2}}{4d} - d\right)^2}$$ Equation 10

Measuring from four points instead of three is equivalent to have four independent trilateration measurements of location *M*, thus reducing the uncertainty by a factor of two.

The determination of the angular orientation of the MSC relatively to the DSC is calculated from the coordinates of two points, particularly selected for each angle, as it is sketched in Figure 7-6.

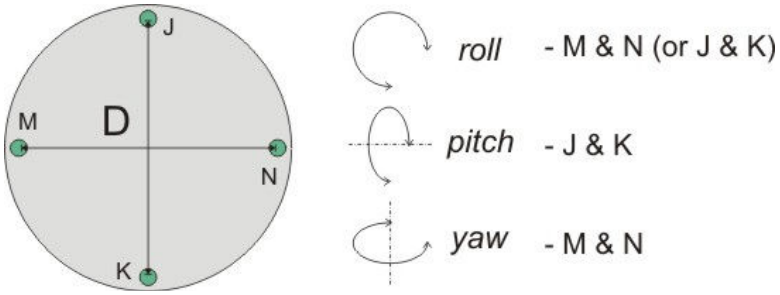

Figure 7-6: Selection of points for the calculation of angular parameters (from trilateration measurements).

7.2.1 XEUS Absolute Distance Metrology requirements from Trilateration

In order to determine the absolute distance measurement accuracy to achieve the metrology requirement presented in Table 7-1, the relationship between parameter uncertainties was determined according to:

$$\delta f = \sqrt{\sum_i \left(\frac{\partial f(x_i)}{\partial x_i} \cdot \delta x_i \right)^2} \qquad \text{Equation 11}$$

where $f(x_i)$ is the parameter equation (point coordinate or attitude angle) and δx_i are the uncertainties for the input variables. The uncertainty corresponds to a coverage probability of approximately 95%.

As it can be seen for Equations 4 to 6, the calculation of the coordinates depends also on the value of the distance d, which is half the size of the square where the detectors are located in the DSC (Figure 7-5). Thus, the final trilateration performances will not only depended on the absolute distance measurement accuracy but also on the uncertainty in the knowledge of d, i.e. the knowledge of the sensor head location. Although this distance could be monitored, it would increase the complexity of the metrology and, as it will be shown ahead, it will be possible to rely only on the calibration of the location considering, in this case, the possible mechanical deformations of the structure as the uncertainty in d.

Figure 7-7 presents the metrology accuracy for all the attitude parameters as a function of the uncertainty in the absolute distance measurement and on the uncertainty in d using four sensor heads.

As it can be seen in Figure 7-7, the MSC attitude parameters uncertainty is mainly a function of only one of the two parameters:

- lateral position, x and y, and angle *roll* are only dependent on the absolute measurement uncertainty;
- longitudinal position, z, and angles *pitch* and *yaw* are basically dependent on the uncertainty in the sensor location d.

In terms of requirement (Table 7-1) fulfillment, it is clear that the governing parameters are the lateral position and the *pitch* and *yaw* angles. The sensor performances should then be set to:

- absolute measurement uncertainty must be < 6.8 μm;
- sensor location (d) uncertainty must be < 1.2 mm.

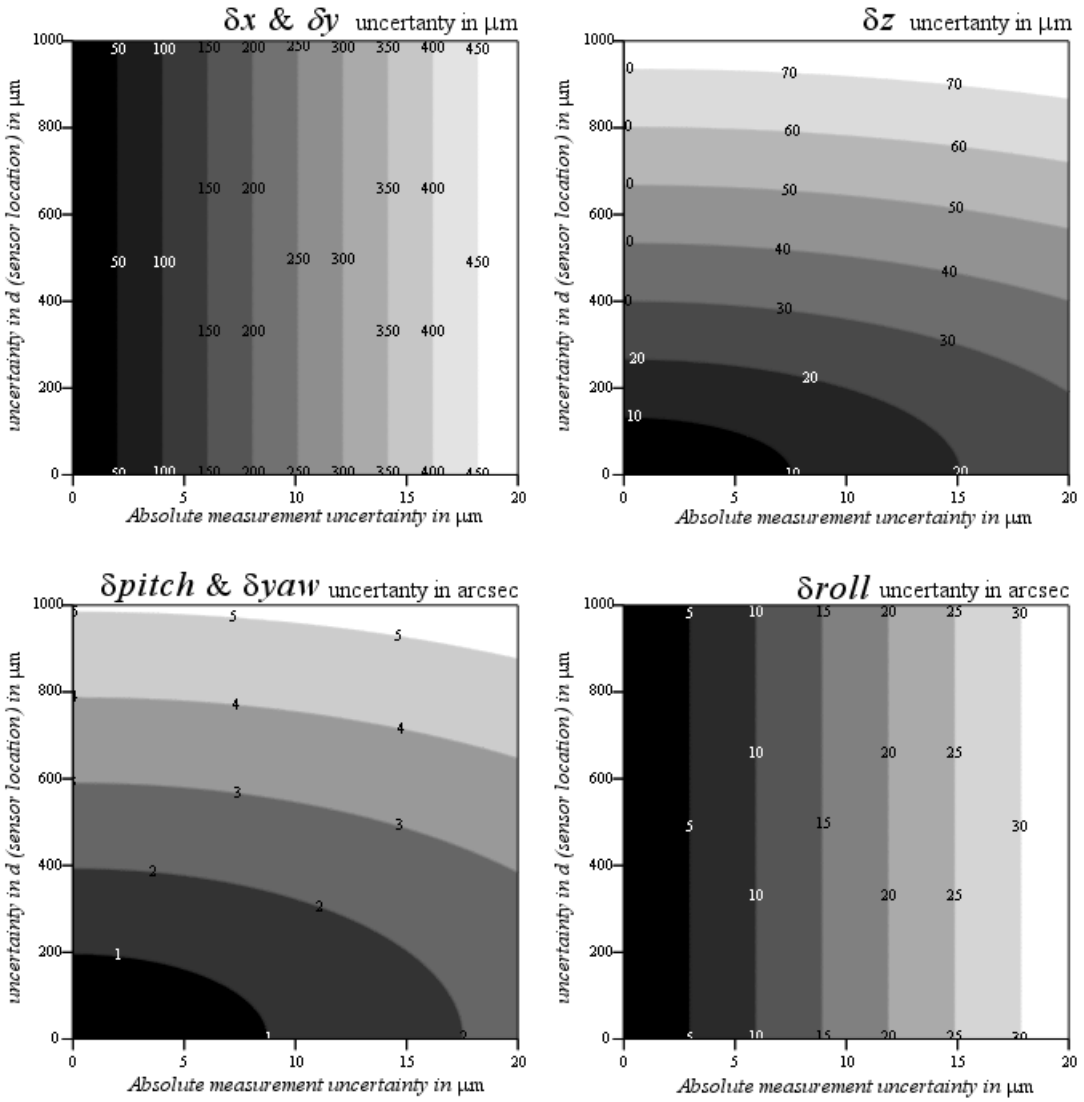

Figure 7-7: Uncertainty of parameters measured by trilateration (with three sensor heads) as a function of the absolute measurement uncertainty and of the uncertainty (of unknown variation) of the sensor location from centre.

The first criteria determine the absolute distance metrology fs-based concept choice. The second has two implications: shows that it is not required to monitor the distance d during the lifetime of the mission, being only necessary to calibrate that distance on-ground with an accuracy at the tenth of millimeter level, and can also give us an indication of how the structure that holds the sensor heads should be implemented. As an example, considering the effect of thermal expansion, by allowing a relative variation of 10^{-4} ($\delta d = 100$ µm for $d = 1$ m) we would permit a thermal variation of ±5 K for an Aluminum structure and ±25 K for SiC. Since it is relatively easy to achieve accuracies for d in the order of 100 µm, the system accuracy will be basically ruled by the ADM performances.

It must be noted that, in the case of four sensor heads, accuracy is basically improved by a factor of 2, besides the fact that it also contributes with redundancy.

7.2.2 MSC 3D Mapping

Instead of having only four retro-reflectors in the MSC, adding extra retroreflectors across its surface, would allow monitoring the tridimensional shape of the MSC (relatively to the DSC), enabling the evaluation of possible structural deformations.

Figure 7-8 shows the accuracy of the metrology in the measurement of the tridimensional parameters in the MSC, considering that the absolute distance metrology as an accuracy of 5 µm and that the distance *d* is known and will not change more than 0.1 mm (in 1 m), for the case of 3 (top) and 4 (bottom) optical heads.

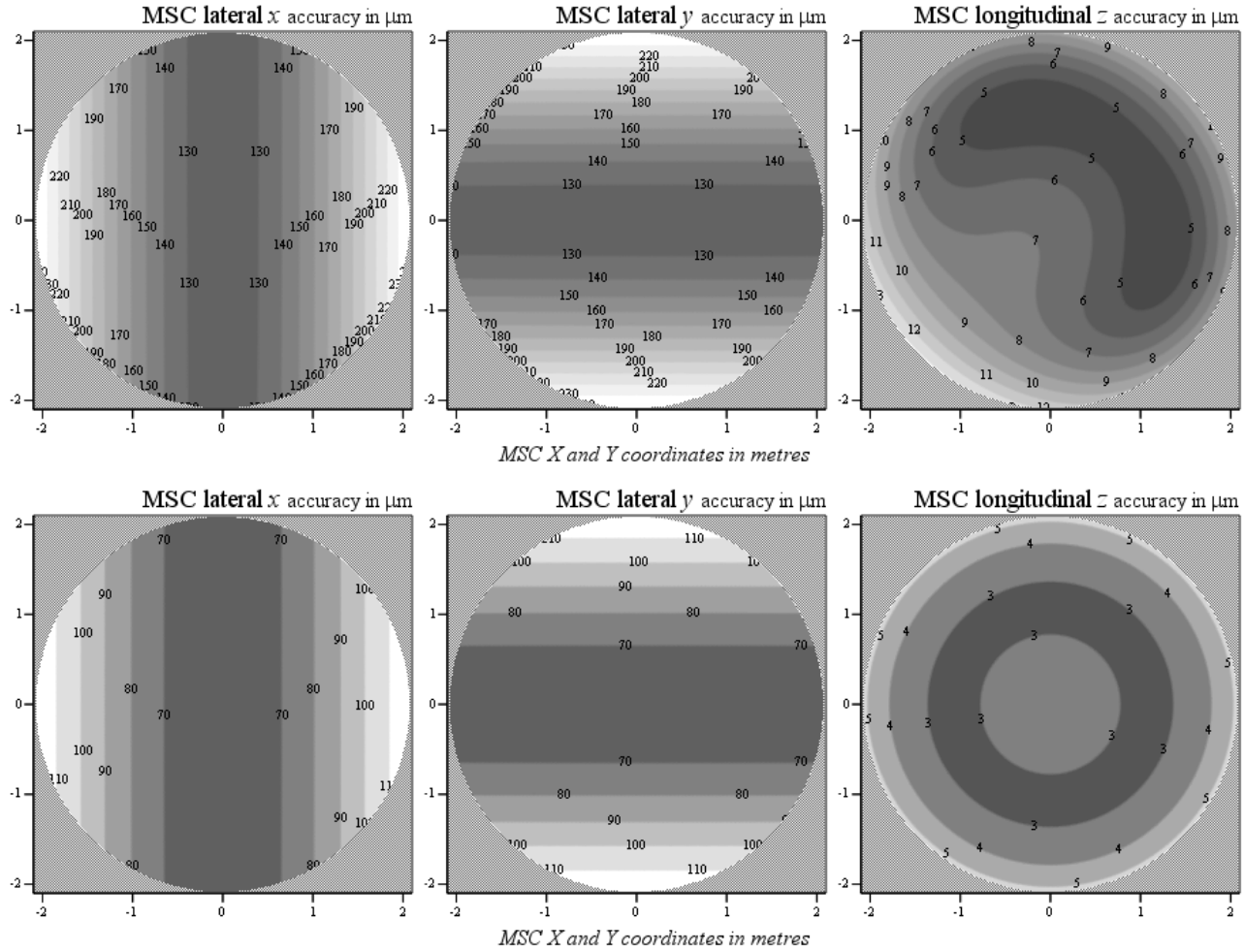

Figure 7-8: Accuracy of the metrology in the measurement of the tridimensional parameters in the MSC (absolute distance metrology with an accuracy of 5 µm and δd = 0.1 mm), for the case of 3 (top) and 4 (bottom) optical heads.

7.3 XEUS Metrology by simplified Trilateration

As discussed before an alternative to the full multi-lateration measurements using at least three optical heads, it's possible to use a single optical head with accurate beam steering measurements. This system is referred to as simplified trilateration.

In general the system performance will not be very different; however this needs to be regarded for each specific performance requirement.

The accuracy lateral displacements δx and δy previously was determined to a large extend by the HAALDM system accuracy, as is depicted in Figure 7-7. This measurement has not been changed directly and hence will give identical accuracies. One has to observe here that MSC pitch and yaw cannot be distinguished from lateral displacements without using the pointing angles.

The distance measurement previously was determined to a large extend by separation between the optical heads d, as is depicted in the top right plot of Figure 7-7. Here this base d does not exist any more. The lateral displacement is determined in the same way, however using the separation between the retroreflectors on the MSC as a baseline. Now this separation s value needs to be known to a similar relative accuracy.

For the accuracies of the pitch and yaw a distinction needs to be made between the MSC and the DSC. The DSC pitch and yaw are directly measured using the beam pointing, whereas the MSC pitch and yaw follow from the combination of the pointing angles and the differences in the measured paths.

Where previously the roll accuracy was dominated by the distance measurement accuracy, now it is given by the differences in the pointing angles towards the different retroreflectors.

8 XEUS System performance

To estimate the trilateration performance of the proposed OHOSE scheme a large number of simulations has been performed. This chapter deals with the perturbations, description of the model and the calculation results. In the last parts these results are compared to the XEUS mission requirements.

8.1 Measurement accuracy and perturbations

The accuracy of the length measurement is determined by a number of parameters and a number of perturbing effects. In general the measurement accuracy is determined by the differences between the pulse shapes, the pulse length, the detected power in a measurement and the accuracy of the reference arm length. Although these are the most important effects, any variation in the system will have some effect in the measurement. Here only the most important parameters are regarded whereas the other effects and combinations of effects are neglected for the time being.

The basis of the perturbation analysis is the function that describes the length measurement. In the proposed cross correlation measurement, the optical power generated by the SHG of the overlapping pulses is detected. In addition the measurement is not performed in a single shot, but is the result of a large number of interacting pulses. The intensity of the SHG signal of two overlapping pulses is described as:

$$I_{Detector}(\tau) = \int_{-\infty}^{+\infty} I_{ref}(t) I_{Meas}(t-\tau) dt \qquad \text{Equation 12}$$

And the centre of the correlation scan is defined by:

$$\tilde{\tau} = \int_{-\infty}^{+\infty} \tau \cdot I_{Detector}(\tau) d\tau \Big/ \int_{-\infty}^{+\infty} I_{Detector}(\tau) d\tau \qquad \text{Equation 13}$$

Two types of error sources can be distinguished: those that affect the overlap position and those that affect the measured intensity. The relation between the impacts of these two is determined by the pulse shape. For a Gaussian pulse shape the correlation pattern will be a Gaussian as well, with a width that is √2 larger than the pulse duration. In that particular case the equation shows no dependence on the actual pulse width. In other words the achievable accuracy doesn't depend on the width of the pulse. This is only true for noiseless pulses. When there are noise sources the pulse width appears as a multiplier for the position error. For the first estimation a Gaussian pulse shape is assumed, which is described by:

$$I(t) = I_0 e^{-t^2/\sigma^2} \qquad \text{Equation 14}$$

Then power P in a pulse is found by integrating over the pulse length to be:

$$P = I_0 \sigma \sqrt{2\pi} \qquad \text{Equation 15}$$

Laser frequency stability

Phase jitter or variation of the repetition frequency of the laser will result in a timing jitter of the overlapping pulses. This jitter is expressed as an inaccuracy of the measurement position.

$$t_{crosscorrelation} = \sqrt{t_1^2 + t_2^2 + t_{jitter}^2} \qquad \text{Equation 16}$$

Laser intensity stability

Pulse to pulse variations of the laser intensity result in a variation of the detected signal intensity.

Detector noise

Due to the low light levels the detector noise will show up in the measurements. As a result a variation in the measured intensities will result.

Delay line position encoder

Inaccuracies of the delay line position encoder will affect the measured position of the best overlap. Statistical variations will add noise to the position measurement, whereas structural errors are interpreted directly as a difference in position. Here one has to keep in mind that due to the folding of the optical path the errors are multiplied by a factor of two.

Delay line dynamic stability

Since the delay line will be operated in a dynamic way, the mechanical part will bend a small bit, creating a variation between the position of the encoder and the retroreflector.

Mechanical stability

Drift between the interferometer arms cannot be distinguished from spacecraft movement and will hence be interpreted as a change of distance. In general changes in the optical paths are due to the (asymmetrical) thermal expansion of the interferometer. More in particular here the distance between the beam splitter (BS) and the beam steering unit (BSU) is included in the measurement path. In the present design this distance is about 200mm, which will not result in errors. However if it is decided that the optics should be combined a longer path will result between the BS and the BSU. Consequently a higher sensitivity to thermal variations will result.

8.2 XEUS performance model

For the XEUS mission a performance model has been made to simulate the achievable accuracies using the proposed trilateration with the OHOSE detection scheme. The model comprises:

- XEUS configurations with 35m nominal separation and 1m Optical Head spacing in the DSC and 4.3m diameter on the MSC
- The Trilateration method using four optical heads and four retro reflectors
- HAALDM based on femto-second lasers
- OHOSE detection scheme with also the functional parameters of its subunits
    - Laser properties such as the pulse repetition rate and pulse length
    - Frequency referencing to an external clock and the resulting frequency jitter
    - Detector and other measurement noise of both the additive type and multiplicative type
- The impact of satellite motion on the measurements

Numbers used in the calculations have been discussed between the partners in order to make them as realistic as possible. As a result the overall model is based on the expertise of the individual project partners.

8.3 XEUS performance

Preferred design

The OPD Scan approach works the best for large f_{rep} values, in order to have a small ambiguity range. To simulate XEUS performances with OHOSE, a frequency comb with f_{rep} of 4 GHz (corresponding to an ambiguity range of 75 mm) and pulse width of 1 ps was considered.

To evaluate the performance of the concept in the XEUS metrology, 250 measurements for each set of parameters were simulated and 2σ dispersion (95% confidence interval) was considered for the determination of absolute measurement uncertainty at a distance of 35 m.

The intensity cross correlation pattern obtained with OHOSE was calculated considering a linear scan in the reference arm, corresponding to a linear scan in the delay τ, and also the timing jitter produced by the f_{rep} instability (dependent on the measured distance), and also the multiplicative, additive and quantification noise introduced by the detector.

Figure 8-1 shows the result of the simulation of a typical intensity cross-correlation pattern, where the horizontal axis of the top graph corresponds to the OPD of the complete ambiguity range.

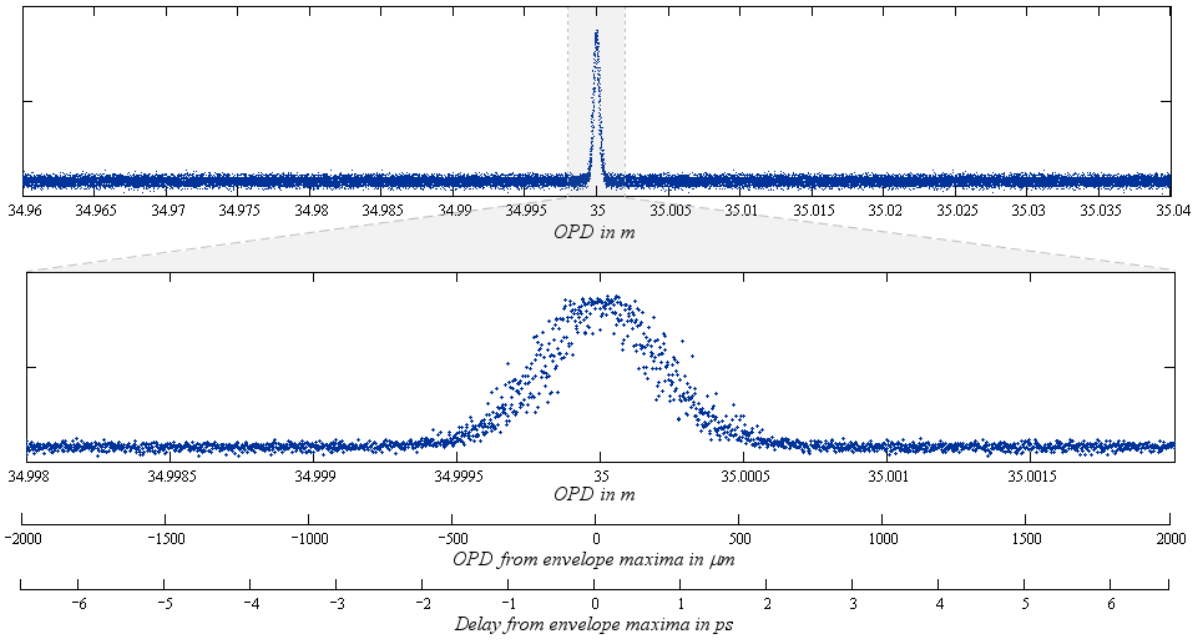

Figure 8-1: Simulation of a typical intensity cross-correlation pattern.

In order to evaluate the requirements on the frequency stability of the laser comb, several simulations were performed for different levels of stability. The main effect on system performances is the instabilities introduced in the pattern, as it is shown in Figure 8-2, that reduces the capability of data processing algorithm to determine the envelope centre more accurately.

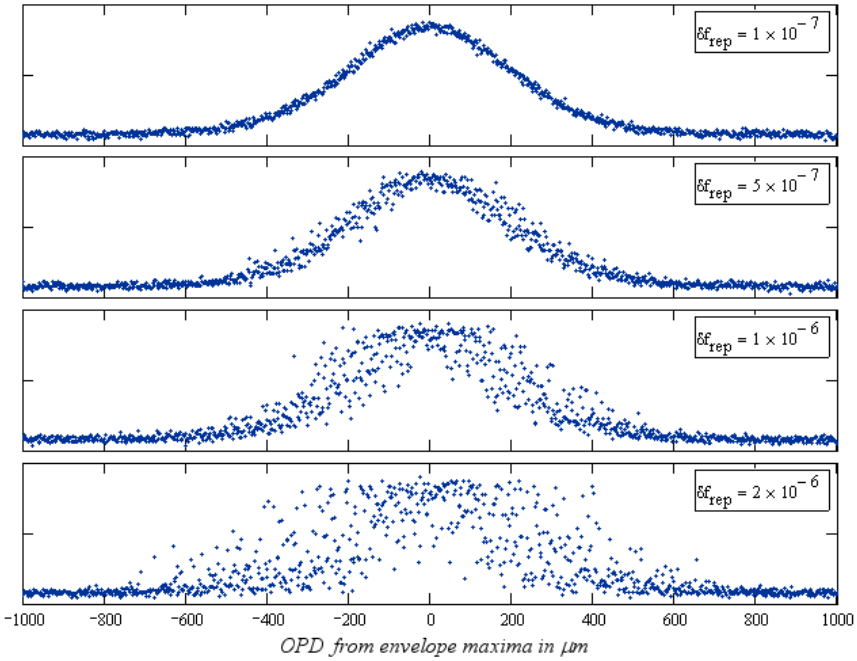

Figure 8-2: Effect of f_{rep} stability on the intensity cross-correlation pattern.

Figure 8-3 shows the absolute distance accuracy of the OHOSE sensor as a function of f_{rep} relative stability. In order to have an accuracy below the required 6.8 μm, it is sufficient to have a stability better than 6×10^{-7}. Comparing with the example level of stability considered in the previous stages of this study[1], this requirement is even lower than the 10^{-7} achieved with a Commercial Cs Clock.

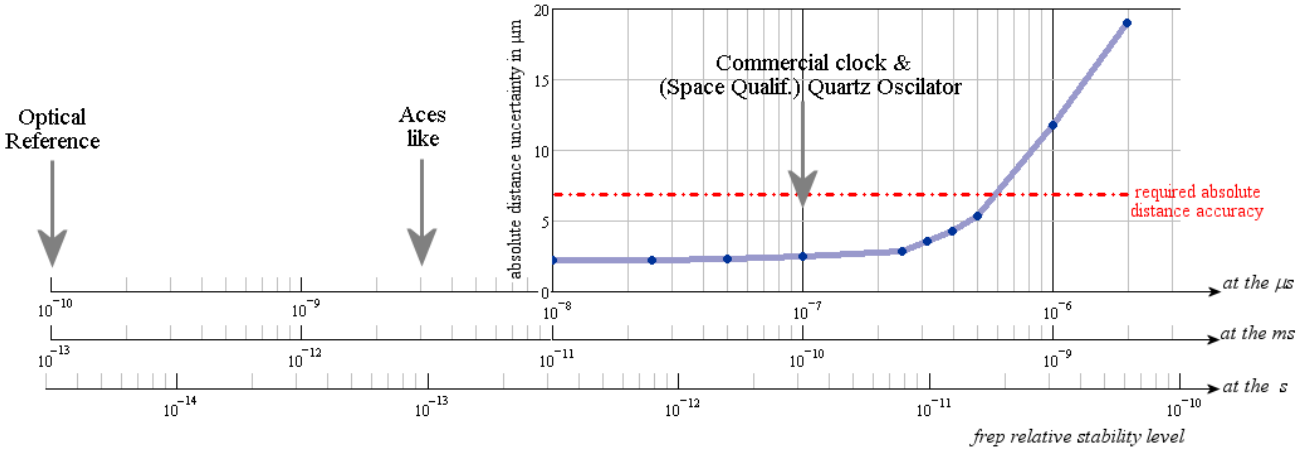

Figure 8-3: Absolute distance accuracy as a function of f_{rep} relative stability with typical clock performances indicated, for the modelocked diode laser.

[1] In the previous TN three frequency references where considered (see Figure 6.3 of TN2 [AD04]): Commercial Cs Clock, ACES like and Optical Reference with, respectively, relative stabilities of 10^{-7}, 3×10^{-9} and 10^{-10}, at the microsecond time scale.

Baseline design

The same procedure applied for the evaluation of the requirements on the frequency stability of the modelocked diode laser in the preferred configuration was also applied to the baseline design, considering a fibre laser with a repetition frequency of 250MHz and a pulse width of 100fs.

Figure 8-4 shows the absolute distance accuracy of the OHOSE sensor as a function of f_{rep} relative stability. In order to have an accuracy below the required 6.8 µm, it is sufficient to have a stability better than 9×10^{-7}, even less demanding than the previous case (1/3 less).

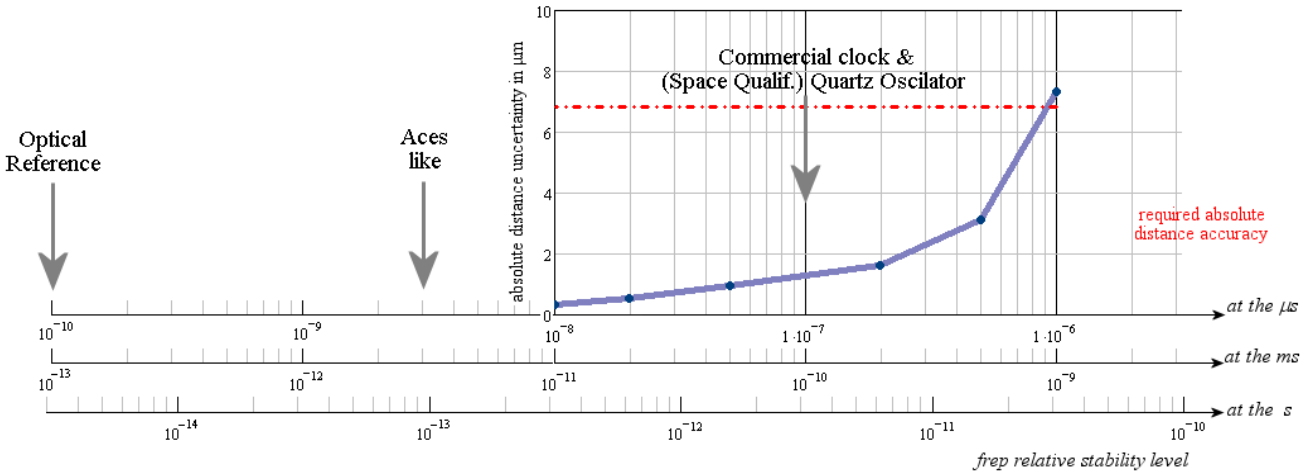

Figure 8-4: Absolute distance accuracy as a function of f_{rep} relative stability with typical clock performances indicated, for the fibre laser.

Comparing Figure 8-3 with Figure 8-4 we can conclude that the use of a fibre laser, instead of a modelocked diode laser, naturally increases the measurement accuracy due to the reduction of the pulse width. This would enable an improvement on the performances of the metrology (by almost a factor of 2) or, as another option, a decrease on the frequency stability requirements (from 6×10^{-7} to 9×10^{-7}). Nevertheless, it must but noted that, due to the larger sensitivity to noise of a smaller pulse width, a stability of 9×10^{-7} in the fibre laser option is very close to the point where a distinct correlation envelope vanishes within the noise.

8.3.1 Effect of spacecraft drift in sensor performances

The mathematical models used to determine the concept performance took already in consideration a large number of parameters, leading to a realistic analysis.

There are, however, other factors not considered in the simulations that might influence the sensor performances like laser coherence length, effect of unbalanced beams in the interferometer, material dispersion, spectral filtering of the measurement beam, and spacecraft drift. All this issues were already described in TN2 [AD4] and, particularly for this OHOSE implementation, the influence in the performances is negligible with a possible exception of the spacecraft drift case.

When a concept is based in an OPD scanning in the reference arm, generating the cross correlation pattern, it is not realistic to assume, at least in space environment, that the distance under measurement is constant during that time frame. Thus, in a situation where the sensor needs some time to perform the measurement, it is important to assess whether the movement during that period of time (drift) can be neglected or must be taken into account.

The effect of drift in an intensity and cross correlation pattern results in a shift in the centre of the envelope and an envelope shrinkage/growth effect (depending on drift signal). To determine if drift can be neglected, three parameters must be taken into account: the drift speed, the measurement duration and the required measurement accuracy. As an example, consider a drift of 10 µm/s and measurement duration of 40 ms (25 Hz). In this case, the maximum error introduced by the drift would be 0.4 µm, which could be neglected for a required accuracy at the micrometre level.

When drift cannot be neglected, assuming that during the measurement duration the drift speed is constant (a condition that is fully acceptable for the current application), it is possible to determine and remove the drift influence using two consecutive measurements with different OPD scan characteristics. Considering that the drift speed is the same for the two measurements, using a symmetrical shape for the OPD variation in the reference arm corresponds to a change in the sign of the OPD variation velocity from scan to scan. In this case, any two consecutive pairs of measurements would be affected by the same amount of drift error but with opposite signs. Simple mathematics would immediately give the correct distance and would also be possible to determine accurately the value of the drift speed.

8.4 Assessment versus XEUS requirements

The XEUS formation flying requirements and the metrology requirements were discussed in paragraphs 7.1.1 and 7.1.2. Here these requirements are mentioned and compared to the simulation results. In Table 8-1 an overview is given.

Parameter	Value and range	Required measurement uncertainty (2σ)	Simulation results
z (ISD)	35 m ± 1 m	300 µm	10 µm
x & y	0 m ± 1 m	170 µm	125 µm
pitch & yaw	0 degrees	10 arcsec	1 arcsec
roll	0 degrees	TBD (>>10 arcsec)	8 arcsec
Required bandwidth	At Hz level		3Hz full cycle

Table 8-1 Comparison of required metrology performance and simulation results

Since the system design was made on the basis of the given requirements it should be no surprise that all requirements met.

The uncertainty of the ISD is dominated by the inaccuracy of the base length. This is the distance between the different optical heads. Here a distance of 2m with an uncertainty of 0.2mm is assumed.

The determination of x any y are clearly the most critical. These measurements are (given the configuration) dominated by the uncertainty of the clock frequency, which is reflected in the laser pulse timing jitter. Here the criticalities occur in the lower part of the frequency spectrum, where the OCXO clock has the limiting performance. At shorter timescales the measurement accuracy will be substantially better.

The uncertainty of the roll measurement show similar sensitivities as the x and y measurements. Consequently these are also dominated by the repetition rate jitter.

These two performances (x and y and the roll) are only marginally within specifications. Here a substantial improvement can be made by improving the reference clock. This will be at the cost of mass and power consumption, of course. In the present design only a simple clock (US-OCXO) is assumed to minimize the mass and power consumption of the overall system.

Pitch and yaw uncertainties again are dominated by the knowledge of the base length. Here also there is room for improvement. Most obvious would be to increase the optical head separation or the position knowledge of the separation.

9 HAALDM system design for XEUS

In the previous chapters the length metrology requirements and the implementation were discussed. As a result the OHOSE system, based on a FS-diode laser was selected to be the preferred design. Using this type of length metrology trilateration measurements are performed from four (three plus one spare) distinct optical heads (in the DSC) to four (three plus one spare) different corner cubes (on the MSC). The overall required accuracy of the length measurement system is 6.8µm. In this paragraph this best fitting HAALDM-scheme is described in more detail and the system elements and their interactions are described to assure that this requirement will be met.

Since the preferred design depends strongly on the development of the required new FSL diode laser technology, a more conservative design is followed as well, as the baseline design. For the baseline design commercially available laser systems are regarded and their impact on the overall design is discussed.

9.1 OHOSE sensor implementation

OHOSE is the acronym for Optical Heterodyning with OPD Scan and Intensity Cross Correlation Envelope Detection. This name already describes to a large extend the operation of the technique. As a reminder the operation principles are repeated. A more detailed explanation of the OHOSE (and the other possible HAALDM-schemes) is given in TN2 [AD05].

Heart of the OHOSE-scheme is pulsed laser, which emits short pulses (~1ps for the preferred design) at a fixed high repetition rate (~4GHz for the preferred design). By changing the length of the reference arm, the interferometer arms are equalized, creating overlapping pulses. At this delay line position, the measurement distance is equal to an integer number of pulse periods (times the speed of light), plus the path length in the delay line. Thus the absolute distance is determined, by knowing how much the length of the reference arm changed from the reference position and the integer number of pulse periods. In our situation the integer number of pulses is determined using the RF-metrology. (Although implementation of a pulse number determination branch into the sensor, is feasible.)

This OHOSE scheme is the least complex HAALDM-system to implement as it does not require any complex control or measurement of the FS-Laser. However, to allow a complete scan between consecutive pulse periods, the required delay line scan range, becomes large for small values of f_{rep}. Although the alignment and operation of this “delay line” in the reference arm are not a critical issue, the maximum achievable OPD scan range is limited to a about a few hundred millimeters (for the preferred design). This limitation is a result delay line dynamical stability for the required position accuracy and the delay line acceleration. As a consequence, this approach is most effective for f_{rep} values at the GHz level.

Still the estimated measurement accuracy is at the micrometer level, and the measurement range, depending on the f_{rep} stabilization, can go up to several tens of km. In addition there is no minimum range limit for this OHOSE-scheme.

9.1.1 Laser and comb

Preferred design

The ideal OHOSE light source is a mode-locked diode laser. Diode lasers are efficient, have a high repetition rate and require only a low complexity control system. For this application only the stabilisation of repetition rate is required, which can be achieved in a relatively simple way. Typical power output levels for this type

of diodes are up to a few to tens of mWatt around a centre wavelength of 1550nm. Typically the pulse duration is about 1-2ps. Two main types of lasers are available here. These are bulk lasers and Quantum Dot (QD) lasers. In general the output power of the QD-lasers is higher and its repetition rate is lower. Anther large difference is that the QD lasers usually show a larger chirp on the pulses than the bulk counterpart. (A chirp doesn't alter the symmetry of the intensity correlation pattern) Finally the noise on the repetition rate of the QD-lasers is lower (mainly on the low frequency side). Both types of diode lasers can be used.

In Figure 9-1 an example of the performance of a bulk diode laser is depicted. Please note that this laser was free running and not repetition frequency stabilised.

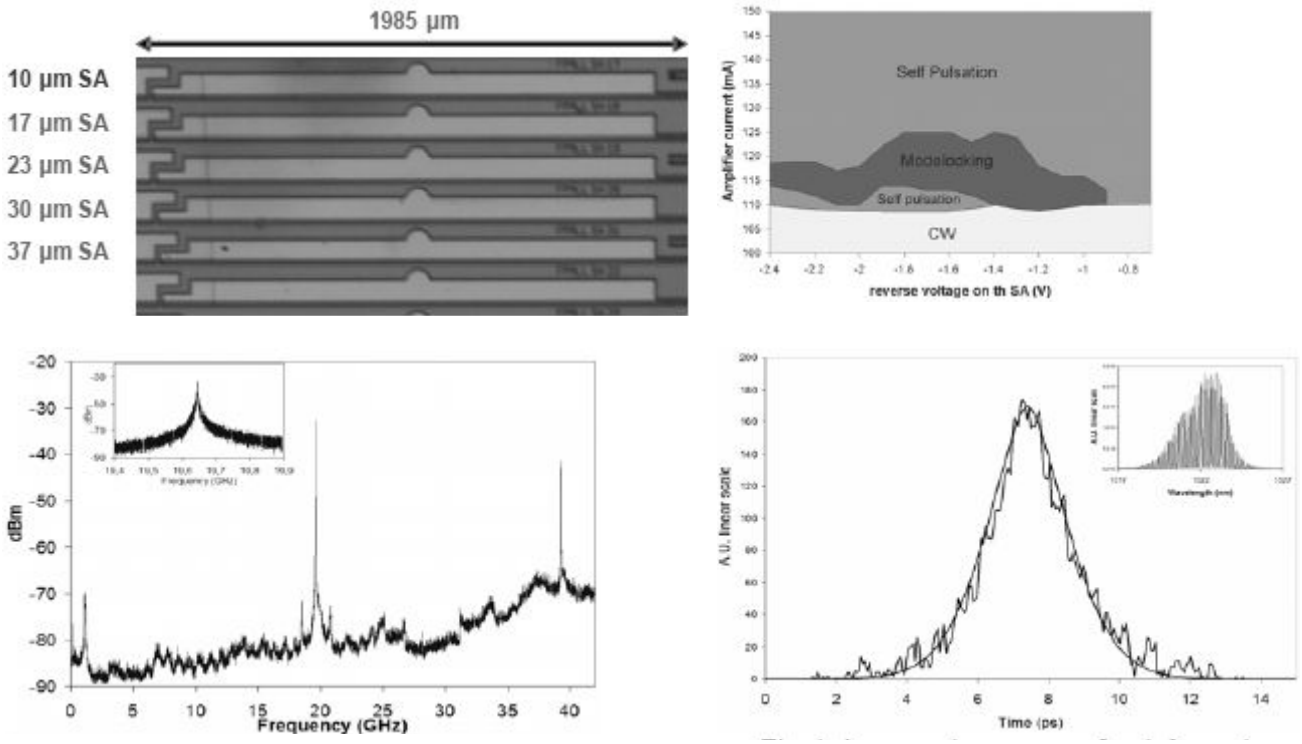

Figure 9-1 Top view picture of the 20GHz FP MLL (Left top), Modelocking regimes versus amplifier current and SA reverse voltage. (right top), RF spectrum of a 20GHz 10µm long SA modelocked laser (I = 121.7 mA V = - 1.9V) (left bottom), Autocorrelator trace of a 1.6ps pulse from a 10µm long SA modelocked laser (right bottom)

Repetition frequency value

Diode lasers offer repetition frequencies from roughly 1GHz to more than 27GHz. For the OHOSE-scheme the optimum value is based on a balance between RF-metrology accuracy and system length. The maximum allowable value for f_{rep} is determined by the accuracy of the RF-metrology. Given the RF-metrology accuracy of +/- 1cm the distance between the consecutive light pulses should be larger then 4cm (OPD is 2 times the ISD) in order to allow the unique identification of the pulse number from the RF metrology. As a result the maximum allowable pulse repetition frequency is 7.5GHz. On the other side the repetition rate should be maximised to minimise the system size. The longer the pulse separation, the longer the delay line stroke has to be. In order to keep some margin a value of 2-5GHz is recommended. (For the further design a value of 4GHz is assumed.)

When selecting the repetition frequency a point of consideration is the availability of frequency references in this frequency range. In particular here the RF-metrology carrier frequency is interesting. If this frequency or an exact multiple of it can be used, this implies that no additional frequency reference, dedicated to the length metrology, is required.

At this stage hybrid mode-locked diode lasers are not commonly available. Recently Anair came to market with a 10GHz diode laser. The main lack here is the relatively low optical power of about few tens of microwatts. However this commercialisation emphasises the realizability of the preferred concept.

Repetition frequency stabilisation

Several methods are available for the stabilization of the repetition frequency. The most direct and hence least complex method is using hybrid mode locking stabilization. Here a SOA is used in the cavity to enhance the modelocking mechanism, see Figure 9-2. In the case of hybrid mode-locking a voltage is applied across the SOA, affecting its efficiency. By modulating the applied voltage at the reference frequency, the laser will take over this frequency and lock onto it. Of course this frequency has to match the cavity length as well. For a 4GHz bulk laser this is about 10mm.

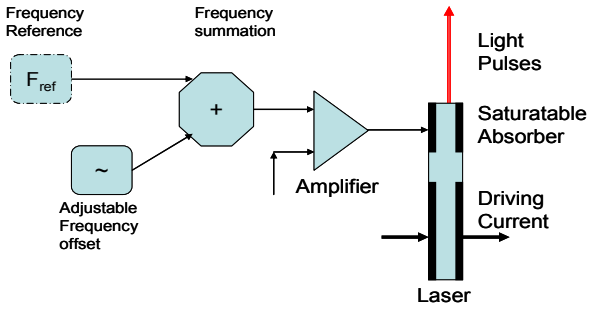

Figure 9-2 Sketch of electronics scheme for hybrid mode-locking of a diode laser

The required quality of the repetition frequency stabilisation is determined by the length of the optical path and length of the pulses. Most importantly the timing jitter between the pulses should allow overlap of pulses at all times. Therefore the timing jitter for frequencies around 4.3MHz (1/TOF) should be smaller than +/- 0.5ps. Noise at frequencies higher than 4.3MHz, shows up as noise on the individual pulse overlapping position measurements. This type of noise can be averaged out. Noise at frequencies below this 4.3MHz, directly affects the measurement accuracy, as it is measured as position drift.

Conclusively it derived that a minimum pulse repetition rate stability is $1.4*10^{-7}$. This number is given by the required measurement accuracy divided by 2 times the ISD. This type of frequency stability is easily achievable using a commercial ultra stable (ovenised crystal clock oscillator) OCXO or the RF-metrology carrier frequency. No optical stabilisation to an etalon or atomic line is required. Typical good OCXO performances are give pulse jitter of tens of ns at short timescales. At longer timescales the frequency stability is reduced, and is not as good as GPS or atomic clock. For these (longer) timescales referencing to (local) GPS is recommended to improve the overall system measurement accuracy.

Laser control

Four parameters of the laser have to be controlled. These are the repetition frequency, the driving voltage and current, and finally the temperature. The control of the repetition frequency has been discussed been discussed before.

The combination of driving current and voltage controls the operation mode of the laser as depicted in the right top plot of Figure 9-1. As can be observed this control is not critical, although the current needs to be controlled better than the voltage. The safest way of operation is to characterize the laser beforehand and then select a point somewhere in the mid range of both the current and voltage range where the laser will be

operated. One should keep in mind here that the laser power is determined by the product of voltage and current. This way one anticipates changes of laser properties due to long term operation or radiation. Implementing active measurement and feedback based on the actual laser performance would imply a large complication of the system complexity.

The temperature control is required to stabilize the cavity length. A proper cavity length is required to match the cavity resonance frequency to the applied reference frequency. Here a slow PID-controller with temperature sensor feedback probably is sufficient, since this adjustment is not required to be perfect. Exact requirements for the accuracy of this temperature control have to be ascertained in an experiment.

Baseline design

The heart of the baseline design is a fibre laser with highest achievable repetition frequency. At this stage this is an Erbium or Ytterbium fiber comb. In Figure 9-3 an overview of typical FS-laser parameters is given. [Taken from TN2]

fs-laser type	***f_{rep} range***	***Phase stability***	***Pulse duration***	***Wavelength***	***Pulse energy***	***f_{ceo} stability (1 ms)***	***f_{ceo} stability (1 s)***
Ti:Sapphire	50 MHz - 1GHz	100 mrad	6-100 fs	800 nm	10 nJ	10^{-7}	10^{-11}
Er-doped fiber	20 MHz - 100 MHz	1 rad	80-200 fs	1550 nm	1 nJ	~ 10^{-6}	~ 10^{-10}
Yb-doped fiber	20 MHz - 300 MHz	<1 rad	80-200 fs	1040 nm	10 nJ	< 10^{-6}	<10^{-10}
Diode laser	1 GHz - 30 GHz	N.A.	1-10 ps	~1500 nm	10 pJ	N.A.	N.A.

Figure 9-3 Overview of the main parameters for various types of femtosecond lasers.

The estimated wall plug efficiencies for these types of lasers are given in Figure 9-4 [Taken from RD2]

Fs-laser type	***Pump source***	***Wallplug efficiency***
Ti:Sapphire	532 nm solid state	1%
Er-doped fiber	980 nm/1480 nm diode	10%
Yb-doped fiber	980 nm diode	15-20%
Cr:LiSAF	650-690 nm diode	5%
Diode laser	--	40-50%

Figure 9-4 Estimated electrical-to-optical conversion efficiencies for various types of fs-lasers.

From these figures it is directly clear why the fibre comb is the best baseline laser for this system. After the diode laser this fibre-comb has the highest repetition frequency and relatively high wall plug efficiency. At this moment the commercial lasers offer repetition rates of 250MHz, however 500MHz has been demonstrated already.

The power consumption of the commercial fibre combs is in the order of 100W-200W electrical to deliver about 50-100mW optical. This efficiency can easily be enhanced to the numbers given in Figure 9-4 by redesigning the electronics. Off the shelf electronics are not designed for efficiency, but for price, availability, flexibility, and so on.

The overall power level is sufficient for the four optical heads simultaneously. This means that using this type of laser only one centralised laser is required. Consequently the increase of the power use is compensated to a large extend.

The main critical point of the fiber lasers is the repetition frequency. We need active repetition rate stabilization and the achievable repetition frequencies are rather low compared to the TiSaf and diode lasers. Fiber lasers in general are tunable over a small frequency range. For the stabilization here an external reference is required and a measurement of the frequency difference between these two. Here direct detection of the pulses and mixing of the electronic signals for difference detection will do. The impact of the fact that the repetition frequency is relatively low is much larger. This has a direct impact on the required path length of the delay line. As a rough estimate the delay line path needs to be increased by an order of magnitude. Even after extra folding of the optical path in the delay line the mechanical outline will be about 5 times larger than in the case where we use a 4GHz laser repetition frequency. This in its turn increases the system mass and power consumption. Due to the increase of the delay line dimensions and weight, the delay line oscillation frequency will be reduced. In other words, the measurement frequency will be reduced to the Hz-level.

A improvement by selecting the fiber laser is that the pulse duration is shorter. Here typically the pulse length is in the order or 100fs instead of the 1-2ps for a diode laser. As a result the detection of the SHG light is more efficient and the pulse overlap position can be determined more accurate. The gain in the detection efficiency can be as large as 2 orders of magnitude, since the SHG efficiency is proportional to the square of the incident power. Since the pulse duration will be an order shorter the overlap measurement can be about 10 times more accurate. Please note that the delay line position decoder is assumed to be the bottle neck. Therefore this gain does not manifest it self directly in the overall accuracy.

One should also note that the blind scanning range is increased substantially, because the pulses are shorter and the spacing between them is larger.

9.1.2 Length measurement using cross-correlator

The core of the OHOSE scheme is a pulse cross-correlator, where an OPD-scan is performed in a reference arm to match its length to the measurement arm. More exactly: The reference arm is scanned continuously in an oscillating movement, whilst measuring the delay line position. From the data analysis the equal arm condition is determined with the corresponding delay line position.

Type of correlation

Three types of pulse correlation exist, these are:

1. Field correlation. Here directly the interfering signals are recorded.
2. Intensity correlation. By combining the two signals in a SHG crystal, or using Two Photon Absorption (TPA) directly on a detector, a frequency doubled pulse is generated when the pulses overlap.
3. Interferometric correlation. When the signals are (phase-) stable enough also fringes in the SHG signal can be created, allowing sub-wavelength (phase) determination of the overlapping pulses.

The direct field correlation is the most direct method, since it doesn't require the use of SHG methods. Therefore this method is the most energy efficient. However when using this technique directly, the signal on

the detector will have a relatively low signal to noise ratio. All pulses arrive on the detector giving a pedestal on the signal. Only the temporal intensity can be doubled when the pulses overlap, which requires fast samples to resolve the signal peak. By applying heterodyning to this method it becomes far more useful. In this case a frequency shift is introduced in one of the arms, by implementing an AOM. Only when the pulses overlap a differential frequency is generated. As a result AC detection can be used and there is hardly any requirement on the equalizing of the intensities in both arms. At the cost of an AOM the method becomes far more robust and has a much larger SNR. (This heterodyning direct field correlation technique is the proposed back-up scenario, in case the light levels appear to be lower than anticipated.)

The second type of pulse cross correlation mentioned is the intensity correlation. This method is the most suitable here, based the combination of the following properties. These are the required accuracy, the laser stability, signal contrast and of course the system complexity, volume and power consumption. In intensity cross-correlation the two pulses are focussed and combined in a SHG crystal (or using TPA). When the pulses overlap a frequency doubled pulse is created, which then is detected. A filter is introduced to block the fundamental wavelength. Important issues here are related to the SHG- or TPA-efficiency. Therefore the power budget and the phase-matching conditions for SHG should be regarded in the design. Intensity cross correlation is the baseline method of detection. In Figure 9-5 a measurement scheme using SHG is depicted.

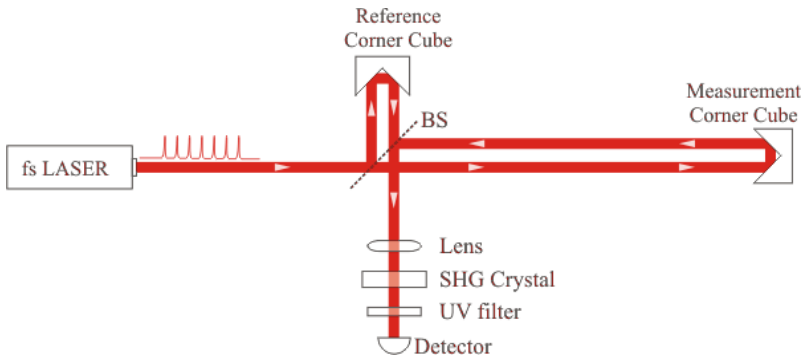

Figure 9-5 Length measurement using Intensity cross-correlation

In Figure 9-6 typical signals of the intensity correlation process are depicted. The measured intensity signal I_{Meas} of the interacting pulses is described as:

$$I_{Meas}(\tau) = \int_{-\infty}^{+\infty} I_{ref}(t) I_{meas}(t-\tau) dt \qquad \text{Equation 17}$$

Where τ is the time difference between the two pulses. For Gaussian shape pulses the length of the intensity pattern is $\sqrt{2}$ times the length of the pulses. Please note that although the pulses interact on very short time scales, the measured signal will only vary as a function of the time difference between the pulses and hence only varies slowly in time. These changes are given by the pulse length and scan speed.

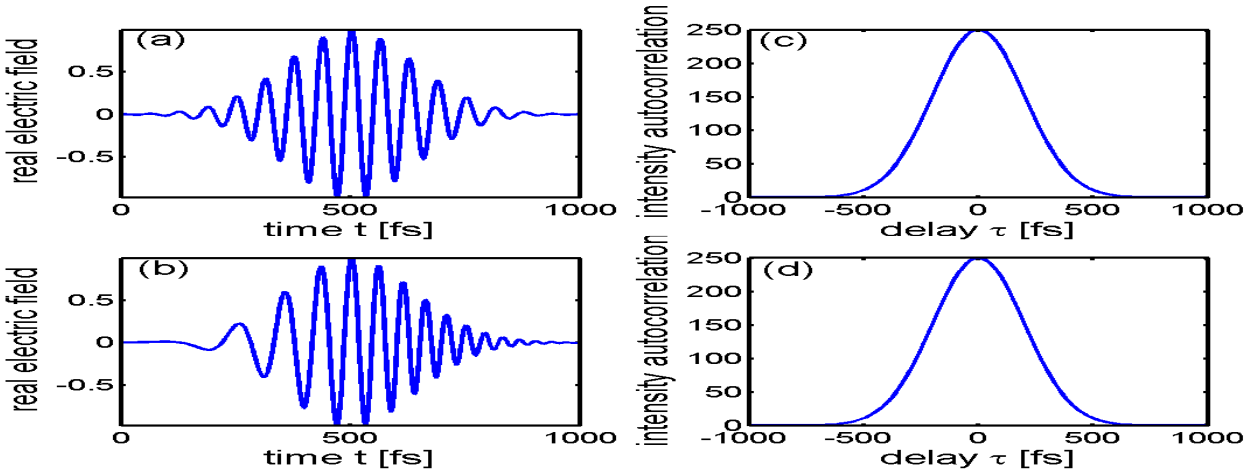

Figure 9-6 Signals in intensity correlation process. On the left the electric field is depicted and on the right the detected intensity pattern

The third correlation type is based on interferometric pulse cross-correlation. For our application this type of correlation is too complex. This interferometric type of detection requires the stabilisation of the laser offset frequency and also more accurate OPD-scanning. For diode lasers this phase-stabilisation is not shown yet, which means that other (larger and less efficient) types of FS-Lasers have to be used.

Second Harmonic Generation or Two Photon Absorption

Two methods of detection exist for the pulse overlap measurement. A first method is based on Second Harmonic Generation and the second is based on Two Photon Absorption.

To achieve SHG the two combined pulses need to be coherent and are combined in a non-linear medium under the right phase matching criterion. Several types of non linear crystals and phase matching types are available. Here one has to make a selection on the basis of the efficiency and the sensitivities. Here BBO appears to be the most promising material option due to the materials high conversion efficiency, large phase matching bandwidth and the small phase matching angles.

Critical in the generation efficiency of second harmonics is the phase matching. In Figure 9-7 the principle of noncollinear phase-matching is depicted. The difference in refractive indices of the incoming wave and the doubled wave is compensated by adjusting the angles between of the incoming waves. Due to the preservation of angular momentum the direction of propagation is along the mean angle.

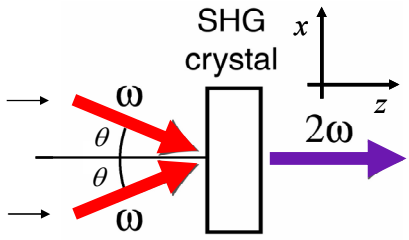

Figure 9-7 Noncollinear phase-matching

The phase matching condition that must be matched then is:

$$n(2\omega) = n(\omega)\cos\theta$$ Equation 18

Where ω is the frequency of the incoming waves, 2ω is the frequency of the frequency doubled waves and n is the corresponding refractive index. This equation holds for a single wavelength. For larger bandwidths the phase matching bandwidth is given by a first order approximation to be:

$$\Delta\lambda_{FWHM} = \frac{4\pi\delta\lambda}{\lambda_0}\left(n'(\lambda_0) - \frac{n'(\lambda_0/2)}{2}\right)$$ Equation 19

The conversion is efficiency is determined by the materials' non-linear constant, the quality of the phase matching and the thickness of the material. A practical approximation is given to be:

$$\frac{I_{2\omega}}{I_\omega} = 5\cdot 10^{-8} I_\omega L^2$$ Equation 20

Where L is the crystal length and the irradiance is given in Watts per square meter. For the *preferred design* the parameters are 1mm crystal thickness, 1ps pulse length, a 4GHz repetition rate and a 100µm spot diameter. This yields an estimated conversion efficiency is found of about 3 x 10^{-5}. This then results in a power on the detector of 30nW. Although not very high, this is sufficient for measurements. For the *baseline design* the parameters are 1mm crystal thickness, 0.1ps pulse length, a 0.25GHz repetition rate and a 100µm spot diameter. This yields an estimated conversion efficiency is found of about 5 x 10^{-3}. This then results in a power on the detector of 1µW.

The SHG efficiency can be boosted by increasing the laser source power, shortening the laser pulses, creating a tighter focus and selecting materials with higher non linear coefficients. As a consequence some other parameters are affected aversely. These are the walk-off angle and the bandwidth over which this SHG efficiency can be achieved. Finally it should be kept in mind that the refractive index depends on the crystal temperature, which might eventually lead to some sort of temperature control, similar to that of a crystal clock.

The alternative technique of two photon absorption (TPA) in semiconductors overcomes several limitations of the SHG based solution, solving the problems related to the phase matching, acceptance angle and walk-off. Although TPA materials being less selective in terms of working wavelengths, they still require that semiconductor materials present a bandgap energy larger the one-photon energy, but smaller than two-photon energy ($h\upsilon < Eg < 2\ h\upsilon$). When choosing a TPA-detector material one should consider that the bandgaps are compatible with spectral bandwidth of the laser diode source.

In practical terms, considering a FS-laser source as a Ti:Saph, detection implementations using a BBO crystal and a PMT (photomultiplier), or a TPA scheme using only a GaAsP diffusion diode show similar conversion efficiencies of 10^{-4} µA/mW2. The critical characteristics of the laser diode, as broad emission spectra, lower energy, larger pulse widths, may however reduce the SHG efficiency in comparison to the TPA solution. In addition a TPA detection scheme is far less sensitive to variations of the alignment.

Conclusively TPA is selected to be the baseline detection method.

Detector

The detector in the cross correlator is used at low light levels and at a relatively low bandwidth (kHz region, set by the delay line scan speed). Therefore a relatively simple low noise detector is sufficiently good. The only special requirement to the detector is that the bandgap energy is smaller than one photon energy and smaller than two photon energy. Since the proposed laser has a centre wavelength of 1550nm and a bandwidth of 20nm, the bandgap should be between 0.8eV and 1.6eV. The material of choice then is Silicon, see Table 9-1. Other advantages of using Silicon detectors are the enormous choice available and the high Quantum Efficiency (QE=0.80) at the two photon wavelength.

Material	Bandgap energy
InSb	0.17 eV
Ge	0.67 eV
Si	1.12 eV
GaAs	1.43 eV
GaP	2.26 eV
6H-SiC	2.9 eV
GaN	3.5 eV

Table 9-1 Overview of semiconductor bandgap energy

Other important detector properties are the detector sensitivity and noise levels. (Low Noise Equivalent Power (NEP) values) For low light level detection Avalanche Photo Detectors (APD) or fast PIN-detectors seem a good choice. Possible good detectors are:

New Focus 1647 with 1.6pW/√Hz NEP, APD

New Focus 2151 with 16fW/√Hz NEP, fast PIN

Thorlabs APD210 0.4pW/√Hz NEP, APD

Besides these detectors there are many other suppliers that have equivalent detectors.

Reference arm scanning

The correlation pattern is measured by scanning the reference arm length. For the *preferred design* the optical path is scanned over 7.5cm, which corresponds to a mechanical path of 3.8cm. By folding the optical path once, the required mechanical scan range has become 1.9cm.

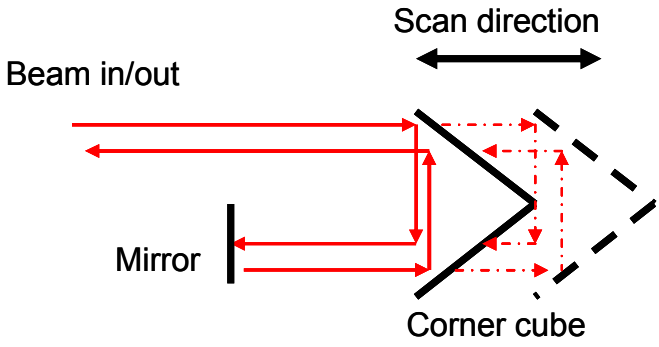

Figure 9-8 Sketch of folded path in delay line

In order to scan the retroreflector a guidance mechanism and an actuator are required. For space operation a magnetic guidance mechanism probably is the best option, since it will have a no friction or particle generation. However parallel spring mount will absolutely do the job.

For the actuator two options were identified to be useful. A first is a piezo stepper (only for direct drive) and the second is a magnetic drive. In both cases a simple position sensor will be required to give reliable position feedback. Here a linear scale with an accuracy of better than 0.5µm is assumed. This will determine the scan accuracy.

In order to minimise vibrations and power consumption of the system a resonant system is advised with a sinusoidal operation (mass on a spring type). Here only the power loss of the system needs to be compensated, rather than the change of impulse directly. Practically the supplied energy is smaller than 1% of the motion energy.

In sinusoidal operation with a 1.9cm full stroke and at 10Hz data rate the maximum scan speed will be 38cm/s. Here it should be noticed that resonant operation of the delay line will result in a non-linear scan movement. This will be dealt with in the data processing.

For the *baseline design* the optical path is scanned over 120cm, which corresponds to a mechanical path of 60cm. (for direct use of a delay line) By folding the optical path twice, the required mechanical scan range has become 30cm. This path is still very long. A further reduction of this path is highly preferred. Due to the developments in the fibre lasers in the last years it is expected that the achievable repetition frequency will go up every year. Therefore 500MHz repetition rates are expected to become available within the next two years. This gain would yield a reduction of the delay line size by a factor of two.

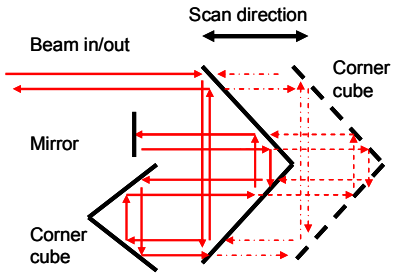

Figure 9-9 systematic sketch of a four pass delay line

Assuming that the driving forces are the same in both the preferred design and the baseline design, then the scan time differs with the root of the path length. This results in a data rate for the baseline design of 2.5Hz.

A large simplification of the overall system can be obtained by centralising the delay lines. In other words use a minimum number of delay lines with a maximum number of beams. From a mechanical point of view a configuration with two delay lines is preferred. An example is given in Figure 9-9.

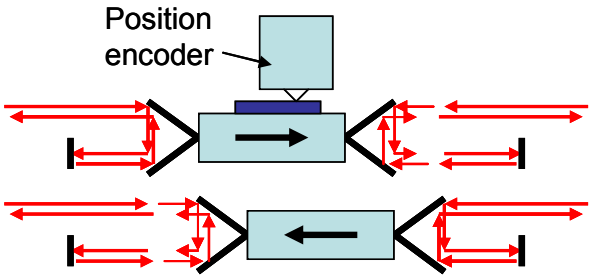

Figure 9-10 Systematic sketch of counter moving delay lines combined with double sided use of the moving parts.

These two delay lines are operated with half an oscillation phase difference to minimises the mechanical vibrations. This way of operation will result in a small amount of angular momentum since the delay lines have to be separated by some distance.

The required lifetime of a delay line is more than 6 $*10^9$ oscillations over the mission duration of 20 years [RD4]. This implies that mechanical contact between moving parts is prohibited. Therefore the magnetic drive is the baseline design for the delay line.

9.1.3 Opto-mechanical design

In Figure 9-11 the outlines of the opto-mechanical components of the preferred design are depicted. It comprises the interferometer, delay line, beam expander, steering mirror, beam splitters, beam dump and the detectors.

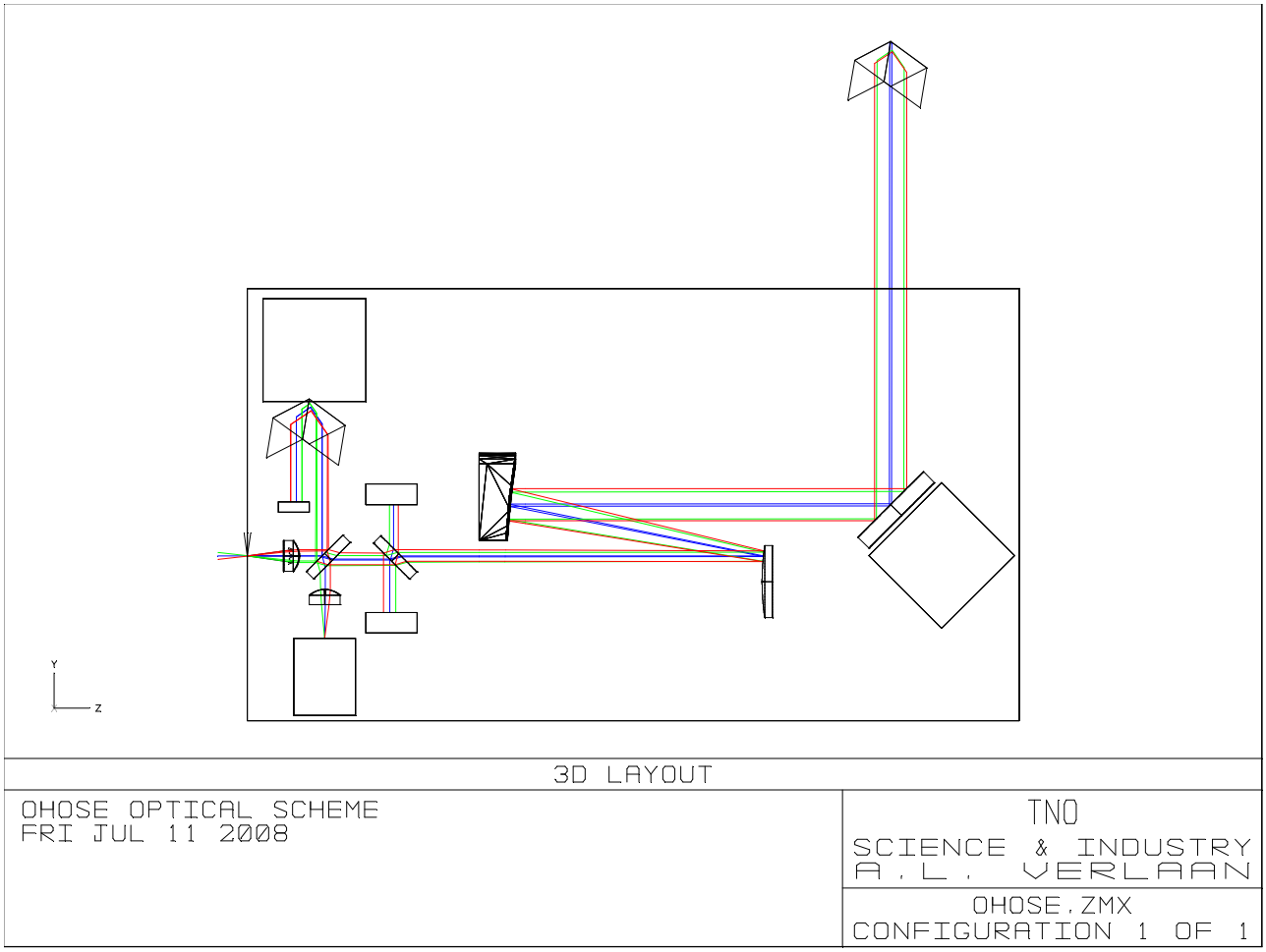

Figure 9-11 OHOSE scheme for XEUS in optical ray tracing package ZEMAX

Light is inserted to the breadboard from the left in an optical fibre. Using a small a-spherical lens the light is collimated to a 3mm beam. Next a beam splitter reflects about 40% of the light towards the reference arm and transmits the other 60%. A second beam splitter transmits the largest part of the beam towards the beam expander and reflects a small part into a beam dump.

Using an off-axis a-focal mirror telescope the beam is expanded 3 times, to a 9mm beam. This type of telescope doesn't create ghost images and has no chromatic effects. The steering mirror on the lower right deflects the beam towards the retro reflector on the other spacecraft. (For displaying purpose the distance is reduced substantially) The returning beam is reflected by the steering mirror again after which is falls on the second beam splitter for the second time. Again the largest part of the light is transmitted and this time a small fraction of the light is reflected towards the PSD for the beam steering control.

On the first beam splitter the measurement and reference beam are recombined and directed towards the detector. Using a small lens the light is focussed onto the detector, where the overlapping beam signal is recorded.

9.2 Beam steering

Beam steering is an essential part of the proposed metrology system. First of all distances are measured towards four different retro reflectors and next also the spacecraft relative positions can vary this requires adjustment of the beam direction. The range over which the angle is adjusted is determined by the allowed variations of the configuration, whereas the required accuracy is determined by the beam and retro reflector dimensions.

In Figure 9-12 a systematic sketch of the beam steering system is given. It shows the mirror, a retro reflector and a sensor to measure the quality of the beam pointing.

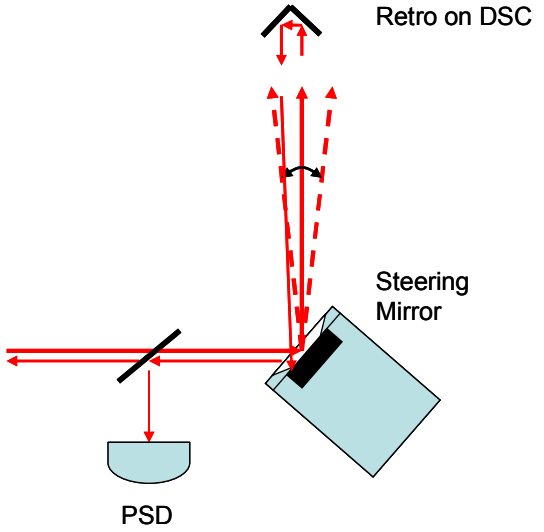

Figure 9-12 Beam steering system

During operation a beam is aimed at the first retro reflector. Next this pointing is maintained while the distance is measured. Then the beam is directed towards the next retro reflector for the second measurement. These steps are repeated for each of the retro reflectors. The overall cycle is repeated continuously. The operation is demonstrated in Figure 9-13. All calculations are located in the central processor to minimise the overall system architecture. Parts of the system are explained in more detail in the paragraphs below.

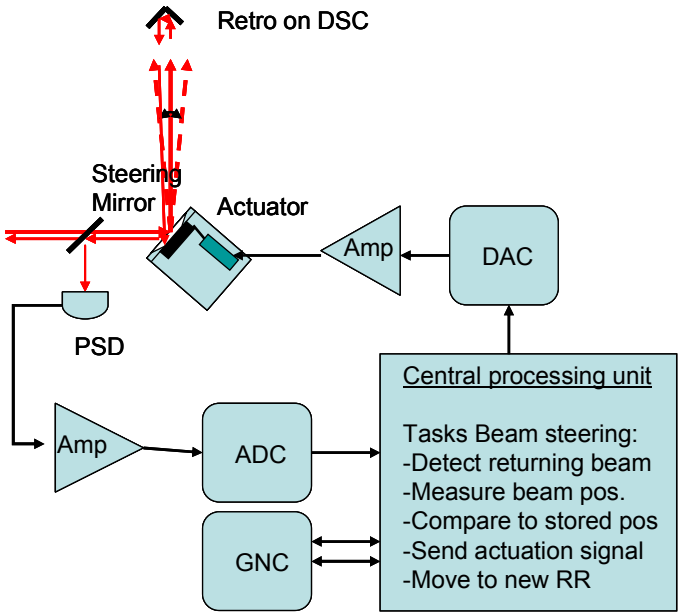

Figure 9-13 Beam steering operation

9.2.1 Requirements

No direct requirements are given in the statement of work for the beam steering mechanism. Here the requirements have to be derived from the higher level metrology requirement. An overview of derived requirements is given in Table 9-2.

Requirement	Value	Remark
Adjustment range	~±4degrees	
Adjustment accuracy	0.3mRad	Few cm at 35m
Adjustment speed	> 5Rad/sec	Required to switch between the different retro reflector
Feedback on achieved pointing	0.3mRad	
Memory of previous pointing angles	4 retro reflectors directions from four optical heads	Required to switch between the different retro reflector

Table 9-2 Beam steering requirements

The required adjustment range is determined by the angle between the retro reflectors and the possible variations of the configuration. Since the RF-metrology typically yields angular accuracies of a few tenths of

a degree, this value will be dominated by the angle between the retro reflectors. This angle is about 3.5degrees, so a total angular range of about ±4degrees is required.

In order for a small light beam to hit the targeted retro reflector, a position accuracy of typically a few cm is required. Dividing this by the ISD gives an angular accuracy of 0.3mRad.

The angular adjustment speed is determined by the measurement frequency and the angles between the targeted retro reflectors. Assuming a few Hz measurement frequency and allowing about half the time for the scanning one finds that the required scan speed is about 3Rad/sec. Larger values are preferred to increase the data rate or allow more time for the measurements.

In order measure the distance to the targeted retro reflector, one needs to target it first. This requires a feedback mechanism on the achieved pointing. This mechanism can be used as well for the beam acquisition. Here the proposed mechanism consists of a Position Sensitive Detector (PSD) that receives a small part of the reflected beam. A shift of the beam position on the targeted retro reflector will yield a shift at the optical head which is twice as large. A PSD sensor works in two directions and has a typical resolution/range of 10^{-5} , which is far more than required here. In addition this type of sensor is robust, has only low power consumption and requires only simple data processing. The estimated angular resolution of this measurement is about tens of nanoradians.

9.2.2 Beam steering design

Several options are available for the mechanical design. In general it should be stated that the requirements are not very critical. In Figure 9-14 two examples are given of such a mechanism where high stability and accuracy have been combined.

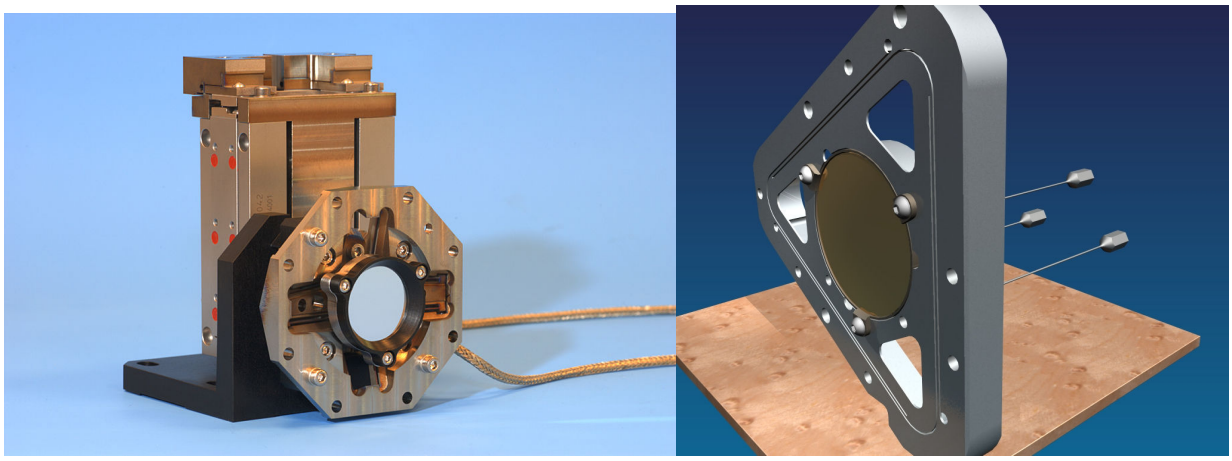

Figure 9-14 2 Examples of high stability and accuracy beam steering mirrors

A beam steering mirror consists of three essential parts. These are:

- Mechanism for the hinge that allows the actual motion
- Actuator to modify the mechanism angles
- Pointing feedback sensor to allow for optimization and remove stability requirements

The hinge with the mirror should have a low weight and low stiffness to minimize the power required to actuate it. Of course the stiffness must be large enough to allow for the operation at the required speed and

frequency. Furthermore the point of rotation should be located on the mirror surface (and the beam should be aligned to this point) to avoid OPD changes due to angular movement.

For the actuator piezos and voice coils are the most promising options. Due to the large development in the field of the voice coils in the last years and the ease of making them space qualified, these are the preferred actuators.

9.2.3 Beam steering operation

The two modes of operation of the beam steering unit are the beam acquisition mode and the measurement mode. These two modes are described below.

Beam acquisition mode

The main objective of the beam acquisition mode is to identify the angles at which the retro reflectors are found. Therefore the output of this mode is a list of 32 angle values given by the four directions from each of the optical heads to each of the retro reflectors. A side objective is to minimize the time required for this procedure, to minimize the time lost during reacquisition after a signal lost event.

When the beam acquisition is started the position and orientation of the DSC and MSC are known from the RF-metrology. Here an angular accuracy of 0.2degrees is assumed and a lateral position accuracy of about 10cm. With these numbers the area that needs to be searched around a retro reflector is a circle with a radius of about 23cm. In relation to this the retro reflector diameter will typically be 2-3cm in diameter. Consequently the chances of hitting the retro reflector directly are about 0.2%.

The most logical approach is to find the retro by starting at the location with the highest probability and then spiraling out, towards the edges of the circular field where it can be found. The maximum total time to find one reflector is simply given by the total scanning cone divided by the angular scan speed and the retro cone angle. This results in an estimated worst case blind scanning time of 2.8seconds for the first retro reflector. The more beam steering angle values are known, the smaller the uncertainty ranges of the other reflectors become.

Measurement mode

During the measurement mode a scan and measure sequence is continuously repeated. This is the main distance measurement system cycle. After each individual distance measurement, or after each cycle over four retro reflectors, a new set of configuration parameters can be calculated. This data then is communicated to the GNC.

In order to allow control and optimisation of the beam steering angles a quality measure is required for the beam pointing. The PSD sensor provides this signal. While aiming the beam at the retro reflector the quality of the aiming is measured using the PSD and the steering mechanism command angles are recorded. These angle values are stored in a cyclic buffer. This way a minimum of time is required for the alignment of the next measurement cycle. Provided that the relative satellite motion is only slow during science operation a simple PID-controller will suffice here as is explained below.

The impact of angular pointing errors is primarily determined by the resulting change in the optical path length. As a simple (first order) approximation a parallel beam on a retro reflector is regarded. In that case the distance from a plane to the reflector and back to the plane does not depend directly on the lateral position. Therefore a lateral displacement on a retro reflector does not induce a measurement error. For the beam combiner and detector combination side a similar explanation is given. Mispointing the beam results in a laterally shifted returning beam. This beam is focussed however on the detector using the same lens. Lateral shifting of a beam has no effect on the path length to the focus. In other words: parts of a plane

wavefront travel identical distances to the focal point behind a lens. Conclusively this argument means that a slight mispointing of the beam steering mirror doesn't lead to measurement errors. Of course this effect should be verified for a final design.

9.3 OHOSE power requirements

The power requirements for the OHOSE detection concept are defined, as general rule for power budget analysis, by: a) intrinsic minimum power levels to obtain a Signal to Noise Ratio (SNR) of, say, 10 dB, related to the detector scheme, materials and amplifier and b) to an extrinsic link budget considering coupling efficiencies, optical transmission, propagation, etc, adding a loss figure to the minimum intrinsic power requirements.

General considerations are presented below.

a) Intrinsic conditions:

In a brief analysis, we considered a general conversion efficiency, common to both SHG or TPA solution, presenting a figure of 10^{-4} μA/mW^2. Dark current at diode level is 100 pA, detection bandwidth of 1MHz and amplifier noise 2pA/√Hz. No background illumination was considered.

b) Extrinsic conditions:

In terms of extrinsic factors, a few assumptions that were taken into account. For the propagation factor, no loss was considered for the particular path of back and forth between the DSC and MSC. A coupling loss on the retroreflector mirror of 8dB to 14dB, may be accounted for, considering spot diameter/ mirror diameter of 2:5 or 1:5 ratio. Assuming minimal beam divergence and lens transparency would produce a 1 dB loss. The Michelson interferometer shall imply a 3 dB loss and the detector coupling 1 dB. All accounted for will produce a total loss of 13 dB to 19 dB loss, depending basically on the ratio of the illuminated area in the mirror SC vs retroreflector area.

The basic SNR requirements are outlined in the following graph.

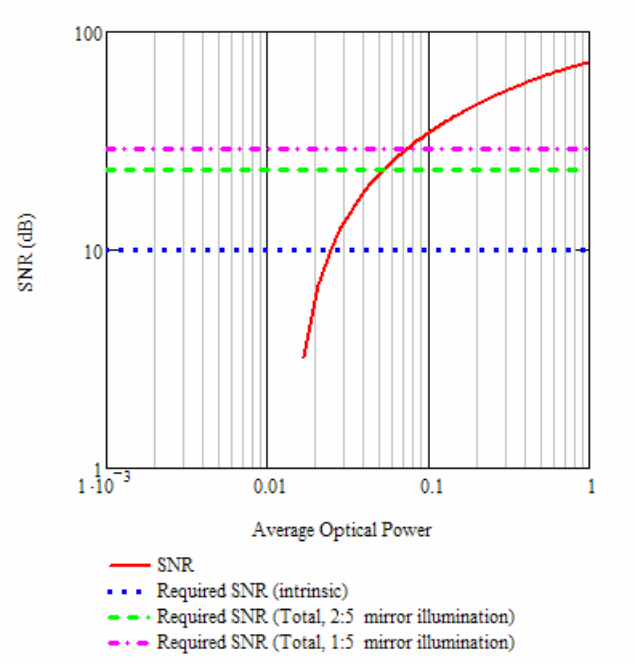

Figure 9-15 Optical Power requirements for different levels of SNR in the MSC/DSC link budget.

From the graph, we can conclude that 15mW (peak) would be required to achieve 10 dB of SNR whilst some 90 mW peak power would be required to obtain the 29 dB, when allowing for worst case of extrinsic factors.

Considering the laser diode (preferred design) is emitting at a 4GHz rate, with 1 ps pulse, one can compute that one requires a 80 µW average power to perform each distance measurements. This level of power requirements will allow using the same laser diode to perform the required 4 simultaneous measurements, even when considering severe beam division losses.

Using the fiber laser (baseline design) the SNR is improved even further. First of all the emitted pulses are ten times shorter and the emitted power is a few times larger. This results in a higher conversion efficiency. Altogether the achievable accuracy will be substantially better. Experiments in air demonstrate that using the OHOSE scheme sub-micrometer accuracies are feasible, even in air. [TU-Delft, results to be published]

9.4 Electronics and control

A number of parts described earlier in this chapter require electrical components and active control. Parts of this have been described in the paragraphs before. Below an overview is given of the complete set of electronics and the signal flow in the diagram of Figure 9-16.

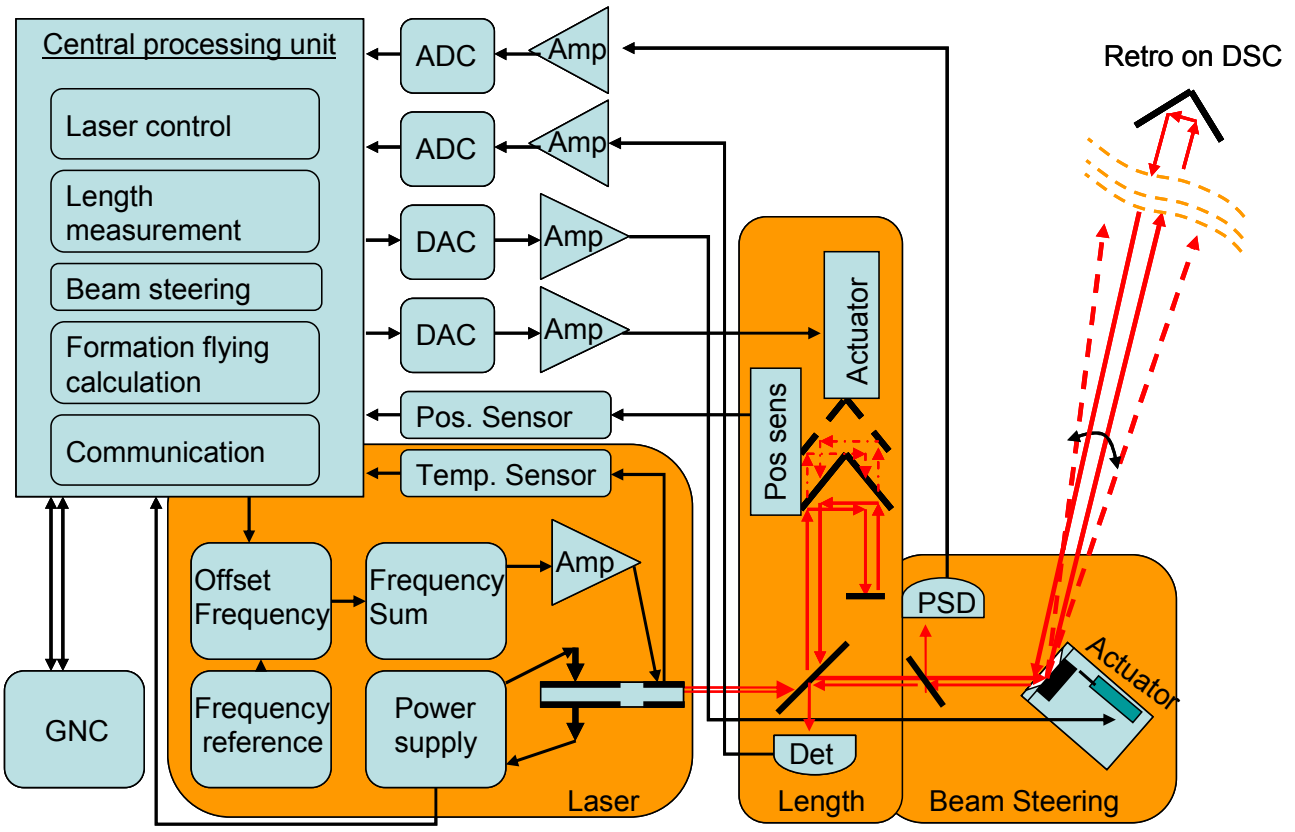

Figure 9-16 Schematical representation of electronics and dataflow of the XEUS measurement system (preferred design depicted)

In this overview a number of functions can be identified. The main three blocks are:

- Laser power supply and control including the reference frequency generator. The diode laser (preferred design) requires a stable power supply and reference frequency. In principle this doesn't

require control. However for the system reliability some degree of control is recommended. (Allow for re-optimisation after changes of system properties.) In addition the laser temperature needs to be stabilised to maintain the cavity length. A temperature sensor will give record the temperature and temperature then is controlled by adjusting the driving current. A simple and slow PID-controller will do this. The controls of the fibre-laser are very similar. Here the reference frequency is not fed to the laser directly but compared to the measured repetition rate. This control basically is the same as the diode laser temperature control.

- Length measurement comprising the OPD scanning and measurement using delay line and the signal detection. For the measurement of distances the maximum detector signal needs to be linked to the delay line position. Here one should correct for the non-linear movement of the delay line. Although the delay line is operated in a continuous way, it still requires a constant update of the actuation signal. This is a constantly repeated sinusoidal cycle, where a very slow control loop could stabilise the oscillation amplitude.
- Beam steering and control. The beam steering is achieved using an actuator. To steer the actuator the retro-reflector positions are read from a memory buffer. Then this buffer is updated using measurements of the PSD.

These blocks describe the core of the system. Performing these processes will yield the raw distance measurement data from each of the optical heads. In addition all data must be combined to calculate the formation flying configuration. Here also some calibration or data correction values are required. For example the base length between the optical heads, between the retro reflectors, the sensor dead path values, and of course the RF-metrology information.

All calculations and control functions are centralised in a central processor to minimise the system complexity. Since the overall data rates are not very high and the processes are not so complex, this will not result in an excessive processor load. As an example an Actel RTAX250S/SL (space qualified) could be used.

9.5 Measurement strategy

The measurement principle used to determine the MSC-DSC relative formation is multiple trilateration. By measuring the distances from three optical heads on the DSC to three retro reflectors on the MSC also the spacecraft rotation and sideways displacement are determined. Since there are four optical heads and four retro reflectors there is a redundancy in the measurement. For the measurement strategy the following mission phases and events are distinguished:

- Formation deployment
- Science operation
- Formation slewing
- Lost link

Formation Deployment

During the formation deployment the trilateration system can be used. The operating range is far larger than the required fixed distance of about 35m. In the current design the operation range will probably be limited by the signal loss due to the small beam diameter and its divergence. It has to be noted of course that the trilateration is operated here as a add-on to the RF-metrology system. Operation of the trilateration system is only useful is the RF-system is operational and more accuracy on the formation accuracy is required. Of

course it is possible to create a self-standing trilateration system, however this implies an increase in system mass, power consumption and complexity.

Science operation

During the science operation the formation of the two spacecraft has to be controlled the most accurately. The science measurements require a stable formation over a long time. During the science operation the external forces that perturb the relative configuration like solar winds have to be compensated for. This requires accurate knowledge of the configuration. Here it has to be pointed out that the formation flying metrology is dependant on the RF-metrology and the science data. The link to the RF-metrology has been explained in the chapters before. The dependence of the science data has not been explained yet. Two requirements for the formation accuracy are used parallel to each other. There is the formation flying accuracy on one side and the absolute X-ray telescope pointing on the other side. These requirements are not identical, but the requirement on the relative formation flying are more strict. In other words, the pointing errors of the MSC are not compensated by the DSC, but will result in an image shift on the DSC-detectors. Provided of course the errors are not too large. Consequently the MSC orientation will be controlled by the science data and hence the DSC will have to follow.

The trilateration system is operated in two steps, the beam acquisition and the measurements as was explained in paragraph 9.2.3 when discussing the beam steering mirror operation. The beam acquisition starts by pointing the laser beam at the location with the highest probability and then spiraling out, towards the edges of the circular field where it can be found. This results in an estimated worst case blind scanning time of 2.8seconds for the first retro reflector. The more beam steering angle values are known, the smaller the uncertainty ranges of the other reflectors become. During the measurement mode a scan and measure sequence is continuously repeated. This is the main distance measurement system cycle. After each individual distance measurement, or after each cycle over four retro reflectors, a new set of configuration parameters can be calculated. This data then is communicated to the GNC. In parallel the optimum beam pointing angles are measured and updated in the memory.

Formation slewing

When a science measurement is completed the MSC will be pointed towards a new science target. During this maneuver the DSC has to follow the MSC and maintain the formation. Of course the formation pointing requirements will be less strict during this operation, however accurate formation data will speed up the process of locking onto the new target since the final formation orientation depends on the data of the science detectors. Conclusively this implies that during these maneuvers the trilateration system should be maintained operational. Since the required speed of the satellites is only small, no substantial degradation of performance is expected here.

Lost link

In case of a single lost link the beam will be directed to the last known good position. If this doesn't result in renewed optical contact the beam acquisition process is started until the link is recovered.

In case of losing all four links, the beam acquisition procedure will be started from the RF-position determination, followed by the normal beam acquisition process.

9.6 Calibration and alignment

The calibration and alignment of the trilateration measurement system is performed a number of steps. The first step is the on ground calibration procedure. In this procedure the elements are characterized and aligned followed by the sub-systems and then the final system. After launch, in the deployment phase the performance has to be validated and related to the science measurement data. Finally during operation over the mission lifetime the link between the trilateration system and the science data should be verified to identify possible drifts due to structural changes or system degradation.

9.6.1 On ground alignment and calibration

On ground one has the best access to all components and therefore this is the best location to assess the performance of all components. Besides this one must be sure that the entire system is operating well before thinking of launching it.

Components and sub-systems

In general all components are required to work within specifications, however some components are more critical to the system performance. Since the measurements are based on the determination of the pulse overlap of a pulsing laser the following parts deserve special attention.

- Laser. The laser is the heart of the system the most important properties that are used in the measurements are:
    - Repetition frequency. A stable reference is used to lock the laser on. Variations of this frequency are directly interpreted as distance changes. Therefore the frequency of the reference and the way the laser follows it should be characterized.
    - Frequency jitter. Smaller variations of the laser frequency also affect the length measurement by reducing the quality of the pulse overlap.
    - Pulse energy. Two photon absorption is a weak process that depends strongly on the incident power. The power levels must be high enough to guarantee the signal to noise ratio over the mission duration.
    - Pulse length and shape. Although the pulse length and shape do not directly affect the measured optimum cross correlation position, a shorter and hence brighter pulse will surely enhance the SNR.
- Delay line. The delay line continuously scans the reference arm to allow the determination of the optimum cross correlation position.
    - Position measurement. The position read-out of the delay-line is used for the length measurement, therefore there should not be a difference between the optical instantaneous position and the position read-out. (The minimum requirement is that the effect is known and stable over time) This requirement implies a calibration of the dynamic behavior of the delay line.
    - Stability of alignment during operation. The beam pointing should not vary with the delay line position to avoid additional OPD changes.
    - Delay line lifetime. The delay line will oscillate over the lifetime of the mission. Although no mechanical contact is anticipated one should be careful that there cannot be mechanical wear. Lifetime simulation at higher oscillating frequencies is recommended.

- Beam steering unit
    - Pointing control performance including the dynamic effects of the mirror. The steering mirror by itself is not critical. The combination of range and resolution can be achieved. What is critical is that its pointing performance can be preserved over the mission lifetime. During operation the mirror is used in a stepping cycle. The angles are changed rapidly and then the position should be stable in the right direction.

Besides the performance assessment of the elements and sub-systems also the parameters for the control loops have to be determined. These are given in Table 9-3 below.

Unit	**Parameter**	**Remark**
Laser	Driving voltage and current	Not very critical
Laser	Nominal repetition frequency	Corresponds to laser crystal length
Laser	Repetition frequency signal amplitude	
Laser	Nominal Temperature set-point	
Delay line	Relation between optical and sensor position	To allow for correction of dynamic effects
Delay line	Required driver signal amplitude for operation	
Beam steering unit	Relation between measured, command and realized angles	Transfer function

Table 9-3 Properties of components and sub-systems used for control

System

On the system level also some calibrations are required. One needs to asses the performance of each of the four systems as well as the relation between the four systems. For each of the systems one should check:

- Range resolution over the working range
- Impact of MSC-DSC motion

On the level of the overall system one needs to asses the relative parameters and the overall triangulation performance. This then comprises:

- Dead path length comparison of the four systems

- Assessment of the formation flying accuracy. This is the ultimate measurement and hence this is the ultimate test. This might be hard to perform full scale due to the large dimensions and the presence of air in a testing facility.

Besides the performance assessment of the systems also the parameters for the control loops have to be determined. These are given in Table 9-4 below.

Unit	Parameter	Remark
Each Optical Head	Dead path length	The distance between the beam splitter and the steering mirror is included in a length measurement
Each Optical Head	Beam pointing angles	These numbers are only required to speed up the first beam acquisition cycle
Overall system	Base lengths	This parameter comes up in the triangulation calculations

Table 9-4 Properties of the overall system used for control

Alignment

Using smart design and constructing the number of alignments can be minimised. For many parts the alignment is not very critical due to the element properties or due to the fact that active elements (like the beam steering unit) are implemented in the system. The anticipated alignments are given in

Unit	Alignment	Remark
Each Laser	Fibre coupling of laser	Optimise the efficiency
Each optical head	Fibre collimator	Aim beam through delay line and beam splitter
Each optical head	Focussing lens wrt. Detector	Optimise detected signal by overlapping measurement and reference beam
Each optical head	Beam expander relative mirror element position	Relative mirror position of telescope is always critical
Each optical head	Centre point of the beam steering unit wrt. the optical beam	To avoid cross coupling the length measurements with mirror tilt angles

Table 9-5 Overview of alignments

9.6.2 Deployment phase

Possible problems that could be expected after launch are element failure and change of alignment. Therefore one needs to asses that the system is performing up to the requirements during the deployment phase. This also implies linking the trilateration system data to the science data. Since four length measurement systems are implemented where only three are required, these systems can be compared to each other to compare the relative performance as a good starting point.

Measurements that one should anticipate during the deployment phase are:

- Individual system performance assessment
    - Signal levels on the detectors and the signal shapes
    - Beam steering control verification
    - Beam acquisition procedure and lost link simulation
- Relative system performance. Comparing the four distance measurement systems allows to identify the errors in one of the systems. This is a fast and low complexity system check, however one does not want to be dependant on all four systems to asses the metrology performance.
- Linking the trilateration data to the Science data
    - Best focus position for each science system
    - and image positions for each science system

9.6.3 Mission lifetime

Over the mission lifetimes optical and electronical elements can degrade and structures can slowly deform. These parameters should therefore be verified over the lifetime. Since these effects usually are slow and the signal levels are indicators of the current performance these verifications are not required frequently.

10 HAALDM system design for Darwin

The OHOSE scheme selected for the XEUS mission, is also applicable to the Darwin mission. Only minor changes to the design have to be made. Therefore this chapter is less elaborate. Here only the most important differences are discussed.

10.1 Darwin requirements overview

This paragraph gives an overview of the technical requirements imposed on the length metrology system for the Darwin mission. This table with requirements is a mixture of the mission documentation (RD2 and RD3) and the ongoing activities and discussions. These numbers are the baseline for the design of the HAALDM-scheme. In Table 10-1 an overview of the Darwin mission parameters is given.

Table 10-1 Overview of Darwin mission parameters

Darwin		
ISD	15m-500m baseline	Slow variation
Required accuracy	Distance accuracy 10μm/√Hz	
Satellite motion	Speed up to few um/s during absolute measurement phase	
Required bandwidth	Control frequency 0.1Hz	
Variations of spacecraft configurations	Continuous ISD variations from 15m to 500m	
Absolute versus relative measurements	Spacecraft separation is absolute	OPD is relative after fringe locking
Metrology function	Measure longitudinal separations to equalize optical paths	Lateral is needed but obtained from configuration or additional metrology

10.2 Darwin metrology design

The OHOSE scheme described in is also applicable to the Darwin mission. The design given in chapter 9 can be copied in terms of laser, laser stabilisation, OPD scanning and detection. Of course here no triangulation is performed and therefore no scanning mirror is required. Consequently the beam steering units and the associated control systems can be omitted, making the system lighter and more robust. In the Darwin configuration the measured distances directly are the required output and no formation calculation is required.

In order to cope with the larger ISD-values the beam expander magnification should be increased from 3 times to about 9 times. This is of course no technical problem. No further changes to the OHOSE scheme are anticipated.

10.3 Performance and Assessment versus Darwin requirements

Directly copying the proposed XEUS OHOSE scheme will result in a measurement accuracy of 5µm. This is about twice as good as the requirements at 1Hz. For the Darwin mission a lower performance is acceptable at lower frequencies, which is less strict than the XEUS requirement, where a flat formation flying performance is required. Since the length measurement is limited by the timing jitter of the laser, this works out very well. The proposed OCXO clock has a lower performance at longer timescales, which was limiting the accuracy for the XEUS configuration. As a result the performance in the Darwin configuration will even better than the 5µm. Practically this means that other perturbations will become dominant.

The 0.1Hz bandwidth requirement is easily met by using the proposed 3Hz system. By reducing the scanning frequency of the delay line the system can be made some more efficient, accurate and produce less vibrations. Therefore this modification would be recommended.

11 Developments towards a space qualified system

11.1 Present status of the prognosed system

Femto-second based metrology has not bee used before in space and a number of components of such a system has not been qualified for space use as well. Consequently any space system design based on this type of metrology inherently has an increased risk of loss of performance or even failure. In order to reduce the system failure risk to acceptable levels the critical elements must be identified and solutions should be found to reduce the risk of component failure.

It must noted that other existing high accuracy absolute distance metrology like DWI and FSI are still in the process of qualification of the several sub-systems involved.

11.2 Critical Parts

In the following chapter all critical parts are listed. Many "new" materials used in the proposed HAALDM instrument are semiconductors, crystals, or special fibres. All these components have to be upgraded for space operation starting from the ground-based performance demonstration. Depending on the mounting on the prime experiment they have to survive extended temperature ranges and the harsh radiation environment. Gamma rays can be often shielded by surrounding the components with suited materials like aluminium but proton radiation cannot be reduced that effectively. Hence, radiation tests with both radiation sources must be performed and if the proton tests fail appropriate redundancy concepts must be applied as work around. This will increase the mass, power consumption, and volume of the HAALDM sensor.

In Figure 11-1 Systematic sketch of the proposed OHOSE system in building blocks a block diagram is given, showing the essential building blocks of the selected HAALDM system.

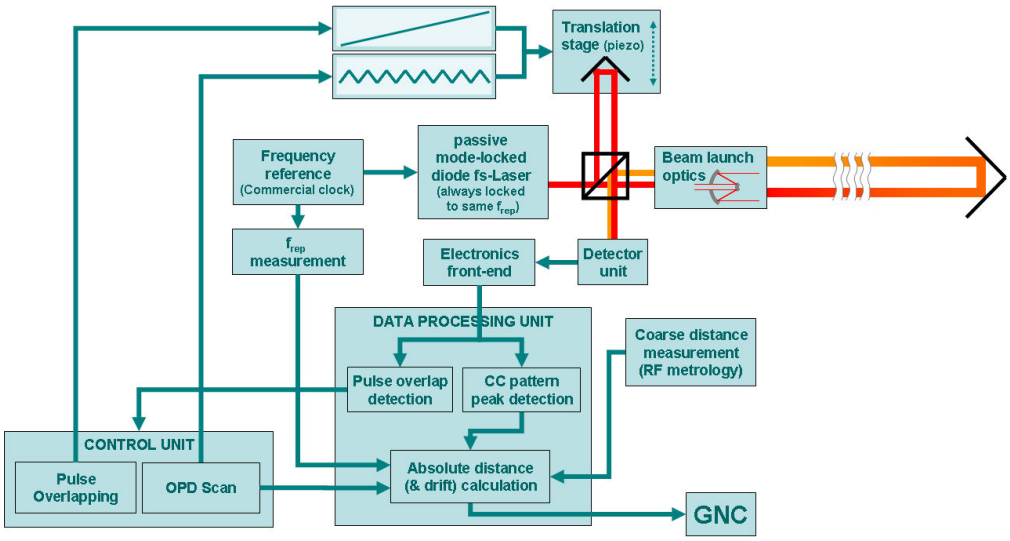

Figure 11-1 Systematic sketch of the proposed OHOSE system in building blocks

The new or still non fully-tested materials and components of the proposed HAALDM sensor for XEUS/Darwin are

- Hybrid mode-locking laser combining a saturable absorber and the proposed very new diode laser in one device
- Frequency reference in the order of 4 GHz
- Intensity correlator using two photon absorption directly on a special detector
- Fast and permanently moving delay line (stroke 19 mm, 5 Hz resonant mode)
- Sub-µm position encoder for the delay line
- Beam steering mechanism (8 degree scan range, 300 µrad accuracy, >5 rad/s scan speed, stepwise scan mode to approach sequentially the target retro-reflectors)

In particular the hybrid mode-locking laser device is completely new and does not exist at the moment (recently the first commercial laser of this type came to market). It has been replaced by a more conservative fibre laser presented as a backup scenario during the study.

The frequency reference determines the accuracy of the distance measurement. As for all formation flying instrument radio frequency metrology is used to employ the arrays until the formation can be captured and tracked we possibly can use the carrier frequency of the rf-metrology as a reference. If it cannot be utilised the clock oscillator must be put in a crystal oven to ensure the high frequency stability.

The beam steering mechanism is needed for both the XEUS application and the Darwin instrument to extract the attitude information. Darwin's formation of the telescope spacecraft is fixed in principal geometry even though the baseline is changed from target to target. Astrium proposed an X-array with a ratio of 1:3. Changing this ratio would also mean that the beam relay optics would have to be changed each time the baseline is varied. The fixed baseline geometry disburdens the scan range of the beam steering. However, the requirements on the resolution increase with growing baseline as the measurement targets are fixed in geometry on the free flyers. XEUS in its old free flying configuration has a fixed focal length and scan range of the beam steering as well as resolution are fixed.

11.3 Laser and detection

To asses the risk associated with the new FS-laser technology, an overview is given of the typical and essential components of such a laser system. See below in Table 11-1. This list is generic and doesn't give exact performance numbers or requirement of these components. These exact numbers will depend on the precise mission requirements and their implementation. Until the precise mission requirements are known, this generic data is more important. This data will tell if a specific component can be build rather than telling us if it already exists. The fact that a component doesn't exist in a space qualified version doesn't mean that it cannot be made, but it often tells us that it has not been needed before. Therefore analogy to earlier missions is a strong argument in favor for any specific component. This will tell if the proposed technology can be made sufficiently robust and radiation tolerant. In the most ideal situation the aging data of the specific components is available from previous missions and the new parts can be made even better. (In terms of performance or lifetime)

Component	Space qualification tested?	Critical issues expected?	Comments
Erbium-doped fiber	yes	yes	Performance degradation may be an issue, can be alleviated by Cerium/Germanium codoping. Radiation-induced damage seems to be correlated more strongly with e.g. Al-concentration rather than with the active ions. See Barnes et al, Proc. SPIE 5897, 67 (2005) and references therein.
Ytterbium-doped fiber	yes	yes	See above.
Waveplates	likely	no	Can be made using air-spaced glass substrates, various (space-grade) glass types possible
Piezo-transducers	yes	no	Already incorporated in various space missions
Diode lasers for pumping	yes	possible	Diode-pumped YAG lasers exist space-qualified, so pump diodes as well. While fiber lasers require different wavelength laser diodes, suitable diodes can be expected to be technically feasible.
Frequency reference standard	yes	no	Depends on the demands. Cs and Rb clocks already exist in space, optical clocks require significant technological work.
PID controllers	yes	no	Standard RF electronics, MHz bandwidths.
Photonic crystal fiber	no	possible	Standard fused silica holey fibers should behave similar to single-mode fibers. Er-doped fiber lasers sometimes use special "highly nonlinear photonic fiber", containing Bismuth-doping which may cause problems.
Avalanche photodiode	yes	no	space-qualified APD's with 65% QE at 532 nm demonstrated: Sun et al, J. Mod. Opt. 51, 1333 (2004)
Mirrors	yes	no	Optical components readily available, broadband Ag, Au or Al-coated mirrors as well as dielectrics
Frequency counters	yes	no	Technology already exists on e.g. GPS satellites
Stepper motor (optional)	yes	no	Developed by e.g. TNO for space-based interferometric delay-lines
Faraday isolator	yes	no	Technology used/tested for space-based LIDAR laser systems. Fiber-based components preferable over bulk systems due to lower vibration sensitivity.
Fiber couplers	likely	no	Widely used in the fiber-optic communications industry, space-qualified components likely to be available
Polarizers	likely	no	Can be made using air-spaced glass substrates, various (space-grade) glass types possible.
Wavelength-division multiplexer	likely	no	Widely used in the fiber-optic communications industry, space-qualified components likely to be available
Single-mode fiber	yes	no	Tested, largely transparent to radiation
SHG crystals	yes	no	KTP, LBO, BBO all tested and qualified. Periodically poled crystals not yet known
Optical filters	likely	possible	Passive glass components, some colored glasses may contain ions that might experience radiation effects
Fiber-Bragg grating	yes	no	Space-qualified components available

Table 11-1 List of FS laser components and the Technology Readiness

Although FS lasers as such have never been flown before, the majority of components required for an FS-laser have been flown before in various missions. In generals it can be said that various types of lasers have been used before in space. These types are diode lasers, gas lasers, Nd-YAG lasers and fiber lasers.

The diode bars for laser pumping are available in space qualified version, but lifetime issues are well known. Often the lasers that are built using these diode bars are situated in small pressurized chambers to avoid certain contamination problems.

The HAALDM-baseline system uses a FS-fiber laser, based on either Ytterbium or Erbium fibers. Both Ytterbium and Erbium fiber amplifiers have been made in space qualified versions. This type of laser amplifier is very similar to a fiber laser itself, showing that this type of laser is suitable for space use. The main parts that are not covered by this analogy to other lasers are the actual mode-locking mechanism and pulse compression.

For the hybrid mode-locking laser diodes the difficulty in producing a space qualified version is not the diode laser itself. Here the application of the actual hybrid mode-locking using the biased saturatable absorber has not been demonstrated. These parts are exactly the difference between commercial telecom components and the diode based frequency combs.

Characteristic for mode-locked lasers are the high peak powers in the beam and in particular in the cavity. These high peak powers enhance the process of glass fault growing. This enlarges the risk of failure. It should be investigated if the radiation induced dislocations will result in component failure. The risk of this effect is the highest where the optical power has the highest value. Consequently the mode-locking element and the photonic crystal fibers are most suspect to this type of aging. Even in ground based application the aging of PCF is a known issue. Since these mode-locking and pulse compression elements are the core components of any frequency comb, the qualification of these materials is the central key in the total qualification process of the laser.

The availability of a stable frequency reference is imperative for the accuracy of the FS-based distance measurement. Although it is clear that stable references exist for space use, the selection of the right source has a large impact on the system mass and power consumption. Atomic clocks based of Cs or Rb are available for space use, however this type of clock probably is an overkill. The standard clocks based on crystal oscillators yield sufficient accuracy, however at a lower frequency. Typical operating frequencies of these clocks vary from 10MHz to 200MHz whereas a frequency in the order of 4GHz is required. Consequently an up conversion of the frequency is required while preserving the accuracy. As an alternative a GPS-like reference can be used. However the availability of such signal is not yet known.

Most of the electronic components are relatively simple and can be composed of space qualified chips. This becomes more critical when the signals are weaker and the bandwidth is higher. In particular the RF-frequency electronics has an increased risk of radiation damage. The closer the frequency is to the technical limits, the higher the risk of failure is. On the other hand the large development in the telecommunication has increased the availability of qualified high frequency electronics substantially. Here one has to be careful of course that the needed components will be used in a similar way they were designed to be. For example the noise on a frequency reference amplitude might not be important for a digital processor, but it could seriously affect the phase jitter of a frequency comb.

11.4 Moving Parts

Moving parts, operating continuously over the full mission duration, are always risky for an instrument. Hence, established or proposed solutions for measuring position and attitude are mainly based on retro-reflectors and non-scanning camera systems. Light sources and/or cameras (CCD-chips) can be easily switched to redundant devices.

Triangulation is proposed within this HAALDM study (and also in the CDF studies) to measure the distance to different retro-reflectors located on the XEUS mirror spacecraft. Therefore, a scanner is needed to sequentially approach the different 3-4 targets. In the proposed scanning mirror design a feedback mechanism is provided, allowing compensation of changes in mechanical properties.

The proposed internal design of the HAALDM sensor requires for both instruments, XEUS and Darwin, a quickly moved internal delay line determining the accuracy of the absolute distance measurement and defining also the speed of the distance measurement.

The reason for this permanently moved part is the cross-correlator performing an OPD-scan in a reference arm to match its length to the measurement arm. The reference arm is continuously scanned in an oscillating movement while measuring the delay line position. A strong correlation is achieved then if the delay line position matches the target distance.

The lifetime of this internal delay time is considered as critical and must be demonstrated before under space environment. Please note that the concept design already anticipates the harsh lifetime requirements. To avoid material wear over the lifetime (approximately 5billion cycles) the delay line has no mechanical contact between moving and static parts. A magnetic bearing and driving is proposed. Here the stiffness is not determined by mechanical dimensions, but by the applied magnetic field. This latter can be adjusted easily if deemed necessary.

Both scanning devices (mirror and delay line) and their reproducibility determine the achievable accuracy in the triangulation concept. The fast internal delay line determines the absolute distance of the measurement, whereas the angle of the sent beam together with the absolute distance must be known for performing the triangulation.

11.5 Necessity for Experimental Verification

Taking up the recommendations given from the subcontractors of the study the following items must be experimentally verified.

- Demonstration of the hybrid mode-locked laser diode source and its stabilisation to an external frequency reference
- Characterisation of phase jitter on emitted laser pulses
- OPD scanning mechanism working at µm-level with sufficiently large stroke at a bandwidth of a few Hz
- Characterisation of stability and lifetime of scanning mirror mechanism and the delay line

The first two topics prove the principle of the high precision distance measurement for the proposed concept. The last topics demonstrate the feasibility of a fast moving scanning device and the reproducibility of steering and OPD position over time in the expected harsh environment. These items together are the heart of the HAALDM applied to formation flying.

11.6 Status of Space Qualification and Lifetime

Currently the technology readiness level of the involved critical components is TRL4.

TRL4 means that the components and/or a breadboard are validated in laboratory environment. The new hybrid laser as a fallback solution to the already established fibre laser is even at TRL3 level.

The detailed definition of TRL4 is as follows below:

Following successful "proof-of-concept" work, basic technological elements must be integrated to establish that the "pieces" will work together to achieve concept-enabling levels of performance for a component and/or breadboard. This validation must be devised to support the concept that was formulated earlier in TRL3, and should also be consistent with the requirements of potential system applications. This validation is relatively "low-fidelity" compared to the eventual system: it could be composed of ad hoc discrete components in a laboratory.

Non of the critical components of a HAALDM sensor are space qualified. Components based on glasses, solid state materials, and semiconductors are always poorly characterised in terms of radiation resistance or lifetime. Hence related environmental tests must be initiated to get serious information on the hardness of the components. Accelerated lifetime tests must be triggered as well to get numbers on the reliability of the components. This will have serious impact on the redundancy concept of the HAALDM sensor and will determine the mass, volume, and power consumption of the sensor.

In the previous chapter most of the critical items were identified and discussed. Due to the similarity between the technical requirements of the Darwin and XEUS missions the proposed HAALDM schemes can be close to identical. The main differences are found in the location of the HAALDM scheme in the overall metrology chain. In the Darwin mission the HAALDM system would serve as an intermediate formation assessment system, whereas in the XEUS configuration the HAALDM system would be operated continuously to maintain the configuration.

Due to the recent developments in the XEUS programme and the current Darwin planning, a development plan dedicated to each of these two missions doesn't seem useful. Rather a development for the use of the HAALDM technology in general is recommended. At the moment the FS-lasers are developing very rapidly, making any design for a mission in more than five years from now outdated from the start. The principles of the HAALDM however remain very promising and the availability of laser systems will only increase in the coming years.

In Figure 11-2 a systematic sketch is given of the HAALDM system proposed for the XEUS mission. A detailed explanation of the system design is given in TN4.

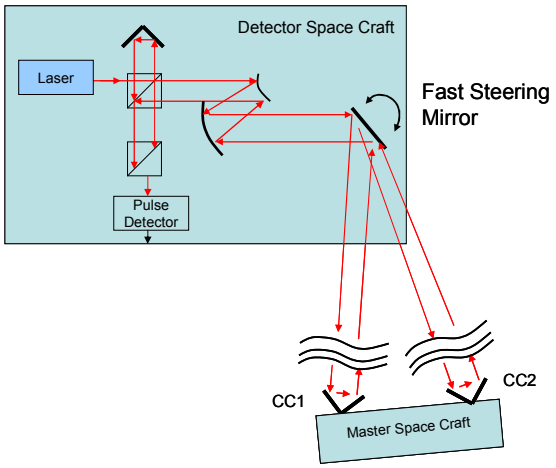

Figure 11-2 Systematic sketch of the proposed HAALDM lay-out for XEUS

11.7 Requirements and interfaces

From the mission requirements and the derived optimum design a number of requirements on the HAALDM system can be derived. The main requirements imposed on (the sub-systems of) a HAALDM system designed for either Darwin or XEUS are:

- Laser
  - Repetition frequency should be in the order of 4GHZ
  - Phase jitter (high frequencies) must be smaller than pulse duration
  - Phase jitter (low frequency variation) must be smaller than the corresponding targeted distance accuracy (~3fs to get ~1µm)
  - Pulse duration between 2ps and 100fs
  - Optical power a few tens of mW
- Optics and detection scheme
  - Optics must be sufficiently achromatic
  - Detection bandwidth >200kHz
  - Two photon detection for SNR-enhancement
- Delay line
  - Stroke should be at least 19mm
  - Repetition frequency should be at least 5Hz
  - Absolute position accuracy better than 1µm
  - Continuous operation over lifetime
- Steering mirror
  - Range +/-4degrees
  - Resolution 300µRad
  - Speed up to 5Rad/sec
  - Continuous operation over lifetime
- Mass and power
  - Total mass <20 kg
  - Total power consumption < 20Watt

11.8 Future technology development

Each of the requirements mentioned in the previous paragraph has been demonstrated separately. Also the principle of HAALDM using frequency combs has been demonstrated. Therefore these separate requirements do not indicate the need for further technological development. It is the combination of requirements and the application to the space situation that calls for development.

As discussed in the previous chapter the stable locking of the hybrid mode-locking laser to a proper RF-reference and the lifetime demonstration of the proposed mechanisms are key to the successful development of the HAALDM systems for Darwin or XEUS like missions. Demonstration of these critical issues is required to gain confidence that the system could be made space worthy.

After performing these developments a continuation of the developments can be addressed to specific mission requirements and the implementation. At this phase it is too early to address this development in detail.

The following key materials required to realise and implement a HAALDM sensor must be space-qualified

- Fibre laser (conservative approach)
- Hybrid mode locked diode laser (very new and compact approach)
- Photonic crystal glass fibre to double the spectral emission
- Fast detector used for pulse correlation
- The fast scanning delay line, permanently moving over the full lifetime
- Precise beam steering mechanism used for triangulation

More details of the subunits of the HAALDM sensor are still not available and the above list must be possibly extended.

In general all components that are not yet space qualified need a performance demonstration in the expected environment. This includes extended temperature excursions (launch, transfer flight to L2-orbit, survival mode of instrument, normal operation) but also radiation environment in terms of gamma radiation and proton impact. Proton degradation cannot be effectively shielded and can seriously affect small semi-conductor structures like the fast detector in the correlation unit. Hence, resistance to proton radiation will determine the redundancy strategy, concept, and implementation.

The required electronics to operate an HAALDM sensor cannot be estimated at this time and needs a careful investigation as well.

A full demonstrator capable of beam steering and of distance measurements with the aid of the fast optical delay line should be realised as a next step to detect and record all devices and components. In a further step all critical devices can be identified then.

The time scale of required technology developments cannot be given in this early state of the Cosmic Vision programme. Darwin has not been selected but could come in again to the CV programme at a later time. XEUS has been recently redefined and no formation flying is needed anymore. After having detected all critical components via the full demonstrator and after identifying a target mission the detailed development plan can be worked out.

12 Conclusions and recommendations

12.1 Conclusions from the literature research

Following the conclusions on TN1, fs-Laser based ADM techniques are considerable candidates to achieve high accuracy at long distances. The frequency comb concept has matured to the point where it can be employed as a workhorse for precision metrology, and is ideally suited to push the limits in high-accuracy absolute long-distance measurement towards sub-µm accuracy. Various frequency comb based metrology concepts were analysed, and promising results were obtained.

The use of coarse absolute distance metrology sensors, normally present in the metrology chain of a space instrument, could be fundamental to both remove the ambiguity of this fs-Laser pulses "time-of-flight" type of sensors and to decrease the level of complexity in the search for the fs pulse overlap location. Nevertheless, if required, these fs-laser based sensors can be self-standing by using its own pulse trains to remove ambiguity.

Two basic techniques where identified: Electrical Heterodyning, based on the measurement of the carrier phase variation , and Optical Heterodyning based in the determination of an overlapping condition between a reference and a measurement pulse train. For Optical Heterodyning, several overlapping procedure and detection scheme were identified, and almost all the possible combinations generated a concept.

All the Optical Heterodyning concepts have to start with a pulse overlapping procedure. Depending on the detection technique, different levels of overlapping will be required. This is clearly one of the critical issues of this measurement process. Several solutions were suggested, with different characteristics that must be tuned for the measurement concept.

From a technological point of view, the development of robust, compact and reliable fs-lasers for use in space-based applications is feasible. Also the additional technological challenges of stabilizing f_{rep} and even f_{ceo} in such a laser system seem achievable.

Due to the large differences in operating parameters between the various types of fs-lasers that have been considered in this study, the choice of the most suitable fs-laser system actually depends to a large extent on the measurement concept that is to be implemented. The most relevant parameters for each type of fs-laser considered in this study have therefore been compiled in tables LCVU1 and LCVU2. To summarize the main conclusions that can be drawn from chapter 4 which influence the selection of a specific fs-laser system:

Ti:Sapphire systems provide the shortest pulses and the highest pulse energy, as well as the fully-stabilized frequency comb with the highest f_{rep} values and the highest demonstrated stability. At present, Ti:Sapphire frequency combs are the only systems that have been demonstrated to allow phase stabilization with a stability that is sufficient for accurate fringe-resolved cross-correlation measurement schemes over large distances.

Erbium-doped fiber lasers are directly diode-pumped systems, which are more robust and much less alignment sensitive than Ti:Sapphire lasers. With this type of laser, frequency combs have been demonstrated that run maintenance-free over weeks, with the potential for much longer uninterrupted operation. Pulse duration, pulse energy and achievable f_{rep}-values are lower than for Ti:Sapphire, but still within the range required for most measurement concepts. The phase coherence that is needed for fringe-resolved cross-correlation measurements has not been unambiguously demonstrated yet, but improved locking schemes and laser design could resolve this issue.

Ytterbium-doped fiber lasers are more powerful and provide shorter pulses than erbium-fiber lasers. The higher doping that can be reached with ytterbium allows higher gain and therefore higher f_{rep} values compared to erbium-based lasers. The shorter wavelength requires careful dispersion management, and pulse

compression is problematic. The phase coherence that may be expected from ytterbium-fiber lasers should be better than for erbium-fiber lasers, due to the faster gain response of ytterbium, and preliminary results support this expectation [RD130].

Modelocked diode lasers with a stabilized f_{rep} can be constructed in a very compact and efficient setup. Even f_{ceo}-stabilization seems feasible, but with significantly more complexity than for the other fs-lasers. The high repetition rates and compact size make diode lasers interesting for applications where only a moderate resolution is required.

The stability of a frequency comb is largely determined by the reference oscillator. Especially on short timescales, optical reference sources can be highly advantageous compared to RF oscillators. When fringe-resolved measurements are required, optical reference sources can provide the required stability and coherence length. Stabilization of f_{ceo} is a major challenge due to the highly nonlinear processes required for f-to-2f interferometry. All-fiber frequency combs could provide the required alignment robustness to allow f-to-2f stabilization, but Ti:Sapphire lasers should preferably be phase-locked using e.g. optical stabilization.

Dispersion can be a serious issue, especially in fringe-resolved measurements. The amount of material in the interferometer arms should preferably be kept identical as much as possible. Longer pulse durations (i.e smaller bandwidth pulses) could be preferable for length measurements, as the distortion experienced by a pulse in a dispersive medium scales inversely proportional to its Fourier-limited pulse duration.

By using two synchronized fs-lasers, a scheme can be devised to measure intensity cross-correlations without mechanical moving parts, by phase-shifting the signal of the reference oscillator that controls f_{rep} for one of the oscillators.

12.2 Conclusions from the HAALDM research

Following the conclusions on TN2, the application of the dispersive time to space conversion to ADM could be specifically dedicated to monitor the pulse proximity when performing OPD or f_{rep} scanning, evaluating how close are the reference and measurement pulse to begin to overlap. This technique would cover a timing range where the current all-electronic architectures fail to provide efficient solutions. In general, this technique could provide time interval counting capacity between 30-40 ps with resolutions down to the few tens of fs.

When correlated with the OPL setting obtained from the reference arm of the interferometer, or a particular f_{rep} configuration of the Fs-laser that maximizes the peak of the envelope function, locating the peak of the envelope function provides an accuracy in the ADM down to the order of the wavelength used can be obtained

In coherent mode detection, that is accomplished mainly when the two interfering beams are close to collinear, measurement accuracy can be improved. When correlated with the OPL setting obtained from the reference arm of the interferometer, or a particular f_{rep} configuration of the Fs-laser that maximizes the peak of the envelope function, an accuracy in the ADM of lower than wavelength magnitude can be obtained, by fringe counting. When laser stabilization and noise conditions are optimised, it is possible to achieve accuracies down to tens of nanometre.

The issue of single-shot shows only its relevance in the interferometric autocorrelation, where each image frame taken by this method will present much less noise and will allow sub-fringe discrimination, thus a nanometer level accuracy. This feature is only evident for the condition of pulse full overlap, being the control of pulse superposition during the scan procedure of the responsibility of other methods, namely the multishot technique.

The single shot solution was found to less performant for any other application, namely for monitoring the pulse separation during the overlap procedure.

Pure TOF methods rely on direct time counting and there are already technologies related to the photodetection that could bring us closer to the requirements, like the family of ultrafast photo detectors and receivers, associated to MSM devices, waveguide integrated photodiodes and others, with which it is expectable to achieve risetimes down to 5 ps.

However, these high speed detectors need complementary technology with similar bandwidths, related to the electronics of time discrimination and counting, in order to produce a measurement system – detector compatible with the requirements of ADM technology.

Considering conservative, but nevertheless high rated specifications, sensitivities achievable with current crosscorrelation detector technology, it is possible to decrease the laser requirements with respect to maximum pulse energies, as the admissible loss range is quite large. Only the laser diode suffers from smaller admissible loss dynamics.

12.3 Conclusions from the concept trade-off

Following the conclusions from TN3, FSL-based systems are new in Space missions and therefore there are many unknown aspects to the usability. Concerning the Space qualification of the new FSL-distance metrology several conclusions can be drawn:

- Lasers sources
  - Pump diodes for lasers are available and used in several systems. Here probably new qualification is required since the required pump wavelength differs from the 808nm for more commonly used Nd-YAG lasers.
  - No continuum generating element has been tested so for radiation hardness. In particular the Erbium fibres pose a risk here. Although some crystals have been tested, they were tested for different parameters, such as transmission and not for continuum generation.
  - Ytterbium fibres however are promising, since it appears they are more radiation resistant than other fibres. However these experiments were not performed on the continuum generation of PCF's but just on transmission.
- Opto-electronic devices can be used as in other laser systems. Of course special designs are required, but there are no extra constraints here with respect to FSL-systems
- Electronic devices will require special design or qualification at least. In general most standard components are available but very fast electronics are not available.
- Fast detectors might deteriorate under the influence of radiation.
- Glasses. Most radiation hard glasses have a relatively low transmission on the bleu side of the visible spectrum. This could be a complication for some frequency combs.

The preliminary perturbation analysis showed that most external perturbations will the same for FSL-systems as for the alternative laser systems. The one aspect that requires attention is the reduced possibility to apply stray-light reduction for an FSL-system due to the large optical bandwidth. However it should be noted that no complications are expected here.

The performance of the different concepts showed a capability to achieve sub-micrometer accuracy for ranges up to several kilometres. Different levels of accuracy and measurement ranges will require different

level of stability and different types of detection schemes. On the whole, there is a gamut of options that allow a sensor tunability in terms of technological complexity versus requirements.

If, for the one hand, Interferometric Cross Correlation Fringe Detection is the key to create a high accuracy sensor, at the tens of nanometre level, on the other hand, its sensitivity to timing jitter reduces the measurement ranges to a few kilometres and puts stringent requirements on the frequency stabilisation technology. Nevertheless, a tens of nanometre level accuracy can be achieved.

Intensity Cross Correlation Envelope Detection can also achieve sub-micrometre (hundreds of nanometre) accuracy providing that a high stabilisation frequency reference is used. Being less sensitive to timing jitters, it can have a larger measurement range, up to several tens of kilometres.

Coherence length is not an issue for measurement up to several hundred metres, due to the inherent narrow linewidth of fs-combs. For larger ranges (> 1 km), coherence must be fully characterised in order to avoid reduction or even loss of fringe contrast.

Optical material dispersion becomes only an issue when interferometer arms are unbalanced with regard to the compensation of this effect. This is not a critical issue but must be taken into account during the sensor design phase.

Satellite drift is a parameter that must be fully characterised, in terms of instrument characteristics, before the sensor parameterisation. After knowing the level of drift, the sensor can be easily design to include, the required level of drift compensation.

Unless accuracies below a tenth of a micrometre are required, there is no advantage in using a small pulse width. Dispersion is more tolerable for large pulses, the maximum measurement range is also larger, and the gamut of available laser technologies is wider, allowing more system solution.

It must be noted that some issues, mainly related with mission details and sensor implementation, where not considered at this stage of the modelling, and might reduce the overall accuracy level. Nevertheless it must be stretched out that some of the parameterisation was over dimensioned, like the f_{rep} stabilisation for short time scales.

After performing the XEUS metrology system design based on HAALDM and performing the associated performance simulations, a number of conclusions can be drawn and recommendations can be made. These are summarised in the paragraphs below.

12.4 Conclusions from detailed design

XEUS formation flying metrology using femto-second lasers

A formation flying metrology system based on femto-second lasers has been configured and designed especially for the XEUS mission. This design comprises sub-system opto-mechanical, electronics scheme design and component selection. As well the data flow and control loops have been identified and described.

The preferred formation flying metrology system will meet all given XEUS requirements. This has been confirmed in numerous simulations where many system parameters, such as repetition frequency, timing jitter, detector noise and other system imperfections have been investigated. An overview of the simulated system performance in relation to the requirements is given in Table 8-1. Here a brief summary is given.

- The predicted longitudinal measurement accuracy is 10 µm where 300 µm is required.
- The predicted lateral measurement accuracy is 125 µm where 170 µm is required.

- The predicted tip-tilt and pitch-yaw measurement accuracy is 1 arcsec where 10 arcsec is required.
- The predicted roll measurement accuracy is 8 arcsec where >10 arcsec is required.

The accuracy of these measurements is limited by the knowledge of the base length knowledge and the timing jitter on the laser repetition frequency at lower frequencies.

Further improvements of the performance are possible by improving the reference clock stability at lower frequencies and using more stable frame design.

The baseline formation flying metrology system will meet all given XEUS requirements. Here the performance can be even better then that of the preferred design. The mayor disadvantage of the baseline design are the somewhat higher system mass and power consumption.

A simplified design based on a combination of angular measurements and distance measurements is also feasible. This simplified system:

- Has similar technical performance
- Requires less optical components and power
- Requires accurate angular measurements of the beam pointing

Darwin absolute distance measurements using femto-second laser

The proposed OHOSE scheme for the XEUS mission is directly applicable to the Darwin mission. Consequently no further design detailing and large modifications were required. When using the proposed XEUS length measurement system for Darwin, this system is only simplified by omitting the beam steering mirror, measurement and associated control. One small modification that has to be made is that the beam expander magnification has to be increased from 3 to about 9 times to match the larger working distances in the Darwin mission.

Metrology simulations demonstrate that the Darwin absolute distance measurement requirements are easily met by directly applying the proposed OHOSE scheme for the XEUS mission.

- The predicted longitudinal measurement accuracy is 5 µm where 10µm/√Hz is required.

These predictions seem somewhat negative, since the proposed OHOSE scheme was most critical at the lower frequencies, where the Darwin requirements are more relaxed at lower frequencies. Therefore the achievable accuracy will be somewhat better.

High bandwidth communication using femto-second lasers

Frequency combs can be used for communication links in different ways. The usefulness depends on the exact requirements, but it is identified that the type of laser used in our system allows for high data rates. (Multiple Gbits)

The most promising option is simple On-Off Keying, simple it yields a high data rate at the cost of just the pulse modulator and the detector on the other side. In addition this implementation has the least impact on the formation flying accuracy. The only impact is that some light will be lost due to the keying and detection.

Furthermore it is easy to implement such a system for DSC to MSC communication. Communication in the other direction is somewhat more complex, since the light source is located on the DSC. In that case the pulse modulation has to be integrated into the retro reflector.

For communication to ground, the power levels in the present system are substantially too low. The metrology system typically uses a few mW, whereas communication to ground required power levels in the Watt range.

12.5 Recommendations from detailed design

In the previous work packages it was already identified that FS-laser based distance measurement systems offer a valid alternative to the existing length metrology systems. In order to move from a paper study towards the application in space it is recommended to breadboard a demonstrator of the proposed length metrology system. During these breadboard activities and experiments special care should be given to the aspects that were identified as critical for the overall performance. A demonstrator should comprise as a minimum:

- The diode laser source and the stabilisation to an external frequency reference.
- An OPD-scanning mechanism that has a sufficiently large stroke and which is accurate to the micrometer level at the operating bandwidth of a few Hz.
- The implementation of the beam expander as well as the beam steering unit would be recommended, in order to complete the distance measurement system. However these parts are less critical and hence not directly required.

Experiments should include:

- Characterisation of the phase jitter on the emitted laser pulses. Since the stabilisation of the hybrid mode-locked laser diodes is new and the achieved jitter directly affects most measurements, a follow-up of this studies should critically asses the achievable performance.
- Characterisation of the stability and lifetime of the OPD-scanning mechanism.
- Comparison of the breadboarded system performance to an alternative length measurement technique like DWI or FSI

In the HAALDM project a thorough analysis has been performed to asses the possibilities of the new frequency comb technology for the application of accurate distance measurements in space (TN1 and TN2). As a result a preliminary design has been derived for the Darwin and XEUS missions. (TN3) and its performance for missions like Darwin and XEUS has been assessed (TN4). The compliance of the FSL for metrology applications has been proven, at the level of raw performance specifications. From a technological point of view, the development fs-lasers for use in space-based applications present a valid solution of a robust, compact and reliable metrology system.

Particular technological challenges are still a hot theme, namely related to the stabilization frep and f_{ceo} in the different laser solutions as a key aspect to an accuracy and range dynamics augmentation. Without excluding any other emerging technology, fiber lasers and monolithic solid-state lasers already present serious advantages justifying further developments.

During the course of this document, several aspects related to the FSL technology were discussed, specifically those related to the system reliability and the required developments for the application in space.

12.6 Conclusions from study review

In terms of metrology, the FS based sensor proposed in this project, showed to be a highly valuable option for absolute distance measurements. Different sensor schemes can be envisaged, allowing for a selection of the most appropriate set of measurement ranges and accuracy, enabling the tuning of the sensor complexity according to the specific requirements.

HAALDM systems for Darwin and XEUS like missions are technically feasible. All essential components and techniques have been demonstrated in a laboratory environment and published. Here the laser source forms an exception and both a base-line and preferred design are described. The baseline design relies on a fibre laser which is available commercially from a number of suppliers, whereas the preferred design utilizes a very efficient and light hybrid mode-locked diode laser. This latter type of light source needs development before it can be used reliably.

The new or still non fully-tested materials and components of the proposed HAALDM sensor for XEUS/Darwin are

- Hybrid mode-locking laser combining a saturable absorber and the proposed very new diode laser in one device
- Frequency reference in the order of 4 GHz
- Intensity correlator using two photon absorption directly on a special detector
- Fast and permanently moving delay line (stroke 19 mm, 5 Hz resonant mode)
- Sub-µm position encoder for the delay line
- Beam steering mechanism (8 degree scan range, 300 µrad accuracy, >5 rad/s scan speed, stepwise scan mode to approach sequentially the target retro-reflectors)

12.7 Recommendations from the study review

The development plan should be focused on the demonstration of the critical issues of the HAALDM technique in general. The following key materials, required to realise and implement a HAALDM sensor, must be space-qualified.

- Fibre laser (conservative approach)
- Hybrid mode locked diode laser (very new and compact approach)
- Photonic crystal glass fibre to double the spectral emission
- Fast detector used for pulse correlation
- The fast scanning delay line, permanently moving over the full lifetime
- Precise beam steering mechanism used for triangulation

A full demonstrator capable of beam steering and of distance measurements with the aid of the fast optical delay line should be realised as a next step to detect and record all devices and components. In a further step all critical devices can be identified then.

Annex 1 Reference documents

Reference Documents

RD01 Claus Jost, Anders Karlsson, Zoran Sodnik, Alain Culoma, "Absolute long distance measurement with (sub-)µm accuracy for formation flight applications", ESA Technical Note, 1-16 (2006).

RD02 "Darwin – Mission Requirements Document" (2005).

RD03 "Darwin – Payload Definition Document" (2005).

RD04 "Xeus CDF Study Report" (2004).

RD05 "Xeus – Payload Definition Document" (2005).

RD06 "Laser Doppler Interferometry Mission for Determination of the Earth's Gravity Field", Executive Summary, (2005).

RD07 "LISA: Study of the Laser Interferometer Space Antenna", Final Technical Report, (2000).

RD08 Jun Ye, "Absolute measurement of a long, arbitrary distance to less than an optical fringe", Optics Letters, **29**, 1153-1155 (2004).

RD09 Seung-Woo Kim, Ki-Nam Joo, Jonghan Jin, Yun Seok Kim, "Absolute distance measurement using femtosecond lasers", Proceedings of the SPIE, 5858, 1-8 (2005).

RD10 Hirokazu Matsumoto, Kaoru Minoshima, Souichi Telada, "High-precision long-distance measurement using a frequency comb of a femtosecond mode-locked laser", Proceedings of the SPIE, 5190, 308-315 (2003).

RD11 K. Minoshima, H. Matsumoto, "High-accuracy measurement of 240m distance in an optical tunnel by use of a compact femtosecond laser", Applied Optics, **39**, 5512-5517 (2000).

RD12 Steven Cundiff, Jun Ye, "Femtosecond optical frequency combs", Review of Modern Physics, **75**, 325-342 (2003).

RD13 S. Witte, R.T. Zinkstok, W. Hogervorst, K.S.E. Eikema, "Control and precise measurement of carrier-envelope phase dynamics", Applied Physics B, **78**, 5-12 (2004).

RD14 Ki-Nam Joo, Seung-Woo Kim, "Absolute distance measurement by dispersive interferometry using a femtosecond pulse laser", Optics Express, **14**, 5954-5960 (2006).

RD15 Jeong Seok Oh, Seung-Woo Kim, "Femtosecond laser pulses for surface-profile-metrology", Optics Letters, **30**, 2650-2652 (2005).

RD16 Kaoru Minoshima, Hirokazu Matsumoto, "Cyclic-error-free long-distance measurement using a frequency comb of a femtosecond mode-locked laser", Proceeding of the Conference on Lasers and Electro-Optics (CLEO), 1-3 (2003).

RD17 Kaoru Minoshima, Thomas R. Schibli, Hirozaku Matsumoto, "Study on cyclic errors in a distance measurement using a frequency comb generated by a mode-locked laser", Proceeding of the Conference on Lasers and Electro-Optics (CLEO), 1-2 (2003).

RD18 Feng-Lei Hong, Kaoru Minoshima, Atsushi Onae, Hajime Inaba, Hirozaku Matsumoto, Yoshibaru Sugiura, Makoto Yoshida, "Broad-spectrum frequency comb generation and carrier-envelope offset frequency measurement using the second harmonic generation of a mode-locked fiber laser", Proceeding of the Conference on Lasers and Electro-Optics (CLEO), 1-2 (2003).

RD19 Feng-Lei Hong, Kaoru Minoshima, Atsushi Onae, Hajime Inaba, Hirozaku Matsumoto, Yoshibaru Sugiura, Makoto Yoshida, "Broad-spectrum frequency comb generation and carrier-envelope offset frequency measurement using the second harmonic generation of a mode-locked fiber laser", Optics Letters, **28**, 1516-1518 (2003).

RD20 Wang Zhongyu, Fu Jihua, Meng Hao, "High precision large scale metrology using a chirped laser pulse", Proc. SPIE, 6280, 1-6 (2006).

RD21 Markus-Christian Amann, "Laser ranging: a critical review of usual techniques for distance measurement", Optical Engineering, **40**, 10-19 (2001).

RD22 Steven Cundiff, Jun Ye, John L. Hall, "Optical frequency synthesis based on mode-locked lasers", Review of Scientific Instruments, **72**, 3749-3771 (2001).

RD23 Tara M. Fortier, David J. Jones, Jun Ye, Steven T. Cundiff, "Long-Term carrier-envelope phase coherence", Optics Letters, **27**, 1436-1438 (2002).

RD24 J. J. McFerran, W. C. Swann, B. R. Washburn, N. R. Newbury, "Elimination of pump-induced frequency jitter on fiber-laser frequency combs", Optics Letters, **31**, 1997-1999 (2006).

RD25 J. J. McFerran, W. C. Swann, B. R. Washburn, N. R. Newbury, "Suppression of pump-induced frequency noise in fiber-laser frequency combs leading to sub-radian Fceo phase excursions", Applied Physics B, **86**, 2426-2430 (2006).

RD26 E. Moon, Chengquan Li, Zuoliang Duan, J. Tackett, K. L. Corwin, B. R. Washburn, Zenghu Chang, "Reduction of fast carrier-envelope phase jitter in femtosecond laser amplifiers", Optics Express, **14**, 9758-9763 (2006).

RD27 U. Keller, F. W. Helbing, G. Steinmeyer, "Carrier-envelope control of femtosecond lasers with attosecond timing jitter", Proceedings of the 11th International Laser Physics Workshop, **13**, 644-651 (2003).

RD28 R. Paschotta, A. Schlatter, S.C. Zeller, H.R. Telle, U. Keller, "Optical phase noise and carrier-envelope offset noise of mode-locked lasers", Applied Physics B, **82**, 265-273 (2006).

RD29 Chengquan Li, Eric Moon, Zenghu Chang, "Carrier-envelope phase shift caused by variation of grating separation", Optics Letters, **31**, 3113-3115 (2006).

RD30 F. W. Helbing, G. Steinmeyer, U. Keller, "Carrier-envelope offset dynamics of mode-locked lasers", Optics Letters, **27**, 194-196 (2002).

RD31 A.K. Sharma, P.A. Naik, P.D. Gupta, "Real-time autocorrelator with enhanced temporal scan range for measurements of ultrashort laser pulses", Optics & Laser Technology, **39**, 465-469 (2007).

RD32 Yan Ling, Fang Lu, "Measurements of femtosecond pulse temporal profile by means of a Michelson interferometer with a Schottky junction", Applied Optics, **45**, 9087-9091 (2006).

RD33 T. M. Fortier, A. Bartels, S. A. Diddams, "Octave-spanning Ti:sapphire laser with a repetition rate > 1 GHz for optical frequency measurements and comparisons", Optics Letters, **31**, 1011-1013 (2006).

RD34 B.R. Washburn, S.A. Diddams, N. R. Newbury, J. W. Nicholson, K. Feder, P. S. Westbrook, C. G. Jorgensen, "Infrared frequency comb for frequency metrology based on a tunable repetition rate fiber laser", Optical Fiber Measurements, 11-14 (2004).

RD35 B. R. Washburn, R. W. Fox, N. R. Newbury, "Fiber-laser-based frequency comb with a tunable repetition rate", Optics Express, **12**, 4999-5004 (2004).

RD36 B. R. Washburn, W. C. Swann, N. R. Newbury, "Response dynamics of the frequency comb output from a femtosecond fiber laser", Optics Express, **13**, 10622-10633 (2005).

RD37 Adler, F., K. Moutzouris, et al. "Phase-locked two-branch erbium-doped fiber laser system for long-term precision measurements of optical frequencies.", Optics Express **12**: 5872 (2004).

RD38 Alcock, A., P. Ma, et al. "Ultrashort pulse Cr4+:YAG laser for high precision infrared frequency interval measurements.", Optics Express **13**: 8837 (2005).

RD39 Barbarin, A., E. Bente and M. J. R. Heck "Realization and modeling of a 27-GHz integrated passively mode-locked ring laser", IEEE Photonics Technology Letters **17**: 2277 (2005).

RD40 Bartels, A., S. A. Diddams, T. M. Ramond and L. Hollberg "Mode-locked laser pulse trains with subfemtosecond timing jitter synchronized to an optical reference oscillator.", Opt. Lett. **28**: 663 (2003).

RD41 Corwin, K. L., N. R. Newbury, et al. "Fundamental amplitude noise limitations to supercontinuum spectra generated in a microstructured fiber.", Applied Physics B **77**: 269 (2003).

RD42 Dudley, J. M. and S. Coen "Coherence properties of supercontinuum spectra generated in photonic crystal and tapered optical fibers.", Optics Letters **27**: 1180 (2002).

RD43 Dudley, J. M., G. Genty and S. Coen "Supercontinuum generation in photonic crystal fiber.", Reviews of Modern Physics **78**(4): 1135 (2006).

RD44 Fuji, T., A. Apolonski and F. Krausz "Self-stabilization of carrier-envelope offset phase by use of difference-frequency generation.", Optics Letters **29**: 632 (2004).

RD45 Fuji, T., J. Rauschenberger, et al. "Monolithic carrier-envelope phase-stabilization scheme.", Opt. Lett. **30**(3): 332 (2005).

RD46 Hansen, K. P. "Introduction to nonlinear photonic crystal fibers.", Journal of Optical and Fiber Communications Reports **2**: 226 (2005).

RD47 Hartl, I., G. Imeshev, et al. "Integrated self-referenced frequency-comb laser based on a combination of fiber and waveguide technology.", Optics Express **13**: 6490 (2005).

RD48 Holzwarth, R., T. Udem, et al. "Optical frequency synthesizer for precision spectroscopy.", Phys. Rev. Lett. **85**(11): 2264-2267 (2000).

RD49 Holzwarth, R., M. Zimmermann, et al. "White-light frequency comb generation with a diode-pumped Cr:LiSAF laser.", Optics Letters **26**: 1376 (2001).

RD50 Hopkins, J. M., G. J. Valentine, et al. "Highly Compact and Efficient Femtosecond Cr:LiSAF Lasers.", IEEE Journal of Quantum Electronics **38**: 360 (2002).

RD51 Inaba, H., Y. Daimon, et al. "Long-term measurement of optical frequencies using a simple, robust and low-noise fiber based frequency comb.", Optics Express **14**: 5223 (2006).

RD52 Jones, D. J., S. A. Diddams, et al. "Carrier-envelope phase control of femtosecond mode-locked lasers and direct optical frequency synthesis.", Science **288**: 635 (2000).

RD53 Jones, R. J. and J.-C. Diels "Stabilization of femtosecond lasers for optical frequency metrology and direct optical to radio frequency synthesis.", Phys. Rev. Lett. **86**(15): 3288--3291 (2001).

RD54 Keller, U., K. J. Weingarten, et al. "Semiconductor saturable absorber mirrors (SESAM's) for femtosecondto nanosecond pulse generation in solid-state lasers.", IEEE Journal of Selected Topics in Quantum Electronics **2**: 435 (1996).

RD55 Kim, K., B. R. Washburn, et al. "Stabilized frequency comb with a self-referenced femtosecond Cr:forsterite laser.", Optics Letters **30**: 932 (2005).

RD56 Kim, K., S. A. Diddams, et al. "Improved stabilization of a 1.3 µm femtosecond optical frequency comb by use of a spectrally tailored continuum from a nonlinear fiber grating.", Optics Letters **31**: 277 (2006).

RD57 Kirchner, M. S., T. M. Fortier, A. Bartels and S. A. Diddams "A low-threshold self-referenced Ti:Sapphire optical frequency comb.", Optics Express **14**: 9531 (2006).

RD58 Kubina, P., P. Adel, et al. "Long term comparison of two fiber based frequency comb systems.", Optics Express **13**: 904 (2005).

RD59 Ludlow, A. D., X. Huang, et al. "Compact, thermal-noise-limited optical cavity for diode laser stabilization at 1×10^{-15}.", Optics Letters **32**: 641 (2007).

RD60 Ma, L. S., Z. Bi, et al. "Optical frequency synthesis and comparison with uncertainty at the 10^{-19} level.", Science **303**: 1843 (2004).

RD61 Mücke, O., R. Ell, et al. "Self-Referenced 200 MHz Octave-Spanning Ti:Sapphire Laser with 50 Attosecond Carrier-Envelope Phase Jitter.", Optics Express **13**: 5163 (2005).

RD62 Naumov, S., E. Sorokin, et al. "Self-starting five optical cycle pulse generation in Cr4+:YAG laser.", Applied Physics B **76**: 1 (2003).

RD63 Naumov, S., E. Sorokin and I. T. Sorokina "Directly diode-pumped Kerr-lens mode-locked Cr4+:YAG laser.", Optics Letters **29**: 1276 (2004).

RD64 Newbury, N. R., B. R. Washburn, K. L. Corwin and R. S. Windeler "Noise amplification during supercontinuum generation in microstructure fiber.", Optics Letters **28**: 944 (2003).

RD65 Notcutt, M., L.-S. Ma, J. Ye and J. L. Hall "Simple and compact 1-Hz laser system via an improved mounting configuration of a reference cavity.", Optics Letters **30**: 1815 (2005).

RD66 Rose, T. S., M. S. Hopkins and R. A. Fields "Characterisation and control of gamma and proton radiation effects on the performance of Nd:YAG and Nd:YLF lasers.", IEEE Journal of Quantum Electronics **31**: 1593 (1995).

RD67 Schibli, T. R., K. Minoshima, et al. "Frequency metrology with a turnkey all-fiber system.", Optics Letters **29**: 2467 (2004).

RD68 Shelton, R. K., L.-S. Ma, et al. "Phase-coherent optical pulse synthesis from separate femtosecond lasers.", Science **293**: 1286 (2001).

RD69 Sorokin, E., I. T. Sorokina and E. Wintner "Diode-pumped ultra-short-pulse solid-state lasers.", Applied Physics B **72**: 3 (2001).

RD70 Sorokin, E. "Solid-State Materials for Few-Cycle Pulse Generation and Amplification.", Topics in Applied Physics **95**: 3 (2004).

RD71 Steinmeyer, G., D. H. Sutter, et al. "Frontiers in Ultrashort Pulse Generation: Pushing the Limits in Linear and Nonlinear Optics.", Science **286**: 1507 (1999).

RD72 Sutter, D. H., G. Steinmeyer, et al. "Semiconductor saturable-absorbermirrorassisted Kerr-lens mode-locked Tisapphire laser producing pulses inthe two-cycle regime.", Optics Letters **24**: 631 (1999).

RD73 Udem, T., R. Holzwarth and T. W. H\"ansch "Optical frequency metrology.", Nature **416**: 233 (2002).

RD74 Uemura, S. and K. Torizuka "Generation of 10 fs Pulses from a Diode-Pumped Kerr-Lens Mode-Locked Cr:LiSAF Laser.", Japanese Journal of Applied Physics **39**: 3472 (2000).

RD75 van Uffelen, M., S. Girard, et al. "Gamma radiation effects in Er-doped silica fibers.", IEEE Transactions on Nuclear Science **51**: 2763 (2004).

RD76 Wagenblast, P., R. Ell, et al. "Diode-pumped 10-fs Cr3+:LiCAF laser.", Optics Letters **28**: 1713 (2003).

RD77 Washburn, B. R., S. A. Diddams, et al. "Phase-locked, Erbium-fiber-laser-based frequency comb in the near infrared.", Opt. Lett. **29**(3): 250 (2004).

RD78 Williams, G. M. and E. J. Friebele "Space radiation effects on erbium-doped fiber devices: sources, amplifiers, and passive measurements.", IEEE Transactions on Nuclear Science **45**: 1531 (1998).

RD79 Zimmermann, M., C. Gohle, et al. "Optical clockwork with an offset-free difference-frequency comb: accuracy of sum- and difference-frequency generation.", Optics Letters **29**: 310 (2004).

RD80 R. Dändliker, K. Hug, J. Politch and E. Zimmermann, “High-accuracy distance measurements with multiple-wavelength interferometry”, Opt Eng. **34**, 2407-2412 (1995).

RD81 R. Dändliker, Y. Salvadé and E. Zimmermann, "Distance measurement by multiple-wavelength interferometry", J. Opt. **29**, 105-114 (1998).

RD82 A. Cabral and J. Rebordão, “Absolute distance metrology with frequency sweeping interferometry”, Recent Developments in Traceable Dimensional Measurements III, J. Decker, Gwo-Sheng Peng; eds. Proc. SPIE 5879, 195-204 (2005).

RD83 B. Swinkels, A. Latoui, N. Bhattacharya, A. Wielders and J. Braat, “Absolute distance metrology for space interferometers”, Recent Developments in Traceable Dimensional Measurements III; Jennifer E. Decker, Gwo-Sheng Peng; eds. Proc. SPIE 5879, 216-222 (2005).

RD84 Alexandre Cabral, José Manuel Rebordão, “Accuracy of frequency sweeping interferometry for absolute distance metrology”, Optical Engineering, Accepted for publication in the 15th of January of 2007

RD85 C Towers, D Reid, W MacPherson, R J Maier, D Towers, “Fibre interferometer for multi-wavelength interferometry with a femtosecond laser”, Journal of Optics A: Pure and Applied Optics, S415–S419 (2005).

RD86 N. Schuhler, Y.Salvade, S. Leveque, R. Dandliker, R. Holzwarth, “Frequency-comb-referenced two-wavelength source for absolute distance measurement”, Optical Letters, **31**, 3101-3103, (2006)

RD87 T. sun, Bosco K.K. Fung, I.K.Sou, G.K.L. Wong, K.S. Wong, G. Lanzani, "Two-photon absorption autocorrelation of visible to ultraviolet femtosecond laser pulses using ZnS-based photodetectors", IEEE Photonics Technology Letters,1041,1-4 (2002).

RD88 William C. Stone, Maris Juberts, Nick Dagalakis, Jack Stone, Jason Gorman, "Performance Analysis of Next-Generation LADAR for Manufacturing, Construction, and Mobility", National Institute of Standards and Technology, NISTIR 7117 (2004).

RD89 Stéphane Poujouly, Bernard Journet, "A two fold modulation frequency laser range finder", JOSA, **4**, 356-363 (2002).

RD90 David Dupuy Marc Lescure, "Improvement of the FMCW laser rangefinder by APD working as an optoelectronic mixer", IEEE Trans. on Instrumentation and measurement, **51**, 5, 1-5 (2002).

RD91 D.T Reid, M. Padgett, C. McGowan, W.E. Sleat, W. Sibbet, "Light emitting diodes as measurement devices for femtosecond laser pulses, Optics Letters, **22**, 4, 233-234 (1997).

RD92 A.K. Sharma, M. Raghuramaiah, P.A. Naik, P.D. Gupta, "Use of commercial grade light emitting diode in autocorrelation measurements of femtosecond and picosecond pulses at 1054 nm", Optics Communications, 246, 195-204 (2004).

RD93 Piotr Wasylczyk, "Ultracompact autocorrelator for femtosecond pulses", Review of scientific instruments, **72**, 4, 2221-2223 (2001).

RD94 G. Perchet ,M. Lescure, "Magnification of phase shift for a laser range finder", Journal of Optics, **29**, 3 ,229-235 (1998).

RD95 Mikulics, M.; Wu, S.; Marso, M.; Adam, R.; Forster, A.; van der Hart, A.; Kordos, P.; Luth, H.; Sobolewski, R.,"Ultrafast and highly sensitive photodetectors with recessed electrodes fabricated on low-temperature-grown GaAs", Photonics Technology Letters, IEEE, **18**, 7, 820-822 (2006).

RD101 "Femtosecond single-shot correlation system: a time-domain approach". Kazutaka Oba, Pang-Chen Sun, Yuri T. Mazurenko, and Yeshaiahu Fainman. APPLIED OPTICS y Vol. 38, No. 17 y 10 June 1999

RD102 "Efficient time-to-space conversion of femtosecond optical pulses" Ayman M. Kan'an and A. M. Weiner. J. Opt. Soc. Am. B/ Vol. 15, No. 3/March 1998

RD103 "Linear and nonlinear operation of a time-to-space processor". Dan M. Marom, Dmitriy Panasenko, Pang-Chen Sun, and Yeshaiahu Fainman . J. Opt. Soc. Am. A/ Vol. 18, No. 2/February 2001

RD104 "Real-Time Detection of Femtosecond Optical Pulse Sequences via Time-To-Space Conversion in the Lightwave Communications Band", Jung-Ho Chung, Andrew M. Weiner, JOURNAL OF LIGHTWAVE TECHNOLOGY, VOL. 21, NO. 12, DECEMBER 2003

RD105 Eric R. Tkaczyk, Sylvain Rivet, Lionel Canioni, Stéphane Santran and Laurent Sarger , "Statistical Description for Assumption-free Single-shot Measurement of Femtosecond Laser Pulse Parameters via Two-photon-induced Photocurrents", IEEE Transations on Magnetics, June 2006.

RD106 "Femtosecond Laser Pulses: Linear Properties, Manipulation, Generation and Measurement". Matthias Wollenhaupt, Andreas Assion and Thomas Baumert. Manuscript to be published in "Springer Handbook of Optics", Editor: F. Träger. 2007 (available at http://www.physik.uni-kassel.de/ome/groups/11/Downloads/Sonstiges/Skript-Version30.pdf)

RD107 Dmitriy Panasenko and Yeshaiahu Fainman, "Interferometric correlation of infrared femtosecond pulses with two-photon conductivity in a silicon CCD" ; APPLIED OPTICS, Vol. 41, No. 18 June 2002

RD108 ECSS-Q-70B "Materials, mechanical parts and processes (14 December 2004), The European Cooperation for Space Standardization

RD109 ECSS-Q-70-71A rev. 1: Space product assurance - Data for selection of space materials and processes (18 June 2004), The European Cooperation for Space Standardization

RD110 "Design of a radiation-hard optical fibre Bragg grating temperature sensor", A.I. Gusarov et al., Photonics for Space and Enhanced Radiation Environments, The EOS/SPIE Symposium on Remote Sensing SPIE Proceedings 3872, 1999

RD111 "Proton and gamma radiation tests on nonlinear crystals", Ulrich Roth et al., APPLIED OPTICS Vol. 41, No. 3, 2002

RD112 K. W. Holman, D. J. Jones, J. Ye and E. P. Ippen, "Orthogonal control of the frequency comb dynamics of a modelocked diode laser", Optics Letters 28, 2405 (2003).

RD113 F. Quinlan, S. Gee, S. Ozharar and P. Delfyett, "Ultralow-jitter and –amplitude-noise semiconductor-based actively modelocked laser", Optics Letters 31, 2870 (2006).

RD114 A.G. Mann, "Ultrastable cryogenic microwave oscillators", Top. Appl. Phys. 79, 37 (2001).

RD115 J.J. McFerran, S.T. Dawkins, P.L. Stanwix, M.E. Tobar and A.N. Luiten, "Optical frequency synthesis from a cryogenic microwave sapphire oscillator", Opt. Express 14, 4316 (2006).

RD116 A. Bartels, C.W. Oates, L. Hollberg and S.A. Diddams, "Stabilization of femtosecond laser frequency combs with subhertz residual linewidths", Opt. Lett. 29, 1081 (2004).

RD117 L.-S. Ma, R.K. Shelton, H.C. Kapteyn, M.M. Murnane and J. Ye, "Sub-10-femtosecond active stabilization of two passively modelocked Ti:Sapphire oscillators", Phys. Rev. A 64, 021802(R) (2001).

RD118 F. Riehle, "Frequency standards: Basics and applications", Wiley-VCH (2004).

RD119 Ch. Spielmann, P.F. Curley, T. Brabec and F. Krausz, "Ultrabroadband femtosecond lasers", IEEE J. Quant. Elect. 30, 1100 (1994).

RD120 T. Brabec, Ch. Spielmann, P.F. Curley and F. Krausz, "Kerr lens mode locking", Opt. Lett. 17, 1292 (1992).

RD121 F.O. Ilday, J.R. Buckley, W.G. Clark and F.W. Wise, "Self-similar evolution of parabolic pulses in a laser", Phys. Rev. Lett. 92, 213902 (2004).

RD122 J.R. Buckley, F.W. Wise, F.O. Ilday and T. Sosnowski, "Femtosecond fiber lasers with pulse energies above 10 nJ", Opt. Lett. 30, 1888 (2005).

RD123 F.O. Ilday, J. Chen and F.X. Kärtner, "Generation of sub-100-fs pulses at up to 200 MHz repetition rate from a passively mode-locked Yb-doped fiber laser", Opt. Express 13, 2716 (2005).

RD124 F.O. Ilday, J.R. Buckley, H. Lim, F.W. Wise and W.G. Clark, "Generation of 50-fs, 5-nJ pulses at 1.03 μm from a wave-breaking-free fiber laser", Opt. Lett. 28, 1365 (2003).

RD125 H. Lim, F.O. Ilday and F.W. Wise, "Femtosecond ytterbium fiber laser with photonic crystal fiber for dispersion control", Opt. Express 10, 1497 (2002).

RD126 C.K. Nielsen, K.G. Jespersen and S.R. Keiding, "A 158 fs 5.3 nJ fiber-laser system at 1 μm using photonic bandgap fibers for dispersion control and pulse compression", Opt. Express 14, 6063 (2006).

RD127 T. Schreiber, C.K. Nielsen, B. Ortac, J. Limpert and A. Tunnermann, "Microjoule-level all-polarization-maintaining femtosecond fiber source", Opt. Lett. 31, 574 (2006).

RD128 A. Malinowski et al., "Ultrashort-pulse Yb3+-fiber-based laser and amplifier system producing >25-W average power", Opt. Lett. 29, 2073 (2004).

RD129 J.R. Buckley, S.W. Clark and F.W. Wise, "Generation of ten-cycle pulses from an ytterbium fiber laser with cubic phase compensation", Opt. Lett. 31, 1340 (2006).

RD130 I. Hartl, M.E. Fermann, P. Pal and W.H. Knox, "Self-referenced Yb-fiber-laser frequency comb using a dispersion micromanaged tapered holey fiber", Conference on Lasers and Electro-Optics (CLEO), Baltimore, paper CMU2 (2007).

RD131 M. Hofer, M.E. Fermann, F. Haberl, M.H. Ober and A.J. Schmidt, "Mode locking with cross-phase and self-phase modulation", Opt. Lett. 16, 502 (1991).

RD132 J.T. Gopinath, et al., "Highly nonlinear bismuth-oxide fiber for smooth supercontinuum generation at 1.5 μm", Opt. Express 12, 5697 (2004).

RD133 W.C. Swann et al., "Fiber-laser frequency combs with subhertz relative linewidths", Opt. Lett. 31, 3046 (2006).

RD134 I. Hartl, M.E. Fermann, et al., "Optical and microwave frequency synthesis with an integrated fiber frequency comb", Conference on Lasers and Electro-Optics (CLEO) , Long Beach, paper CPDB10 (2006).

RD135 R.J. Jones, I. Thomann and J. Ye, "Precision stabilization of femtosecond lasers to high-finesse optical cavities", Phys. Rev. A 69, 051803(R) (2004).

RD136 J. Ye, L.-S. Ma and J. Hall, "Molecular iodine clock", Phys. Rev. Lett. 87, 270801 (2001).

RD137 A. Bartels, S.A. Diddams, et al., "Femtosecond-laser-based synthesis of ultrastable microwave signals from optical frequency references", Opt. Lett. 30, 667 (2005).

RD138 Heinz Gunter Bach, "Ultrafast photodetectors and Receivers". J. Opt. Fiber Communications Rep. 2, 293-344 (2005)

RD139 M. Collins, B.M. AL-Hasimi, P.R. Wilson, "On chip timing resolution architectures with femtosecond resolution", Electronics Letters, 27 April 2006, Vol 42, No. 9

RD140 M.S. Kirchner, S.A. Diddams et al., "A low-threshold self-referenced Ti:Sapphire optical frequency comb", Opt. Express **14**, 9531 (2006)

RD141 C. Xu, J.M. Roth, W.H. Knox and K. Bergman; "Ultra-sensitive autocorrelation of 1.5 μm light with single photon counting silicon avalanche diode". ELECTRONICS LETERS 17th January 2002 Vol. 38 No. 2

RD142 Jeffrey M. Roth , T. E. Murphy, Chris Xu. " Ultrasensitive and high dynamic range two-photon absorption in a GaAs photomultiplier tube". OPTICS LETTERS / Vol. 27, No. 23 / December 1, 2002

RD143 L.P. Barry, B.C. Thomsen, J.M. Dudley and J.D. Harvey; " Autocorrelation and ultrafast Optical thresholding at 1.5 μm using a commercial InGaAsP 1.3 μm laser diode". ELECTRONICS LETTERS. Vol. 34 No. 4, 19th February 1998

RD144 S. Yang ; A. M. Weiner, Fejer, Martin; " 400 photon per pulse ultrashort atocorrelation measurement with aperiodicaly poed lithium niobate waveguides at 1.55 μm" OPTICS LETTERS / Vol. 29, No. 17 / September 1, 2004

RD145 Peter M. Skovgaard, Rory Mullane, David Nikogosyan, John McInerney. “Two photon conductivity in semiconductor waveguides”. Optics Communications 153, 78-82 (1998)

RD146 H. Folliot, M. Lynch, A.L.Bradley, L.A. Dunbar, J. Hegarty, J.F. Donegan, L.P.Barry, J.S. Roberts, G. Hill. “Two photon absorption photocurrent enhancement in bulk AlGaAs semiconductor microcavities”. Applied Physics Letters, Volume 80, 9

RD147 Victor Torres-Company et al., “Coherence theory of noise in ultrashort-pulse trains”, J. Opt. Soc. Am. B/ Vol. 24, No. 7/July 2007

RD148 Victor Torres-Company et al., “Effects of partial coherence on frequency combs”, J. of the European Opt. Soc. 2, 07007, 2007

RD149 PROBA 3 Mission Requirements Issue 1 Rev 1, March 6th, 2006

RD150 Preliminary XEUS Pointing Requirements SCI-A/2006.111/NR, August 25th, 2006